Silver nanoparticles – From the synthesis to the biological application

Dissertation
Zur
Erlangung des Doktorgrades
der Naturwissenschaften
(Dr. rer. nat.)

dem
Fachbereich Physik
der Philipps-Universität Marburg
vorgelegt von

Christian Pfeiffer

aus
Elmshausen

Marburg/Lahn, 2013

Vom Fachbereich Physik der Philipps-Universität (Hochschulkennziffer: 1180) als Dissertation angenommen am 12.11.2013

Erstgutachter:	Prof. Dr. Wolfgang J. Parak
Zweitgutachter:	Prof. Dr. Mackillo Kira
Prüfer:	Prof. Dr. Jörg Sundermeyer
Prüfer:	Prof. Dr. Marc Schneider

Tag der mündlichen Prüfung: 04.12.2013

Die vorliegende Arbeit wurde am Fachbereich Physik
der Philipps-Universität Marburg unter Anleitung von

Herrn Prof. Dr. Wolfgang J. Parak

in der Zeit von Februar 2010 bis August 2013 angefertigt.

Acknowledgement / Danksagung

First of all I would like thank Professor Wolfgang J. Parak for giving me the possibility to work in his workgroup and to supervise me during my PhD student time. It was an honor and a pleasure for me to work with him and the whole Biophotonics group. Here I want to set my supervisor and good friend José Maria apart for a lot of constructive discussions and advices.

I want to thank the whole group for let me work in a very pleasant and friendly atmosphere. In special I want to thank Sherry, Nani and Lena for making all the cell experiments with my particles. Special thanks for a lot of good times and interesting discussions go to my office colleagues (Andrea, Christiane, Lena, Verena, Moritz, Raimo and Xiang) including our special member Prof. Bauer for the catering with fresh fruits.

I want to thank Sebastian from the workgroup of Prof. Heimbrodt for measuring the time resolved fluorescence of my particles and Javier from the workgroup of Prof. Laborda for doing the ICP measurements.

Further I want to thank Bea, Dorleta and José Maria for proofreading this thesis.

And of course I want to thank all the once, who I forgot to mention.

Also I want to thank the BMBF and the members of the project “UMSICHT” for funding this work and for a lot of interesting discussions.

Ein ganz besonderer und extrem wichtiger Dank geht an dieser Stelle natürlich an meine Familie und meine Freunde, die immer zu mir gestanden haben und mich immer unterstützt haben. Ohne eure Unterstützung hätte ich weder mein Studium noch meine Doktorarbeit machen können.

Zusammenfassung

Das Hauptaugenmerk dieser Doktorarbeit lag auf der Synthese und Charakterisierung von definierten Silbernanopartikeln (Ag NPs). Die Partikel wurden in zwei unterschiedlichen Größen und veränderter Oberflächenchemie hergestellt. Erstens sehr kleine (~2 nm Kerndurchmesser) mit hydrophilen Liganden auf der Oberfläche und zweitens größere (~4,2 nm Kerndurchmesser), bei denen verschiedene Beschichtungen untersucht wurden. Zusätzlich wurde das Potential der Partikel auf die Anwendung in biologischen Systemen untersucht. Hierzu mussten die Partikel in wässrigen Medien stabil sein. Um dies zu gewährleisten, wurde die Stabilität in Natriumchloridlösungen gemessen. Ein weiterer wichtiger Punkt, besonders für Silbernanopartikel, ist die Zytotoxizität der unterschiedlichen Partikel. Die Zytotoxizität der Silbernanopartikel ist von besonderer Bedeutung aufgrund der zu beobachteten antimikrobiellen Wirkung. Hierzu wurde die Toxizität in zwei unterschiedlichen Zelllinien untersucht.

Die sehr kleinen Partikel (~2 nm), sogenannte Nanocluster (NCs), wurden in zwei Stufen hergestellt. Nach der Reduktion des Silberprecursors wurde zunächst ein Ätzschritt und im Anschluss daran eine Ligandenaustauschreaktion durchgeführt. Dieser Austausch ermöglichte den Partikeln auch die Stabilität in wässrigen Medien. Während der gesamten Synthese änderten sich sowohl Größe als auch Größenverteilung der Partikel. Zu Beginn herrschte eine breite Größenverteilung und es lagen Größen bis zu ca. 30 nm vor. Nach dem Ätzen war die Verteilung bereits erheblich enger und auch die Größen waren auf ungefähr 5 nm geschrumpft. Die schlussendliche Kerngröße von beinahe 2 nm mit einer sehr engen Verteilung wurde nach der Austauschreaktion erreicht, wonach die Cluster in einer wässrigen Suspension vorlagen. Ein großer Vorteil dieser Cluster war ihre rote Fluoreszenz, wodurch sie für die Betrachtung *in vitro* nicht mit einem zusätzlichen Farbstoff versehen werden mussten.

Die zweite Art der Partikel wies eine Kerngröße von ca. 4,2 nm auf und wurde durch eine einfache chemische Reduktion hergestellt. Allerdings musste hierfür zunächst ein Vorläufer des eigentlichen Liganden hergestellt werden. Nach der Synthese lagen die Partikel als graues Pulver vor und besaßen eine hydrophobe Oberfläche. Um diese nun in die wässrige Phase zu überführen, wurden zwei unterschiedliche Wege untersucht. Einerseits wurde eine Ligandenaustauschreaktion mit einem hydrophilen Liganden und andererseits das Beschichten der Partikel mit einem amphiphilen Polymer durchgeführt. Ein Vorteil der Beschichtung der Partikel ist die einfache, zusätzliche Veränderung der Oberfläche. Hierzu wurden die Oberflächen mit einem Farbstoff und/oder Polyethylenglycol (PEG) versehen. Ein weiterer Vorteil ist, dass die Toxizität der Partikel hierdurch erheblich reduziert wurde. Diese geringere Toxizität basiert einerseits auf der gestiegenen Stabilität der Partikel und andererseits auf der geringeren Aufnahme durch die Zellen für den Fall einer vollständigen Bedeckung der Partikeloberfläche mit PEG. Ein Anstieg der Stabilität gegenüber Natriumchlorid wurde zudem auch für kommerzielle Goldnanopartikel gefunden, insofern diese der gleichen Behandlung wie die Silbernanopartikel unterzogen wurden. Da diese kommerziellen Goldpartikel allerdings mit Zitrat stabilisiert wurden, mussten diese zunächst in die organische Phase überführt werden, um die gleiche Oberfläche wie Silberpartikel aufzuweisen.

Nichtsdestoweniger zeigten die Silbernanopartikel einen zytotoxischen Effekt, was auf die Freisetzung von Silber(I)ionen zurückzuführen ist. Die Freisetzung wurde bei zwei unterschiedlichen pH Werten untersucht. Bei einem neutralen pH Wert zeigten weder die mit hydrophilen Liganden stabilisierten Partikel noch die mit Polymer umwickelten Partikel eine Freisetzung von mehr als 0,1% nach 14 Tagen. Unter sauren Bedingungen hingegen (pH 3) zeigten alle Partikel eine Freisetzung von rund 1% nach nur 7 Tagen. In Relation der Gesamtmenge an Silber mit einem Silbersalz war die Konzentration an Silberionen aus den Partikeln recht gering. Allerdings zeigten diese eine erhöhte Toxizität aufgrund ihrer besseren Aufnahme bzw. der Freisetzung im Inneren der Zellen.

Abschließend lässt sich sagen, dass die definierte Synthese und Modifikation von verschiedenen Silbernanopartikeln durchgeführt werden konnte und obwohl diese eine erheblich gesteigerte Stabilität aufweisen, haben sie niemals ihre zytotoxischen Eigenschaften verloren.

Summary

The main topic of this doctoral thesis was the synthesis and characterization of defined silver nanoparticles (Ag NPs). These particles were synthesized with different sizes and modified surface chemistry. Two core sizes were synthesized. One, very small particle (~2 nm core) with hydrophilic ligands at the surface and second, bigger particles (~4.2 nm core) with different kinds of coatings were prepared. Additionally, the potential of these particles were tested for their use in biological systems. For this, they had to be stable in aqueous media. To assess this, their stability against different salt concentration was measured. Another important point, especially for silver nanoparticles, was its cytotoxicity. The cytotoxicity of the silver particles is a very important research topic due to the antimicrobial effect observed in silver NPs. Here, the toxicity of the different particles was measured in two different cell lines.

The very small particles (~2 nm), so called nanoclusters (NCs), were prepared in two steps. After the reduction of the silver precursor first an etching step and afterwards a ligand exchange reaction were done. This ligand exchange also allowed the particles to be stable in aqueous media. During the whole synthesis the size and the distribution of the particles changed. At the beginning the particles showed a broad distribution and sizes up to almost 30 nm. After the etching the distribution decreased a lot and the sizes shrunk to 5 nm. The final core size of about 2 nm with a narrow distribution was reached after the ligand exchange being the particles stable in an aqueous suspension. A big advantage of these nanoclusters was that they showed fluorescence in the red and did not need to be labeled with an additional dye for *in vitro* experiments.

The second type of particles showed a core size of around 4.2 nm and was synthesized in a simple reduction reaction. For this reaction first a precursor of the stabilizing ligand had to be synthesized. After the synthesis the particles were stable as a gray powder and showed a hydrophobic surface. To get the particles into aqueous phase two different methods were used. First a ligand exchange reaction with a hydrophilic ligand and second the coating of the particles with an amphiphilic polymer. One advantage of the coating process was the easy modification of the surface afterwards. This was shown by the modification of the particles with a dye and/or polyethylene glycol (PEG) chains. A further advantage was that the toxicity of the particles was highly reduced by this process. This reduced toxicity was on one hand due to the increased stability of the particles and on the other hand due to the reduced uptake of the particles when their surface was saturated with PEG. An increase of the stability against sodium chloride could also been shown for commercial gold particles using the same coating process. The commercial gold nanoparticles were stabilized by citrate molecules at the beginning and so first a ligand exchange including a phase transfer to the organic phase had to be done to reach the same surface like the silver nanoparticles.

Nevertheless, the Ag NPs showed a cytotoxic effect, which was due to the release of Ag(I) ions. This release was measured under different pH conditions. Under neutral pH values neither the Ag NPs stabilized by hydrophilic ligand molecules nor the once stabilized by the polymer coating showed a release of more than 0.1% of ions up to 14 days. Under acidic conditions (pH 3) all the particles showed a release of about 1% of ions already after 7 days. In comparison of the total amount of silver with a silver salt the concentration of silver ions from the particles are low but they are “more toxic” because of the better uptake respectively their release inside the cell.

To summarize it can be said that a defined synthesis and modification of different Ag NPs could be done but although they showed a very high stability they never lost their cytotoxicity.

Table of Contents

1 Introduction

1.1 General Information

To talk about silver nanoparticles (Ag NPs), first the two fields *silver* and *nanoparticles* have to be introduced. The use of silver is known since ancient times and already 3000 BC man were able to separate silver from lead. The electrical and thermal conductivity of silver is the highest of all metals, and it possesses the lowest contact resistance, which leads to its use as electrical contacts. Alloys of silver, like sterling silver, are widely used in jewelry and other silver ware. Also silver salts are of high interest. Silver iodide for example is used in seeding clouds to produce rain. Silver nitrate was extensively used in photography but its importance was reduced by upcoming of digital photography. In former times silver was widely used for coinage by many countries in the world. But this ended when the value of the coins get greater than their exchange value. Bulk silver is not considered to be toxic but most silver salts show certain toxicity[1]. Already Hippocrates of Kos knew about the bioactivity of silver[2]. Because of this biological activity silver was used for treatment of wounds as wound dressing until development of modern antibiotics in the 1940s[3]. Since more and more bacteria started to be resistant to antibiotics, the use of silver get back into the focus[4].

The definition of a nanoparticle or a nanomaterial is not as easy as one might think. A common definition says that materials, which show at least in one dimension a size between 1 and 100 nm, is a nanomaterial. But this is not a general definition. In other definitions the maximum size of a nanomaterial can also increase up the less than 1 µm (1000 nm). Here the first mentioned definition, that at least one dimension has to be smaller than 100 nm, will be used. Nanoparticles show special physical and chemical properties in comparison to their bulk material. These properties are due to the small size and their huge surface area compared to the same amount in bulk form. One famous example is gold: while bulk gold shows the typical golden color, nanoparticles made of gold show red color. This change in color is due to the appearing of surface plasmon absorption of the visible light at 520 nm[5]. By increasing the size of the particles, this absorption shifts to higher wavelength which leads to a changed color of the particles.

Nanomaterials and nanoparticles (NPs) are everywhere in our daily life. With every breath one inhales several different nanoparticles. The two main categories of nanoparticles are *naturally occurring NPs* and *synthetic NPs*. Natural sources of nanoparticles are for example dust and ashes but also some organisms show sizes of a few nanometers[6]. Although the biggest amount of particles produced in a dust storm show sizes of a few micrometers, they can also decrease to less than 100 nm. The amount of nano- and microparticles can be so big, that it can be seen by satellites. The ashes produced in forest fire or an eruption of a volcano is also a source of nano- and microparticles. These particles can reach the upper troposphere and can be found all over the world during years. Organisms like viruses and some bacteria also show sizes of a few nanometers up to a few hundred nanometers, which makes them part of the nanomaterial, which can be found in the air. But of course they are not nanoparticles. Not only outdoor nano- and microparticles can be found but especially indoor. Here the air can be ten times more polluted than outdoor, according to the US Environmental Protecting Agency[7]. The main sources here are cooking, smoking, dust, skin particles, spores and combustion (from e.g. candles). The World Health Organization estimates that worldwide 1.6 million people annually die because of indoor air pollution[8].

Ahead from the *naturally occurring nanoparticles* the *synthetic nanoparticles* also can be found in a huge number in our daily life. Here most nanoparticles can be found in cosmetics (e.g. creams, face powder, lipsticks etc.) and personal care products (e.g. deodorants, soaps, toothpaste etc.) but also in other consumer products[9,10]. Their use in cosmetics is due their special properties for example that some can penetrate deeper into the skin or show antioxidant properties or show intensive color. Another important field for synthetic nanoparticles is *nanotechnology*. Here the special properties of the different particles are used for example to deliver a drug or sensing or labeling.

All this leads to the question: "Why are nanoparticles important in nanotechnology and in special silver nanoparticles?" To answer this question first one must have a look at the different kinds of synthetic NPs and what they are used for.

The two main synthesis routes are *top down* or *bottom up*. A *top down* synthesis starts from the bulk material and ends with the nanoparticles. Laser ablation is a typical *top down* synthesis route. In a *bottom up* synthesis the starting point is a precursor, which reacts to generate the final nanoparticle. Some kind of particles (e.g. Au NPs) can be produces by using both synthesis routes, *top down*[11] or *bottom up*[5]. The two main types of nanoparticles are *organic* and *inorganic*. Here the focus will be placed on the *synthetic, inorganic* NPs, in special the Ag NPs, their *bottom up* synthesis and their behavior in biological systems. All the other types of particles will just be mentioned in a few words describing a possible synthesis and a possible use.

1.2 Organic nanoparticles

Starting with the *organic nanoparticles*, here the first subtype of NPs are carbon nanoparticles. For this type of particles, in special carbon nanotubes, the most common synthesis are arc discharge[12], laser ablation[13] and chemical vapor deposition[14]. Arc discharge and laser ablation are *top down methods* and will be unaccounted. The chemical vapor deposition is a *bottom up synthesis* for carbon nanotubes. In this method a catalyst metallic particle is heated in a furnace and a hydrocarbon gas is flowing through the reactor for a while. The metallic particles are used as a type of "seed" for the tubes. The size, shape and orientation of the nanotubes can be modified by changing different parameters like substrate, type of gas, metallic particle, etc.[14]. The two most common uses for carbon nanotubes are in catalysis[15] and also for biological applications[16].

Also special polymers can form nanoparticles. This can happen by self assembling for example with block copolymers or just by the architecture of the polymer like dendrimers. Both types of polymer particles can be used for example for drug or gene delivery in gene therapy as non-viral vectors. Block copolymers, like poly(2-(dimethyl amino)ethyl methacrylate)-block-poly(2-hydroxyl methacrylate), form stable ,so called, *polyplexes* with the DNA. In these *polyplexes* the DNA can be transfected into the cell and can be protected from degradation by DNase[17,18]. Dendrimeres are polymerized by starting from a central molecule and growing of defined *generations* around this inner molecule, which leads to a three-dimensional tree like structure. They are also widely used in gene therapy[19]. Because of their tree like architecture, they form stable complexes with the DNA, making them good vectors for gene delivery. The exact synthesis of these particles depends on the type of polymer, on the monomers and other factors.

1.3 Inorganic nanoparticles

We can find a wide variety of nanoparticles with an inorganic core, showing optical, magnetic or thermal properties depending on the material and on the size. The first type of *inorganic* nanoparticles are quantum dots (QDs). These particles are made of semiconductor crystals. One interesting property of these particles is that they show different fluorescence emission depending on their size. Fluorescence occurs by the relaxation of an electron from an excited energy state back to the ground state by emitting a photon. In a dye molecule the energy of the emitted photon is given by the energy difference between the HOMO and the LUMO orbital. In a QD the energy gap between the valence band and the conduction band is important. This gap can be modified by changing the size of the particle. The smaller a QD, the bigger the gap and the higher is the energy of the emitted photon (blue shifted). The bigger the QD, the closer the edges of valence and conduction band and the lower the energy of the emitted photon is leading to a red shift. The widely used particles are made of a

core/shell structure of CdSe/ZnS[20] or CdTe/ZnS[21] but also QDs without a shell are used[22,23]. The advantage of core/shell like QDs is that the recombination of the electron is done in the core and the shell can act as a protective layer, which reduces photobleaching. The fluorescence, its intensity and high yield, as well as the reduced photobleaching due to the mechanism of the emission are the main reasons why QDs are an useful tool for sensing and labeling in biomedicine[24,25]. Another possible use for QDs is the use in solar cells[26]. The synthesis of this kind of particles is based on the reaction of organometallic precursors in a hot coordinating organic solvent forming first the CdSe core and afterwards the ZnS shell around this core[27,28].

Magnetic nanoparticles are another type of inorganic NPs. Important particles in this field are for example Fe_2O_3 NPs[29]. Also other types of particles including magnetic elements, like Cobalt, are used[30] and also alloys, like FePt nanoparticles, are used[31]. The two main synthetic routes are thermal decomposition of precursors or the (co-)precipitation[32]. In thermal decomposition, the metal precursor is heated in a high-boiling temperature organic solvent containing stabilizing surfactants until decomposition and formation of the nanoparticles. The co-precipitation is a convenient way to synthesize iron oxide nanoparticles. In this methodology, aqueous iron salt solutions react by the addition of a base under inert atmosphere at RT or at elevated temperature. Because of the magnetic nature of the particles one field is the use in magnetic resonance imaging (MRI) for contrast enhancement[33,34]. Magnetic hyperthermia is another important use for magnetic NPs in nanobiotechnology[35]. The particles produce heat due to the oscillation of the internal magnetic moment of the superparamagnetic particles, induced by an external alternating magnetic field of suitable frequency. This heat can be used for selective death of tumor cells, which taken up the particles. If the produced heat keeps moderate healthy cell will keep unaffected because they are less sensitive to temperature[36].

In the field of metal nanoparticles two types of metals are dominant, gold and silver. But also other metals like Copper[37], Platinum[38], Cobalt[39] and Nickel[40] are used. Gold nanoparticles (Au NPs) were used since Ancient Roman times for coloring glass, without knowing that they used Au NPs.

Figure 1: The Lycurgus cup and a part of a church window in the cologne cathedral. Red color is due to Au NPs inside the glass.

This was done because of the intensive red color of gold nanoparticles. This color is due to a typical surface plasmon of the particles at 520 nm[5]. This Plasmon peak is used for example for localized surface plasmon resonance (LSPR) spectroscopy[41]. In this method the shift of the absorption of the NP due to the absorption of (bio-) samples is measured. One of the first scientific practical synthesis of gold nanoparticles was published in 1951 from Turkevich *et al.*[42]. The first syntheses were based on the reduction of Au(III) ions in aqueous solutions. The disadvantage of this method was that sizes smaller than 10 nm could hardly be realized. A good methodology to solve this problem, based in the reduction of the Au(III) ions in organic solvent, reaching smaller sizes, was published in 1994 by Brust *et al.*[5]. Nowadays the sizes and shapes as well as the surface of the Au NPs can be tuned[43–47]. Hyperthermia, which was introduced in the former paragraph, can also be provoked by Au NPs. Here the particles are irradiated with a laser beam. Due to the absorbed light, the particles heat up[48]. The use of Au NPs in biological systems require high stability of the NPs in aqueous solution. There are at

least two ways to manage this; one is to use hydrophilic ligand at the surface[43,45]. The other one is in case that the particle itself shows a hydrophobic surface. The use of an amphiphilic polymer to cover the surface, creating hydrophilic properties at the surface of the particle can solve the problem[49,50]. These methods are not special for Au NPs but can be used for every kind of particle described before and for silver nanoparticles too[24,49,51].

Because of the above mentioned biological activity the silver nanoparticles are the most used nanoparticles in the daily life[9,10]. Ag NPs are in all regions of life from clothes to cosmetics and from toys to medicine. All these different particles have one thing in common, they come in contact with the human and afterwards with the environment[52–54]. But still there is a big gap of knowledge why silver products and silver nanoparticles are toxic and what happens with the Ag NPs in the body and later in the environment. Another huge disadvantage of the most used Ag NPs used in daily life is, that the sizes and/or shapes are not well defined, so that one cannot say which effect is due to which parameter. The synthesis of silver nanoparticles can be done in aqueous[55] or organic solvent[44,45,56,57]. The aqueous synthesis deals with same disadvantage like the former mentioned Au NPs synthesis, the difficult realization of sizes smaller than 10 nm. Additionally the oxidation of the Ag particles will be done automatically just by the presence of oxygen. Also the solution of the problem of small particle synthesis was done in same way, by using synthesis in organic solvents. Silver nanoparticles also show a typical surface plasmon at 430 nm[51], which gives them a yellowish color. The cytotoxicity is one key factor for the use of nanoparticles in biological systems[58–60], not only for Ag NPs. Another important factor, which correlates with the toxicity, is the uptake of the particles[61] in cells and their dissolution behavior[62]. Also the surface chemistry is different in almost all the different particles, although the most common capping ligands are citrate and polyvinylpyrrolidone (PVP). The surface chemistry and with this the stabilization is very important for the behavior of the nanoparticles[51,56,63,64]. The amount of particles for example, which were taken up a cell, is actively influenced by the surface chemistry of a particle. This is very important for the case that the particles release toxic ions, like silver[65]. For Ag NPs the toxicity was tested in many studies from unicellular organisms[65–67] to cell lines[4,51,63,68–71] up to higher organisms[72]. All these studies show that the toxicity of silver ions is greater than from silver nanoparticles, in the case that one look at the total amount of silver.

1.4 Biological applications of the nanoparticles

In principal, nanoparticles can be found is a wide range of applications in *biotechnology*. In the field of diagnosis they are used for labeling, sensing and imaging. By the uptake of a particle by a cell the fluorescence for example can be used for labeling these cells and tracking them with a confocal laser scanning microscope (CLSM)[73]. Here the particle itself can show fluorescence, like QDs[73–76] or very small metallic nanoclusters (NCs)[43,56], or the particles can be labeled with a dye. But QDs as well as Ag NCs can release toxic ions, like Cd^{2+} or Ag^{+} inside the cells, which give them certain toxicity. If the used particles are big enough (>20 nm for Au NPs), they can also be imaged directly with optical microscopy in phase contrast mode[77]. For biosensors, the plasmon resonance of metallic particles is used. In localized surface plasmon resonance (LSPR) spectroscopy the shift of the plasmon resonance peak of the particles is measured, which appears due to the adsorption of (biological) samples. For this method, it is very important that the particles are uniform in size and shape because the plasmon resonance peak can be shifted by changing one of these factors[78]. Also the particles can be modified in a way that only specific samples can absorb so that also selectivity is given[41,77,79]. Another way of sensing is that the particles are modified for example with an ion sensitive dye and so detect the environmental ion concentration[80]. But for this application it is important to mention that the particles themselves influence the “nanoenvironment” around the particle because of their charged surface[81]. A negative charged particle will attract more positive ions in its closest environment and vice versa, so that the concentration of the ions differs from the real bulk concentration, if the sensor dye is located at the surface of the particle. To solve this problem the introduction of spacers between the particle surface and the sensitive dye can be done[82]. The nanoparticles can also be used for treatment of cells.

The hyperthermia for example can be used to induce cell death[35] or to open other carrier systems, like microcapsules, inside a cell[48]. The opening of the polymer microcapsule can be done for example by irradiating the capsule with a laser beam. The Au NPs, which are included in the shell of the capsule, start to produce heat, which leads to the melting of the polymer shell and the release of the cargo material inside the cell (*cf.* Figure 2). Also the nanoparticle itself can act as a cargo system to bring for example drugs or DNA inside a cell[17] or to enlarge the circulation time in a body[83].

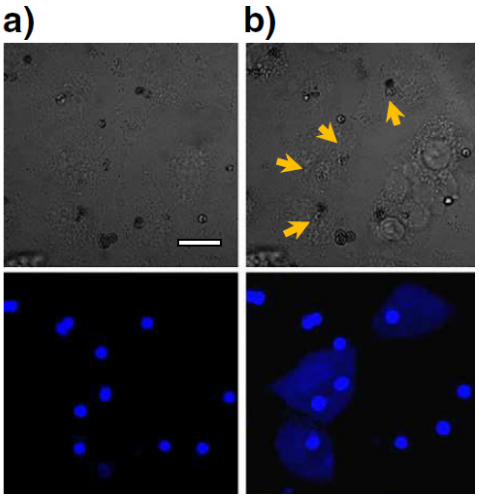

Figure 2: Release of 10 kDa Cascade Blue-dextran inside A549 cells by irradiation of microcapsules by a laser beam, done by Carregal-Romero et al.[48].

1.5 Interaction of nanoparticles with cells

Nevertheless the fate of a nanoparticle, when it enters a cell or is in biological media, is also very important[84]. The first barrier for the particle by entering a cell is the cell membrane[85]. Here the surface chemistry of the nanoparticle is very important. For example, if the particle surface is modified with a cell penetrating peptide or an antibody, they can be used for active targeting. Or if the surface is coated with an antifouling coating like polyethylene glycol (PEG), the particles can be used for passive targeting. The suspension of nanoparticles in biological medium can release ions, which can be toxic depending on the coating, the core material, the time present in the biological sample and its location. In this case the formation of reactive oxygen species (ROS) can happen, which lead to oxidative stress, which is a main factor for the toxicity of particles. The formation of a so called *protein corona* happens to all particles as soon as proteins are around[31,86–88]. This can lead eventually to opsonization and recognition by macrophages or in worst case to uncontrolled aggregation of the particles. In both cases the uptake of the particles is blocked, besides the particles should be taken up by the macrophages. The surface charge of the nanoparticle is another important factor for the uptake of a particle. Positively charged particles show in general a higher uptake than negatively charged particles[89]. This effect is due to the negative charge of the cell membrane, which leads to a repulsion of the negative particles. The other side of the medal is that the positive charged particles show a higher toxicity compared to the negative charged particles.

If all these facts are considered, one can say that all the NPs and in special the Ag NPs are important and that it is important to use defined particles and systems to draw the right conclusions.

2 Materials and Methods

In this Chapter all the methods are described just in general words. For a detailed description see the attached articles and supporting information in the Appendix of this thesis.

2.1 Materials

Chemicals

The following chemicals were used for the preparation of the different nanoparticles and the different modifications. Chemicals were used without further purification before use.

British BioCell International: Colloidal gold (5 nm #EM.GC5)

Carl Roth: Chloroform (#Y015.2), Ethanol (#9065.2), Methanol (#8388.6), Sodium chloride (#HN00.2), Tetrahydrofuran (#AE07.1), Toluene (#9558.2)

Dyomics: DY-636 amino derivate (#636-02)

Invitrogen: Ultra-Pure Agarose (#7606037200)

Rapp Polymere: α-Methoxy-ω-amino Polyethylene Glycol (PEG-NH_2) (2 kDa #122000-2, 10 kDa #1210000-2), α-Methoxy-ω-thiol Polyethylene Glycol (PEG-SH) (5 kDa #125000-40)

Sigma-Aldrich: 11-Mercaptoundecanoic acid (MUA) (#450561), Decanoic acid (#W236403), Didodecyldimethylammonium bromide (DDAB) (#36785), Dodecanethiol (#47,136-4), Dodecylamine (#D222208), L-Ascorbic acid (#255564), Lipoic acid (#T5625), *N*-(3-Dimethylaminopropyl)-*N*′-ethylcarbodiimide hydrochloride (EDC) (#E7750), Poly-isobutylene-alt-maleic anhydride (6 kDa) (#531278), Silver nitrate (#204390), Sodium borohydride (#452874), Tetra-n-butylammonium borohydride (TBAB) (#23,017-0), Tetraoctylammonium bromide (TOAB) (#294136), Tris-Borate-EDTA buffer (TBE) (#T3913),

Strem Chemicals: Bis(p-sulfonatophenyl)phenylphosphine dihydrate dipotassium salt (Phosphine) (#15-0463)

Techniques

The following techniques and equipments were used for the purification and characterization of the different nanoparticles.

Gel electrophoresis: Bio Rad PowerPac Basic

Centrifuge and Filters: Heraeus Variofuge 3.0RS and Satorius Vivaspin 20 (100 kDa MWCO, 30 kDa MWCO, 3 kDa MWCO)

Size-exclusion chromatography (SEC): Agilent Technologies 1100 Series with a column filled with GE Healthcare Sephacryl S-300 high resolution

UV-Vis- and Fluorescence spectra: Agilent Technologies 8453 UV-Vis and Horiba FluoroLog

Dynamic light scattering (DLS) and laser Doppler anemometry (LDA): Malvern Zetasizer Nano ZS

Transmission electron microscopy (TEM): Jeol JEM-3010 TEM, copper grids from Plano (#160-3)

Inductively coupled plasma mass spectrometry (ICP-MS): Agilent Technologies 7700 Series ICP-MS

2.2 Synthesis of silver nanoclusters (Ag NCs)

The synthesis of the silver nanoclusters was done in two steps. The first step was the synthesis of silver nanoparticles which were etched down to nanoclusters in a second step. This method is based on a similar synthesis of gold nanoclusters[43].

2.2.1 Synthesis of 2 nm sized silver nanoparticles

The synthetic pathway was divided in two steps. For the first step four precursor solutions had to be freshly prepared. The first one was 25 mM AgCl in 100 mM didodecyldimethylammonium bromide (DDAB) in toluene. This product needed a few hours to be completely dissolved and must be protected from light. The other solutions were 25 mM of DDAB in toluene, 100 mM decanoic acid in 25 mM DDAB in toluene and 100 mM tetrabutylammonium borohydride (TBAB) in 25 mM DDAB in toluene.

First, 156.3 µL of the decanoic acid solution, 200 µL of the AgCl solution and 250 µL of the TBAB solution were mixed and stirred for 10 minutes at RT in a small glass vial. Immediately after the addition of the three solutions the mixture turned light brown, which indicated the formation of Ag NPs. To improve the size distribution of the particles an etching step was done. Therefore, 2500 µL of the AgCl solution were added by adding one drop each three seconds to the Ag NPs reaction mixture and stirred it for 10 minutes at RT. The color of the mixture changed during the addition from light brown to dark brown almost black.

Very important in the second step was to prepare the precursor solutions during the synthesis of the Ag NPs. First a solution of 200 mM lipoic acid in 25 mM DDAB in toluene and a solution of 50 mM TBAB in 25 mM DDAB in toluene were prepared. By mixing both solutions in a ratio of 1:1 the lipoic acid was reduced into dihydrolipoic acid (DHLA), which bound to the surface of the nanoclusters.

During the last 10 minutes of stirring the Ag NPs 1600 µL of both, the lipoic acid solution and the TBAB solution, were mixed and stirred. Then the freshly prepared Ag NPs were added under vigorous stirring into this mixture one drop every three seconds. During this addition the Ag NCs started to precipitate. After the addition the reaction was stirred for 10 minutes and afterwards divided into four lockable glass vials and locked. These vials were exposed to UV light (366 nm) for 10 minutes. Then each vial was gently shaken and again exposed for 10 minutes. Afterwards the vials were heated at 70°C for one minute. Then the steps of exposure, shaking and exposure were repeated. Afterwards the Ag NCs should be aggregated and stuck to the wall of the vials. If not, the former steps had to be repeated until the clusters stuck to the wall. Now, the vials were unlocked and the yellowish solution was trashed. The nanoclusters were dissolved in Methanol and combined again. Afterwards the Methanol was removed under reduced pressure at 40°C. To remove excess ligand molecules 2 mL of Chloroform was added and gently shaken. The Chloroform was trashed afterwards. The clusters were again dissolved in Methanol and dried completely under reduced pressure at 40°C. Finally, the clusters were dissolved in 50 mM sodium borate buffer (pH 9). The dispersed clusters were heated over night at 55°C. For removing of aggregates the suspension was passed through a syringe filter (0.22 µm pore size). For separating the different sizes clusters were placed into a 100 kDa MWCO centrifuge filter were only the small once can pass the membrane. These clusters were placed into a 30 kDa MWCO centrifuge filter were they pass again the membrane. For the final concentrating of the clusters a 3 kDa centrifuge filter was used. When the particles were washed and concentrated they were purified as described in Chapter 2.8.

2.3 Synthesis of dodecanethiol capped silver nanoparticles (Ag NPs)

Silver nanoparticles with a diameter of about 4.2 nm were prepared following the route described by Mari *et al.*[57]. The first step was the preparation of the sodium S-dodecylthiosulfate. This molecule was needed for the synthesis of the silver nanoparticles (Ag NPs) leading to the final stabilization ligand (*cf.* Figure 3). During the reaction the disulfide bond gets cleaved and the final particles were stabilized with dodecanethiol.

First, 25 mmol of sodium thiosulfate pentahydrate (6.21 g) were dissolved in 50 mL water and 25 mmol of 1-bromododecane (5.187 ml) were dissolved in 50 mL ethanol. The solutions were mixed and stirred under reflux for 3 hours. After cooling down to RT the obtained white crystals (sodium S-dodecylthiosulfate) were filtered, crystallized again from ethanol and dried.

The particles were synthesized dissolving 1.26 mmol of the sodium S-dodecylthiosulfate (390 mg) in 90 mL of ethanol at 50 °C. 1.68 mmol of $AgNO_3$ (282 mg) were added to the solution and the mixture was stirred for 10 minutes. The white mixture started to turn brown after a few minutes. 8.4 mmol sodium borohydride (318 mg) were dissolved in 15 mL ethanol and added to the mixture which turned almost black immediately. After 5 minutes 0.42 mmol ascorbic acid (74 mg) was added to the reaction. Three hours later the heat source was removed and the reaction cooled down to RT. The Ag NP were collected by centrifugation at 3000 rpm for 15 minutes, washed with water, ethanol and acetone and dried in the vacuum and stored as gray powder. For further use the particles were suspended in chloroform.

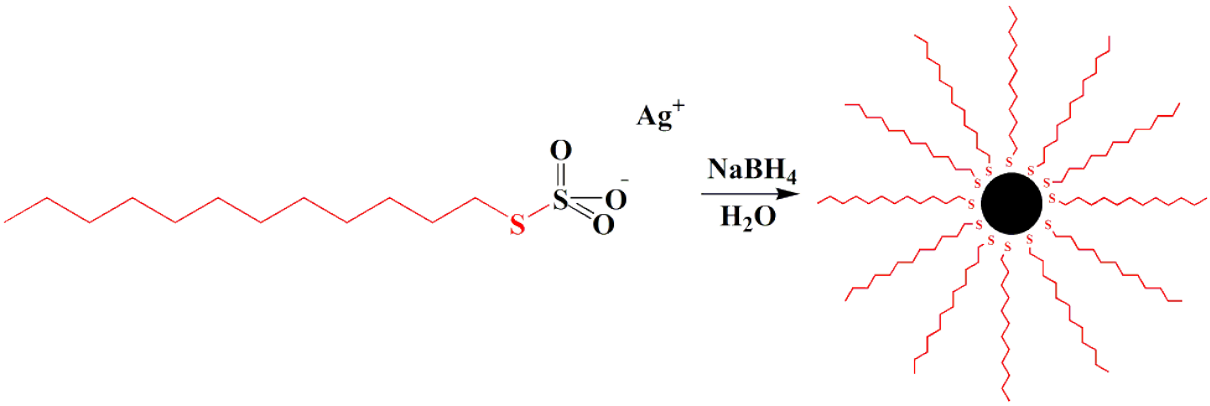

Figure 3: Scheme of the synthesis of 4 nm silver nanoparticles.

2.4 Ligand exchange of Ag NPs with 11-mercaptoundecanoic acid

To obtain water soluble Ag NPs, the hydrophobic dodecanethiol molecules were exchanged by hydrophilic 11-mercaptoundecanoic acid (MUA). Therefore 10 mL of a suspension of 0.5 $mg \cdot mL^{-1}$ of the Ag NPs in Chloroform was prepared. Additionally 7.3 mmol of MUA was dissolved in 130 mL of Tris-Borate-EDTA (TBE) buffer (0.5x) by placing it into an ultrasonic bath for 45 minutes. Afterwards both suspensions were mixed and shaken for 5 minutes. During this time the Ag NPs underwent a phase transfer to the aqueous phase. A separation funnel should not be used for this because the MUA was used at such excess that it could block the chock during the separation. For separating the organic from the water phase and the biggest amount of excess ligand molecules, the mixture was placed into 40 ml lockable glass vials and centrifuged for 20 minutes at 2000 rpm. After the centrifugation the phases were well separated and the excess ligand created a white solid phase on top of the organic phase. The aqueous phase, which included the Ag NPs and was on top of all phases, could be easily removed by using a pipette. For a first purification, washing and concentration step the MUA stabilized Ag NPs (Ag-MUA NPs) were placed into a centrifuge filter (MWCO 100 kDa) and washed three times with water. When the particles were washed and concentrated they were purified as described in Chapter 2.8.

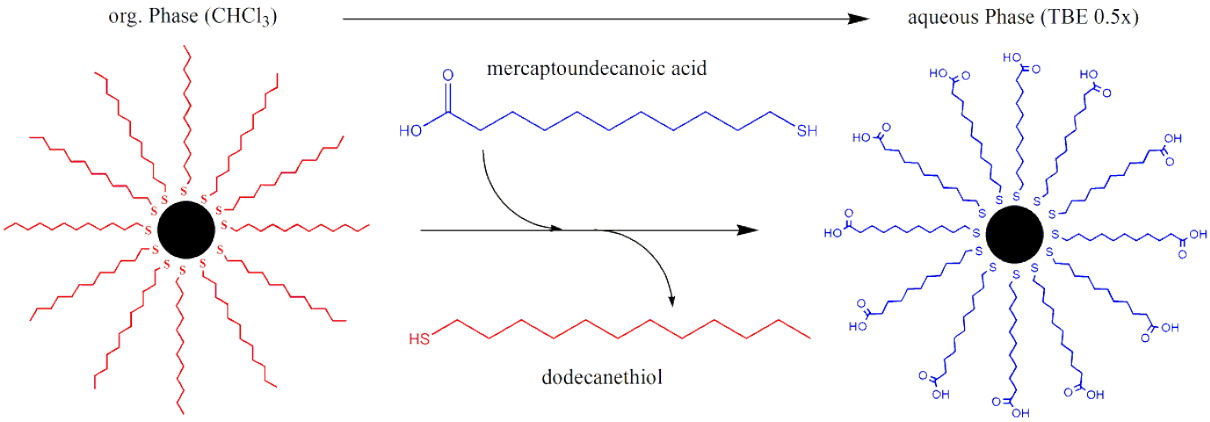

Figure 4: Ligand exchange of dodecanethiol with mercaptoundecanoic acid.

2.5 Polymer coating of Ag NPs with an amphiphilic polymer

One way to transfer the hydrophobic Ag NPs (or other hydrophobic nanoparticles) into aqueous solutions is to coat the particles with an amphiphilic polymer. The Polymer used here, was a modified Poly-isobutylene-alt-maleic anhydride (PMA) with a final molecular weight of about 11 kDa. The modification was done by the reaction of 75% of the anhydride rings with Dodecylamine. This reaction was performed in Tetrahydrofuran (THF) at 67°C overnight. The anhydride rings were opened by the amine group of the Dodecylamine forming an amide bond. This leaves 25% of the anhydrides unreacted, making possible postmodification and the linkage of other molecules like dyes, polymers or biological molecules like peptides. After the modification the polymer was dried under reduced pressure at 40°C. A stock solution of the polymer in Chloroform was prepared with a concentration of 0.05M. The rest of the unreacted anhydride rings were opened during the last step of the coating process, described below. The Dodecylamine side chains represent the hydrophobic part, whereas the opened rings (=> carboxylic acid groups) represent the hydrophilic part. This modification reaction and also the additional modification with for example a dye is already established and known in the literature[49].

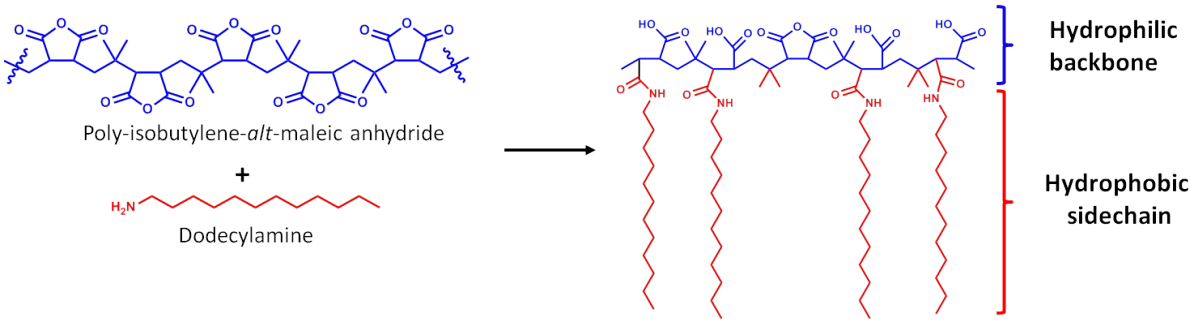

Figure 5: Scheme of the synthesis of the modified PMA used for polymer coating.

For the coating of hydrophobic dodecanethiol capped Ag NPs, a suspension of particles in chloroform was mixed with a calculated amount of modified PMA. The quantity of polymer was calculated using Eq. 1.

$$V = \frac{A_P \cdot R_P}{c_p \cdot N_A} \text{ (Eq. 1),}$$

where A_P is the surface area of all the particles in the sample; Rp is the value how many polymer units should be used per nm² (100 worked the best); c_P is the concentration of polymer solution (0.05 M) and N_A is the Avogadro constant ($6.022 \cdot 10^{23}$ mol^{-1}).

For calculating the surface area of the particles it was assumed that all particles have a spherical shape and the same diameter. The mixture of the particles and the polymer was stirred for 5 minutes at 40°C and afterwards the chloroform was removed under reduced pressure. When the chloroform was completely removed the coated particles were resuspended in basic aqueous media (50 mM sodium borate buffer, pH 12 (SBB12)). During this suspension all the anhydride rings of the PMA were opened so that afterwards carboxylic acid groups were present at the surface of the particles. To remove bigger aggregates the particle suspension was filtered through a 0.22 µm syringe filter. Afterwards the PMA coated particles (Ag-PMA NPs) were placed into a centrifuge filter washed with water and concentrated. When the particles were washed and concentrated they were purified as described in Chapter 2.8.

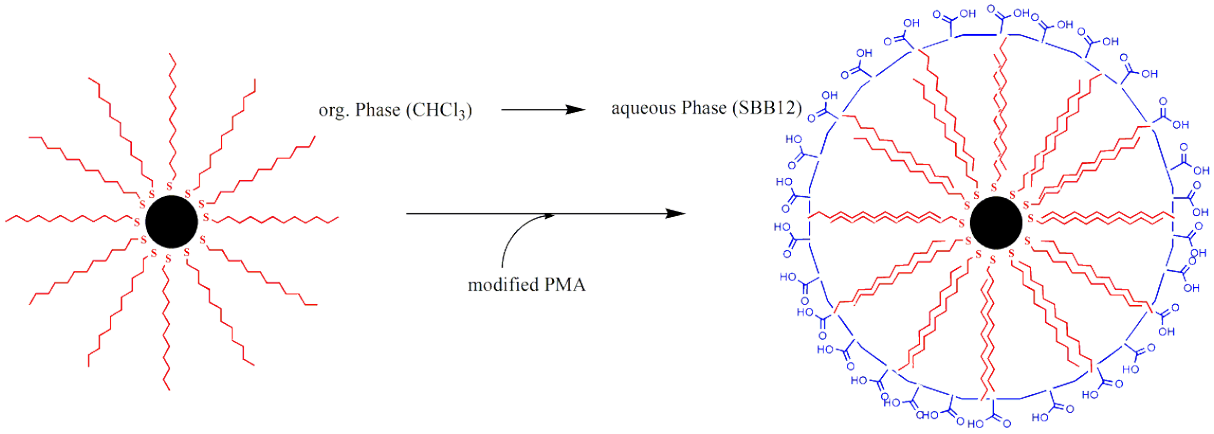

Figure 6: Polymer coating of a Ag NP with modified PMA.

2.6 Surface modification of Ag-MUA NPs and Ag-PMA NPs

Ag-MUA NPs can be modified in the same way like the Ag-PMA NPs. The modification of PMA coated particles is well established and known in the literature[49,59]. The presence of the COOH groups permit to modify the surface as esters or amides, using standard methodology. Here it was done using carbodiimides chemistry, with *N*-(3-Dimethylaminopropyl)-*N'*-ethylcarbodiimide hydrochloride (EDC). To use EDC chemistry two conditions have to be fulfilled. First, one molecule must carry a carboxylic acid group; here this is done by the PMA coated particles and the MUA stabilized particles. Second, the other molecule has to carry an amine group and both reactants have to be soluble in water. In peptide synthesis, where EDC is also used[90,91], it could be added to the reaction in a ratio of 1:1 to the carboxylic acid groups but for the reaction with nanoparticles a high excess of the EDC is necessary. To find the ratio which is needed for the reaction, first a test-reaction was done.

The procedure of the reaction is the same for both types of particles, so it will be explained here in general words. For the test-reaction 10 µL of the Ag NPs in water were mixed with a certain amount of amine modified PEG so that 500 amine groups were available per nanoparticle. To this mixture an amount of EDC in water was added which corresponds to a certain ratio of EDC per particle. This ratio was varied from 1:500 up to 1:128000 depending on the particles and the amount you want to add to the surface. After 2.5 h of reaction the particles were run through an Agarose gel to see the result. Afterwards the ratio which fits the best was chosen to modify the rest of the particles. To make it more clear, here an example of Ag-PMA NPs, which were modified with 10 kDa PEG.

10 µL of Ag-PMA NPs (2 µM) were mixed with 10 µL of PEG-NH_2 (1 mM) and 64 µL of EDC (10 mM) which correlates to a ratio of 1:32000. Additionally ratios of 1:16000 down to 1:2000 were prepared and after 2.5 h of reaction all the samples were run through a 2% Agarose gel for comparison (*cf.* Figure 7). Depending on the ratio several bands of different modified particles were visible. With this result the ratio for the modification could be chosen and the rest of the particles could be modified. For example to add one PEG molecule per particle a ratio of 1:2000 up to 1:8000 could be chosen. But in all the cases the particles had to be separated from the "wrong" modified particles (0 or 2 PEG per particle) by cutting the "right" modified band out of the gel and extracting the particles.

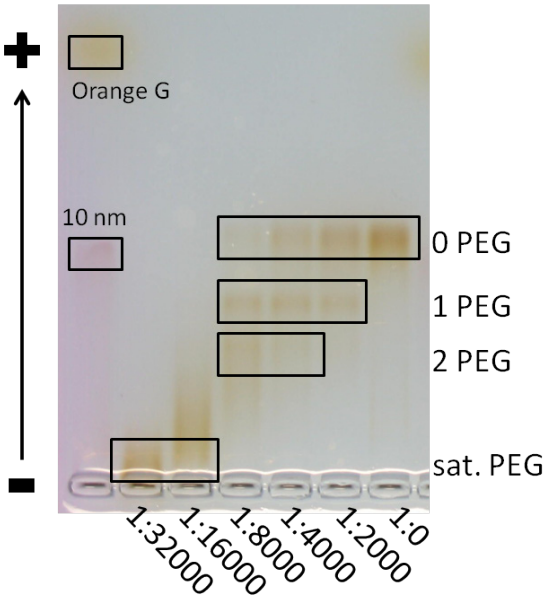

Figure 7: Result of a test-reaction of Ag NPs with 10 kDa PEG and different amounts of EDC. As reference 10 nm BBI Au NP and Orange G were used.

2.7 Surface modification of commercial gold nanoparticles

Commercial gold nanoparticles (Au NPs) from British BioCell (BBI) with a diameter of 5 nm were chosen for the following experiments. The particles are stabilized with citrate in the beginning. These commercial particles were chosen to show that the used methodologies are from general nature.

2.7.1 Ligand exchange with Phosphine

The ligand exchange with Bis(p-sulfonatophenyl)phenylphosphine dihydrate dipotassium salt (Phosphine) was done by simple stirring at room temperature. Therefore 10 mL of the nanoparticle suspension was mixed with 3 mg (5.6 µmol) of Phosphine. The mixture was stirred for 4 hours. Afterwards the particles were washed in a centrifuge filter (100 kDa MWCO) with water until the filtrate showed no yellow color. When the particles were washed and concentrated they were purified as described in Chapter 2.8. The exchange worked because the binding of the citrate molecules on the surface of the Au NP is less stable in comparison to the bond between the phosphor of the Phosphine and the gold atoms on the surface.

2.7.2 Ligand exchange with Polyethylene Glycol

For the exchange of the citrate molecules with Polyethylene Glycol (PEG) a 5 kDa MeO-PEG-SH was used. The thiol group was used to bind at the surface of the Au NP because of the strong thiol-gold binding. The ligand exchange was done as followed. A stock solution of the 5 kDa thiol-PEG (PEG-SH) with a concentration of 5 mM in water was prepared. The concentration of the particles was given from BBI[92]. The total surface of the particles was calculated and an amount of 50 PEG molecules per nm^2 was added. The mixture was stirred for 24 h at RT. Afterwards the particles were concentrated and washed with water in a centrifuge filter (100 kDa MWCO, 2500 rpm) until the filtrate showed no yellow color. When the particles were washed and concentrated they were purified as described in Chapter 2.8.

2.7.3 Phase transfer and polymer coating

To use the same methodologies for the commercial 5 nm sized Au NPs which were used for the synthesized Ag NPs (*cf.* Chapter 2.3) including the polymer coating (*cf.* Chapter 2.5) the Au NPs first have to be transferred to the organic phase. Therefore a solution of Tetraoctylammonium bromide (TOAB) in toluene with a concentration of 6.5 µM was prepared. A ratio of 2500 TOAB molecules per Au NP was set and the amount of the TOAB solution was placed together with the Au NP in a separation funnel. The mixture was shaken for 10 minutes. During this time the Au NPs move from the aqueous phase to the organic phase. The colorless aqueous phase was discarded and the organic phase was two times washed with water. Before the coating step could be done the TOAB had to be exchanged with dodecanethiol. The washed organic phase was reduced to 1/3 of its original volume. A ratio of 11 dodecanethiol molecules per TOAB molecule was set and the amount was added. The mixture was heated up to 65 °C and stirred for 4 hours. To remove the excess ligand molecules acetone (4 times the volume of the toluene) was added to the particle suspension. The suspension was placed into lockable glass vials and centrifuged for 5 minutes at 2000 rpm. The slightly yellow supernatant was discarded and the precipitated Au NPs were suspended in $CHCl_3$. The concentration of the Au NPs was measured *via* UV/Vis spectroscopy using the extinction coefficient from BBI. The coating step and the saturation of the Au NPs surface with 2 kDa PEG could be done as described in Chapter 2.5 and 2.6.

2.8 Purification and characterization

After their surface modification Ag NPs were purified from free chains or empty polymer micelles with two methodologies. After purification, they were characterized measuring their physical and optical properties.

2.8.1 Gel electrophoresis

The first purification step of the particles and/or clusters was the Gel electrophoresis. This was done in a 2% Agarose gel, using TBE (0.5x) as electrolyte buffer in a Bio Rad PowerPac Basic system. The gel was placed into the electrophoresis chamber and the chamber was filled with TBE buffer. Afterwards the sample was placed into a pocket in the gel. For keeping the sample inside the pocket it was mixed with 10% of a gel-loading-buffer consisting of 2/3 of glycerol and 1/3 of TBE to increase the density of the sample. An electric field of 10 $V \cdot cm^{-1}$ was applied and the particles started to move because of their surface charge. As an internal reference 10 nm commercial gold particles from BBI were used. These reference particles also had to undergo a ligand exchange with Phosphine as described in Chapter 2.7.1 but without the purification. The electric field was applied for one hour. The particles, excess polymer micelles or ligand molecules or free dye molecules moved through the gel. The different parts of the samples moved with different speed because of their surface charge, size and molecular weight (*cf.* Figure 8). A small, highly charged molecule like a free dye molecule moved fast, whereas bigger molecules with less charge per size, like excess polymer micelles, moved slower. Coated NPs, which are even bigger than polymer micelles because of the metallic core, were more retained. If these particles were modified with additional polymer at the surface, they lose charge and increase the size and weight and were even more retained. After one hour bands of the different parts of the sample (for example free dye, excess polymer micelles and coated NPs) were clearly separated inside the gel (*cf.* Chapter 3). The band, containing the NPs, was cut out of the gel and placed into a dialysis membrane (MWCO 50 kDa for Ag NPs or 10 kDa for Ag NCs). To extract the particles from the gel, the membrane was filled up with TBE buffer, locked and placed back into the electrophoresis chamber. The electric field was again applied for ca. 20 min (depending on the NPs) until the particles went out of the gel. Because of their size the particles could not pass through the membrane and were trapped inside the dialysis tube but out of the gel. The piece of gel inside the tube was removed and trashed. The particle suspension was washed with water and concentrated using a centrifuge filter for further purification and characterization.

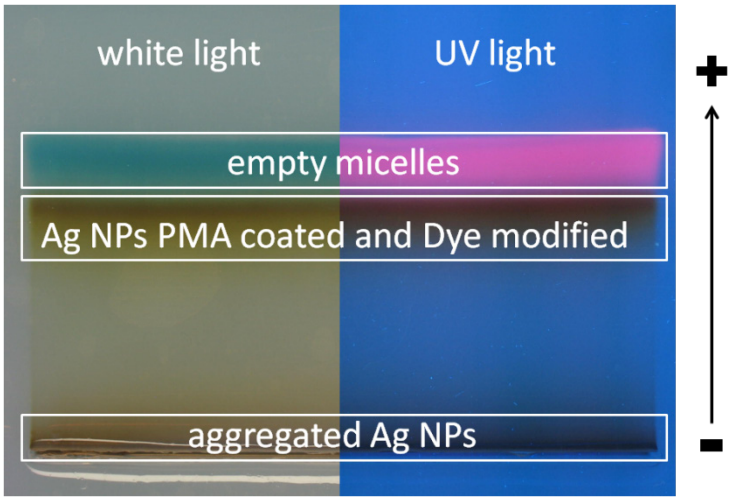

Figure 8: Example of a 2% Agarose gel after gel electrophoresis (1 h, 10 $V \cdot cm^{-1}$) of polymer coated Ag NPs modified with DY-636.

2.8.2 Size-exclusion chromatography

The second purification and characterization step for all the different particles and cluster was the size-exclusion chromatography (SEC) by using a high pressure liquid chromatography (HPLC) system. Therefore an Agilent Technologies 1100 Series with a column filled with GE Healthcare Sephacryl S-300HR was used. The system was run with a flow rate of 1 $mL \cdot min^{-1}$. Different solvents (like water, PBS, SBBS9) could be used for elution. The nanoparticles were separated from excess polymer, which were not removed during the gel electrophoresis by passing the column. The sample was detected by an absorbance detector and a fluorescence detector and finally collected with a fraction collector. Afterwards the cleaned sample was concentrated and washed with water in a centrifuge filter. When the sample was concentrated, it was clean and ready for further characterization.

2.8.3 Ultraviolet-visible spectroscopy and Fluorescence spectroscopy

To get Information about the absorption of the samples an Agilent Technologies 8453 UV-Vis spectrometer was used. If the extinction coefficient of the measured sample is known, the concentration of the sample could also be calculated *via* UV-Vis spectroscopy by using the Beer-Lambert law. For the commercial gold nanoparticles the extinction coefficient was given from the company[92]. For the Ag NPs the coefficient was calculated, see Chapter 3.2. For the measurement the sample was filled in a 1 cm pathway single using polystyrene cuvette. To measure only the absorbance of the particles a blank spectrum of the solvent was measured before and used as background.

For fluorescent samples also the fluorescence emission was measured. To measure the fluorescence of the samples the Horiba FluoroLog was used. The excitation and the emission were selected for each sample. The samples were placed in a three window glass cuvette for the measurements.

2.8.4 Dynamic light scattering and laser Doppler anemometry

For measuring the hydrodynamic diameter and the zeta-potential, the Malvern Zetasizer Nano ZS with a red laser (632.8 nm) as light source was used at 173° backscatter detection mode. All the samples were measured using polystyrene cuvettes and the settings which were set for the UMSICHT project. The settings for the size measurements were: Temperature 25 °C (15 minutes equilibration time); 10 measurements (60 seconds each measurement); fixed measurement position at 1.5 mm. zeta-potential measurements were performed using the Malvern Dip Cell Kit. For these measurements the same temperature and equilibration time were used but the other parameters were set to “auto”.

The colloidal stability of the samples was measured by measuring the hydrodynamic diameter at different concentrations of sodium chloride from 0 mM to 2.5 M. These measurements were repeated after 24 hours.

2.8.5 Transmission electron microscopy

For measuring the samples with transmission electron microscopy the Jeol JEM-3010 TEM was used. The preparation of the sample was done in two different ways. For samples in organic solvents 8 µl of the sample were placed at the copper grid and directly dried at RT. Samples in aqueous solvents were treated in a different way. The copper grid was placed in an upside down lid of a 40 ml lockable glass vial. 8 µl of the sample were placed at the grid and the vial was locked with the lid still upside down. Then the sample was kept in the dark like this for four days for the particles to settle down slowly. After three days the vial was opened a little bit that the water can evaporate over night.

3 Results and Discussion

This thesis represents a cumulative work and should demonstrate different synthetic methods of silver nanoparticles, their surface modification and the behavior of the particles after the modification in cell lines. The methods of stabilization and modification are general methods, which could also be used for other kinds of nanoparticles. Because of this, commercial gold nanoparticles were modified in a similar way to show, that similar results belong to the similar surface chemistry and that different results are due to the different core materials. To be sure that a certain property or a change in behavior of a particle is not random but due to a special feature of the particle or a certain change, which was made, the synthesis of defined particles with defined surface chemistry is important. Also the purity of the sample is of vital importance to be sure that the results belong to the particles and not any kind of impurity. In this chapter first the synthesis of the different silver particles will be shown and afterwards the different characteristics of the modified Ag and Au NPs. At the end of this chapter the effect of the different kinds of silver nanoparticles on two different cell lines will be shown. For the Ag NCs MCF-7 breast cancer cells and for the different modified Ag NPs NIH/3T3 fibroblast cells were used. The uptake and the cytotoxicity were considered. These experiments were performed and evaluated by Sherry Huang (Taipei, Taiwan) for the Ag NCs and Lena Kastl (Marburg) for the Ag NPs. The time resolved fluorescence measurements of the Ag NCs were performed and evaluated by Sebastian Friede (Marburg). The ICP measurements were done by Javier Jiménez-Lamana (Zaragoza, Spain).

3.1 Size controlled synthesis of Ag NCs and Ag NPs

3.1.1 Silver nanoclusters

With the above mentioned method (*cf.* Chapter 2.2) very small and fluorescent silver nanoparticles, so called silver nanoclusters (Ag NCs), could be produced. During the synthesis first big and not uniform particles were produced, which were etched down in a second step to smaller and more uniform particles. These particles were finally shrunk to almost 2 nm sized clusters, which were stable in aqueous media. As described, the size of the particles changed during the synthesis. This change was observed by taking TEM pictures of the different stages of the synthesis. These pictures and the corresponding size distribution are shown in figure 9. Before the etching of the particles the size distribution is very broad up to almost 30 nm. Afterwards the distribution is way smaller and the particles show a size of about 5 nm. But after the ligand exchange the final Ag NCs show a sharp distribution and a size of about 2 nm.

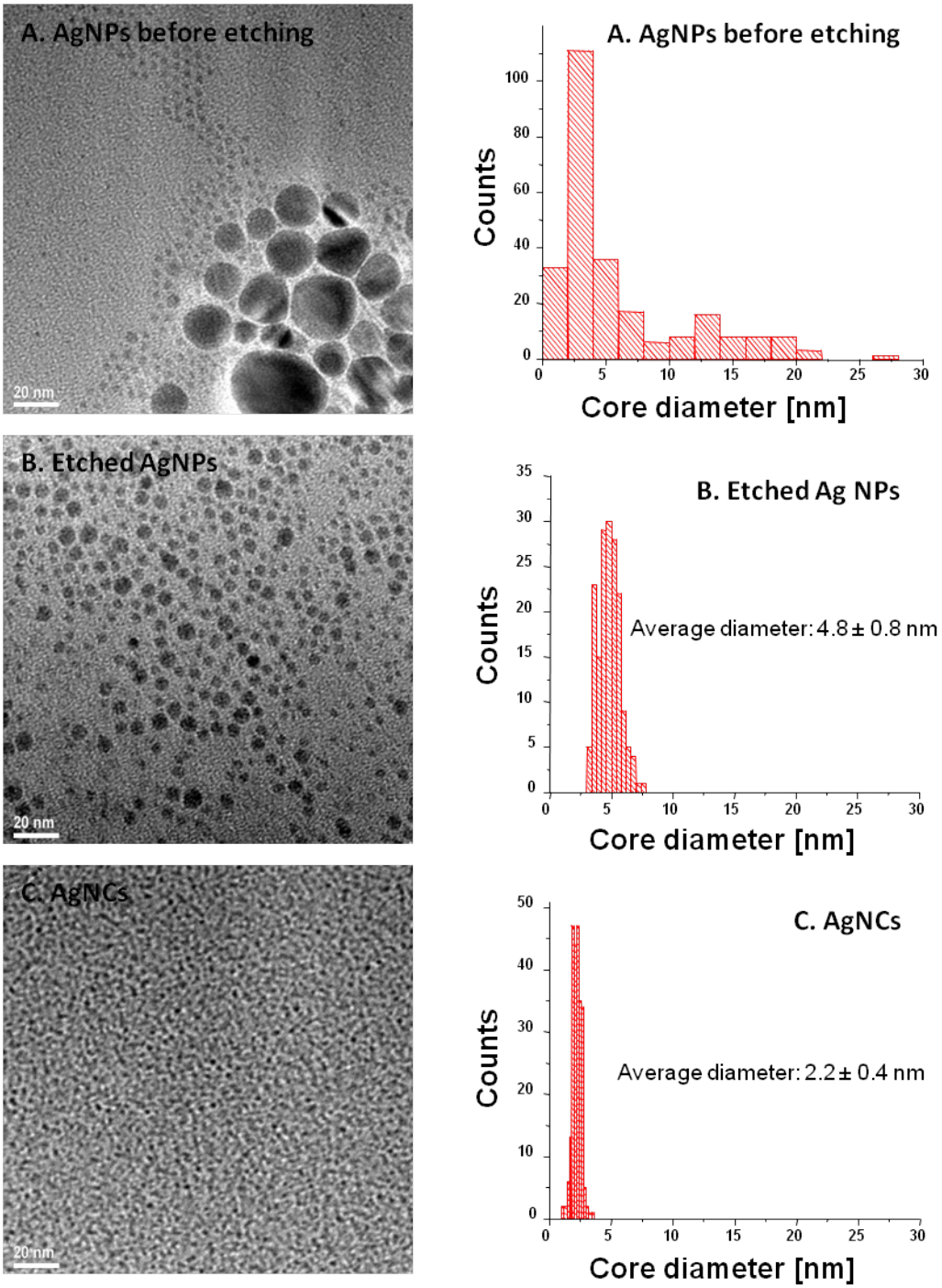

Figure 9: Tracing of the size distributions during the synthesis and after the ligand exchange. On the left side TEM pictures of the different states of the synthesis and on the right side the size distributions are shown. The scale bar of the TEM pictures corresponds to 20 nm.

A high resolution TEM picture and the fast Fourier transformation (FFT) of a small NC is shown in figure 10, in which the reflexes of the Ag {111} lattice planes can be seen. The image also displays a linescan along the NC. The fringe distance corresponds to Ag {111}.

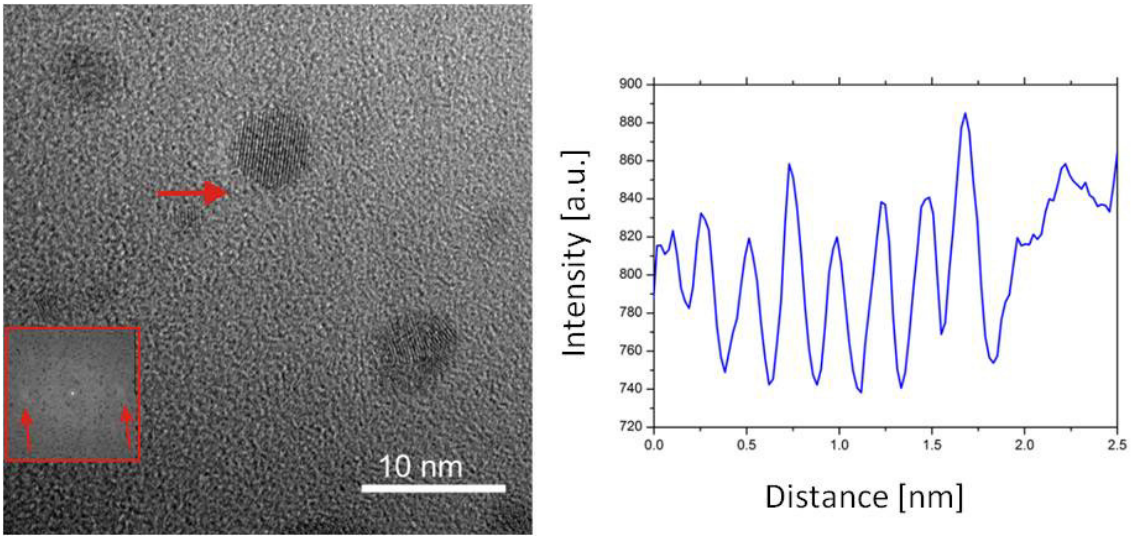

Figure 10: High resolution TEM picture of a mixture of Ag NPs after etching and Ag NCs. The images shows an overview, with the fast Fourier transformation of one small NC as inset. On the right a linescan across the NC (as indicated by the red arrow) is shown.

The Ag NCs also show a certain colloidal stability and could be purified and characterized by different methods. In Gel electrophoresis (1 h, 10 $V \cdot cm^{-1}$) they passed a 2% Agarose gel and showed a small band (figure 11). This band runs as fast as a reference dye (Orange G) and much faster than 10 nm commercial gold nanoparticles. This is a second proof of the small size of the clusters. The slight fluorescence of the clusters is already visible in the picture of the Agarose gel under UV light.

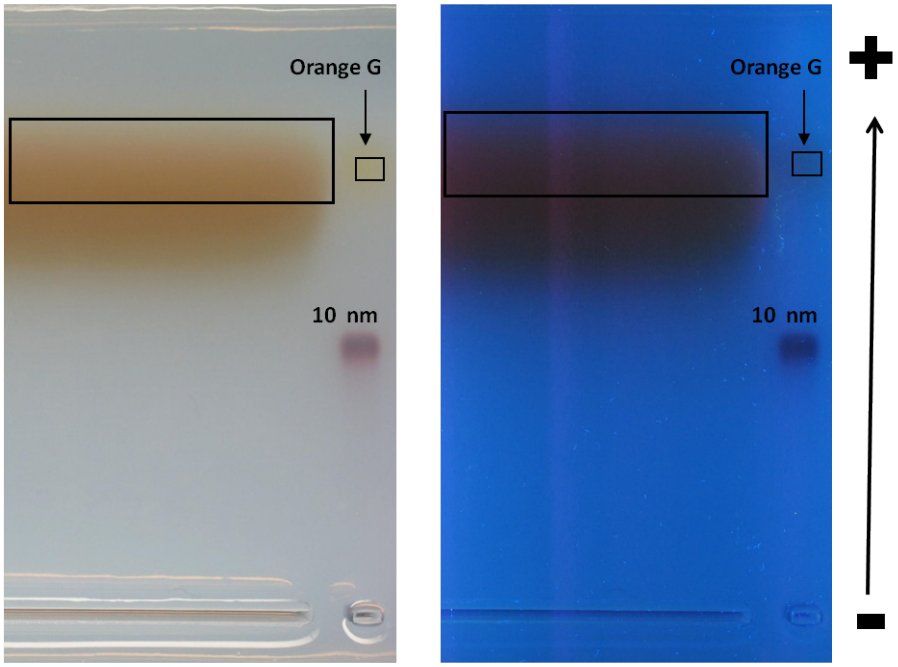

Figure 11: Pictures of the Ag NCs after gel electrophoresis (1 h, 10 Vcm^{-1}, 2% Agarose gel) under white (left) and UV light (right). The clusters run faster than the internal reference 10 nm Au NPs but as fast as the reference dye Orange G.

By purification *via* SEC the colloidal stability could be shown again and that the fluorescence belongs to the Ag NCs and not to any kind of impurity (figure 12). The fluorescence increases at the same time as the Ag NCs passes the detector (79-94 min) whereas no increase of the fluorescence is detected when a very small amount of impurity passed the detector after 50 min. The chromatogram shows also the narrow size distribution of the nanoclusters.

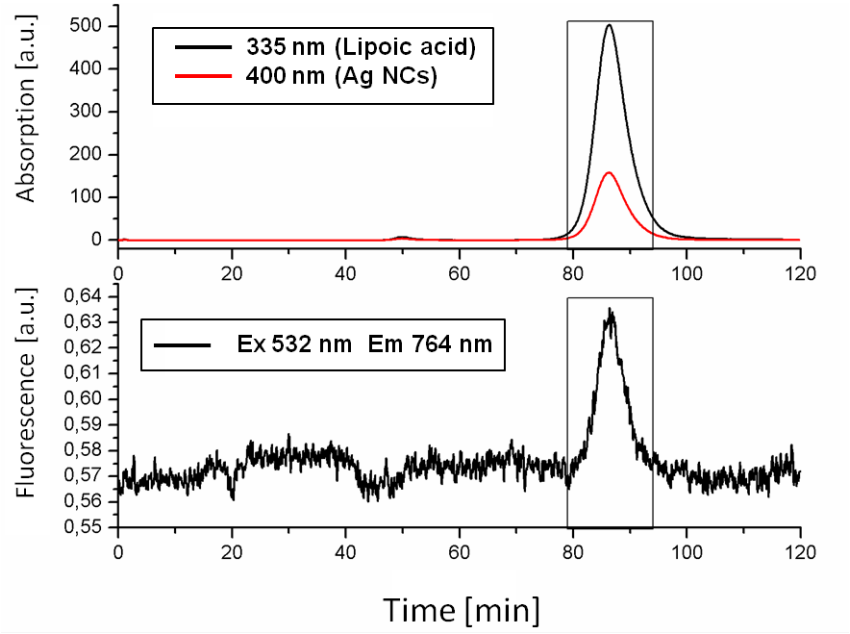

Figure 12: SEC chromatograms of the Ag NCs passing a column filled with Sephacryl S-300HR. A simultaneous increasing of the absorbance and the fluorescence from 79 to 94 minutes is shown which shows that the fluorescence belongs to the Ag NCs and not to any kind of impurity.

A short summary of the synthesis and how the particles look like is shown in figure 13. Further characterizations are shown in the following chapters.

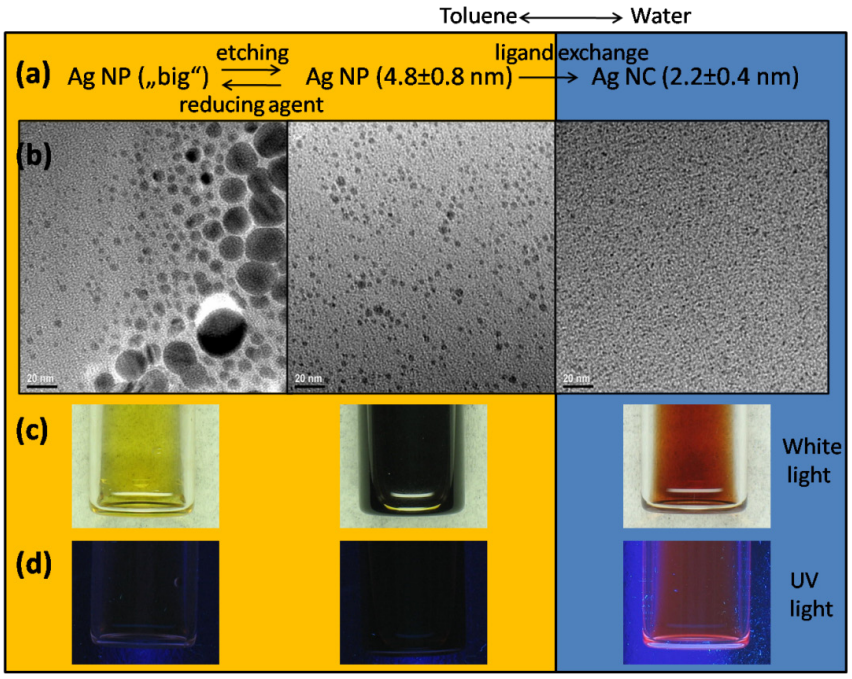

Figure 13: Summary of the Results of the Synthesis of the Ag NCs. (a) theoretical; (b) TEM; (c) with light; (d) UV light

3.1.2 Silver nanoparticles

Another type of Ag NPs was produced using the method mentioned in Chapter 2.3. Here just the TEM picture of the particles is shown. The other characterization results are shown in the following chapters. The size distribution of the dodecanethiol capped Ag NPs is sharp and shows a main size of 4.17 ± 0.44 nm.

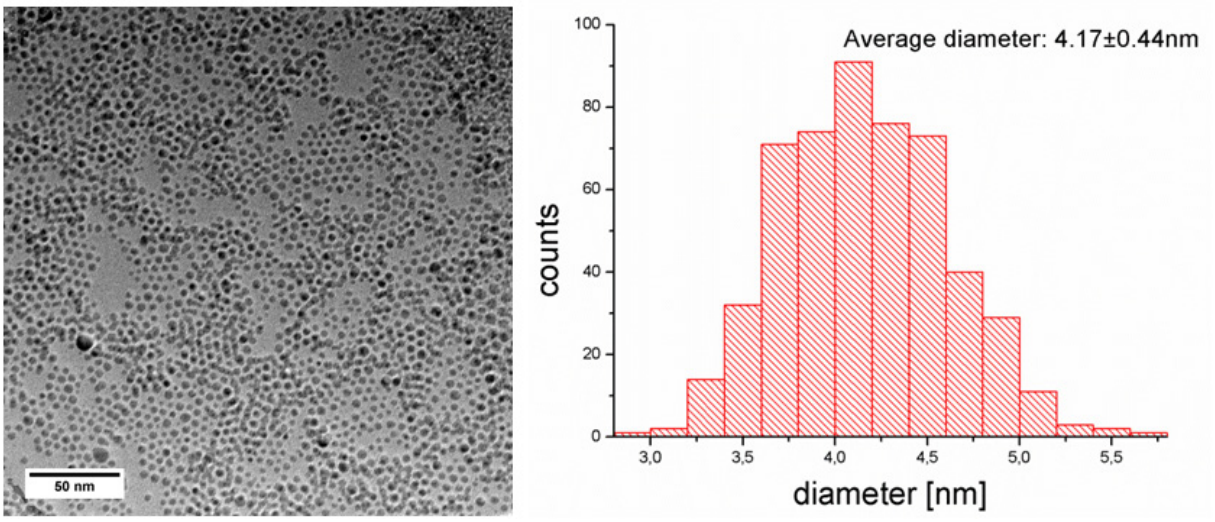

Figure 14: TEM picture of the Ag NPs (left) the scale bar corresponds to 50 nm; Histogram of the size distribution the average size is calculated to 4.17 nm.

3.2 Optical properties

3.2.1 Silver nanoclusters

The absorption of UV- and visible light of the Ag NCs changed during the synthesis, depending on the size and the quantity of the particles. At the beginning a slight plasmon peak at 420 nm was visible. This peak starts to increase during the etching process due to the bigger amount of uniform Ag NPs. At the end of the etching step the peak starts to decrease again due to the formation of small particles. After the ligand exchange the size of the particles shrank so much that the plasmon peak disappears so that the final clusters showed no peak.

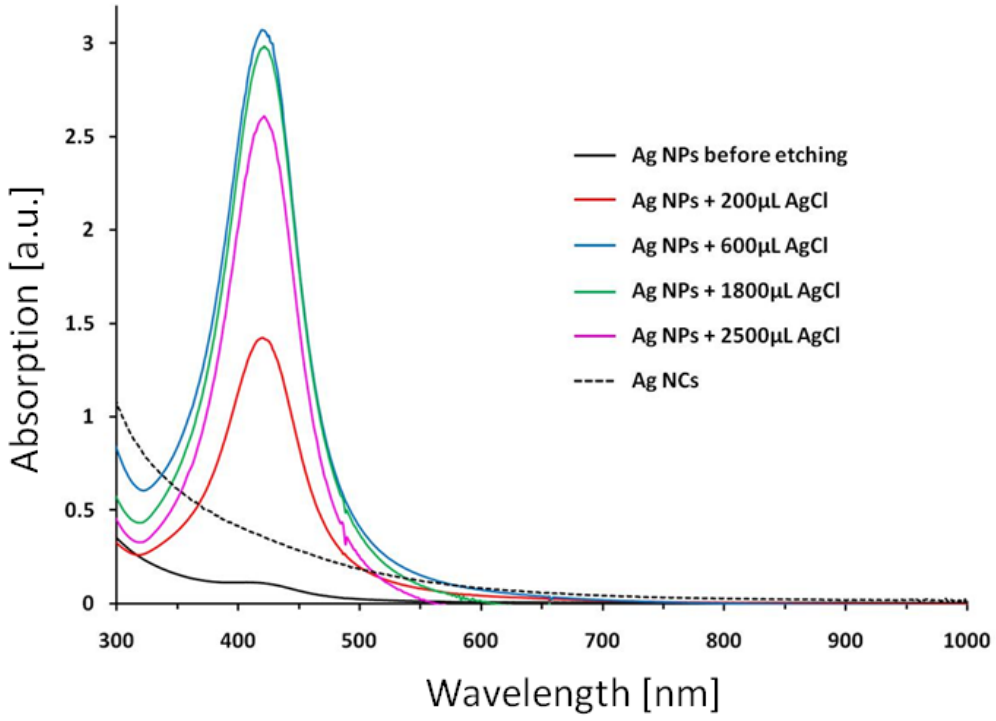

Figure 15: UV/Vis absorption spectra of the Ag NPs during the synthesis in toluene (straight lines) and of the Ag NCs after the ligand exchange in water (dashed line). The Ag NPs show the typical plasmon peak during the whole synthesis. First an increase of the peak is visible but with an increasing amount of the silver precursor the etching increases and the peak decreases. After the ligand exchange when the Ag NCs reached their final size (~2 nm) no plasmon peak is visible.

With the decreasing size the fluorescence of the Ag NCs comes along. The fluorescence is placed in the red spectral range and shows a broad maximum at 680 nm (figure 16). Although the quantum yield is quiet low with 0.024% calculated by the method of Lakowicz[93], using quinine sulfate in 0.1 M sulfuric acid as reference dye. The quantum yield was calculated by

$$Q = Q_R \frac{I}{I_R} \frac{OD_R}{OD} \frac{n^2}{n_R^2} \quad \text{(Eq. 2)},$$

with Q as quantum yield, I as integrated intensity, OD as the absorbance and n as the refractive index. The subscript R refers to the reference dye.

The long lifetime of the fluorescence decay up to 3 µs is typical for forbidden electronic transitions.

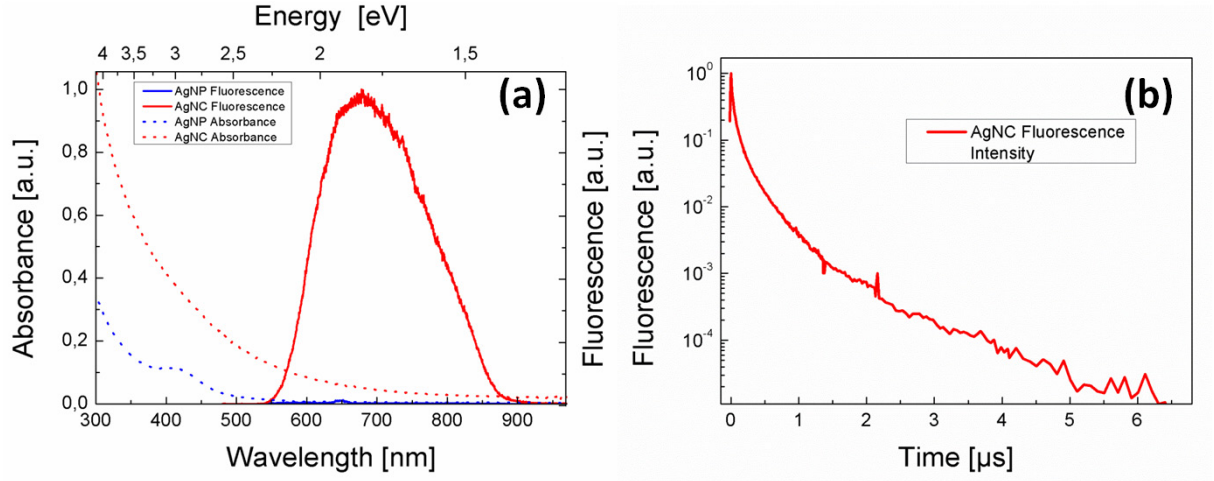

Figure 16: (a) Absorbance (dotted lines) and fluorescence (full lines) spectra of silver nanoparticles (Ag NP) and silver nanoclusters (Ag NC). (b) Transient of the Ag NC fluorescence.

3.2.2 Silver nanoparticles

The dodecanethiol capped Ag NPs show the typical plasmon peak at 430 nm. In the case that the polymer coated particles were modified with a dye (e.g. DY-636) to introduce fluorescence the absorption of the dye could also be clearly seen (figure 17).

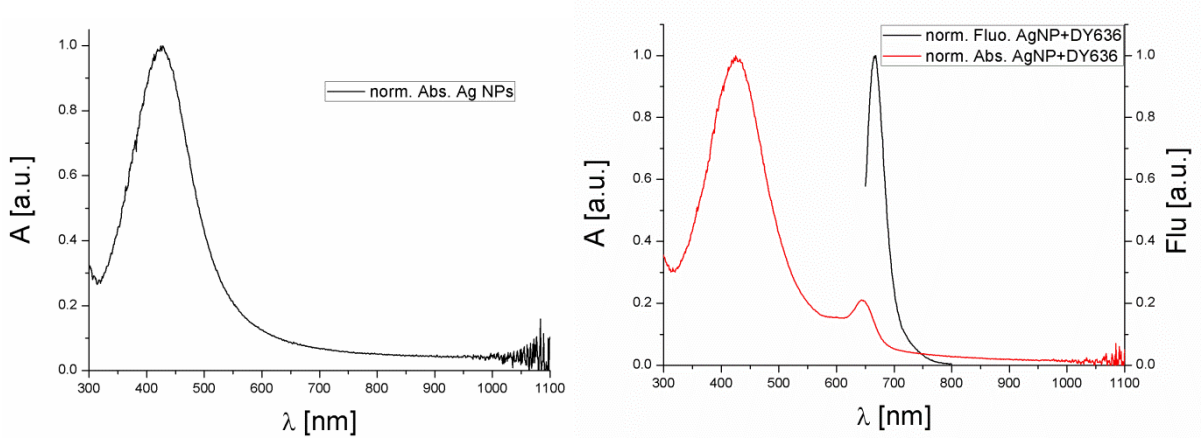

Figure 17: UV/Vis absorbance of the Ag NPs (left) and UV/Vis absorbance and Fluorescence of Ag NPs modified with DY-636.

To calculate the concentration of the Ag NPs via UV-Vis spectroscopy the molar extinction coefficient was experimentally determined to $\varepsilon = 16.9 \cdot 10^6\ M^{-1} \cdot cm^{-1}$. This was done by measuring the absorbance at 430 nm depending on the concentration in $mol \cdot L^{-1}$ of the Ag NP suspension with a cuvette of 1 cm pathlength. The slope of the linear fit gives the experimental extinction coefficient (figure 18). First the amount of silver c(Ag) $[kg \cdot L^{-1}]$ of a Ag NPs suspension was measured *via* ICP-MS and the absorbance of a dilution series was measured. The mass of a single core was calculated to be

$$m(Ag\ NP) = \rho_{Ag} \cdot V(Ag\ NP) = \rho_{Ag} \cdot \left(\frac{4\pi}{3}\right)\left(\frac{d_c}{2}\right)^3 = 3.99 \cdot 10^{-22} kg = 3.99 \cdot 10^{-16} mg \quad \text{(Eq. 3)},$$

based on the experimental determined diameter d_c = 4.17 nm and the density of bulk silver ρ_{Ag} = 10.49 g·cm^{-3}. The volume of a single core is V(Ag NP) = 38 nm^3. The concentration of the samples of the dilution series in mol·L^{-1} was then calculated by using Eq. 4 with N_A as Avogadro constant.

$$c(Ag\ NP)[mol \cdot L^{-1}] = \frac{c(Ag\ NP)[kg \cdot L^{-1}]}{m(Ag\ NP)[kg]} / N_A[mol^{-1}] \quad \text{(Eq. 4)}$$

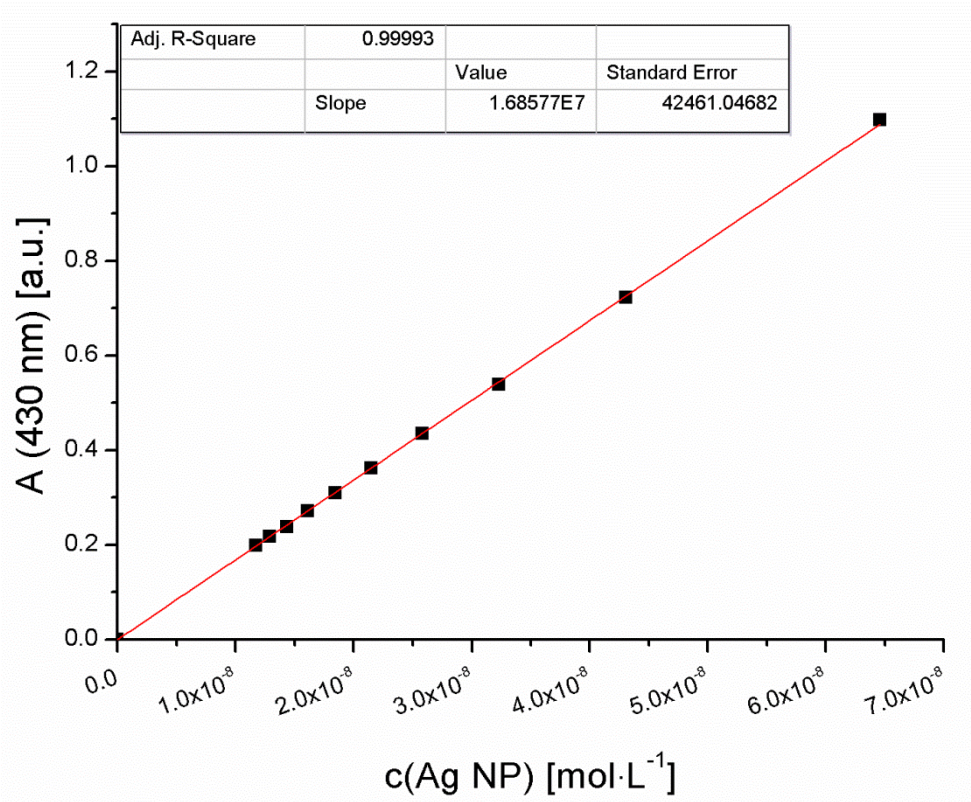

Figure 18: Plot of the absorbance at 430 nm versus the concentration of dilution series. The slope gives the experimental extinction coefficient.

3.2.2 Commercial Au NPs

The commercial Au NPs show the typical plasmon peak for 5 nm sized particles at 520 nm. This peak is independent from the ligand which is at the surface of the particle for stabilizing the particle. Like the absorption of the dye in the case of the Ag NPs belong additional absorption peaks to the stabilizing ligand molecules like citrate.

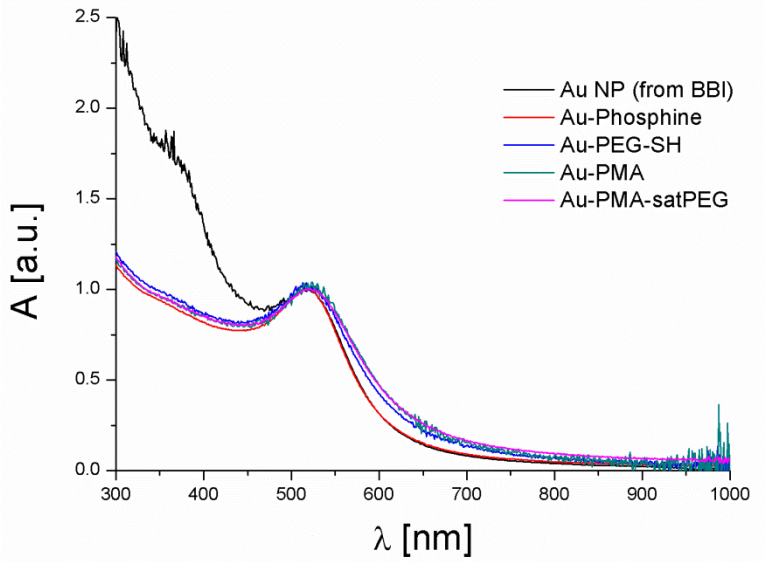

Figure 19: UV/Vis spectra of all the modified commercial gold nanoparticles and the original particles. All the samples were normalized at the typical plasmon peak at 520 nm. The citrate stabilized particles from BBI show additional absorption at ca. 370 nm depending to the citrate.

3.3 Surface modifications

3.3.1 Modification of Ag NPs

The Ag NPs, which were capped by dodecanethiol after synthesis, were modified in two different ways to make them colloidal stable in aqueous solutions. The first way was to exchange the hydrophobic dodecanethiol with a hydrophilic molecule like 11-mercaptoundecanoic acid (MUA) (*cf.* Chapter 2.4). The advantage of this method is that it is fast and also additional modifications *via* EDC chemistry are possible. The disadvantage is that the molecules can be replaced by other molecules decreasing the particle stability and even leading to particle aggregation (*cf.* Chapter 3.4). The other method to transfer the hydrophobic particles into aqueous phase is to wrap an amphiphilic polymer around the particle. Here a modified poly-isobutylene-alt-maleic anhydride (PMA) was used. This polymer is already known in literature[49,59] and has the advantage that it can easily be modified after the coating process *via* EDC chemistry (*cf.* Chapter 2.5 + 2.6). Another advantage of this method is that the coating is very stable at the surface and could not be removed in an easy way from other molecules or ions (*cf.* Chapter 3.4).

With these two methods four samples of particles were synthesized with different surface chemistry. The first was the as described Ag-MUA NPs (figure 20A). The second were Ag-PMA NPs without any further modification (figure 20B). The third sample was the Ag-PMA particles with one additional 10 kDa PEG at the surface (Ag-PMA-1PEG NPs) (figure 20C). For the fourth sample the surface of the Ag-PMA NPs were saturated with 10 kDa PEG molecules (Ag-PMA-satPEG NPs) (figure 20D). The addition of PEG at the surface of the particles should lead to a reduced uptake in the cell experiments.

Due to the different surface modifications the particles behave differently. To assess their different properties, these particles were characterized by different techniques. A first example is their behavior in gel electrophoresis (figure 20). Here the Ag-MUA NPs run the fastest because of their small size, weight and high surface charge. The Ag-PMA NPs run a little bit slower because of the bigger weight. The zeta-potential and the hydrodynamic diameter of both particle types are in the same range (*cf.* Chapter 3.4.1) and although the Ag-MUA NPs show a smaller zeta-potential their faster movement through the Agarose gel is due to the different weight. These two samples show faster movement than the 10 nm reference Au NPs. The behavior of the other two types of particles is also due to their bigger weight and in case of the Ag-PMA-satPEG NPs even due to the smallest zeta-potential (*cf.* Chapter 3.4.1).

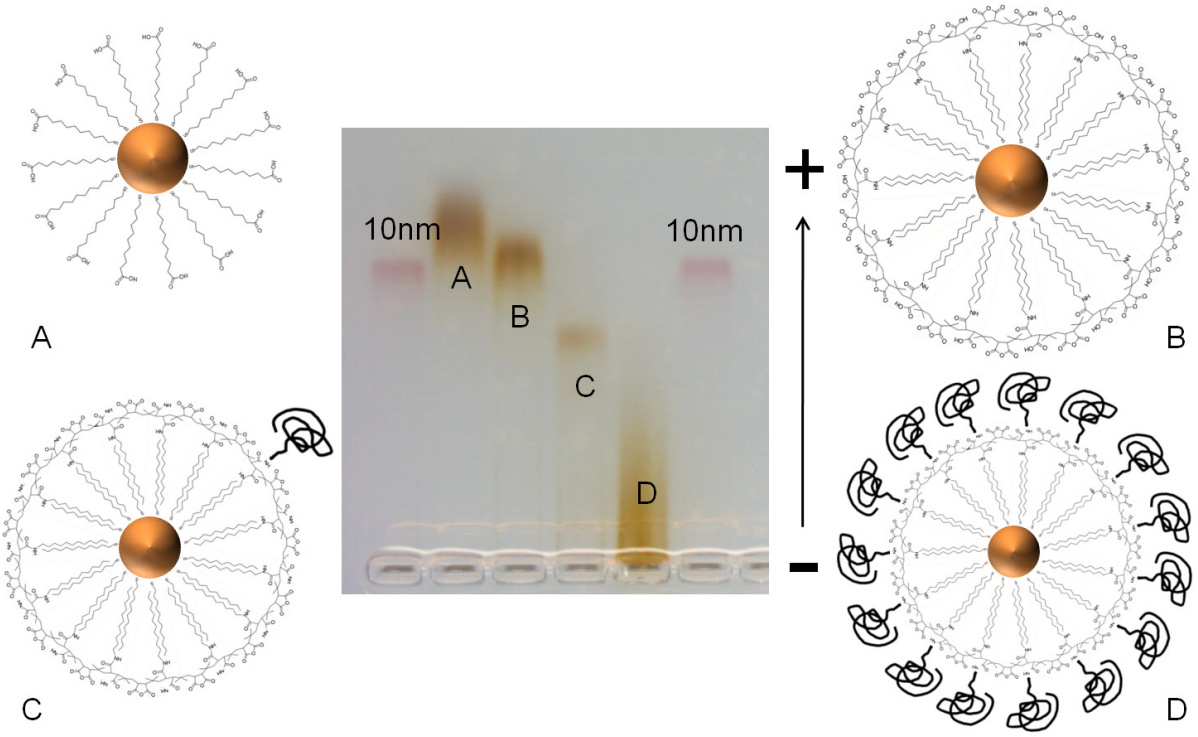

Figure 20: Picture of the 2% Agarose gel after one hour of gel electrophoresis with 10 V·cm^{-1} of the four different Ag NPs and the internal reference 10 nm Au NPs. Next to the picture sketches of the different modified particles are shown (A: Ag-MUA NPs; B:Ag-PMA NPs; C: Ag-PMA-1PEG NPs; D: Ag-PMA-satPEG NPs).

The result of the characterization/purification of the different particles by SEC confirmed the result of the gel electrophoresis. Here, the Ag-PMA-satPEG NPs passed the separation column and showed the lowest retention time because of their bigger size and weight. The next sample was the Ag-PMA-1PEG NPs. The Ag-PMA and the Ag-MUA NPs show again a similar result but like in the gel the Ag-MUA particles show again the smaller size (figure 21), which leads to the highest retention time.

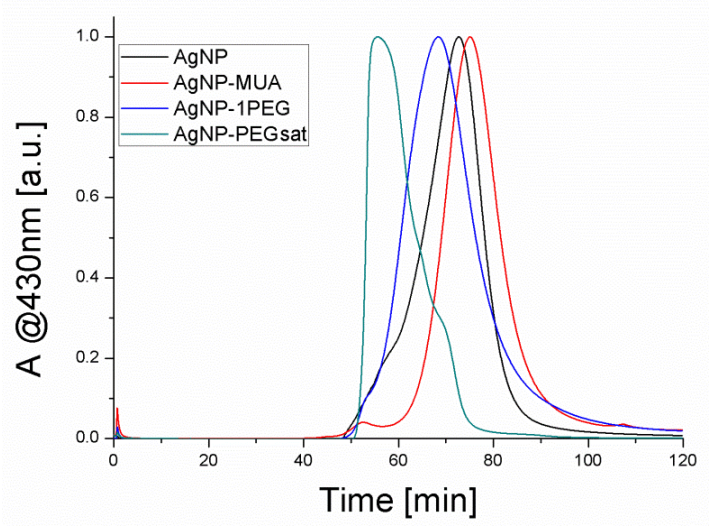

Figure 21: SEC chromatogram of the four different modified Ag NPs (1 ml·min^{-1}, PBS).

3.3.2 Modification of commercial Au NPs

To show that the modifications are general methods also commercial Au NPs from British Biocell International (BBI) were modified (*cf.* Chapter 2.7). The original coating of the Au NPs was done by citrate molecules (Au-citrate). Four other modifications were done starting from the original stock. Two samples were modified by simple ligand molecule exchange (Au-Phosphine and Au-PEG-SH, figure 22A+B). The other two samples were coated with the modified PMA and the surface of one of these was saturated with 2 kDa PEG (Au-PMA, Au-PMA-satPEG, figure 22C+D).

To compare/purify the five different samples they were run in gel electrophoresis. The original, citrate stabilized Au NPs stuck in the Agarose gel, that is why in figure 22 only four different samples are shown. The Au-Phosphine and the Au-PMA NPs run faster or as fast the reference 10 nm Au NPs. The Au-PEG-SH and the Au-PMA-satPEG NPs show the expected retardation. The fact that the Au-PEG-SH NPs run to the negative pole although the zeta-potential is negative (*cf.* Chapter 3.4.1) is due that the gel electrophoresis is done in TBE buffer (pH 8). It is possible that the PEG molecules at the surface of the particles catch ions from the buffer and so change the surface charge of the particle.

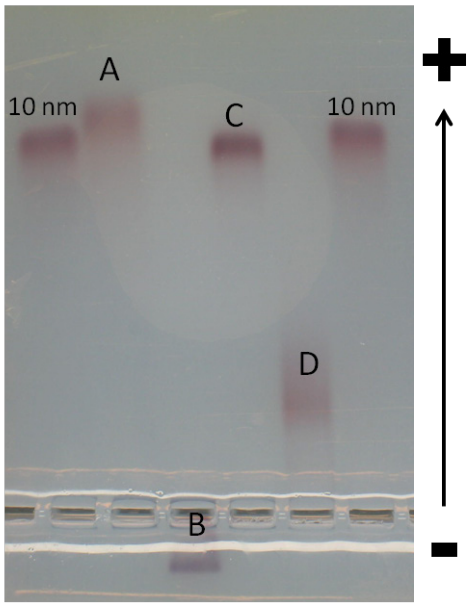

Figure 22: Picture of the 2% Agarose gel after one hour of gel electrophoresis (10 V·cm^{-1}) of four of the different modified commercial gold particles as internal reference 10 nm Au particles from BBI were used. (A) Bis(p-sulfonatophenyl)phenylphosphine dihydrate dipotassium salt (Phosphine) modified Au NPs (Au-Phosphine), (B) Au NPs modified with 5 kDa PEG-SH (Au-PEG-SH), (C) Au NPs coated with PMA (Au-PMA) and (D) Au NPs coated with PMA and saturated with 2 kDa PEG-NH_2 (Au-PMA-satPEG). The original citrate stabilized Au NPs from BBI did not run through the gel.

The stability from two of the five different Au samples was even too weak to purify the particles by SEC (figure 23). The original particles and the Au-Phosphine particles stuck in the column and could not purified/characterized in this way. The results of the other three samples were as expected. The Au-PMA-satPEG NPs showed the biggest size. The Au-PEG-SH particles showed the smallest size.

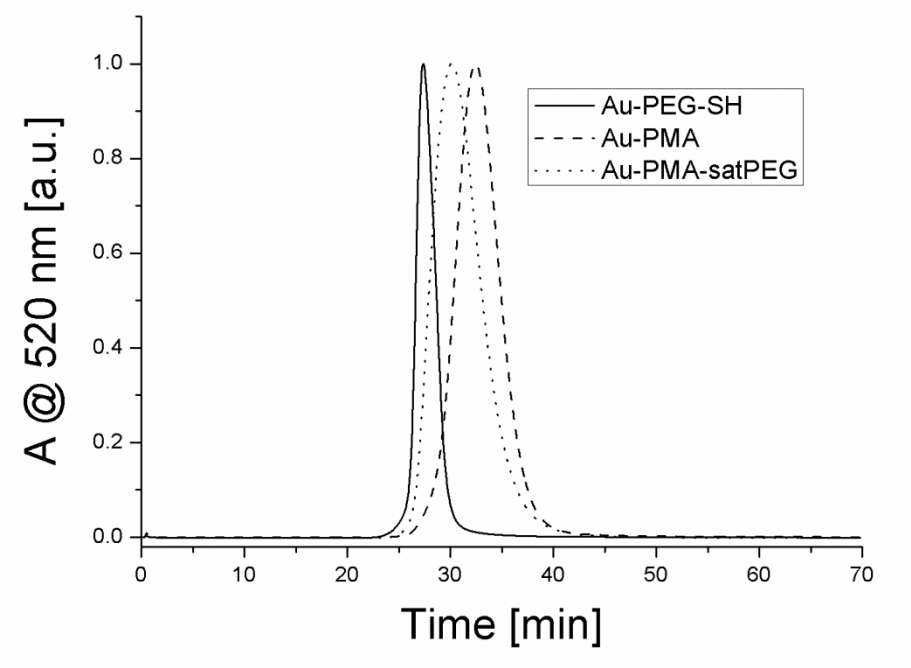

Figure 23: SEC chromatogram of three of the modified Au NPs (1 mL·min^{-1}, PBS). The original citrate stabilized particles and the Phosphine modified once did not pass the column.

3.4 Colloidal stability

3.4.1 Hydrodynamic diameter and zeta-potential

All the synthesized particles were characterized by dynamic light scattering (DLS) for measuring the hydrodynamic diameter and by laser Doppler anemometry (LDA) for measuring the zeta-potential. The Ag NCs showed the smallest hydrodynamic diameter in comparison to the other Ag NPs, which confirmed the TEM results. The hydrodynamic diameter of the Ag NCs was measured to 2.7 ± 0.4 nm and zeta-potential to -30 ± 2 mV. This value was in the same range than the Ag-PMA and also the Au-PMA particles but these particles showed a three to four times greater hydrodynamic diameter (Table 1 + 2).

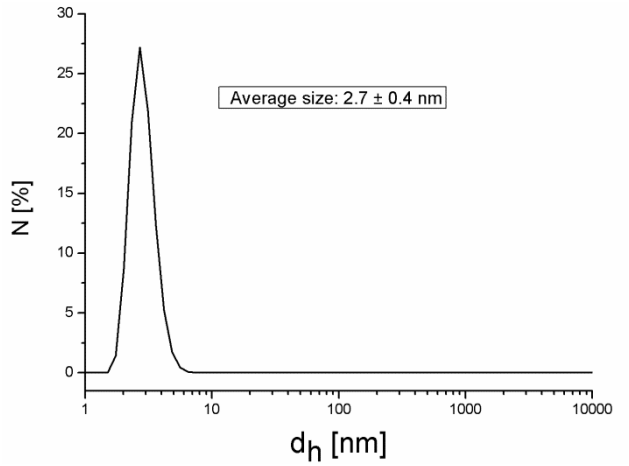

Figure 24: Hydrodynamic diameter of the Ag NCs measured in SBB9 measured by DLS. The zeta-potential was measured to -30 ± 2 mV.

The hydrodynamic diameters of the four different Ag NPs samples were in the same range. This was somehow surprising because for the Ag-PMA-satPEG NPs a much higher value were expected because of the results of the gel electrophoresis and the SEC. One possible explanation for this is that the flexible PEG molecules were wrapped around the particles because of the surface charge of the polymer. This wrapping of the polymer around the particle is also possible for the Ag-PMA-1PEG NPs. One point to support this statement was the low zeta-potential of the Ag-PMA-satPEG NPs. The higher zeta-potential of the Ag-PMA-satPEG NPs was a sign that the stability of these particles belong to steric repulsion. The three other samples showed a lower zeta-potential and this was a sign that the stability of these particles was due to electrostatic repulsion.

Sample	d_h [nm]	ζ [mV]
Ag-MUA	11 ± 4	-24.9 ± 1.7
Ag-PMA	12 ± 3	-31.0 ± 1.3
Ag-PMA-1PEG	13 ± 4	-41.1 ± 1.5
Ag-PMA-satPEG	12 ± 3	-10.9 ± 0.4

Table 1: Hydrodynamic diameter d_h and zeta-potential ζ of Ag NPs with different surface coating, with a core diameter of d_c = 4.2 nm.

The results of the measurements of the different Au NPs showed the expected results. The original and the Au-Phosphine NPs showed the smallest hydrodynamic diameter. Also the size of the Au-PEG-SH particles was in the expected range. Here a wrapping of the PEG molecules around the particle was not expected because of the gold-thiol bond. This bond is so stable[94] that a "wrapped polymer" will be removed from other molecules to enter the gold-thiol bond. The results of the Au-PMA NPs were in the same range like the Ag-PMA NPs. One possible explanation for the fact that the hydrodynamic diameter of the Au-PMA-satPEG was bigger than the one of the Ag-PMA-satPEG NPs was that smaller PEG molecules were used to saturate the surface (Au: 2 kDa PEG; Ag: 10 kDa PEG) and because of this more molecules could be linked to the surface.

Sample	d_h [nm]	ζ [mV]
Au-citrate	7 ± 2	-19.0 ± 2.5
Au-Phosphine	6 ± 2	-51.0 ± 4.8
Au-PEG-SH	22 ± 6	-44.5 ± 7.7
Au-PMA	10 ± 3	-33.0 ± 6.4
Au-PMA-satPEG	19 ± 5	-25.3 ± 2.4

Table 2: Hydrodynamic diameter d_h and zeta-potential ζ of commercial Au NPs with different surface coating, with a core diameter of d_c = 5 nm.

3.4.2 Dissolving behavior of the Ag NPs

Because of the cytotoxic effect of the Ag NPs their dissolving behavior, releasing silver cations, under different pH values was a critical factor. The released Ag^+ ions were measured *via* ICP-MS at different times and under two different pH values. First, a pH value of 7 (pure water) was chosen and second a value of pH 3, which is even 2 pH units less than in the late endosome[95,96]. This was done by separating the solid Ag NPs from the released Ag^+ ions by ultrafiltration, using 3 kDa MWCO filters with a speed of 9000 rpm for 15 minutes. The detection limit of the ICP-MS was measured and calculated to 0.0015% of the used Ag^+ ions. For this purpose the attainable dilution limit of a standard solution, which gives a signal 10 times the standard deviation of a blank sample, was measured.

At the beginning the total amount of silver in the different samples were measured ($c_{tot}(Ag)$). Then an aliquot of each sample was taken and the dissolved silver was separated from the Ag NPs by ultrafiltration, described above. The dissolved silver cations were quantified ($c(Ag^+)$) *via* ICP-MS and the amount of released silver was calculated by calculating $c(Ag^+)/c_{tot}(Ag)$. This was done at day 0, day 7 and day 14 for neutral conditions and at day 0 and day 7 for acidic conditions. Under neutral conditions even after 14 days the Ag particles were stable. A release of silver cations could just been measured in one sample. Even this value was very low, around 0.1%. This showed again the good stability of the different Ag NPs. Under acidic conditions (pH 3) the release of Ag^+ ions should be increased and could been measured. After one day all three samples released silver cations. The measured values were between 0.7 and less than 1.2%. These values increased just a little bit after 7 days under the acidic conditions up to 0.73 und less than 1.4%. Even under these extreme conditions the Ag NPs show a good stability.

Sample	released Ag (water): $c(Ag^+)/c_{tot}(Ag)$ [%]		
	day 0	day 7	day 14
Ag-MUA	< 0.0015	< 0.0015	< 0.0015
Ag-PMA	< 0.0015	< 0.0015	0.146 ± 0.001
Ag-PMA-satPEG	< 0.0015	< 0.0015	< 0.0015

Sample	released Ag (pH 3): $c(Ag^+)/c_{tot}(Ag)$ [%]	
	day 1	day 7
Ag-MUA	0.781 ± 0.002	1.316 ± 0.002
Ag-PMA	1.120 ± 0.004	1.390 ± 0.003
Ag-PMA-satPEG	0.701 ± 0.001	0.735 ± 0.001

Table 3: The amount of released Ag^+ ions $c(Ag^+)/c_{tot}(Ag)$, in dependence on their exposure to water or acidic solution. At day 0 all residual Ag^+ had been removed by ultrafiltration.

3.4.3 Stability of Ag NPs under different sodium chloride concentrations

For using the Ag NPs in cells it is important that the particles keep the colloidal stability with high salt concentrations over a longer time period. Therefore the hydrodynamic diameters of the different modified particles were measured first directly after adding the salt and a second time after 24 h. The results are shown in figures 25 and 26.

The Ag-MUA particles differ in the behavior to the other three modified particles. Only the Ag-MUA NPs show an increasing hydrodynamic diameter with an increasing salt concentration. Additionally these particles aggregated and precipitated after 24 h with a NaCl concentration higher than 160 mM. The hydrodynamic diameters of the other three samples kept constant for 24 h even at very high salt concentrations up to 2.5 M.

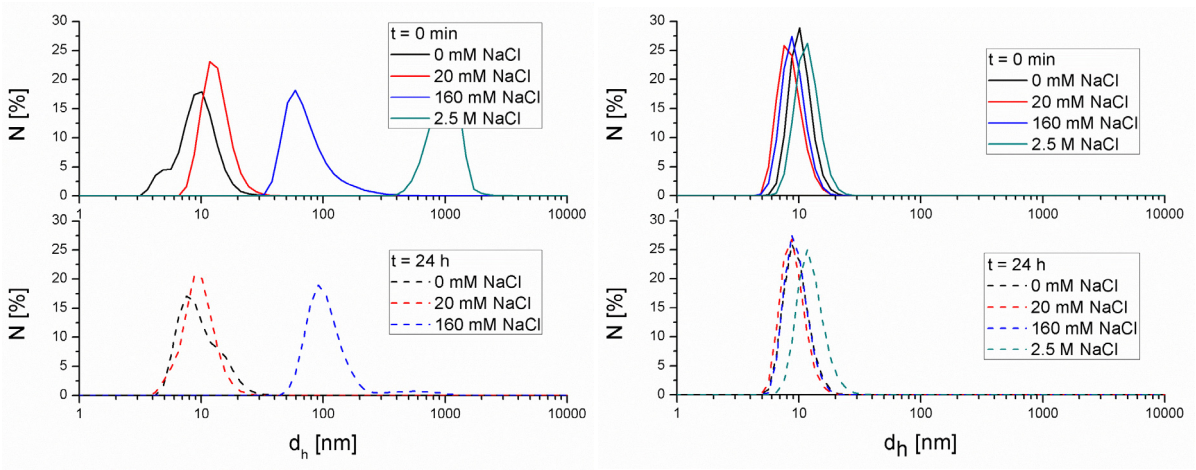

Figure 25: Selected results of DLS measurements for stability test of Ag-MUA (left) and Ag-PMA (right) NPs vs. NaCl from 0 mM slat to 2.5 M salt concentration. The results directly after mixing is shown in straight lines and the results after 24 h in dashed lines. The Ag-MUA NPs kept constant up to 160 mM of salt and aggregated at higher concentrations. The Ag-PMA NPs kept constant up to a concentration of salt of 2.5 M.

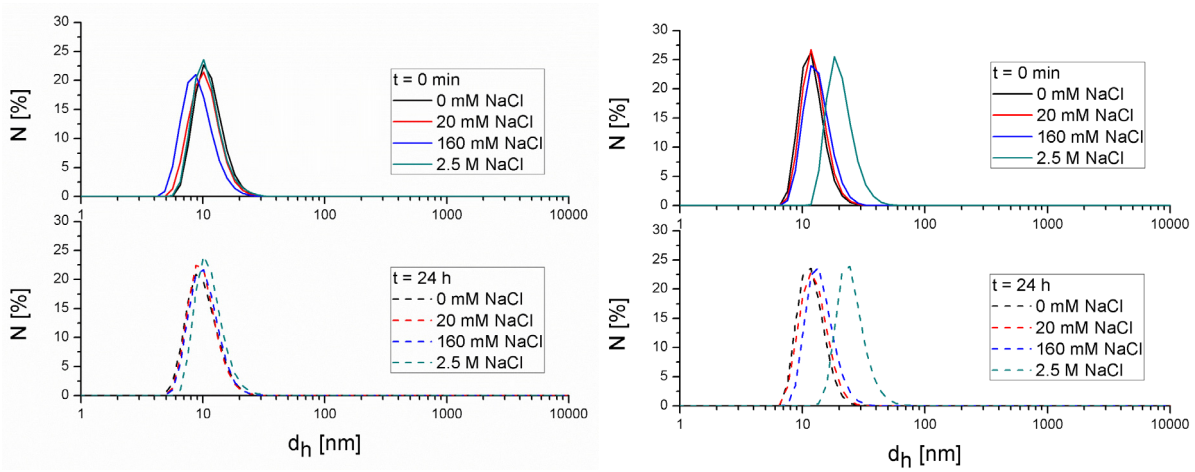

Figure 26: Selected results of DLS measurements for stability test of Ag-PMA-1PEG (left) and Ag-PMA-satPEG (right) NPs vs. NaCl from 0 mM salt to 2.5 M salt concentration. The results directly after mixing is shown in straight lines and the results after 24 h in dashed lines. Both types of Ag NPs kept constant up to a concentration of 2.5 M of salt.

The hydrodynamic diameters of the four Ag NP samples with different salt concentrations directly after addition of the salt are shown in figure 27. Some concrete values including the standard deviations of the above measurements are shown in table 4. It is clearly shown that the hydrodynamic diameter of the Ag-MUA NPs increases to more than 1000 nm by salt concentrations higher than 625 mM.

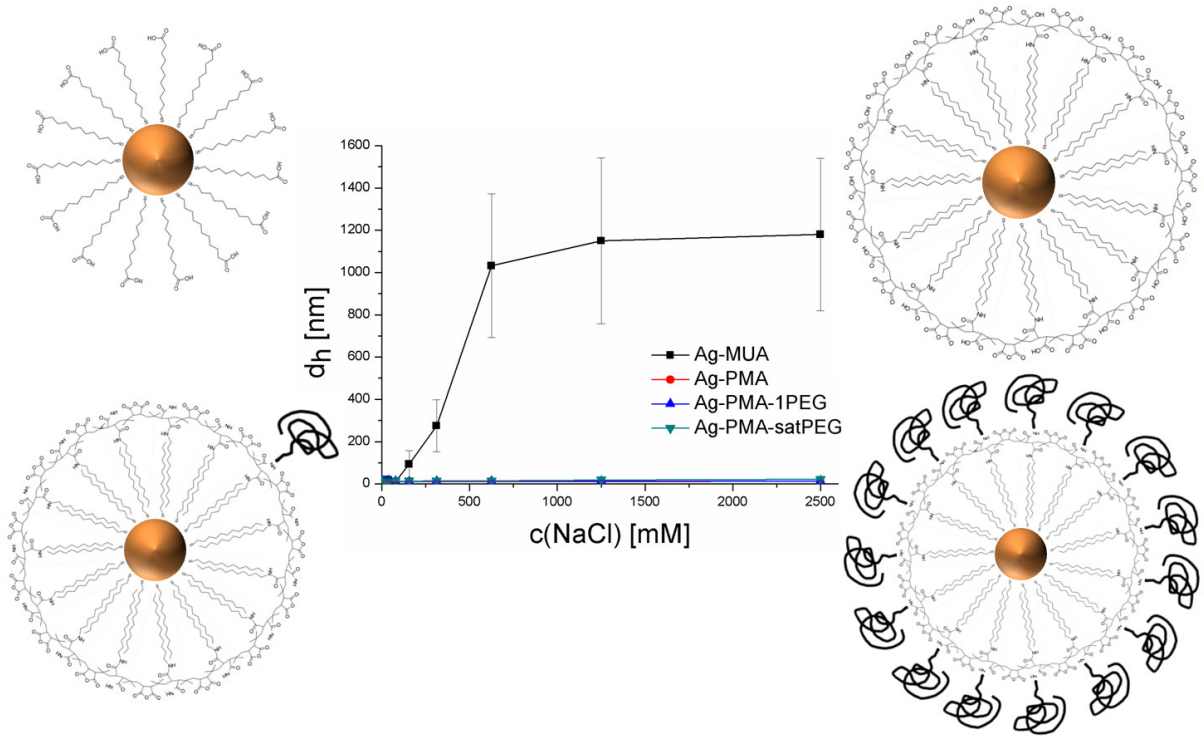

Figure 27: Sketches of the four different modified particles and summary of the hydrodynamic diameter of the different modified Ag NPs vs. NaCl directly after addition of the salt. Only the Ag-MUA particles show an increasing diameter with higher salt concentrations. The other three samples keep the same diameter up to 2.5 M.

t = 0 h

c(NaCl)	0 mM	20 mM	160 mM	2.5 M
Ag-MUA	11.23±4.4nm	13.54±4.2nm	93.48±63.9nm	1180±361nm
Ag-PMA	12.04±2.7nm	9.97±2.4nm	10.60±2.4nm	13.77±3.3nm
Ag-PMA-1PEG	13.22±3.8nm	12.36±3.8nm	10.87±3.5nm	12.88±3.9nm
Ag-PMA-satPEG	12.16±3.0nm	12.68±3.2nm	13.49±3.6nm	20.84±5.9nm

t = 24 h

c(NaCl)	0 mM	20 mM	160 mM	2.5 M
Ag-MUA	11.91±5.2nm	11.46±3.9nm	122.3±42.1nm	$\rightarrow\infty$
Ag-PMA	11.27±2.8nm	10.52±2.5nm	11.19±2.6nm	14.82±4.1nm
Ag-PMA-1PEG	11.87±3.7nm	11.87±3.5nm	12.19±3.6nm	13.43±3.9nm
Ag-PMA-satPEG	12.09±3.2nm	12.67±3.4nm	14.26±3.9nm	25.64±7.6nm

Table 4: Summary of mean hydrodynamic diameters d_h and their corresponding standard deviation, as derived from the data presented in Figures 23 + 24.

3.4.4 Commercial gold nanoparticles vs. NaCl

The stability of commercial Au NPs against NaCl was also measured with different modifications. The results directly after the addition of the salt and after 24 h are shown in figure 28 - 30. The Au NPs without modification (Au-citrate) showed the worst stability. By increasing the salt concentration above 40 mM, the hydrodynamic diameter started to increase up to almost 900 nm with a concentration of 2.5 M salt. After 24 hours all the particles with a concentration higher than 80 mM were aggregated.

The Au-Phosphine particles behaved similar. Here the hydrodynamic diameter also started to increase by increasing the salt concentration to more than 160 mM up to 700 nm with a concentration of 2.5 M. The particles with concentrations higher than 625 mM were aggregated after 24 h.

The Au NPs stabilized by PEG-SH or PMA coating and additional PEG modification did not show any increase of the hydrodynamic diameter up to a salt concentration of 2.5 M and were also stable for at least 24 hours.

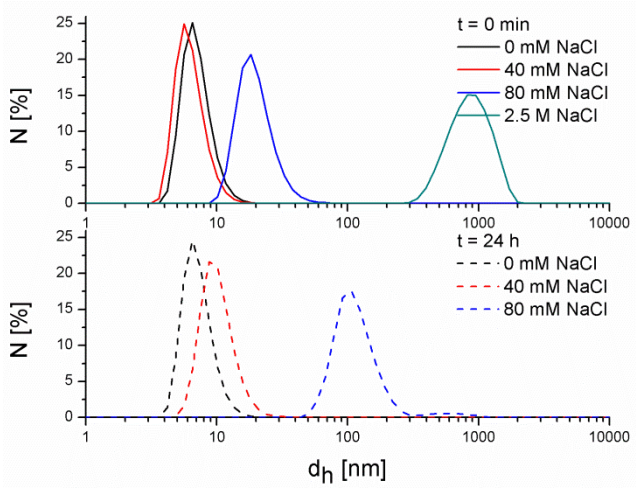

Figure 28: Selected results of DLS measurements for stability test of Au-citrate NPs vs. NaCl from 0 mM slat to 2.5 M salt concentration. The results directly after mixing is shown in straight lines and the results after 24 h in dashed lines. All the samples containing salt showed an increased diameter after 24 h and samples with more than 80 mM salt were aggregated and precipitated.

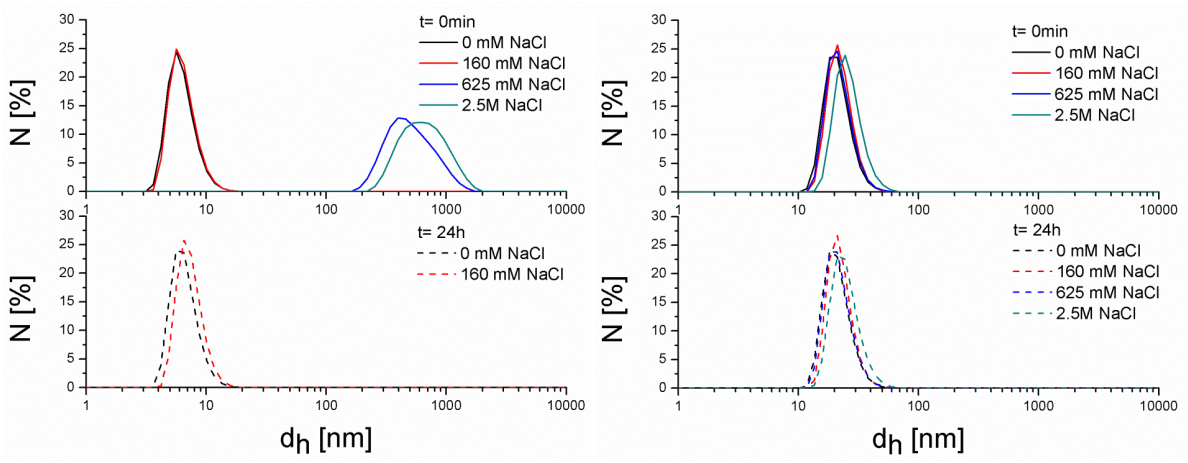

Figure 29: Selected results of DLS measurements for stability test of Au-Phosphine (left) and Au-PEG-SH (right) NPs vs. NaCl from 0 mM slat to 2.5 M salt concentration. The results directly after mixing is shown in straight lines and the results after 24 h in dashed lines. The Au-Phosphine samples kept constant for 24 h up to a concentration of 625 mM of salt. With higher concentrations the samples aggregated and precipitated. The Au-PEG-SH NPs kept constant up to a concentration of 2.5 M of salt.

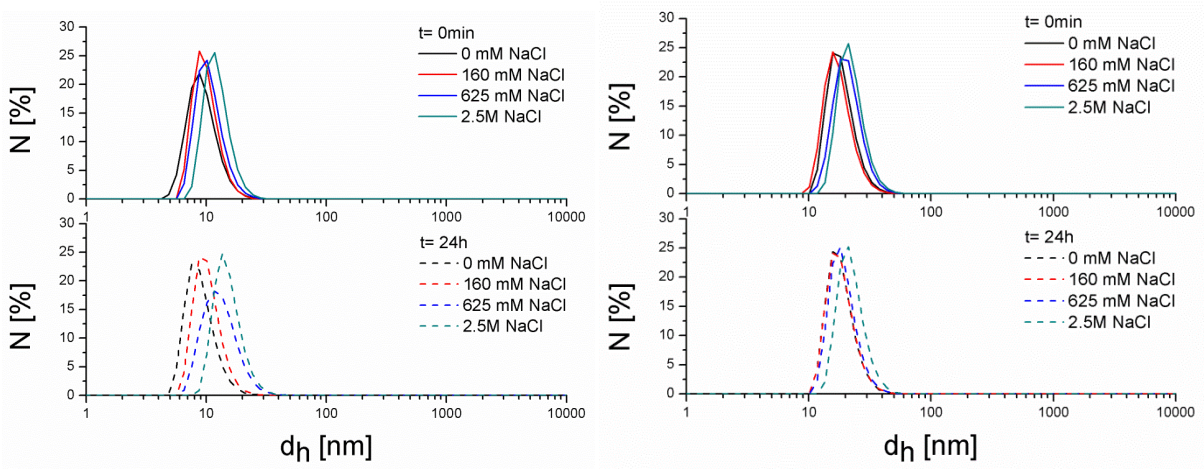

Figure 30: Selected results of DLS measurements for stability test of Au-PMA (left) and Au-PMA-satPEG (right) NPs vs. NaCl from 0 mM slat to 2.5 M salt concentration. The results directly after mixing is shown in straight lines and the results after 24 h in dashed lines. Both types of Au NPs kept constant up to a concentration of 2.5 M of salt.

The results of the measurements directly after addition were summarized in figure 31. A summary of the measured values shown in above figures is presented in table 5.

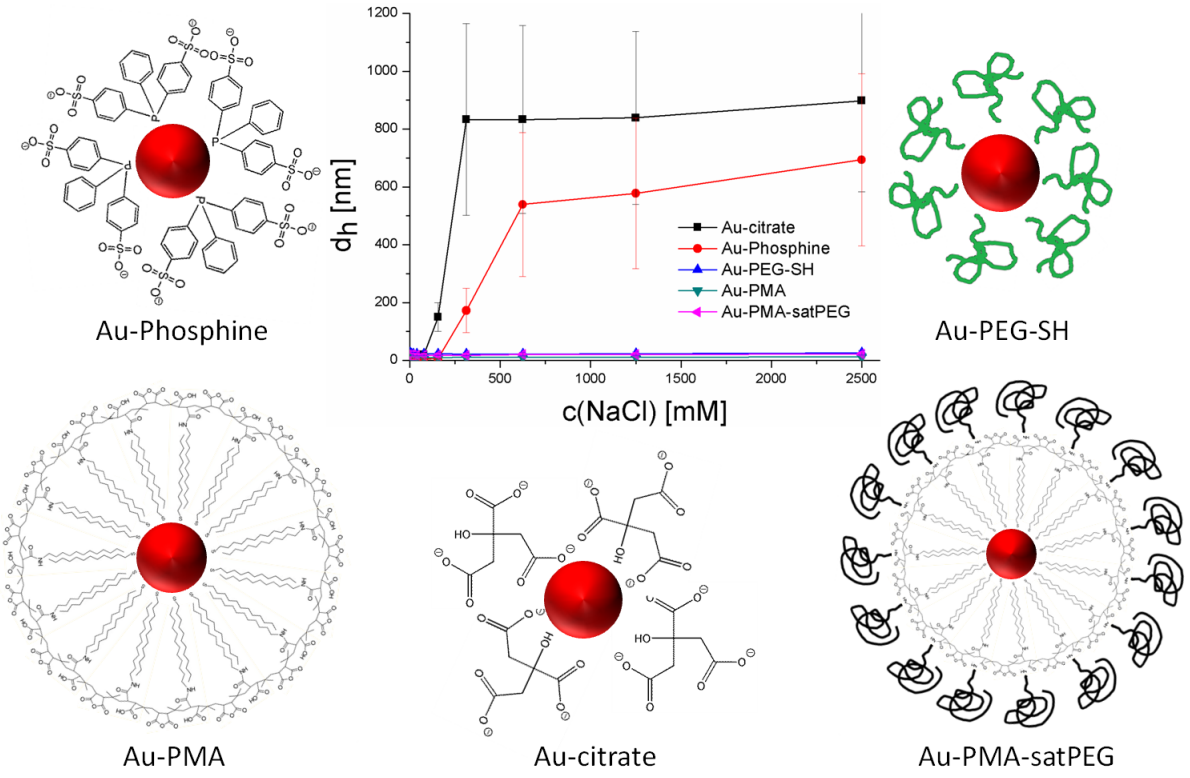

Figure 31: Summary of the hydrodynamic diameter of the Au NPs vs. NaCl direct after addition and sketches of the different modified Au NPs.

t = 0 h

c(NaCl)	0 mM	160 mM	625 mM	2.5 M
Au-citrate	7.10±1.9nm	149.8±49.4nm	833±324nm	898±315nm
Au-Phosphine	6.30±1.8nm	6.49±1.8nm	539±248nm	693±297nm
Au-PEG-SH	21.47±5.8nm	23.08±5.7nm	22.16±5.9nm	26.51±7.4nm
Au-PMA	9.48±2.9nm	10.00±2.6nm	10.78±3.0nm	12.34±3.1nm
Au-PMA-satPEG	18.64±5.1nm	17.75±5.0nm	21.06±5.7nm	22.50±5.9nm

t = 24 h

c(NaCl)	0 mM	160 mM	625 mM	2.5 M
Au-citrate	7.26±2.0nm	$\rightarrow\infty$	$\rightarrow\infty$	$\rightarrow\infty$
Au-Phosphine	6.68±1.8nm	7.40±1.9nm	$\rightarrow\infty$	$\rightarrow\infty$
Au-PEG-SH	21.31±5.8nm	22.47±4.9nm	21.80±5.9nm	25.08±7.2nm
Au-PMA	9.10±2.7nm	10.43±2.9nm	13.39±4.7nm	15.39±4.4nm
Au-PMA-satPEG	18.57±5.1nm	18.65±5.2nm	18.65±5.2nm	22.63±6.1nm

Table 5: Summary of mean hydrodynamic diameters d_h and their corresponding standard deviation, as derived from the data presented in Figures 27 - 29.

3.5 Effect on cells

3.5.1 Effect of Ag NCs on MCF-7 cells

The uptake and the cytotoxicity of the Ag NCs were measured with MCF-7 breast cancer cells (figure 32). After 6 h of incubation the red fluorescent Ag NCs could be distinguished from the blue labeled cell nucleus and from autofluorescence. Unfortunately the quantum yield was too low to observe a distribution in intracellular vesicular structures. The blank sample is not shown here.

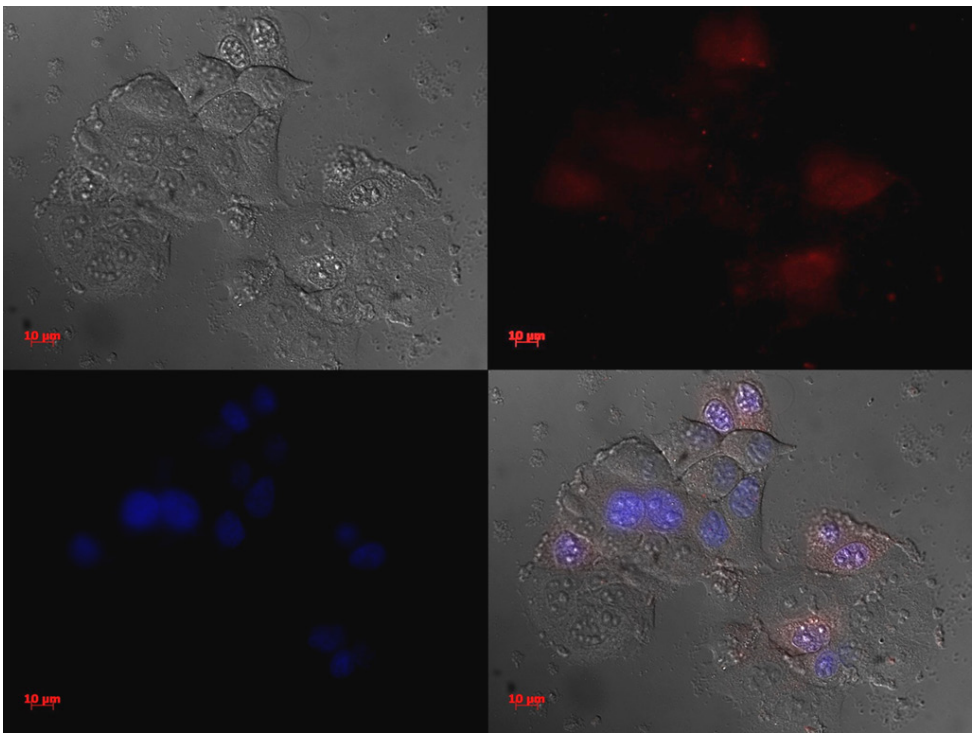

Figure 32: Fluorescence microscopy image of live MCF-7 cells after 6 hours of incubation with Ag NCs. (A) Differential interference contrast (DIC) image, (B) red fluorescence signal of Ag NCs, (C) blue fluorescence signal of Hoechst 33342, (D) merged picture of A, B, and C. Scale bars represent 10 µm.

For measuring the cytotoxicity a CellTiter Blue viability test was done[97]. This viability test is similar to the resazurin assay, used for the cytotoxicity test of the Ag NPs (*cf.* Chapter 3.5.2). Here the metabolism of viable cells from not fluorescent resazurin to the fluorescent resofurin was measured (*cf.* figure 35). The result is shown below in figure 33. For this test the cells were treated with the CellTiter Blue reagent and the absorbance at 570 nm was measured. The results showed that the Ag NCs show a tolerable toxicity after 24 h of incubation up to a concentration of 0.48 $mg \cdot mL^{-1}$.

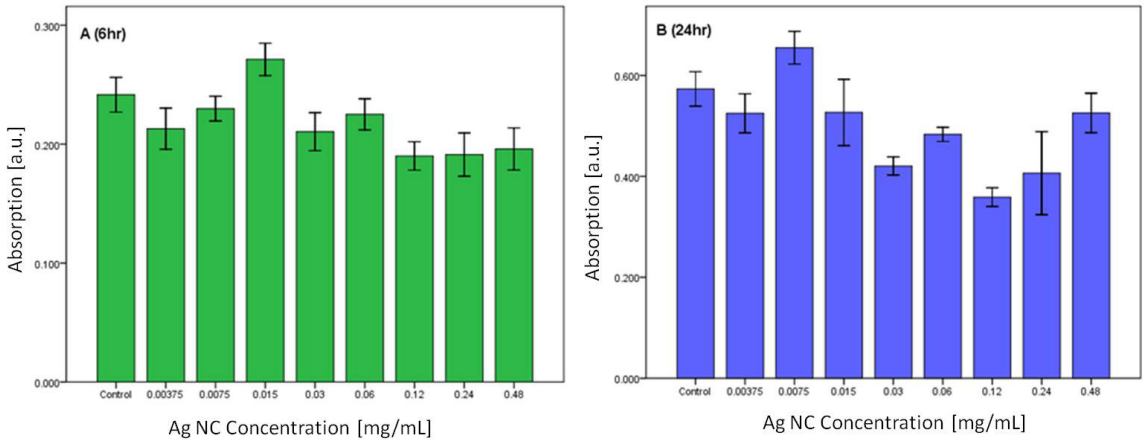

Figure 33: Cell viability assay using the CellTiter-Blue reagent with MCF-7 cells exposed to Ag NCs with serial dilutions for (A) 6 or (B) 24 hours. As read-out the OD at 570 nm is displayed. The results are represented as mean values ± standard error of the mean and were analyzed statistically using one-way ANOVA followed by Scheffé's test using SPSS version 17.0 to establish the significance of any differences. The level of statistical significance was set at $p < 0.05$.

3.5.2 Effect of Ag NP on NIH/3T3 cells

The uptake and the cytotoxicity of the four different modified Ag NPs were measured by using the NIH/3T3 fibroblast cells. The difference in the uptake between not PEGylated and PEGylated NPs after 15 h of incubation is shown in figure 34 for the example of Ag-PMA and Ag-PMA-satPEG NPs. Here both types were additionally modified with the dye DY-636 to get a fluorescent label. It is clearly seen that the uptake is reduced dramatically by saturating the surface of the particle with PEG. Unfortunately the uptake could not be quantified. The uptake of the Ag-MUA particles is not shown but it is qualitatively in the same range like the Ag-PMA NPs. For the Ag-PMA-1PEG particles the uptake is also in the same range.

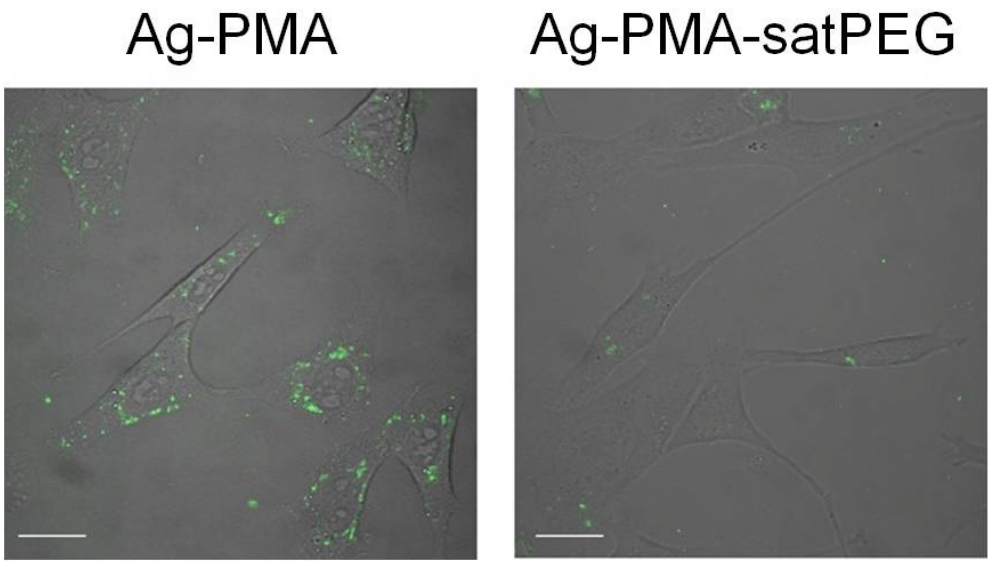

Figure 34: Fluorescence images of NIH/3T3 fibroblasts which had been exposed for 15 hours to fluorescence (DY636) labeled (A) polymer-coated Ag NPs or (B) polymer coated Ag NPs whose surface has been saturated with 10kDa PEG molecules. The images correspond to the overly images of the transmission and fluorescence channel. Scale bars correspond to 20 µm.

The toxicity of the Ag NPs was probed with a standard resazurin assay[98](*cf.* figure 34). For the positive control silver nitrate was used. The summarized results are shown in the response curves in figure 35. As expected the silver nitrate showed the highest toxicity. By comparing just the different Ag NPs, Ag-MUA NPs showed the highest toxicity with a LD_{50} value of 0.04 mM. The toxicity of the Ag-PMA and the Ag-PMA-1PEG is in the same range with LD_{50} values of 0.65 mM and 0.73 mM. The toxicity of the Ag-PMA-satPEG showed the lowest toxicity (LD_{50}: 1.34 mM). This low toxicity is due to the lower uptake of the Ag-PMA-satPEG NPs.

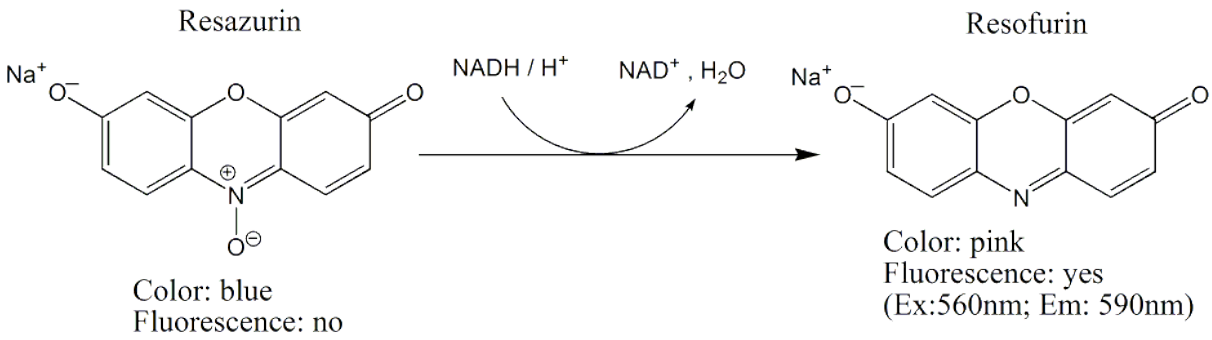

Figure 35: Reduction of resazurin to the fluorescent resofurin, which is done by living cells.

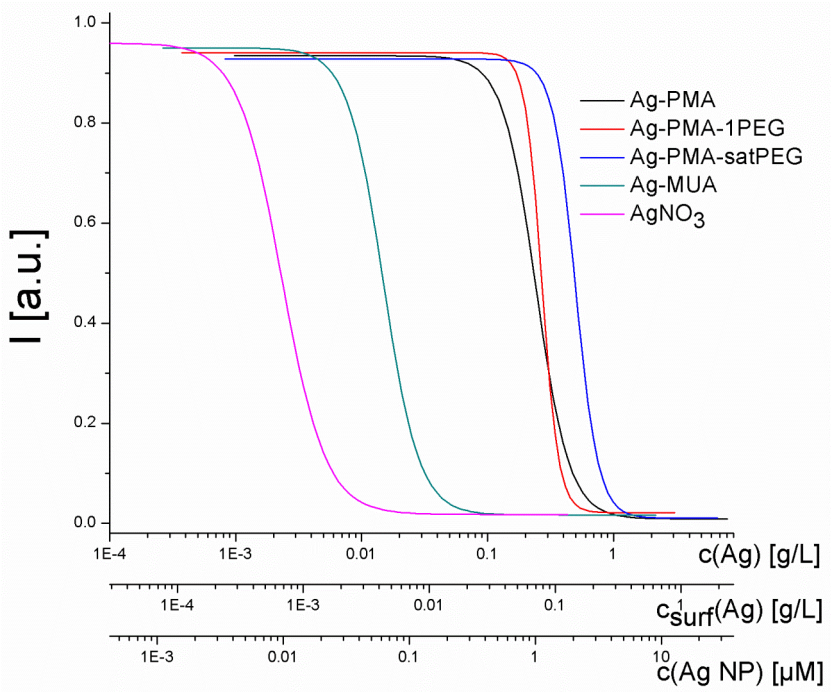

Figure 36: Resazurin-based viability test of 3T3 fibroblasts which had been incubated for 24 hours with Ag NPs. Onset of fluorescence (as quantified by the measured intensity I) is an indicator for viability of cells. The amount of Ag is quantified in a) the total amount of Ag (c(Ag)), b) the amount of Ag atoms which are present on the NP surface ($c_{surf}(Ag)$), and c) the amount of Ag NPs (c(Ag NP)). The following scaling factors were used: $c_{surf}(Ag) = 0.29 \cdot c(Ag)$ and $c(Ag\ NP) = 4.2 \cdot 10^{-9}$ mol/mg·c(Ag). In case of $AgNO_3$ as silver source only the c(Ag) concentration scale is valid, in case of all the NPs all three concentration scales are valid.

4 Conclusion

The synthesis of defined Ag NPs is very important in the field of particle science because the effect of a particle belongs to its size, shape or not at least to its surface chemistry. Two different wet chemical syntheses were established for well defined and stable Ag NPs. First, very small (2.2 nm) and fluorescent nanoparticles were synthesized *via* an etching step and afterwards a ligand exchange with a hydrophilic ligand. Second, bigger (4.2 nm) and not fluorescent particles were synthesized *via* simple reduction and capping with a hydrophobic ligand. In both cases the particles were stable enough that several purification and/or modification steps could be done without endanger the colloidal stability of the different nanoparticles. Both types and their modifications were tested for their use in biological systems.

The first type of Ag NPs, the small Ag NCs, showed a red fluorescence, a tolerable toxicity and an unspecific uptake in MCF-7 cells. Unfortunately, the presented particles showed a limited use for labeling cells due to their low quantum yield (QY). By solving the problem of the low QY in further studies, maybe by using of other ligands, the use of this kind of particles for labeling will get more possible. One major advantage of these particles was their small size. Because of the size it could be possible that they could penetrate tissue locations which are impenetrable for bigger particles. Another important point of these particles was that they could be used, with a more detailed photophysical characterization, for increasing the further understanding on their optical properties.

The, as produced, second type of Ag NPs were not soluble in water because of the hydrophobic ligand at the surface. To transfer the particles into the aqueous phase two different methods were used. The transfer to the aqueous phase was necessary for the investigation of the uptake and the cytotoxicity in cells. The first method was an exchange of the hydrophobic ligands with hydrophilic ligand molecules. The second method was the coating of the hydrophobic particle with an amphiphilic polymer. Both methods showed different advantages. Both methods were easy to do and also an additional modification was still possible at a later time point. An advantage of the simple ligand exchange reaction was that the ligand molecules do not need to be modified before they were used. The preparation of the amphiphilic polymer for the polymer coating, which first needed to be synthesized, cost an additional day. But this disadvantage is negligible because of the advantage that the colloidal stability of the coated Ag NPs was increased dramatically in comparison to the Ag NPs, which were stabilized by hydrophilic ligands. This increased stability was the main factor why the PMA coated particles showed a lower toxicity than the MUA stabilized particles. The polymer coated particles showed a reduced toxicity. This effect could be explained by clouding the cell membrane with the aggregated Ag-MUA particles[58].

PEGylation was another key factor for the cytotoxicity of the Ag NPs. Here not the release of Ag^+ ions but the uptake of the whole particle in the cell was the most important factor. If the surface of a particle was saturated with PEG molecules and showed because of this almost no surface charge, the uptake was reduced compared to the same but “naked” particle. Already the addition of one big (10 kDa) PEG molecule to the surface reduced the cytotoxicity. So here it was clearly seen that extracellular silver was less toxic than intracellular silver.

The modification of the different Ag NPs showed no influence to the corrosion of the Ag cores. After two weeks under neutral conditions, the release of free silver cations could not been detected. Just one sample showed a release of around 0.1%. Under acidic condition (pH 3) the release of silver cations was increased. After one day release rates between 0.7 and less than 1.2% could be measured. These values increased after one week up to 0.7 – 1.4%. These small amounts of released silver ions confirm the good stability of the Ag NPs.

By comparing the cytotoxicity of the different Ag NPs to silver nitrate, the particles showed a lower toxicity referred to the absolute amount of silver. But one had to consider that only 30% of the silver of the Ag NPs was located to the surface. An additional point was that just about 1% of this surface

silver was released into the surrounding media under acidic conditions. With the silver salt 100% of the Ag ions were free in the media and these Ag(I) ions are not permeable for the cell membrane (trough they can be complexed by serum proteins). So there were a lot of silver ions in the extracellular medium of the cells for the silver salt but only a few ions in the intracellular medium of the cells for the Ag NPs.

Summarizing all these facts one can say that the synthesis of different Ag NPs with difference in size, optical properties, stability and surface chemistry was done in a defined way. These particles could be taken up by cells and show that intracellular Ag is more toxic than extracellular and that the Ag NPs are an efficient carrier to bring the silver inside the cells.

In addition to the silver nanoparticles commercial gold nanoparticles were used to show that the here used methods to increase the stability of a particle against salt can be used in a general way. It could be shown that the coating of particle increased the stability it than using hydrophilic ligand molecules. By replacing the weak citrate ligand molecules with strong binding thiol-PEG molecules, the stability could also be increased showing comparable results like the coated particles. For using the coating procedure, the commercial particles first were transferred to the organic phase by replacing hydrophilic ligand molecules with hydrophobic molecules in two steps. First, the weak hydrophilic ligand was preplaced by a weak phase transfer ligand, which was replaced by a strong binding thiol ligand in a second step. Afterwards the gold nanoparticles showed the same surface chemistry like the silver nanoparticles and could be used in the same manner.

5. Publications

This cumulative thesis displays parts of the results of the scientific research assembled and published in the time from 2010 to 2013. Here the publications will be listed and the contribution to the articles, done by myself, will be outlined below. The released articles are attached to this thesis in the Appendix.

5.1 Reviews

One of the topics of this thesis is the interaction of nanoparticles with biological systems. For this reason three reviews are or will be published.

The first review [A1] deals with the biological fate of engineered NPs in physiological media. The fate of the NP depends on several parameters like the core material, the coating which is used to stabilize the particle, the functionalization for active or passive targeting, etc.. These parameters influence the absorbed protein corona which is another important point for the fate of a NP and its toxicity.

The focus of review [A2] is placed on the interaction of NPs with cell membranes. The before mentioned parameters which influence the fate of the NPs, as well as the compositions of the membranes are very important for the interaction between the NPs and the cell membrane. Due to the different compositions of the membranes the same NPs can show different behavior with different membranes.

In review [A3] we have a closer look to the NP and their closest environment the so called nano-environment. The closest environment plays an important role, if the particles are used as sensors. Because of their charged surface the NPs are actively influence this closest environment, which can be positive or negative for their use as sensors.

[A1][84] B. Pelaz, G. Charron, C. Pfeiffer, Y. Zhao, J. M. de la Fuente, X.-J. Liang, W. J. Parak, P. del Pino, "Interfacing engineered nanoparticles with biological systems: Anticipating adverse nano-bio interactions", *Small* **2013**, 9(9-10), 1573-1584.

[A2][85] M. Mahmoudi, J. Meng, X. Xue, X. J. Liang, M. Rahman, C. Pfeiffer, R. Hartmann, P. Rivera Gil, B. Pelaz, W.J. Parak, P. del Pino, S. Carregal-Romero, A.G. Kanaras, S. T. Selvan, "Interaction of stable colloidal nanoparticles with cellular membranes", *Recent Biotechnology Advances* submitted.

[A3][81] C. Pfeiffer*, C. Rehbock*, D. Hühn, C. Carrillo, D. Jimenez de Aberasturi, V. Merck, S. Barcikowski, W. J. Parak, "Interaction of colloidal nanoparticles with their local environment – the (ionic) nanoenvironment around nanoparticles is different from the bulk and determines the phyisco chemical properties of the nanoparticles", in preparation.

* Authors contribute equal to this article.

My contribution to the presented articles was the detailed search and description of scientific fact of the interaction from different kinds of nanoparticles with different types of biological systems in general or more detailed with the cell membrane. Additionally a closer look of the closest environment of a nanoparticle was taken. I did editorial work for all the articles like proofreading and improving of the text, the figures and the cited literature.

5.2 Synthesis and modification of nanoparticles

The main topic of this thesis is the synthesis and the modification of nanoparticles. In this field six articles were published or will be published. The publications deal with different kinds of particles e.g. core materials or sizes or modifications. Each factor was chosen depending on the main topic of the article and the task of the particle. The presented results in this thesis belong to the articles [A5], [A8] and [A9].

The article [A4] deals with the coating of Au NPs and CdSe/ZnS QDs with different charged polymers. Depending on the polymer different techniques of the coating procedure have been used. These coatings were compared with the established coating with modified PMA.

In article [A5] the synthesis of ultra small and red fluorescent Ag NCs is shown. The possible use of these clusters for biological applications and their cytotoxicity against MCF-7 breast cancer were investigated.

The reversible aggregation of casein coated Ag NPs is shown in article [A6]. The aggregation of these particles depend on the pH value of the medium and were analyzed using different techniques. Additionally the uptake and the toxicity of the particles in NIH/3T3 fibroblast cells were measured.

The focus of article [A7] is placed on the effect of the temperature at the formation of the protein corona at the surface of different NPs and proteins. It was shown that the degree of protein coverage and the composition of the absorbed proteins on the surface depend on the temperature.

The toxicity of Ag NPs can change a lot depending on the uptake in cells which is the main topic of article [A8]. Ag NPs with identical cores but different surface chemistry were synthesized and the uptake and cytotoxicity in NIH/3T3 fibroblast cells were investigated. The different surface chemistries were an important factor for the uptake and with this for the toxicity of the particles.

In article [A9] the impact of the colloidal stability for the formation of the protein corona was measured. For this reason commercial Au NPs were modified showing different surface chemistry and different stabilities. The formation and composition of the protein corona was measured using different techniques.

[A4][50] C. Geidel, S. Schmachtel, A. Riedinger, C. Pfeiffer, K. Muellen, M. Klapper, W. J. Parak, "A general synthetic approach for obtaining cationic and anionic inorganic nanoparticles *via* encapsulation in amphiphilic copolymers", *Small* **2011**, 7(20), 2929-2934.

[A5][56] S. Huang*, C.Pfeiffer*, J. Hollmann, S. Friede, J. J.-C. Chen, A. Beyer, B. Haas, K. Volz, W. Heimbrodt, J. M. Montenegro Martos, W. Chang, W. J. Parak, "Synthesis and characterization of colloidal fluorescent silver nanoclusters", *Langmuir* **2012**, 28(24), 8915-8919.

[A6][63] S. Ashraf, A.Z. Abbasi, C. Pfeiffer, S. Z. Hussain, Z. M. Khalid, P. Rivera Gil, W. J. Parak, I. Hussain, "Protein-mediated synthesis, pH-induced reversible agglomeration, toxicity and cellular interaction of silver nanoparticles", *Colloids and Surfaces B: Biointerfaces* **2013**, 102, 511-518.

[A7][31] M. Mahmoudi, A. M. Abdelmonem, S. Behazadi, J. Clement, S. Dutz, M. R. Ejtehadi, R. Hartmann, K. Kantner, U. Linne, P. Maffre, S. Metzler, M. K. Moghadam, C. Pfeiffer, M. Rezaie, P. Riuz-Lozano, V. Serpooshan, M. A. Shokrgozar, G. U. Nienhaus, W. J. Parak, "Temperature – The "ignored" factor at the nanobio interface", *ACS Nano* **2013**, 7(8), 6555-6562.

[A8][51] E. Caballero-Díaz*, C. Pfeiffer*, L. Kastl, P. Rivera-Gil, B. Simonet Suau, M. Valcárcel, J. Jiménez-Lamana, F. Laborda, W. J. Parak, "The toxicity of silver nanoparticles depends on their uptake by cells and thus on their surface chemistry", *Particle & Particle Systems Characterization*; ahead of print.

[A9][86] C. Pfeiffer*, B. D. Johnston*, W. G. Kreyling, W. J. Parak, "Colloidal stability in addition to surface chemistry as key factor of the composition of the protein corona of nanoparticles", in preparation.

* Authors contribute equal to this article.

My contribution to the article [A4] was to synthesize hydrophobic Au NPs (~4 nm core diameter) and to coat these particles with modified PMA. Afterwards the particles were purified and characterized by gel electrophoresis, SEC, TEM, DLS, LDA and UV-Vis spectroscopy. Additionally I did editorial work for the main article and supporting information.

For article [A5] first I had to establish the synthesis of the Ag NCs. Again the nanoclusters were purified using gel electrophoresis, SEC, TEM, DLS, LDA, UV-Vis spectroscopy and fluorescence spectroscopy. Parts of the main paper and all the parts of the supporting information belonging to afore mentioned synthesis and characterization were written by me.

In [A6] my contribution was the characterized the Ag NPs *via* TEM. Here the degree of aggregation of the Ag NPs could be influenced by the pH value, which was observed by TEM. Additionally I did editorial work for the main paper and the supporting information.

My contribution to article [A7] was to coat FePt NPs with modified PMA. Afterwards the surface of some of coated FePt NPs was modified by an additional dye (DY-636). All these particles were purified by gel electrophoresis, SEC, TEM, DLS, LDA, UV-Vis spectroscopy and fluorescence spectroscopy. Also I did editorial work for the main article and wrote big parts of the supporting information.

The first thing I had to do for article [A8] was to search for and establish a method for the synthesis of Ag NPs. Afterwards the particles were coated by modified PMA and the surface of the particles were modified described in this thesis. The different particles were purified by gel electrophoresis, SEC, TEM, LDA, UV-Vis spectroscopy and fluorescence spectroscopy. Additionally stability tests of the particles against NaCl concentration were done *via* DLS measurements. The extinction coefficient of the Ag NPs was experimentally determined to measure the concentration of the Ag NPs suspension by UV-Vis spectroscopy. The parts belonging to these things in the main paper are partly written by me. In the supporting information everything belonging to these things is written by me.

For article [A9] my contribution was the complete modification of the commercial Au NPs. Before some of the modification could be done I first had to find a way to bring the hydrophilic particles into the organic phase. Afterwards I could purify and characterize the different modified particles by gel electrophoresis, SEC, TEM, LDA and UV-Vis spectroscopy. The colloidal stability of the modified particles was tested by measuring the hydrodynamic diameter with different NaCl concentrations. Up to now there is just a first draft of the article and the supporting information results written by me.

The in all the articles mentioned editorial work was to improve the text, the literature, the figures and the tables.

References

1. Hammond, C. R. The Elements. In *Handbook of Chemistry and Physics*; CRC Press, 2005.

2. Yapijakis, C. Hippocrates of Kos, the Father of Clinical Medicine, and Asclepiades of Bithynia, the Father of Molecular Medicine. Review. *In vivo (Athens, Greece)* **2009**, *23*, 507–514.

3. Chopra, I. The Increasing Use of Silver-based Products as Antimicrobial Agents: a Useful Development or a Cause for Concern? *Journal of Antimicrobial Chemotherapy* **2007**, *59*, 587–590.

4. Morones, J.; Elechiguerra, J.; Camacho, A.; Holt, K.; Kouri, J.; Ram, J.; Yacaman, M. The Bactericidal Effect of Silver Nanoparticles. *Nanotechnology* **2005**, *16*, 2346–2352.

5. Brust, M.; Walker, M.; Bethell, D.; Schiffrin, D. J.; Whyman, R. Synthesis of Thiol-derivatised Gold Nanoparticles in a Two-phase Liquid-liquid System. *J. Chem. Soc., Chem. Commun.* **1994**, *7*, 801–802.

6. Buzea, C.; Pacheco, I. I.; Robbie, K. Nanomaterials and Nanoparticles: Sources and Toxicity. *Biointerphases* **2007**, *2*, MR17 – MR 71.

7. United States Environmental Protecting Agency http://www.epa.gov/iaq/index.html.

8. World Health Organization http://www.who.int/heli/risks/indoorair/indoorair/en/index.html.

9. BUND Nanoproduktdatenbank http://www.bund.net/nanodatenbank.

10. Project on Emerging Nanotechnologies http://www.nanotechproject.org/inventories/consumer/analysis_draft/.

11. Machmudah, S.; Goto, M.; Kuwahara, Y.; Sasaki, M. Gold Nanoparticles Fabricated by Pulsed Laser Ablation in Supercritical CO2. *Research on Chemical Intermediates* **2011**, *37*, 515–522.

12. Ebbesen, T. W.; Ajayan, P. M. Large-scale Synthesis of Carbon Nanotubes. *Nature* **1992**, *358*, 220–222.

13. Fischer, J. E.; Dai, H.; Thess, a.; Lee, R.; Hanjani, N. M.; Dehaas, D. L.; Smalley, R. E. Metallic Resistivity in Crystalline Ropes of Single-wall Carbon Nanotubes. *Physical Review B* **1997**, *55*, R4921–R4924.

14. Dai, H. Carbon Nanotubes: Synthesis, Integration, and Properties. *Accounts of chemical research* **2002**, *35*, 1035–44.

15. Serp, P.; Corrias, M.; Klack, P. Carbon Nanotubes and Nanofibers in Catalysis. *Applied Catalysis A: General* **2003**, *253*, 337–358.

16. Kam, N. W. S.; Jessop, T. C.; Wender, P. a; Dai, H. Nanotube Molecular Transporters: Internalization of Carbon Nanotube-protein Conjugates into Mammalian Cells. *Journal of the American Chemical Society* **2004**, *126*, 6850–1.

17. Samsonova, O.; Pfeiffer, C.; Hellmund, M.; Merkel, O. M.; Kissel, T. Low Molecular Weight pDMAEMA-block-pHEMA Block-Copolymers Synthesized via RAFT-Polymerization: Potential Non-Viral Gene Delivery Agents? *Polymers* **2011**, *3*, 693–718.

18. Samsonova, O.; Glinca, S.; Biela, A.; Pfeiffer, C.; Dayyoub, E.; Sahin, D.; Klebe, G.; Kissel, T. The Use of Isothermal Titration Calorimetry and Molecular Dynamics to Show Variability in DNA Transfection Performance. *Acta biomaterialia* **2013**, *9*, 4994–5002.

19. Dufès, C.; Uchegbu, I. F.; Schätzlein, A. G. Dendrimers in Gene Delivery. *Advanced drug delivery reviews* **2005**, *57*, 2177–2202.

20. Gerion, D.; Pinaud, F.; Williams, S. C.; Parak, W. J.; Zanchet, D.; Weiss, S.; Alivisatos, A. P. Synthesis and Properties of Biocompatible Water-Soluble Silica-Coated CdSe/ZnS Semiconductor Quantum Dots. *Journal of Physical Chemistry B* **2001**, *105*, 8861–8871.

21. Law, W.-C.; Yong, K.-T.; Roy, I.; Ding, H.; Hu, R.; Zhao, W.; Prasad, P. N. Aqueous-phase Synthesis of Highly Luminescent CdTe/ZnTe Core/shell Quantum Dots Optimized for Targeted Bioimaging. *Small* **2009**, *5*, 1302–1310.

22. Peng, Z. A.; Peng, X. Formation of High-Quality CdTe, CdSe, and CdS Nanocrystals Using CdO as Precursor. *Journal of the American Chemical Society* **2001**, *123*, 183–184.

23. Guzelian, a. a.; Banin, U.; Kadavanich, a. V.; Peng, X.; Alivisatos, a. P. Colloidal Chemical Synthesis and Characterization of InAs Nanocrystal Quantum Dots. *Applied Physics Letters* **1996**, *69*, 1432–1334.

24. Fernández-Arguelles, M. T.; Yakovlev, A.; Sperling, R. A.; Luccardini, C.; Gaillard, S.; Medel, A. S.; Mallet, J.-M.; Brochon, J.-C.; Feltz, A.; Oheim, M.; *et al.* Synthesis and Characterization of Polymer-Coated Quantum Dots with Integrated Acceptor Dyes as FRET-Based Nanoprobes. *Nano Letters* **2007**, *7*, 2613–2617.

25. Drummen, G. P. C. Quantum Dots From-Synthesis to Applications in Biomedicine and Life Sciences. *International Journal of Molecular Sciences* **2010**, *11*, 154–163.

26. Wang, J.; Vennerberg, D.; Lin, Z. Quantum Dot Sensitized Solar Cells. *Journal of Nanoengineering and Nanomanufacturing* **2011**, *1*, 155–171.

27. Murray, C. B.; Noms, D. J.; Bawendi, M. G. Synthesis an Characterization of Nearly Monodisperse CdE (E= S, Se, Te) Semiconductor Nanocrystallites. *Journal of the American Chemical Society* **1993**, *115*, 8706–8715.

28. Peng, X.; Schlamp, M. C.; Kadavanich, A. V; Alivisatos, A. P. Epitaxial Growth of Highly Luminescent CdSe/CdS Core/Shell Nanocrystals with Photostability and Electronic Accessibility. *Journal of the American Chemical Society* **1997**, *119*, 7019–7029.

29. Gupta, A. K.; Gupta, M. Synthesis and Surface Engineering of Iron Oxide Nanoparticles for Biomedical Applications. *Biomaterials* **2005**, *26*, 3995–4021.

30. Hyeon, T. Chemical Synthesis of Magnetic Nanoparticles. *Chem. Commun.* **2003**, *8*, 927–934.

31. Mahmoudi, M.; Abdelmonem, A. M.; Behzadi, S.; Clement, J. H.; Dutz, S.; Ejtehadi, M. R.; Hartmann, R.; Kantner, K.; Linne, U.; Maffre, P.; *et al.* Temperature - The "Ignored" Factor at the NanoBio Interface. *ACS nano* **2013**, *7*, 6555–6562.

32. Lu, A. H.; Salabas, E. L.; Schuth, F. Magnetic Nanoparticles: Synthesis, Protection, Functionalization, and Application. *Angewandte Chemie-International Edition* **2007**, *46*, 1222–1244.

33. Babes, L.; Denizot, B.; Tanguy, G.; Jeune, J. J. Le; Jallet, P. Synthesis of Iron Oxide Nanoparticles Used as MRI Contrast Agents: A Parametric Study. *Journal of Colloid and Interface Science* **1999**, *212*, 474–482.

34. Schweiger, C.; Gil, P.; Parak, W.; Kissel, T. MRI Contrast Enhancement Potential of Different Superparamagnetic Iron Oxide Nanoparticle (SPION) Formulations. *Journal Of Controlled Release* **2010**, *148*, E67–E68.

35. Gao, F.; Cai, Y.; Zhou, J.; Xie, X.; Ouyang, W.; Zhang, Y.; Wang, X.; Zhang, X.; Wang, X.; Zhao, L.; *et al.* Pullulan Acetate Coated Magnetite Nanoparticles for Hyper-thermia: Preparation, Characterization and in Vitro Experiments. *Nano Research* **2010**, *3*, 23–31.

36. Hildebrandt, B.; Wust, P.; Ahlers, O.; Dieing, A.; Sreenivasa, G.; Kerner, T.; Felix, R.; Riess, H. The Cellular and Molecular Basis of Hyperthermia. *Critical Reviews in Oncology Hematology* **2002**, *43*, 33–56.

37. Zhu, H.; Zhang, C.; Yin, Y. Rapid Synthesis of Copper Nanoparticles by Sodium Hypophosphite Reduction in Ethylene Glycol Under Microwave Irradiation. *Journal of Crystal Growth* **2004**, *270*, 722–728.

38. Wang, C.; Daimon, H.; Onodera, T.; Koda, T.; Sun, S. A General Approach to the Size- and Shape-controlled Synthesis of Platinum Nanoparticles and Their Catalytic Reduction of Oxygen. *Angewandte Chemie (International ed. in English)* **2008**, *47*, 3588–3591.

39. Osorio-Cantillo, C.; Santiago-Miranda, a. N.; Perales-Perez, O.; Xin, Y. Size- and Phase-controlled Synthesis of Cobalt Nanoparticles for Potential Biomedical Applications. *Journal of Applied Physics* **2012**, *111*, 07B324.

40. Wu, S.-H.; Chen, D.-H. Synthesis and Characterization of Nickel Nanoparticles by Hydrazine Reduction in Ethylene Glycol. *Journal of colloid and interface science* **2003**, *259*, 282–286.

41. Haes, A. J.; Duyne, R. P. Van A Nanoscale Optical Biosensor: Sensitivity and Selectivity of an Approach Based on the Localized Surface Plasmon Resonance Spectroscopy of Triangular Silver Nanoparticles. *Journal of the American Chemical Society* **2002**, *124*, 10596–10604.

42. Turkevich, J.; Stevenson, P. C.; Hillier, J. A Study of the Nucleation and Growth Processes in the Synthesis of Colloidal Gold. *Discussions of the Faraday Society* **1951**, *11*, 55–75.

43. Lin, C. A. J.; Yang, T. Y.; Lee, C. H.; Huang, S. H.; Sperling, R. A.; Zanella, M.; Li, J. K.; Shen, J. L.; Wang, H. H.; Yeh, H. I.; *et al.* Synthesis, Characterization, and Bioconjugation of Fluorescent Gold Nanoclusters Toward Biological Labeling Applications. *ACS Nano* **2009**, *3*, 395–401.

44. Sun, Y.; Xia, Y. Shape-Controlled Synthesis of Gold and Silver Nanoparticles. *Science* **2002**, *298*, 2176–2179.

45. Link, S.; Wang, Z. L.; and M. A. El-Sayed Alloy Formation of Gold-Silver Nanoparticles and the Dependence of the Plasmon Absorption on Their Composition. *Journal of Physical Chemistry B* **1999**, *103*, 3529–3533.

46. Ohno, K.; Koh, K.; Tsujii, Y.; Fukuda, T. Synthesis of Gold Nanoparticles Coated with Well-Defined, High-Density Polymer Brushes by Surface-Initiated Living Radical Polymerization. *Macromolecules* **2002**, *35*, 8989–8993.

47. Brust, M.; Fink, J.; Bethell, D.; Schiffrin, D. J.; Kiely, C. Synthesis and Reaction of Functionalised Gold Nanoparticles. *J. Chem. Soc., Chem. Commun.* **1995**, 1655–1656.

48. Carregal-Romero, S.; Ochs, M.; Rivera Gil, P.; Gana, C.; Pavlov, A. M.; Sukhorukov, G. B.; Parak, W. J. NIR-light Triggered Delivery of Macromolecules into the Cytosol. *Journal Of Controlled Release* **2012**, *159*, 120–127.

49. Lin, C. J.; R. A. Sperling; Lee, J. K.; Zanella, M.; T. Yang; Li, P.; Chang, W. H.; Parak, W. J. Design of an Amphiphilic Polymer for Nanoparticle Coating and Functionalization. *Small* **2008**, *4*, 334–341.

50. Geidel, C.; Schmachtel, S.; Riedinger, A.; Pfeiffer, C.; Müllen, K.; Klapper, M.; Parak, W. J. A General Synthetic Approach for Obtaining Cationic and Anionic Inorganic Nanoparticles via Encapsulation in Amphiphilic Copolymers. *Small* **2011**, *7*, 2929–2934.

51. Caballero-Díaz, E.; Pfeiffer, C.; Kastl, L.; Rivera-Gil, P.; Simonet, B. M.; Valcarcel, M.; Jiménez-Lamana, J.; Laborda, F.; Parak, W. J. The Toxicity of Silver Nanoparticles Depends on Their Uptake by Cells and Thus on Their Surface Chemistry. *Particle and Particle Systems Characterization* **2013**, ahead of print.

52. Christian, P.; Kammer, F. Von der; Baalousha, M.; Hofmann, T. Nanoparticles: Structure, Properties, Preparation and Behaviour in Environmental Media. *Ecotoxicology (London, England)* **2008**, *17*, 326–343.

53. Wijnhoven, S. W. P.; Peijnenburg, W. J. G. M.; Herberts, C. a.; Hagens, W. I.; Oomen, A. G.; Heugens, E. H. W.; Roszek, B.; Bisschops, J.; Gosens, I.; Meent, D. Van De; *et al.* Nano-silver – a Review of Available Data and Knowledge Gaps in Human and Environmental Risk Assessment. *Nanotoxicology* **2009**, *3*, 109–138.

54. Benn, T.; Cavanagh, B.; Hristovski, K.; Posner, J. D.; Westerhoff, P. The Release of Nanosilver from Consumer Products Used in the Home. *Journal of Environment Quality* **2010**, *39*, 1875–1882.

55. Pal, T.; Sau, T. K.; Jana, N. R. Reversible Formation and Dissolution of Silver Nanoparticles in Aqueous Surfactant Media. *Langmuir* **1997**, *7463*, 1481–1485.

56. Huang, S.; Pfeiffer, C.; Hollmann, J.; Friede, S.; Chen, J. J.-C.; Beyer, A.; Volz, K.; Heimbrodt, W.; Martos, J. M. M.; Chang, W.; *et al.* Synthesis and Characterization of Colloidal Fluorescent Silver Nanoclusters. *Langmuir* **2012**, *28*, 8915–8919.

57. Mari, A.; Imperatori, P.; Marchegiani, G.; Pilloni, L.; Mezzi, A.; Kaciulis, S.; Cannas, C.; Meneghini, C.; Mobilio, S.; Suber, L. High Yield Synthesis of Pure Alkanethiolate-capped Silver Nanoparticles. *Langmuir* **2010**, *26*, 15561–15566.

58. Kirchner, C.; Liedl T.; S. Kudera; T. Pellegrino; A. Muñoz Javier; H. E. Gaub; S. Stölzle; N. Fertig; Parak, W. J. Cytotoxicity of Colloidal CdSe and CdSe/ZnS Nanoparticles. *Nano Letters* **2005**, *5*, 331–338.

59. Soenen, S. J.; Manshian, B.; Montenegro, J. M.; Amin, F.; Meermann, B.; Thiron, T.; Cornelissen, M.; Vanhaecke, F.; Doak, S.; Parak, W. J.; *et al.* Cytotoxic Effects of Gold Nanoparticles : A Multiparametric Study. *ACS Nano* **2012**, *6*, 5767–5783.

60. Hoecke, K. Van; Schamphelaere, K. a C. De; Ali, Z.; Zhang, F.; Elsaesser, A.; Rivera-Gil, P.; Parak, W. J.; Smagghe, G.; Howard, C. V; Janssen, C. R. Ecotoxicity and Uptake of Polymer Coated Gold Nanoparticles. *Nanotoxicology* **2013**, *7*, 37–47.

61. Brandenberger, C.; Mühlfeld, C.; Ali, Z.; Lenz, A.-G.; Schmid, O.; Parak, W. J.; Gehr, P.; Rothen-Rutishauser, B. Quantitative Evaluation of Cellular Uptake and Trafficking of Plain and Polyethylene Glycol-Coated Gold Nanoparticles. *SMALL* **2010**, *6*, 1669–1678.

62. Ma, R.; Levard, C.; Marinakos, S. M.; Cheng, Y.; Liu, J.; Michel, F. M.; Brown, G. E.; Lowry, G. V Size-controlled Dissolution of Organic-coated Silver Nanoparticles. *Environmental science & technology* **2012**, *46*, 752–759.

63. Ashraf, S.; Abbasi, A. Z.; Pfeiffer, C.; Hussain, S. Z.; Khalid, Z. M.; Gil, P. R.; Parak, W. J.; Hussain, I. Protein-mediated Synthesis, pH-induced Reversible Agglomeration, Toxicity and Cellular Interaction of Silver Nanoparticles. *Colloids and surfaces. B, Biointerfaces* **2013**, *102*, 511–518.

64. Badawy, A. M. El; Scheckel, K. G.; Suidan, M.; Tolaymat, T. The Impact of Stabilization Mechanism on the Aggregation Kinetics of Silver Nanoparticles. *The Science of the total environment* **2012**, *429*, 325–331.

65. Navarro, E.; Piccapietra, F.; Wagner, B.; Marconi, F.; Kaegi, R.; Odzak, N.; Sigg, L.; Behra, R. Toxicity of Silver Nanoparticles to Chlamydomonas Reinhardtii. *Environ. Sci. Technol.* **2008**, *42*, 8959–8964.

66. Sondi, I.; Salopek-Sondi, B. Silver Nanoparticles as Antimicrobial Agent: a Case Study on E. Coli as a Model for Gram-negative Bacteria. *Journal of Colloid and Interface Science* **2004**, *275*, 177–182.

67. Kvitek, L.; Vanickova, M.; Panacek, A.; Soukupova, J.; Dittrich, M.; Valentova, E.; Prucek, R.; Bancirova, M.; Milde, D.; Zboril, R.; *et al.* Initial Study on the Toxicity of Silver Nanoparticles (NPs) Against Paramecium Caudatum. *Journal of Physical Chemistry C* **2010**, *113*, 4296–4300.

68. Hussain, S. M.; Hess, K. L.; Gearhart, J. M.; Geiss, K. T.; Schlager, J. J. In Vitro Toxicity of Nanoparticles in BRL 3A Rat Liver Cells. *Toxicology in Vitro* **2005**, *19*, 975–983.

69. Braydich-Stolle, L.; Hussain, S.; Schlager, J. J.; Hofmann, M.-C. In Vitro Cytotoxicity of Nanoparticles in Mammalian Germline Stem Cells. *Toxicol. Sci.* **2005**, *88*, 412–419.

70. Asharani, P. V; Low, G.; Mun, K.; Hande, M. P.; Valiyaveettil, S. Cytotoxicity and Genotoxicity of Silver. *ACS Nano* **2009**, *3*, 279–290.

71. Singh, R. P.; Ramarao, P. Cellular Uptake, Intracellular Trafficking and Cytotoxicity of Silver Nanoparticles. *Toxicology letters* **2012**, *213*, 249–259.

72. Heckmann, L.-H.; Hovgaard, M. B.; Sutherland, D. S.; Autrup, H.; Besenbacher, F.; Scott-Fordsmand, J. J. Limit-test Toxicity Screening of Selected Inorganic Nanoparticles to the Earthworm Eisenia Fetida. *Ecotoxicology (London, England)* **2011**, *20*, 226–233.

73. Liedl, T.; Pellegrino, T.; Parak, W. J. Bological Application of Fluorescent Quantum Dots. *New Drugs* **2005**, *February 2*, 14–16.

74. Lin, C.-A. J.; Liedl, T.; Sperling, R. a.; Fern?ndez-Arg?elles, M. T.; Costa-Fern?ndez, J. M.; Pereiro, R.; Sanz-Medel, A.; Chang, W. H.; Parak, W. J. Bioanalytics and Biolabeling with Semiconductor Nanoparticles (quantum Dots). *Journal of Materials Chemistry* **2007**, *17*, 1343–1346.

75. Gu, W.; Pellegrino, T.; Parak, W. J.; Boudreau, R.; Gros, M. A. Le; Alivisatos, A. P.; Larabell, C. A. Measuring Cell Motility Using Quantum Dot Probes. *Methods in Molecular Biology* **2007**, *374*, 125–131.

76. Zhang, F.; Ali, Z.; Amin, F.; Riedinger, A.; Parak, W. J. In Vitro and Intracellular Sensing by Using the Photoluminescence of Quantum Dots. *Analytical And Bioanalytical Chemistry* **2010**, *397*, 935–942.

77. Sperling, R. A.; Rivera-Gil, P.; Zhang, F.; Zanella, M.; Parak, W. J. Biological Applications of Gold Nanoparticles. *Chemical Society Reviews* **2008**, *37*, 1896–1908.

78. Mock, J. J.; Barbic, M.; Smith, D. R.; Schultz, D. a.; Schultz, S. Shape Effects in Plasmon Resonance of Individual Colloidal Silver Nanoparticles. *The Journal of Chemical Physics* **2002**, *116*, 6755–6759.

79. Parak, W. J.; Gerion, D.; Pellegrino, T.; Zanchet, D.; Micheel, C.; Williams, S. C.; Boudreau, R.; Gros, M. A. Le; Larabell, C. A.; Alivisatos, A. P. Biological Applications of Colloidal Nanocrystals. *Nanotechnology* **2003**, *14*, R15–R27.

80. Amin, F.; Yushchenko, D. A.; Montenegro, J. M.; Parak, W. J. Integration of Organic Fluorophores in the Surface of Polymer-Coated Colloidal Nanoparticles for Sensing the Local Polarity of the Environment. *Chemphyschem* **2012**, *13*, 1030–1035.

81. Pfeiffer, C.; Rehbock, C.; Hühn, D.; Carrillo-Carrion, C.; Jimenez de Aberasturi, D.; Merk, V.; Barcikowski, S.; Parak, W. J. Interaction of Colloidal Nanoparticles with Their Local Environment - the (ionic) Nanoenvironment Around Nanoparticles Is Different from Bulk and Determines the Physico Chemical Properties of the Nanoparticles. *in preparation*.

82. Riedinger, A.; Zhang, F.; Dommershausen, F.; Röcker, C.; Brandholt, S.; Nienhaus, G. U.; Koert, U.; Parak, W. J. Ratiometric Optical Sensing of Chloride Ions with Organic Fluorophore - Gold Nanoparticle Hybrids: a Systematic Study of Distance Dependency and the Influence of Surface Charge. *Small* **2010**, *6*, 2590–2597.

83. Cho, K.; Wang, X.; Nie, S.; Chen, Z.; Shin, D. M. Therapeutic Nanoparticles for Drug Delivery in Cancer. *Clin Cancer Res* **2008**, *14*, 1310–1316.

84. Pelaz, B.; Charron, G.; Pfeiffer, C.; Zhao, Y.; la Fuente, J. M. de; Liang, X.-J.; Parak, W. J.; Pino, P. del Interfacing Engineered Nanoparticles with Biological Systems: Anticipating Adverse Nano-Bio Interactions. *Small* **2013**, *9*, 1573–1584.

85. Mahmoudi, M.; Meng, J.; Xue, X.; Liang, J.; Rahman, M.; Pfeiffer, C.; Hartmann, R.; Rivera Gil, P.; Pelaz, B.; Parak, W. J.; *et al.* Interaction of Stable Colloidal Nanoparticles with Cellular Membranes. *Recent Biotechnology Advances*.

86. Pfeiffer, C.; Johnston, B.; Kreyling, W. G.; Parak, W. J. Colloidal Stability in Addition to Surface Chemistry as Key Factor of the Composition of the Protein Corona of Nanoparticles. *in preparation*.

87. Walkey, C. D.; Chan, W. C. W. Understanding and Controlling the Interaction of Nanomaterials with Proteins in a Physiological Environment. *Chemical Society reviews* **2012**, *41*, 2780–2799.

88. Röcker, C.; Pötzl, M.; Zhang, F.; Parak, W. J.; Nienhaus, G. U. A Quantitative Fluorescence Study of Protein Monolayer Formation on Colloidal Nanoparticles. *Nature Nanotechnology* **2009**, *4*, 577–580.

89. Chung, T.-H.; Wu, S.-H.; Yao, M.; Lu, C.-W.; Lin, Y.-S.; Hung, Y.; Mou, C.-Y.; Huang, D.-M. The Effect of Surface Charge on the Uptake and Biological Function of Mesoporous Silica Nanoparticles in 3T3-L1 Cells and Human Mesenchymal Stem Cells. *Biomaterials* **2007**, *28*, 2959–2966.

90. Wong, S. S. *Chemisrtry of Protein Conjugation and Cross-linking*; CRC Press, 1991.

91. Hermanson, G. T. *Bioconjugate Techniques*; Academic Press, second edition, 2008.

92. British Biocell International http://www.buybbi.com/GC215nm_271.aspx.

93. Lakowicz, J. R. *Principles of Fluorescence Spectroscopy*; Third Edit.; Springer: New York, 2006; p. 954.

94. Grönbeck, H.; Curioni, A.; Andreoni, W. Thiols and Disulfides on the Au (111) Surface : The Headgroup - Gold Interaction. *Journal of the Americal Chemical Society* **2000**, 3839–3842.

95. Huotari, J.; Helenius, A. Endosome Maturation. *The EMBO journal* **2011**, *30*, 3481–500.

96. Mellman, I.; Fuchs, R.; Helenius, A. Acidification of the Endocytic and Exocytic Pathways. *Annual Review of Biochemistry* **1986**, *55*, 663–700.

97. Promega CellTiter-Blue Cell Viability Assay http://www.promega.de/products/cell-health-assays/cell-viability-assays/celltiter_blue-cell-viability-assay/?origUrl=http://www.promega.com/products/cell-health-assays/cell-viability-assays/celltiter_blue-cell-viability-assay/.

98. O'Brien, J.; Wilson, I.; Orton, T.; Pognan, F. Investigation of the Alamar Blue (resazurin) Fluorescent Dye for the Assessment of Mammalian Cell Cytotoxicity. *European journal of biochemistry / FEBS* **2000**, *267*, 5421–5426.

Wissenschaftlicher Werdegang

Persönliche Daten

Name:	Christian Pfeiffer
Geburtsdatum:	19.08.1984
Geburtsort:	Marburg/Lahn
Staatsangehörigkeit:	Deutsch

Ausbildung

02/2010 – 08/2013	Doktorarbeit, Philipps-Universität Marburg Thema: Silbernanopartikel – Von der Synthese bis zur biologischen Anwendung Betreuer: Prof. Dr. W. J. Parak
01/2009 – 07/2009	Diplomarbeit, Philipps-Universität Marburg Thema: Diblockcopolymere aus Poly-2-(dimethylamino)ethyl- methacrylat und Poly-2-hydroxyethylmethacrylat mittels RAFT Polymerisation zur Herstellung von Polyplexen für die Gentherapie Betreuer: Prof. Dr. T. Kissel
10/2003 – 07/2009	Chemie Haupt- und Grundstudium, Philipps-Universität Marburg
09/1996 – 06/2003	Abitur, Gymnasium Lahntalschule Biedenkopf

Wissenschaftliche Veröffentlichungen

[1] O. Samsonova*, C. Pfeiffer*, M. Hellmund, O. M. Merkel, T. Kissel, "Low molecular weight pDMAEMA-block-pHEMA block-copolymers synthesized *via* RAFT-polymerization: potential non-viral gene delivery agents?" *Polymers* **2011**, 3(2), 693-718.

[2] C. Geidel, S. Schmachtel, A. Riedinger, C. Pfeiffer, K. Muellen, M.Klapper, W. J. Parak, "A general synthetic approach for obtaining cationic and anionic inorganic nanoparticles *via* encapsulation in amphiphilic copolymers", *Small* **2011**, 7(20), 2929-2934.

[3] S. Huang*, C.Pfeiffer*, J. Hollmann, S. Friede, J. J.-C. Chen, A. Beyer, B. Haas, K. Volz, W. Heimbrodt, J. M. Montenegro Martos, W. Chang, W. J. Parak, "Synthesis and characterization of colloidal fluorescent silver nanoclusters", *Langmuir* **2012**, 28(24), 8915-8919.

[4] O. Samsonova, S. Glinca, A. Biela, C. Pfeiffer, E. Dayyoub, D. Sahin, G. Klebe, T. Kissel, "The use of isothermal titration calometry and molecular dynamics to show variability in DNA transfection performance", *Acta Biomaterialia* **2013**, 9, 4994-5002.

[5] B. Pelaz, G. Charron, C. Pfeiffer, Y. Zhao, J. M. de la Fuente, X.-J. Liang, W. J. Parak, P. del Pino, "Interfacing engineered nanoparticles with biological systems: Anticipating adverse nano-bio interactions", *Small* **2013**, 9(9-10), 1573-1584.

[6] S. Ashraf, A.Z. Abbasi, C. Pfeiffer, S. Z. Hussain, Z. M. Khalid, P. Rivera Gil, W. J. Parak, I. Hussain, "Protein-mediated synthesis, pH-induced reversible agglomeration, toxicity and cellular interaction of silver nanoparticles", *Colloids and Surfaces B: Biointerfaces* **2013**, 102, 511-518.

[7] M. Mahmoudi, A. M. Abdelmonem, S. Behazadi, J. Clement, S. Dutz, M. R. Ejtehadi, R. Hartmann, K. Kantner, U. Linne, P. Maffre, S. Metzler, M. K. Moghadam, C. Pfeiffer, M. Rezaie, P. Riuz-Lozano, V. Serpooshan, M. A. Shokrgozar, G. U. Nienhaus, W. J. Parak, "Temperature – The "ignored" factor at the nanobio interface", *ACS Nano* **2013**, 7(8), 6555-6562.

[8] E. Caballero-Díaz*, C. Pfeiffer*, L. Kastl, P. Rivera-Gil, B. Simonet Suau, M. Valcárcel, J. Jiménez-Lamana, F. Laborda, W. J. Parak, "The toxicity of silver nanoparticles depends on their uptake by cells and thus on their surface chemistry", *Particle & Particle Systems Characterization*; ahead of print.

[9] M. Mahmoudi, J. Meng, X. Xue, X. J. Liang, M. Rahman, M. S. Strano, S. Kruss, C. Pfeiffer, R. Hartmann, P. Rivera Gil, B. Pelaz, W.J. Parak, P. del Pino, S. Carregal-Romero, A.G. Kanaras, S. T. Selvan, "Interaction of stable colloidal nanoparticles with cellular membranes", submitted Recent Biotechnology Advances 2013.

[10] C. Pfeiffer*, B. D. Johnston*, W. G. Kreyling, W. J. Parak, "Colloidal stability in addition to surface chemistry as key factor of the composition of the protein corona of nanoparticles"; in preparation.

[11] C. Pfeiffer, D. Hühn, C. Carrillo, B. Pelaz, S. Barcikowski, W. J. Parak, "Effects of colloidal nanoparticles on their local environment – the nanoenvironment around nanoparticles is different from the bulk"; in preparation.

*Gleichberechtigte Erstautorenschaft

Marburg, 06.12.2013

Erklärung

Hiermit versichere ich, dass ich meine Dissertation

Silver nanoparticles – From the synthesis to the biological application

selbständig ohne unerlaubte Hilfe angefertigt und mich dabei keiner anderen als der von mir ausdrücklich bezeichneten Quellen und Hilfen bedient habe.

Die Dissertation wurde in der jetzigen oder einer ähnlichen Form noch bei keiner Hochschule eingereicht und hat noch keinem sonstigen Prüfungszweck gedient.

Name, Vorname: Pfeiffer, Christian

Marburg,06.12.2013 .....

Unterschrift

small
NANO MICRO

Interfacing Engineered Nanoparticles with Biological Systems: Anticipating Adverse Nano–Bio Interactions

*Beatriz Pelaz, Gaëlle Charron, Christian Pfeiffer, Yuliang Zhao, Jesus M. de la Fuente, Xing-Jie Liang, Wolfgang J. Parak, and Pablo del Pino**

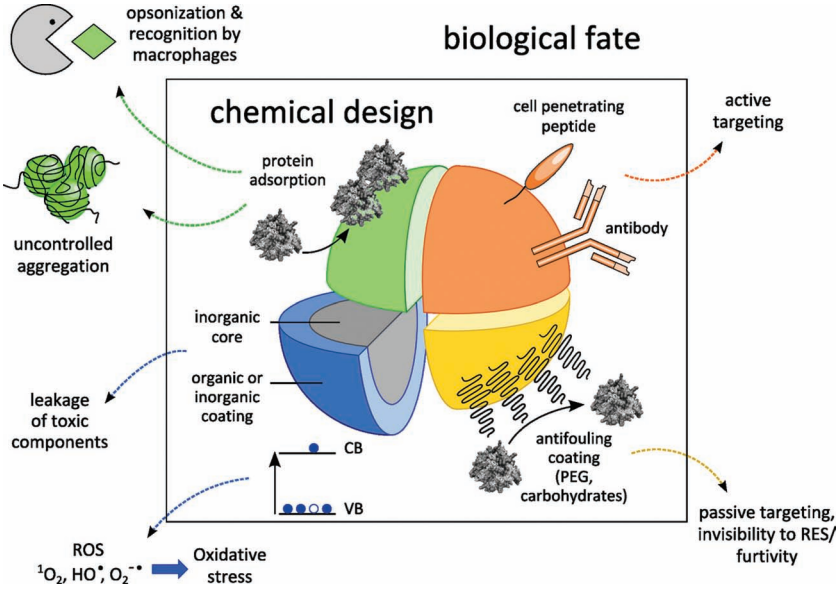

From the Contents

The innovative use of engineered nanomaterials in medicine, be it in therapy or diagnosis, is growing dramatically. This is motivated by the current extraordinary control over the synthesis of complex nanomaterials with a variety of biological functions (e.g. contrast agents, drug-delivery systems, transducers, amplifiers, etc.). Engineered nanomaterials are found in the bio-context with a variety of applications in fields such as sensing, imaging, therapy or diagnosis. As the degree of control to fabricate customized novel and/or enhanced nanomaterials evolves, often new applications, devices with enhanced performance or unprecedented sensing limits can be achieved. Of course, interfacing any novel material with biological systems has to be critically analyzed as many undesirable adverse effects can be triggered (e.g. toxicity, allergy, genotoxicity, etc.) and/or the performance of the nanomaterial can be compromised due to the unexpected phenomena in physiological environments (e.g. corrosion, aggregation, unspecific absorption of biomolecules, etc.). Despite the need for standard protocols for assessing the toxicity and bio-performance of each new functional nanomaterial, these are still scarce or currently under development. Nonetheless, nanotoxicology and relating adverse effects to the physico-chemical properties of nanomaterials are emerging areas of the utmost importance which have to be continuously revisited as any new material emerges. This review highlights recent progress concerning the interaction of nanomaterials with biological systems and following adverse effects.

1. Introduction

Since the term nanomaterial includes many different materials, i.e. inorganic nanocrystals, organic nanoparticles, films, inorganic/organic hybrid materials, etc., for the sake of clarity, this review focuses on colloidal nanoparticles (NPs) containing inorganic materials (typically these are referred to as nanocrystals or inorganic NPs), although many of the critical aspects discussed here also apply to other nanoparticulate materials, e.g. purely organic nanoparticles.

Functional inorganic colloids have been used in modern biology and medicine for long time. Already in 1971, an original antibody–colloidal gold complex was proposed for cell surface antigen localization for electron microscopy.[1] In the last decade, nanoscience has grown to what appears to be one of the richest research areas in terms of spin-off effects on our society.[2] Importantly, engineered nanomaterials have been proven to deliver important technological features in a wide variety of medical applications (e.g. imaging,[3] therapy,[4] sensing,[5] diagnosis[6]). Maybe since the pioneering works where semiconductor nanocrystals were proposed as cellular probes,[7] and DNA to arrange NPs,[8] there has been an increasing and widely extended interest for 'mixing' inorganic NPs with living organisms and biomolecules. This is motivated by three main reasons: (i) NP size lies in the "right" range where most bio-interactions occur, (ii) when bulk materials are reduced to the nanoscale (increasing the surface to volume ratio dramatically), they present useful properties such as bright fluorescence, plasmonic effects or superparamagnetism[9] and, remarkably, (iii) these 'nano' properties can be accessed synthetically by controlling the design of the NPs (e.g. size, shape, structure), enabling tailoring for specific purposes.

Recent progress in nanotechnology applied to medicine, also called nanomedicine, has spread the general optimism that this applied discipline can solve many medical issues (therapy, early diagnosis, sensing, limits of detection, etc.).[10] However, many challenges must be overcome before nanomedicine becomes available for all and an actual breakthrough for our society.[11] Among a variety of challenges, one could highlight the following: (i) technology transference to the healthcare system (hospitals, pharmaceutical industry, etc.); (ii) regulation of application of nanomaterials in healthcare, or (iii) guidelines for nanosafety, i.e. the safe manipulation of nanomaterials and prevention of accidental exposure to nanomaterials. Most importantly, anticipating the effects of the interaction of nanomaterials with biological systems such as their potential toxicity and bio-performance is crucial. Although there are many recent and ongoing investigations in this direction, nanotoxicology, nanopharmacology, or nano-biosensing are still very young areas of research.[11b] We would like to highlight that, ultimately, the targeted delivery of functional nanomaterials remains the key issue for achieving 'real' medical approaches.

In this review, we discuss important issues concerning the functionalization and characterization of inorganic NPs for bioapplications and, importantly, how the outermost layer on the NP design affects the suitability and performance of nanomaterials.

2. Hybrid Nature of 'Inorganic' Functional NPs for Bioapplications

This review focuses on inorganic NPs where the term 'inorganic' refers to the nature of the core component of the material. Actually, the term 'inorganic NPs' is misleading since the nanomaterials designed for a bioapplications need to be of hybrid nature. A NP comprises an inorganic core, a purposely designed primary coating made of organic or inorganic material and, typically, an organic outermost layer incidentally derived from the interaction with the surrounding medium. In the following, we take a closer look at the structure and composition of these Russian doll-like structures while focusing on the inorganic core and the chemically designed primary coating (**Figure 1**). The principles governing the formation of the outermost biomaterial layer are discussed in detail in Section 3.

2.1. The Inorganic Core

Importantly, evaluation of the inorganic material itself represents the first task prior to success in any bioapplication. There is nowadays tremendous chemical expertise in the synthesis of inorganic nanocrystals. Size, shape, and composition, the parameters that govern their physical properties, can be varied almost continuously while retaining monodispersity.[12] These parameters not only govern the physical properties of the nanocrystals (quantum yield, position of the plasmon band, saturation magnetization) but will also strongly affect their bio-performance through their interaction with physiological media. For instance, in the context of passive targeting in cancer treatments, larger NPs are preferred over their smaller counterparts as large ones (greater than 100 nm) accumulate in areas of leaky vasculature (as in solid tumors)

Dr. B. Pelaz, Dr. J. M. de la Fuente, Dr. P. del Pino
Instituto de Nanociencia de Aragon (INA)
Universidad de Zaragoza
50018 Zaragoza, Spain
E-mail: pdelpino@unizar.es
Dr. G. Charron
Univ. Paris Diderot
Sorbonne Paris Cité
ITODYS, UMR CNRS 7086
15 rue J-A de Baïf, 75205 Paris Cedex 13, France
C. Pfeiffer, Prof. W. J. Parak
Fachbereich Physik and WZMW
Philipps Universitaet Marburg
35037 Marburg, Germany
Prof. Y. Zhao, Prof. X.-J. Liang
Laboratory of Nanomedicine and Nanosafety
Division of Nanomedicine and Nanobiology
National Center for Nanoscience and Technology
China, and CAS Key Laboratory for Biomedical Effects
of Nanomaterials and Nanosafety
Chinese Academy of Sciences
Beijing 100190, P.R. China

DOI: 10.1002/smll.201201229

small NANO MICRO

to a higher degree than smaller NPs by the enhanced permeability and retention (EPR) effect.[13] For details regarding tumor-selective delivery of macromolecular drugs via the EPR effect, we refer to the recent review of Maeda.[14] On the other hand, small NPs with a hydrodynamic diameter less than 5 nm can be excreted very conveniently, which is normally preferred over unintended accumulation in organs for extended periods of time.[15] Similarly, the shape of the nanocrystal can control the rate of internalization by cells; for instance, gold nanostars are less readily internalized than gold nanospheres of equivalent dimension.[16] In addition, the composition of the core material strongly affects the toxicity response, as will be detailed later on. Some inorganic materials are more prone to corrosion than others and, thus, the 'dissolution' of NPs and metal ion shedding is different depending on the identity of the core.[17]

2.2. Organic Coatings for Stabilization

Bare inorganic NPs are colloidally unstable due to attractive interparticle van der Waals interactions, and tend to form large agglomerates. Therefore, any bioapplications based on colloidally stable NPs will require their stabilization with a coating which prevents these interactions from being dominant. Stabilization in water is usually achieved through electrostatic repulsion between like-charged NPs or through steric hindrance using hydrophilic moieties, such as polyethylene glycol (PEG) chains,[18] carbohydrates,[19] or zwitterionic appended arms.[20]

Generally, for bioapplications, any as-synthesized NP will require a coating, whether it is initially synthesized in organic media or in water. The chosen coating represents a crucial part of the design of the hybrid inorganic NP as it ultimately determines their colloidal and chemical stabilities through imparting resilience to high ionic strengths, various pH, or nonspecific protein adsorption, and shielding them against corrosion. Ideally, the coating should ensure that the NPs do not agglomerate, dissociate, or suffer any chemical reaction with the surrounding media. The coating can also open the possibility to further derivatize the nanomaterials with molecules of biological relevance by adding functional groups on their surface (Figure 1).

There are a number of strategies to derive water colloidally stable inorganic nanocrystals including ligand exchange with small, macro, or biomolecules, polymerization of a silica shell, wrapping in organic polymers, encapsulation (e.g. polymer coating, micelles, liposomes), or combinations of the aforementioned.[21]

The ligand exchange strategy is based on the displacement of the ligands surrounding as-synthesized nanocrystals by ligands with a higher affinity for the inorganic core. The choice of ligand type (i.e., thiols, amines, or alcohols) depends on the composition of the core. The selection of a ligand chain relies on the type of stabilization sought (electrostatic or steric repulsions).[18,20] Silanization consists of growing a glass shell around the NPs.[22] Polymer coating methods can involve intercalating amphiphilic polymers in the aliphatic shell of the NPs[23] or sequentially wrapping them in layers of polymers of alternating charges, a method known as the layer-by-layer (LbL) technique.[24] Finally, inorganic NPs can be derivatized into inorganic/organic hybrid materials by trapping inorganic NPs within other organic structures such as liposomes or lipospheres.[21,25]

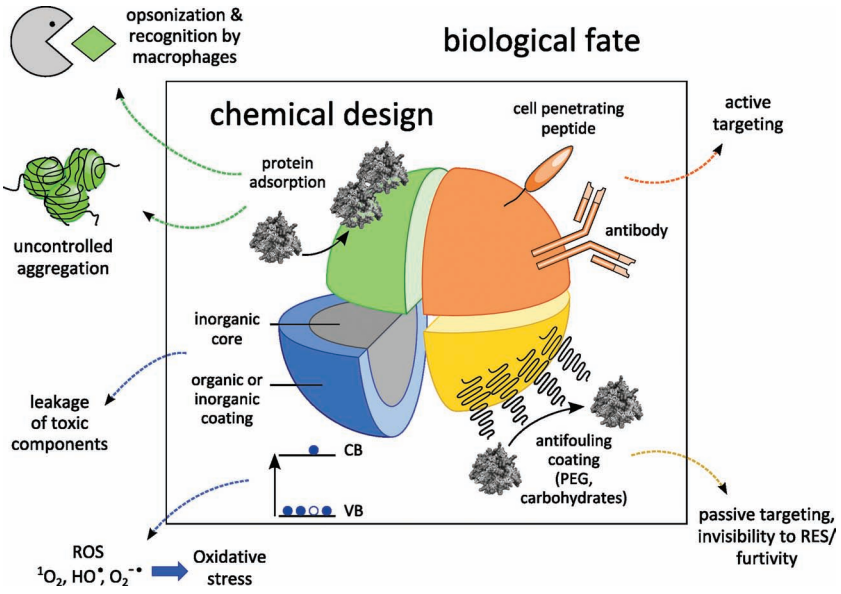

Figure 1. Schematic representation of the biological fate of engineered NPs in physiological media. The green scenario illustrates some potential adverse effects following protein adsorption; the orange scenario represents the functionalization of NPs with cell-penetrating peptides (CPPs) and antibodies; the yellow scenario emphasize the possibility of passivating NPs with suitable coatings; the blue scenario represents adverse effects such as NP dissolution and ROS generation.

2.3. Derivatization with Molecules of Biological Interest for Biofunctionalization

Once stabilization has been achieved in physiological environments by one or

Pablo del Pino graduated in Physics from Universidad de Sevilla (Spain) in 2002 and obtained his PhD from the Technische Universität München (Germany) in 2007. He then joined the group of Wolfgang Parak as postdoctoral fellow at the Ludwig-Maximilians-Universität München (Munich, Germany). Since 2009, he has been a junior scientist of the Institute of Nanoscience of Aragon (INA) from the University of Zaragoza, Spain. His work is focused on the synthesis and functionalization of inorganic NPs aimed as nanomedicines.

more of the aforementioned methods, NPs can be engineered into complex functional materials for a particular bioapplication. Nowadays, there is a wide variety of chemical methods to anchor molecules of biological relevance onto NPs, such as fluorescent tags, PEG chains, proteins, carbohydrates, DNA, peptides, siRNA, enzymes, antibodies, cyclodextrins, biotin, etc.[8,19,26] There are different approaches depending on the chemical groups present on the NPs and the ligand of interest. For instance, conjugation of NPs bearing carboxylates with amine-containing molecules/proteins can be achieved by classical carbodiimide cross coupling approaches;[27] linkage to sulfhydryl groups can be similarly achieved by way of maleimide-terminal ligands which are widely commercially available.[28] Copper(I) catalyzed azide-alkyne cycloaddition, a reaction from the click family, has been similarly employed in a number of gold nanoparticle conjugation strategies.[29] However, click cycloaddition in its copper(I) catalyzed form cannot be apply to the conjugation of quantum dots (QDs) without impairing the luminescence quantum yield. Indeed, Chan et al. demonstrated that Cu(I) ions can displace cations in the QD and subsequently quench the luminescence.[30] However, click cycloaddition can be performed in catalyst-free conditions when using a cyclooctyne derivative. This has been successfully used by Bernardin et al. in the derivatisation of CdSe/ZnS QDs.[31]

Different derivatization approaches allow for an extraordinary control over the arrangement of ligands onto NPs which can be used to tailor and predict how a nanomaterial of interest is for instance internalized by cells, among other biointeractions.[32] The pioneering work of Stellacci and coworkers showed that by patterning the coating of Au NPs the internalization process can be controlled.[33] The authors made "stripes" or defined hydrophobic/hydrophilic domains on monolayer protected NPs. Remarkalby, 'striped' NPs penetrate the plasma membrane without bilayer disruption, whereas the equivalent NPs but 'non-striped' are mostly trapped in endosomes.

The type of coating, the physico-chemical principle of stabilization, and the terminal groups control the interaction the nanomaterial not only with other NPs, but also with the surrounding biomolecules in physiological media.[34] This phenomenon has strong consequences for the performance of the nanomaterial (as a sensor, diagnostic tool, drug carrier, or more complex multitask systems),[11,35] as will be detailed in the next section.

3. NP–Protein Interactions: Insights into the Protein Corona

Biomolecules adsorbed on the surface of NPs can be responsible for many of the toxicological effects of nanomaterials as well as for defining the fate of the newly formed hybrid NP. For instance, protein adsorption can lead to the nonspecific uptake of nanomaterials into cells by receptor-mediated endocytosis.[36] Indeed, when a NP is presented to a cell, what the cell actually sees is a patchwork made of all the different organic molecules shaping the outermost layer of the NP, which can be the result of synthetic design or of nonspecific biomaterial absorption.[37] Proteins are the most abundant biomolecules in biological fluids (blood, plasma, interstitial fluids, and cytoplasm) and will therefore be the main constituent of the biomaterial layer adsorbed around NPs in physiological media. This fact has been known for long time for planar surfaces. To be able to tune, optimize, or predict the performances of engineered nanoparticles for bioapplications, one needs to understand the driving forces and parameters of the formation of the so-called protein corona. This topic has been recently reviewed in a comprehensive manner by Walkey and Chan.[38] In the following, we highlight their main findings, but the reader is referred to the original publication for more detailed insights. We later exemplify how the protein corona can affect the bioapplications of nanoparticles.

Although the physico-chemical description and characterizations of the interactions of proteins with nanoparticles are still in their infancy, it now appears that these interactions are controlled by the surface chemistry and curvature of the nanoparticle. The interaction can proceed through electrostatic attraction, hydrogen bonding, or van der Waals interactions. Nanoparticles with hydrophobic or charged surfaces interact more readily and form more stable complexes with proteins than their hydrophilic neutral counterparts. They also tend to absorb more of them. The interactions of proteins with a NP of a given core material differ from those with extended surfaces. They are also subject to variations when the curvature radius is decreased. To date, there seems to be a general trend indicating that the lower the curvature radius, the lower the affinity of the protein for the NP. Several physico-chemical effects might be responsible for this observation. First, as the curvature radius is decreased, the contact area between the protein and the surface of the nanomaterial decreases, thus weakening the interaction. Second, it has been suggested that protein–protein interactions might act as an additional driving force for the adsorption of proteins on the NP surface. Therefore, lowering the curvature radius, which increases the deflection angle between adsorbed proteins, tends to decrease protein adsorption because of weaker cooperativity. In many bioapplications of nanoparticles, minimizing the adsorption of proteins is highly desirable. This can be achieved by coating the NPs with anti-fouling, hydrophilic, charge-neutral polymers, such as PEG, polysaccharide, or zwitterionic poly(carboxybetaine methacrylate).[18–20] The surface of the NP is then said to be 'passivated'. The development of anti-fouling polymers is an active area of research (Figure 1, yellow scenario).

One should bear in mind that, although trends for protein–NP interactions have emerged, counter-examples are not rare. It is to be expected that finer descriptions will emerge as the field matures. But for now, each supramolecular interaction between NPs and proteins is a nontrivial phenomenon determined by the intrinsically complex nature of NPs and proteins. It should be assayed systematically when designing a nanomaterial for a bioapplication.

For most proteins interacting with nanomaterials, adsorption is associated with some conformational change, the degree of which is highly variable and can span the entire range from overall structural integrity to full denaturation. Within this range, loss or impairment of biological activity can

small NANO MICRO

be expected. The extent of conformational distortion largely depends on the surface chemistry of the nanomaterial. As for the extent of the interaction, charged or hydrophobic nanoparticles tend to give rise to larger conformational changes than their hydrophilic neutral counterparts. Likewise, the larger the NP, the greater the distortion. However, it is important to acknowledge here that small enough NPs are capable of introducing local denaturation effects.[39] The structure of the protein also strongly influences the degree of the conformational change, with protein capable of strong internal stabilizing interactions such as disulfide or salt bridges, displaying superior resilience to distortion.

Importantly, as it strongly depends on the surface chemistry of the NPs, denaturation of a protein or impairment of its biological activity can be avoided or tailored by tuning the organic coating. Adsorption of proteases deserves special attention as some of them can be involved in the 'digestion' of endocytosed NPs. For instance, Chymotrypsin (ChT), whose enzymatic activity is well characterized, is particularly attractive for in vitro investigations. Based on amino acid-functionalized gold nanoparticles, Rotello and co-workers demonstrated how surface charge and hydrophobic side chains affect the binding affinity and denaturation of ChT. Although electrostatic interactions between NPs and ChT were proven to be the predominant driving force contributing to the complex formation, the hydrophobic interaction between the hydrophobic patches of the NP's ligands (receptors) and proteins enhanced the complex stability. Remarkably, control over association/dissociation as well as stabilization/denaturation of ChT onto NPs could be readily tailored by introducing diverse terminal derivatizations (i.e. tuning the organic coating).[40]

Recently, Au NPs of different sizes (5 to 100 nm) stabilized by citrate ligands were mixed with the most abundant plasma protein, namely human serum albumin (HSA).[41] The authors evidenced the formation of a protein corona via electrostatic interactions and hydrogen bonding. In contrast to previous examples, the structure of the adsorbed proteins was largely retained upon the interaction with the metal surface, although distortion increased as the curvature decreased, in line with the trends exposed earlier. Importantly, adsorbed HSAs became more resistant to complete thermal denaturation than free proteins.

Impairment of biological activity is likely to arise when large conformational changes occur but do not necessarily mean that the structural integrity is lost. Indeed, interaction with the NP surface can bury the active sequence of a given protein in the protein corona and hide it from the physiological environment. In addition, protein adsorption on the nanomaterials does not necessarily occur through interaction with the NP surface but can also stem from protein–protein interactions between free proteins and the primary protein corona. Burying of the primary binding protein or of the active domain of a secondary binder can result in the loss of biological activity.

In addition, it is important to stress the dynamic character of the protein corona, which reflects the instantaneous composition of the physiological environment surrounding the nanomaterial. As a NP traffics across different cell compartments, the protein corona is likely to be modified in structure or in composition. For instance, studies on the serum albumin model protein, i.e. bovine serum albumin (BSA), have shown that, under different pH conditions, this protein could undergo various conformational changes.[42] Therefore, trafficking from endosomes to lysosomes is expected to affect the overall structure of a given NP.

The protein corona not only affects the structure and biological activity of the adsorbed proteins but may also strongly influences the properties of the NP and hence its physical performance and biological fate. First, adsorption of a primary and secondary corona increases to a large extent the effective diameter of the nanoparticle in the physiological medium. For instance, the corona of 30–50 nm citrate-stabilized gold NPs has been reported to be 21–23 nm thick, evidencing in this case adsorption of multiple layers of proteins.[41,43] In contrast, other studies have pointed out the formation of only one saturated monolayer of proteins which depends on the NP geometry and NP-to-protein ratio.[44] Clearly, different concepts about the protein layer exist, and those depend on the NP model, the proteins, and the detection techniques used. In any case, the thickness of the protein corona increases the minimal interparticle distance compared to buffer conditions, a fact that has strong consequences on applications where optical coupling of NPs is required. The reverse situation can also be observed, namely, uncontrolled NP aggregation through interparticle bridging by proteins, possibly triggered upon protein denaturation.[38,45] Finally, adsorption of a protein corona can affect the physical properties of the individual NP itself, for instance by shifting its plasmon resonance[41] or altering its luminescence quantum yield.[46]

The aforementioned examples regarding protein-NP interactions illustrate how complex and diverse the structures resulting from interfacing NPs with proteins can be. The protein corona has a large influence on the performances of the nanomaterials as it impacts both its biological fate and its physical properties, as will be illustrated later on. Guidelines have been drawn to understand and sometimes predict the formation of this protein corona, although there is still much to do in this direction. More importantly, the chemical availability of various coatings allows for tailoring of this interaction and optimization of the bio-performances.

4. Toxicological Effects Related to Engineered NPs

In the following section, we aim at illustrating how the structure and composition of engineered nanoparticles may adversely affect the interplay between the nanoparticle and the biological system. We focus on both the fate of the NPs in the biological system and the fate of the biological system exposed to the nanomaterial.

4.1. Leakage of Toxic Material

Leakage of toxic components from the nanomaterial is possibly the simplest mechanism responsible for nanoparticle

cytotoxicity. The toxic components can be released from either the inorganic core, as toxic ions, or from the stabilizing coating shell, as surfactants, ligands, or polymers (Figure 1, blue scenario).[17,47]

The shape and composition of the inorganic material are determining factors in the dissolution or corrosion of the core. For instance, Au NPs are believed to be less prone to corrosion than their Ag counterparts, which may leak toxic Ag^+ ions. For this reason, Au NPs are often preferred over Ag NPs in surface-enhanced Raman spectroscopy (SERS) experiments, despite the superior enhancement abilities of the latter.[48] However, the sensitivity of Ag NPs to corrosion can be turned into an advantage in anti-bacterial applications.[49]

The dissolution of NPs can also be tailored synthetically by modifying the composition of the core material. For instance, doping ZnO NPs with Fe reduces their cytotoxicity.[50] Encapsulation into a robust inorganic matrix can also prevent dissolution of the core material. Following this principle, silanization helps prevent the release of toxic Cd ions from QDs.[51]

Organic coatings can also be responsible for cytotoxicity. For instance, gold nanorods have been believed for a while to be cytotoxic while later studies indicated that the actual cytotoxicity stems from the surfactant used for their anisotropic growth, namely cetyltrimethylammonium bromide (CTAB).[36,52] Common strategies to avoid leakage of toxic organic components involve surface cross-linked coatings such as silica shells, or wrapping in cross-liked polymers.[21b]

4.2. Production of ROS

Inorganic nanoparticles can produce reactive oxygen species (ROS), such as singlet oxygen, radical hydroxide, or superoxide, through photochemical or Fenton-like reactions.[53] These ROS in turn trigger oxidative stress in the biological system (Figure 1, blue scenario).

In vitro, this phenomenon needs to be taken into account when monitoring cellular analytes or parameters as this brings about cellular defense mechanisms that can interfere with the measurements. Hence, prior to SERS measurement of intracellular potential via a redox probe adsorbed on gold nanoshells, Auchinvollet et al. checked that the SERS substrate did not induce ROS production compared to pristine cells using independent ROS fluorimetric assays.[54]

In vivo, ROS production is thought to be the main mechanism responsible for nanotoxicity affecting the blood, spleen, kidney, respiratory system, liver, or immune system (immunotoxicity).[55] Sequestration of NPs by phagocytic cells in the organs of the reticuloendothelial system (RES) makes organs such as the liver and spleen major targets of oxidative stress.[56] Other organs exposed to high blood flow such as the kidneys and lungs are also subject to oxidative stress.[57]

4.3. Interaction with Organelles and Organelle Impairment

In the context of in vitro studies, cationic NPs are generally observed to be more toxic to cells than their neutral or anionic counterparts.[33,,36,58] This phenomenon may be due to their higher degree of cell interaction and/or internalization compared to neutral and negatively charged NPs,[24,,58,59] although the 'big picture' seems to be more complex.[60] A variety of mechanisms have been proposed to explain the observed cytotoxicity of cationic NPs. These are largely dependent on the NP model, cell line, concentration of NPs, and possibly other experimental variables. Among distinct cytotoxic processes, there are examples for hole formation, membrane thinning, and/or erosion due to the strong interaction of cationic NPs and the cell membrane.[58,60,61] The proton sponge effect by which acidic endosomal compartments can be damaged have been also widely proposed as leading to toxicity. This is typically followed by mitochondrial injury[58,62] and also by membrane depolarization.[58,63] In general, cationic nanomaterials, once introduced into the circulatory system, have been shown to strongly interact with red blood cells, destabilize cell membranes, and cause cell lysis.[55a]

NPs coated with a variety of cationic molecules such as polyamidoamine (PMAM) and polypropylenimine (PPI) dendrimers of different generations, cell penetrating peptides, amine molecules, polyethyleneimine (PEI), and diethylaminoethyl-dextran, to name a few, have been proven to induce defects in lipid membranes.[60,61,64] A recent work of Lin et al. addressed the interaction of NPs with model lipid membranes by molecular dynamics (MD) simulations.[65] Their simulation results reveal that the sign as well as the surface charge density on NPs determine their fate, i.e., repulsion of, adhesion to, or penetration into lipid membranes. Cationic NPs are shown to strongly adhere to and penetrate into the membrane but more critical is the fact that at high surface-charge density, cationic NPs are able to disrupt the membrane and introduce defects. Although these simulations do not take into account the presence of biomolecules in the environment (e.g. protein coronae), which are likely to absorb in such cationic surfaces, they are in excellent agreement with previous equivalent experimental works.[33,58,61] Disruption of the cellular membrane can lead to exchange of the medium between extracellular fluid and cytosol, whichmay cause acute cytotoxicity.[60] To add complexity to the big picture, the work of Xia et al. showed that cationic particles exert differential toxicity on different cell lines (i.e. either viable or apoptotic and/or necrotic features) upon NP uptake.[66]

4.4. Impairment of Biomolecule Functions

As explained earlier, the adsorption of proteins onto NPs is paired with conformational changes, which can lead to loss of biological activity and impair the cell machinery. Cathepsins are proteases found in lysosomes and endosomes of different mammalians cells which are mainly involved in protein degradation and antigen presentation (for adaptative immune response).[67] In a recent work, the ability of a number of Ag and Au NPs of different sizes and coatings to distort cathepsin activity to different degrees was confirmed, even when the cytotoxicity of the type of NP was not an issue.[68] Although these results should be considered with caution because they were performed with one cell line and a limited set of NPs,

NANO MICRO small

misregulation of cellular cathepsin activity can be a critical issue as it may alter the adaptative immune response.

Alteration of biological activity can trigger defense mechanisms from the cell, such as an inflammatory response. Recently, Minchin and co-workers[69] showed that negatively charged NPs (polyacrylic acid-coated gold NPs) can strongly bind to (forming a 'hard' protein corona) and consecutively induce unfolding of fibrinogen, a plasma protein. As a result, a chain of activation (receptor Mac-1) and corresponding signaling pathway (NF-$\alpha\beta$) trigger the release of inflammatory cytokines.

4.5. Recognition by the Immune System, and Complement Activation and Opsonization

A major fate of nanomaterials in physiological media is opsonization, which typically leads to phagocytosis of the opsonized body by macrophages.[55,70] Opsonization is mediated by the recognition by macrophages of plasma proteins called opsonins. As proteins, opsonins also take part in the formation of the protein corona and are therefore responsible for the opsonization of the NPs.[38,71] This immunological response leads to rapid clearance of the nanomaterial from the blood stream and accumulation in the liver and spleen.[55a]

In the process of secondary protein corona formation, proteins adsorb onto nanoparticles via protein–protein interactions. These protein interactions can be specific, meaning that they would occur in the absence of the nanomaterial, or nonspecific. The secondary nonspecific binding events are driven by electrostatic or hydrophobic interactions between free proteins and charged or hydrophobic protein domains on the corona that have been exposed as a result of conformational changes. These interactions do not occur in the native system in the absence of the nanomaterial. The resulting complexes are detected as an abnormality by the biological system and therefore trigger an immune response.[38,72] Importantly, NPs decorated with anti-fouling coatings that minimize protein adsorption (as described in Section 3) can reduce the interaction with the phagocytic system.[19,73]

5. Limitations Derived from Interfacing Sensing Nanoplatforms and Physiological Environments

In the following, we review the limitations of two relevant and widely used bio-sensing nanoplatforms, SERS and Förster resonant energy transfer (FRET), related to the complexity of biological systems.

5.1. SERS

SERS is a spectroscopic technique by which the Raman signal of an analyte is strongly enhanced when sitting in close proximity to the surface of a nanostructured noble metal (Au, Ag).[74] Enhancement factors (EFs) are strongly localization-dependent and drop dramatically when moving away from the surface of the metal. In general, isolated nanoparticles do not provide EFs high enough to be responsible for the observed SERS signal of a nonresonant analyte. The signal then stems from 'hot spots', gaps of a few nanometers within agglomerates of NPs. Some nanoparticles displaying sharp apexes or strong roughness give rise to EFs comparable to that of coupled nanoparticles and can even enable single molecule detection.[75]

Intracellular SERS experiments mainly focus on two objectives: (i) the measurement of intracellular analytes of endogenous or exogenous nature or, alternatively, of cell chemical parameters (pH, redox potential); (ii) the tracking of cellular moieties or organelles through their labelling with SERS-encoded substrates.

Due to the narrow bandwidth of Raman signals, intracellular SERS allows for the detection of various biological species having specific vibrational peaks such as DNA, lipids, or specific amino acids within proteins.[76] When recorded with high spatial resolution, SERS spectra can be exploited to map the distribution of molecular species.[77] Exogenous molecules attached to or adsorbed onto SERS substrates can also be detected. Their SERS spectra can be exploited for instance to monitor the kinetics of uptake or metabolization of a drug within a cell.[78] The most advanced intracellular SERS applications involve the measurement of cell parameters through the use of SERS substrates encoded with molecular probes that are strongly adsorbed onto the substrate. The SERS spectra of these probes are sensitive to the targeted parameters and can therefore be exploited for the ratiometric quantitative determination of the parameters of interest, e.g. pH values,[79] or intracellular redox potentials.[54]

Alternatively, intracellular SERS can be used as a labelling technique for a given cell moiety. This strategy was followed by Rector and co-workers to track the fate of an internalised IgE receptor.[79b] Their sensor consisted of a SERS substrate encoded with a pH-senstive Raman reporter and bearing 2,4-dinitrophenol-L-lysine (DNP) ligands. The DNP ligands could be recognised by DNP-specific IgE which in turn associated with IgE receptors on the cell membrane. The SERS encoded substrate allowed for the monitoring of the traffic of IgE receptor within the cell. In addition, the pH-sensitive SERS spectrum enabled the identification of the compartment in which the receptor stood (endosome or lysosome).

SERS substrates can be cytotoxic (Figure 1, blue scenario) and, therefore, the first key to meaningful SERS measurements of biological activity is to ensure that the SERS probe does not largely impair the normal functioning of the cell on the timescale of the measurement. In the same line, when measuring endogenous analytes or cell parameters, it is important to make sure that the SERS substrate or integrated probe does not affect the target of the measurement.[54]

Cellular mapping of the distribution of analytes has been routinely done through the use of molecular fluorophores or genetically encoded fluorescent proteins. SERS imaging is advantageous compared to fluorescence imaging because of the narrow signal bandwidth that enables multiplexion. However, SERS can have a major disadvantage compared

to molecular probe based techniques: When using smooth SERS nanoparticles (nanospheres, nanorods), which are the most common type of substrate for intracellular measurements, the obtaining of a SERS spectrum requires the formation of agglomerates. These agglomerates, let alone the SERS substrates themselves, are generally not evenly distributed throughout the cells and, therefore, not all cell areas are probed with equal probability.[76] Accordingly, the absence of an analyte signal in a cell compartment does not necessarily mean that the analyte is not present. This difficulty may be overcome by cross-referencing SERS mapping with TEM imaging to map the areas that are rich in agglomerates and by enlarging the random sample size. However, in most intracellular mapping, it is not enough to identify a given analyte or to co-localise two target species throughout the cell. One aims to quantify the relative concentrations. This task is rendered tedious by the distribution of EFs throughout agglomerates within the cell. Indeed, the protein corona might increase the NP-to-NP distance in the agglomerates and either strongly affect the EF within the hot spot or prevent the formation of hot spots altogether (Figure 1, green scenario).[38] The reverse effect can also be observed. Denatured proteins within protein coronas can cross-link NPs and lead to uncontrolled agglomerates of unknown EFs. An elegant strategy to overcome both the issues of mapping and of reproducible EFs over the cell involves the use of nanoparticles displaying sharp apexes that provide strong enough EFs to give rise to decent SERS spectra as single NPs. This has been achieved by Brust and co-workers using SERS-encoded gold nanostars.[16] Another strategy is based on the building of agglomerates made of smooth NPs prior to cell exposure. This idea has been recently developed by Kotov and co-workers, who synthesised controlled assemblies made of a central gold nanorod and surrounding gold nanospheres of various topologies (end, side, and satellite).[80] Using these nanostructures, intracellular lipids were detected with sensitivities that depended on the type of assembly (**Figure 2**).

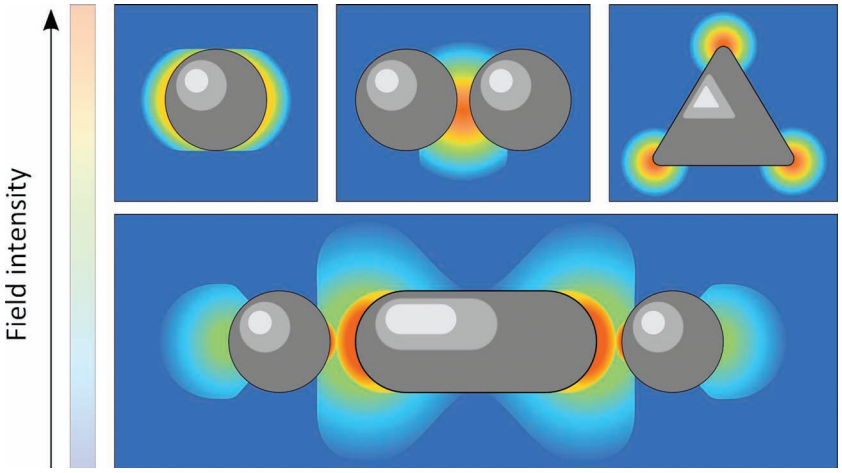

Figure 2. Electromagnetic field intensity maps for a spherical plasmonic NP, a dimer, a prism as an example of anisotropic NP and an 'end assembly' as described in reference 80.

Quantification can also be a hassle due to the complexity of the intracellular environment. Difficulties arise when attempting to quantify a given protein in a physiological environment because of the presence of a large amount of proteins surrounding the SERS substrate.[76] Any protein present within a few nanometers of the SERS substrate surface will see its spectrum enhanced. Hence, the resulting SERS spectrum is expected to be very complex as it will display not only the vibrational signature of the protein of interest, but also the contribution of all other proteins within the protein corona. Moreover, as proteins are made of similar building blocks, namely amino-acids, they display very close spectral signatures that can lead to peak overlaps, further complicating the spectrum. Advanced deconvolution techniques are then required to assess the presence of the targeted protein and further quantification is expected to be challenging. The targeted protein is not even guaranteed to see its Raman spectrum enhanced since it might never reach the metal surface. Indeed, proteins with different affinities compete for adsorption on the nanomaterial surface. Hence, if the targeted protein has a relatively weak affinity for the SERS substrate compared to other surrounding proteins, and/or if its relative concentration is low, it might never be detected. The same observation holds relevance for other physiological molecules of interest, such as lipids or sugars which might never reach the hot spots if they cannot efficiently compete with the protein corona.

In several intracellular SERS experiments aimed at monitoring exogenous analytes or Raman reporters, the molecule of interest is adsorbed onto the SERS substrate prior to its internalisation by the cells.[78,79] The Raman-active molecule can be either physisorbed (as, for example, Rhodamine 6G or Nile Blue) or more firmly anchored to the SERS substrate through a thiol or amine coordination to the metal.[81] Physisorbed dyes are usually chosen because, as resonant molecules in the visible range, they provide very intense SERS spectra with high signal-to-noise ratios. However, their SERS signals rapidly vanish due to displacement of the Raman label by the protein corona (Figure 1, green scenario).[81] In contrast, coordinated molecules (examples so far were nonresonant) display intracellular SERS signals that are stable on a 24 h timescale. Therefore, to monitor cell parameters such as pH or redox potential, it is advisable to use thiol- or amine-bearing probes. In addition, the use of ratiometric probes appears particularly appealing since they enable quantification independent of the amount of probe or of the EF, provided that the latter gives rise to a sufficient signal-to-noise ratio.[82]

5.2. FRET

Förster resonant energy transfer has long since been exploited for the sensing of biomolecular recognition processes using organic dyes and green fluorescent protein (GFP) derivatives. The transfer of quantum dots (QDs) into aqueous solutions

NANO MICRO small

has enabled their integration into new FRET set-ups where the QDs are mostly exploited as donors. This research field has been highly active in the past ten years because of the advantageous optical properties of QDs over conventional molecular fluorophores.[83] However, FRET sensing of biomolecules or bio-events using nanomaterials faces challenges inherent to the interaction of biomaterials with NPs. These can be foreseen at two developmental stages: (i) the optimisation of the sensor 'in synthetico', that is, in buffers and relatively simple analytical media; (ii) the implementation of the sensor 'in physiologico', that is, in physiological conditions (in protein-rich environments, such as plasma or cells).

The protein corona and the related conformational changes induced by it have tremendous impact on FRET sensing since they can affect the recognition mechanism involved in the formation or dissociation of the FRET pair (cf. Section 3 and Figure 1, green scenario). To the best of our knowledge, there is no general trend and each case should be examined carefully. For instance, Dezhurov et al. have observed that BSA retains its folding capability upon recognition of oleic acid once supported on QDs.[84] This enabled the sensing of oleic acid through the modulation of FRET efficiency between the QD and the dye-labelled BSA upon binding. This result is in contrast with the loss of substrate ability of siRNA adsorbed onto up-converting nanocrystals (upCNs) for RNA-ase, observed by Jiang and Zhang (**Figure 3**).[85] This impairment of activity was turned into an advantage because it prevented degradation of the siRNA prior to delivery into the cytoplasm. To avoid impairment of biological activity of a ligand, recognition unit, or enzyme, several strategies have proven successful. Introducing rigid or long spacers into the linkers between the NP and biomolecules prevents their strong interaction, thus preserving biological activity.[86] Conjugating the nanocrystals with an anti-fouling coating (Figure 1, yellow scenario) also provided good results.[87] However, the advantages of long spacers or anti-fouling coatings for preserving bioactivity may come at the price of reduced optical performance. Indeed, the accumulation of conjugation-coating spacer and biomolecules can lead to rather high donor-to-acceptor distances and therefore poor FRET efficiencies that limit the sensitivity of the sensor. This is particularly true for sandwich immunoassays, where the recognition of the target necessitates assembly of two antibodies, which are rather heavy proteins (Figure 1, orange scenario). This constraint puts more pressure on finely tuning the spectral properties of donor–acceptor pairs to maximise the Förster radius. Several materials look appealing to address this issue. First, aptamers can be considered as lighter alternative recognition units,[88] although their comparatively lower complexation constants can lead to cross-talk in multiplexed assays. Second, as acceptors, gold nanoparticles tend to give rise to larger Förster radii than conventional dyes.[89] Finally, the use of a lanthanide complex as a donor and a QD as an acceptor enables maximal spectral overlap between their respective emission and absorption spectra and consequently provides Förster radii on the order of 10 nm.[87]

Another difficulty in optimising the sensitivity of the FRET sensor stems from the distribution of FRET configurations within the sample, which originate from the distribution of donor-to-acceptor ratios and the distribution or relative orientations and distances between them.[84,89] Control over stoichiometry or geometrical parameters is especially difficult to achieve when there is significant nonspecific interaction between the biomolecules and the nanocrystals (Figure 1, green scenario). However, anti-fouling coatings seem to overcome this issue, and control over donor–acceptor stoichiometry has been reported using this strategy (Figure 1, yellow scenario).[87]

As protein-rich environments have very different physico-chemical properties (optical index, polarity, etc.) compared to buffer solutions, the photophysical performances of each component of the FRET pair are likely to be modified. Indeed, Hildebrandt and co-workers observed both dynamic and static quenching of QDs upon introduction into various protein-rich media, in agreement with the formation of a protein corona.[46] Importantly, the extent of dynamic and static quenching varied depending on the composition of the medium, on the size, composition and surface coating of the QD. No general trend could be formulated, leading to the conclusion that 'not every QD is alike'. Hence, the photophysical properties must be re-evaluated for each medium and each nanocrystal sample.

Much like for the SERS assays, nanocrystal-based FRET sensors can see their performances brought down by competitive adsorption of one part of the donor–acceptor construction and proteins. For instance, attachment of polyhistidine-containing peptides tagged with a Tb complex to CdSe/ZnS core–shell QDs has been shown to be unsuccessful in plasma, while the reverse was true in TRIS- or BSA-containing buffers (tris(hydroxymethyl) aminomethane (TRIS) and bovine serum albumin (BSA)).[46] The polyhistidine moiety, which has a strong affinity for the Zn-rich QD shell, is also present in plasma proteins in rather abundant concentration. Competitive adsorption of these histidine-rich proteins was thought to be the main cause of poor FRET performance in plasma. A stronger linker, possibly crosslinked around the NP surface, might circumvent this limitation.

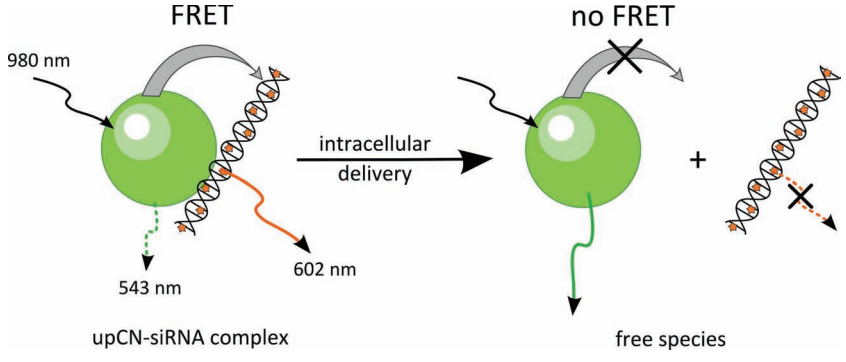

Figure 3. FRET scheme between siRNA and up-converter nanocrystals (upCN) used in reference 85 to monitor the intracellular delivery of siRNA.

The protein corona, even if it does not displace components of the FRET edifice,

can prevent successful FRET events by sterically hindering the pairing of donor and acceptor. The use of FRET assays in which a preformed donor–acceptor pair dissociates upon recognition of the analyte, or alternatively in which the FRET path is broken, might overcome this hindrance,[85,90] although the intracellular assembly of a donor–acceptor pair from initially free components has also been reported.[91]

6. Conclusion

Despite the need for standard protocols for assessing the toxicity and bioperformance of each new functional nanomaterial, these are still scarce or still under development. Interfacing engineered nanomaterials with biological fluids and predicting their biological fate are not trivial issues, since the interplay between nanomaterials and biological components is dictated by a complex scenario of interactions. The structural integrity and function of nanomaterials can be greatly compromised by the presence of components of physiological fluids. The most relevant parameters in the NP design are: synthesis of the inorganic core (composition, size, shape, and structure, e.g., solid or hollow), stabilization (i.e. derivatization techniques towards enhanced colloidal stability in physiological media) and, lastly, functionalization with molecules of biological relevance for enhanced bioperformance. Any new nanomaterial has to be critically analyzed, as many adverse effects can be triggered accidentally (e.g. toxicity, allergy, genotoxicity, etc.) and/or the performance of the nanomaterial (e.g. as a therapeutic or diagnosis agent, or nano-biosensor) can be compromised. However, some trends concerning physicochemical descriptions are emerging and these 'nano' attributes can be accessed synthetically, enabling tailoring for specific purposes and partly preventing adverse effects such as cytotoxicity, opsonization, leakage of toxic NP components, nonspecific NP–protein interactions, distortion of biological relevant proteins.

Acknowledgements

B.P. and G.C. contributed equally to this work. This work was supported by the grant ERC-Starting Grant 239931-NANOPUZZLE project and the MAT2011-26850-CO2-01 project of the Spanish Ministry of Science and Innovation. J.M.F. thanks ARAID for financial support. W.J.P. acknowledges funding by BMBF Germany (project UMSICHT). This work was also supported by the Chinese Academy of Sciences visiting professorship for senior international scientists Grant No. 2012T1J0021 to W.J.P.

[1] W. P. Faulk, G. M. Taylor, *Immunochemistry* **1971**, *8*, 1081.
[2] P. S. Weiss, *ACS Nano* **2010**, *4*, 1771.
[3] N. Kotov, *Nat. Mater.* **2011**, *10*, 903.
[4] M. E. Davis, J. E. Zuckerman, C. H. J. Choi, D. Seligson, A. Tolcher, C. A. Alabi, Y. Yen, J. D. Heidel, A. Ribas, *Nature* **2010**, *464*, 1067.
[5] A. Z. Abbasi, F. Amin, T. Niebling, S. Friede, M. Ochs, S. Carregal-Romero, J.-M. Montenegro, P. R. Gil, W. Heimbrodt, W. J. Parak, *ACS Nano* **2011**, *5*, 21.
[6] X. Wang, X. Qian, J. J. Beitler, Z. G. Chen, F. R. Khuri, M. M. Lewis, H. J. C. Shin, S. Nie, D. M. Shin, *Cancer Res.* **2011**, *71*, 1526.
[7] a) M. Bruchez, M. Moronne, P. Gin, S. Weiss, A. P. Alivisatos, *Science* **1998**, *281*, 2013; b) W. C. W. Chan, S. Nie, *Science* **1998**, *281*, 2016.
[8] a) A. P. Alivisatos, K. P. Johnsson, X. Peng, T. E. Wilson, C. J. Loweth, M. P. Bruchez, P. G. Schultz, *Nature* **1996**, *382*, 609; b) C. A. Mirkin, R. L. Letsinger, R. C. Mucic, J. J. Storhoff, *Nature* **1996**, *382*, 607.
[9] W. J. Parak, D. Gerion, T. Pellegrino, D. Zanchet, C. Micheel, S. C. Williams, R. Boudreau, M. A. Le Gros, C. A. Larabell, A. P. Alivisatos, *Nanotechnology* **2003**, *14*, R15.
[10] S. Rannard, A. Owen, *Nano Today* **2009**, *4*, 382.
[11] a) A. Nel, T. Xia, L. Mädler, N. Li, *Science* **2006**, *311*, 622; b) P. Rivera Gil, G. n. Oberdörster, A. Elder, V. c. Puntes, W. J. Parak, *ACS Nano* **2010**, *4*, 5527.
[12] a) W. J. Parak, *Science* **2011**, *334*, 1359; b) E. C. Scher, L. Manna, A. P. Alivisatos, *Philos. Trans. Roy. Soc. A* **2003**, *361*, 241.
[13] Y. Cheng, J. D. Meyers, A.-M. Broome, M. E. Kenney, J. P. Basilion, C. Burda, *J. Am. Chem. Soc.* **2011**, *133*, 2583.
[14] H. Maeda, *Bioconjugate Chem.* **2010**, *21*, 797.
[15] X.-D. Zhang, D. Wu, X. Shen, P.-X. Liu, F.-Y. Fan, S.-J. Fan, *Biomaterials* **2012**, *33*, 4628.
[16] L. Rodriguez-Lorenzo, Z. Krpetic, S. Barbosa, R. A. Alvarez-Puebla, L. M. Liz-Marzan, I. A. Prior, M. Brust, *Integr. Biol.* **2011**, *3*, 922.
[17] a) R. Ma, C. Levard, S. M. Marinakos, Y. Cheng, J. Liu, F. M. Michel, G. E. Brown, G. V. Lowry, *Environ. Sci. Technol.* **2011**, *46*, 752; b) X. Li, J. J. Lenhart, H. W. Walker, *Langmuir* **2011**, *28*, 1095; c) J. Zook, S. Long, D. Cleveland, C. Geronimo, R. MacCuspie, *Anal. Bioanal. Chem.* **2011**, *401*, 1993; d) K.-H. Kim, J.-U. Kim, S.-H. Cha, J.-C. Lee, *J. Am. Chem. Soc.* **2009**, *131*, 7482; e) Y. Yang, J. M. Mathieu, S. Chattopadhyay, J. T. Miller, T. Wu, T. Shibata, W. Guo, P. J. J. Alvarez, *ACS Nano* **2012**, *6*, 6091.
[18] B. C. Mei, K. Susumu, I. L. Medintz, J. B. Delehanty, T. J. Mountziaris, H. Mattoussi, *J. Mater. Chem.* **2008**, *18*, 4949.
[19] M. Moros, B. Pelaz, P. Lopez-Larrubia, M. L. Garcia-Martin, V. Grazu, J. M. de la Fuente, *Nanoscale* **2010**, *2*, 1746.
[20] V. V. Breus, C. D. Heyes, K. Tron, G. U. Nienhaus, *ACS Nano* **2009**, *3*, 2573.
[21] a) R. Mout, D. F. Moyano, S. Rana, V. M. Rotello, *Chem. Soc. Rev.* **2012**, *41*, 2539; b) S. K. Basiruddin, A. Saha, N. Pradhan, N. R. Jana, *J. Phys. Chem. C* **2010**, *114*, 11009; c) T. Pellegrino, L. Manna, S. Kudera, T. Liedl, D. Koktysh, A. L. Rogach, S. Keller, J. Radler, G. Natile, W. J. Parak, *Nano Lett.* **2004**, *4*, 703; d) Y. Chen, Y. Gao, H. Chen, D. Zeng, Y. Li, Y. Zheng, F. Li, X. Ji, X. Wang, F. Chen, Q. He, L. Zhang, J. Shi, *Adv. Funct. Mater.* **2012**, *22*, 1586.
[22] L. M. Liz-Marzan, M. Giersig, P. Mulvaney, *Langmuir* **1996**, *12*, 4329.
[23] T. Pellegrino, S. Kudera, T. Liedl, A. M. Javier, L. Manna, W. J. Parak, *Small* **2005**, *1*, 48.
[24] T. S. Hauck, A. A. Ghazani, W. C. W. Chan, *Small* **2008**, *4*, 153.
[25] P. del Pino, A. Munoz-Javier, D. Vlaskou, P. Rivera Gil, C. Plank, W. J. Parak, *Nano Lett.* **2010**, *10*, 3914.
[26] a) S. Puertas, P. Batalla, M. Moros, E. Polo, P. del Pino, J. M. Guisàn, V. Grazú, J. M. de la Fuente, *ACS Nano* **2011**, *5*, 4521; b) M. Moros, B. Hernáez, E. Garet, J. T. Dias, B. Sáez, V. Grazú, Á. González-Fernández, C. Alonso, J. M. de la Fuente, *ACS Nano* **2012**, *6*, 1565; c) H. W. Child, P. A. del Pino, J. M. de La Fuente, A. S. Hursthouse, D. Stirling, M. Mullen, G. M. McPhee, C. Nixon, V. Jayawarna, C. C. Berry, *ACS Nano* **2011**, *5*, 7910; d) B. Pelaz, V. Grazu, A. Ibarra, C. Magen, P. del Pino, J. M. De La Fuente, *Langmuir* **2012**, *28*, 8965; e) W. R. Algar, D. E. Prasuhn, M. H. Stewart, T. L. Jennings, J. B. Blanco-Canosa, P. E. Dawson, I. L. Medintz, *Bioconjugate Chem.* **2011**, *22*, 825.

[27] a) D. Bartczak, A. G. Kanaras, *Langmuir* **2011**, *27*, 10119; b) D. A. East, D. P. Mulvihill, M. Todd, I. J. Bruce, *Langmuir* **2011**, *27*, 13888.

[28] a) H. Ba, J. Rodríguez-Fernández, F. D. Stefani, J. Feldmann, *Nano Lett.* **2010**, *10*, 3006; b) T. L. Jennings, S. G. Becker-Catania, R. C. Triulzi, G. Tao, B. Scott, K. E. Sapsford, S. Spindel, E. Oh, V. Jain, J. B. Delehanty, D. E. Prasuhn, K. Boeneman, W. R. Algar, I. L. Medintz, *ACS Nano* **2011**, *5*, 5579.

[29] a) A. Gole, C. J. Murphy, *Langmuir* **2008**, *24*, 266; b) D. Baranov, E. N. Kadnikova, *J. Mater. Chem.* **2011**, *21*, 6152; c) N. Li, W. H. Binder, *J. Mater. Chem.* **2011**, *21*, 16717.

[30] Y.-H. Chan, J. Chen, Q. Liu, S. E. Wark, D. H. Son, J. D. Batteas, *Anal. Chem.* **2010**, *82*, 3671.

[31] A. Bernardin, A. l. Cazet, L. Guyon, P. Delannoy, F. o. Vinet, D. Bonnaffé, I. Texier, *Bioconjugate Chem.* **2010**, *21*, 583.

[32] A. Verma, F. Stellacci, *Small* **2010**, *6*, 12.

[33] A. Verma, O. Uzun, Y. Hu, Y. Hu, H.-S. Han, N. Watson, S. Chen, D. J. Irvine, F. Stellacci, *Nat. Mater.* **2008**, *7*, 588.

[34] C. M. Niemeyer, *Angew. Chem. Int. Ed.* **2001**, *40*, 4128.

[35] A. E. Nel, L. Madler, D. Velegol, T. Xia, E. M. V. Hoek, P. Somasundaran, F. Klaessig, V. Castranova, M. Thompson, *Nat. Mater.* **2009**, *8*, 543.

[36] a) S. George, S. Pokhrel, T. Xia, B. Gilbert, Z. Ji, M. Schowalter, A. Rosenauer, R. Damoiseaux, K. A. Bradley, L. Mädler, A. E. Nel, *ACS Nano* **2009**, *4*, 15; b) B. D. Chithrani, A. A. Ghazani, W. C. W. Chan, *Nano Lett.* **2006**, *6*, 662; c) A. M. Alkilany, P. K. Nagaria, C. R. Hexel, T. J. Shaw, C. J. Murphy, M. D. Wyatt, *Small* **2009**, *5*, 701.

[37] I. Lynch, A. Salvati, K. A. Dawson, *Nat. Nanotechnol.* **2009**, *4*, 546.

[38] C. D. Walkey, W. C. W. Chan, *Chem. Soc. Rev.* **2012**, *41*, 2780.

[39] M.-E. Aubin-Tam, K. Hamad-Schifferli, *Langmuir* **2005**, *21*, 12080.

[40] a) C.-C. You, M. De, G. Han, V. M. Rotello, *J. Am. Chem. Soc.* **2005**, *127*, 12873; b) M. De, C. C. You, S. Srivastava, V. M. Rotello, *J. Am. Chem. Soc.* **2007**, *129*, 10747.

[41] S. Goy-López, J. Juárez, M. Alatorre-Meda, E. Casals, V. F. Puntes, P. Taboada, V. Mosquera, *Langmuir* **2012**, *24*, 13186.

[42] R. S. Kane, A. D. Stroock, *Biotechnol. Prog.* **2007**, *23*, 316.

[43] M. A. Dobrovolskaia, A. K. Patri, J. Zheng, J. D. Clogston, N. Ayub, P. Aggarwal, B. W. Neun, J. B. Hall, S. E. McNeil, *Nanomed.-Nanotechnol. Biol. Med.* **2009**, *5*, 106.

[44] a) C. Rocker, M. Potzl, F. Zhang, W. J. Parak, G. U. Nienhaus, *Nat. Nanotechnol.* **2009**, *4*, 577; b) S. Milani, F. Baldelli Bombelli, A. S. Pitek, K. A. Dawson, J. Rädler, *ACS Nano* **2012**, *6*, 2532.

[45] a) D. Walczyk, F. B. Bombelli, M. P. Monopoli, I. Lynch, K. A. Dawson, *J. Am. Chem. Soc.* **2010**, *132*, 5761; b) Y. Hong, P. Shaw, B. Tattam, C. Nath, J. Earl, K. Stephen, A. McLachlan, *Eur. J. Clin. Pharmacol.* **2007**, *63*, 165; c) D. Zhang, O. Neumann, H. Wang, V. M. Yuwono, A. Barhoumi, M. Perham, J. D. Hartgerink, P. Wittung-Stafshede, N. J. Halas, *Nano Lett.* **2009**, *9*, 666.

[46] F. Morgner, S. Stufler, D. Geißler, I. L. Medintz, W. R. Algar, K. Susumu, M. H. Stewart, J. B. Blanco-Canosa, P. E. Dawson, N. Hildebrandt, *Sensors* **2011**, *11*, 9667.

[47] a) J. Bear, G. Charron, M. T. Fernández-Argüelles, S. Massadeh, P. McNaughter, T. Nann, in *Systems Biology*, Vol. *2* (Eds: B. Booß-Bavnbek, B. Klösgen, J. Larsen, F. Pociot, E. Renström), SpringerNew York, **2011**, pp. 185–220; b) F. Wang, C. He, M.-Y. Han, J. H. Wu, G. Q. Xu, *Chem. Commun.* **2012**, *48*, 6136.

[48] E. C. Dreaden, A. M. Alkilany, X. Huang, C. J. Murphy, M. A. El-Sayed, *Chem. Soc. Rev.* **2012**, *41*, 2740.

[49] a) T.-S. Wu, K.-X. Wang, G.-D. Li, S.-Y. Sun, J. Sun, J.-S. Chen, *ACS Appl. Mater. Interfaces* **2010**, *2*, 544; b) J. D. Oei, W. W. Zhao, L. Chu, M. N. DeSilva, A. Ghimire, H. R. Rawls, K. Whang, *J. Biomed. Mater. Res. Part B* **2012**, *100B*, 409; c) D. V. Quang, P. B. Sarawade, A. Hilonga, J.-K. Kim, Y. G. Chai, S. H. Kim, J.-Y. Ryu, H. T. Kim, *Colloid Surf. A-Physicochem. Eng. Asp.* **2011**, *389*, 118.

[50] a) C. R. Thomas, S. George, A. M. Horst, Z. X. Ji, R. J. Miller, J. R. Peralta-Videa, T. A. Xia, S. Pokhrel, L. Madler, J. L. Gardea-Torresdey, P. A. Holden, A. A. Keller, H. S. Lenihan, A. E. Nel, J. I. Zink, *ACS Nano* **2011**, *5*, 13; b) T. A. Xia, Y. Zhao, T. Sager, S. George, S. Pokhrel, N. Li, D. Schoenfeld, H. A. Meng, S. J. Lin, X. Wang, M. Y. Wang, Z. X. Ji, J. I. Zink, L. Madler, V. Castranova, S. Lin, A. E. Nel, *ACS Nano* **2011**, *5*, 1223.

[51] C. Kirchner, T. Liedl, S. Kudera, T. Pellegrino, A. Muñoz Javier, H. E. Gaub, S. Stölzle, N. Fertig, W. J. Parak, *Nano Lett.* **2004**, *5*, 331.

[52] A. Alkilany, C. Murphy, *J. Nanopart. Res.* **2010**, *12*, 2313.

[53] a) P. Kovacic, R. Somanathan, *J. Nanosci. Nanotechnol.* **2010**, *10*, 7919; b) K. Unfried, C. Albrecht, L.-O. Klotz, A. Von Mikecz, S. Grether-Beck, R. P. F. Schins, *Nanotoxicology* **2007**, *1*, 52; c) E. J. Petersen, B. C. Nelson, *Anal. Bioanal. Chem.* **2010**, *398*, 613; d) H. Chibli, L. Carlini, S. Park, N. M. Dimitrijevic, J. L. Nadeau, *Nanoscale* **2011**, *3*, 2552; e) D. R. Cooper, N. M. Dimitrijevic, J. L. Nadeau, *Nanoscale* **2010**, *2*, 114.

[54] C. A. R. Auchinvole, P. Richardson, C. McGuinnes, V. Mallikarjun, K. Donaldson, H. McNab, C. J. Campbell, *ACS Nano* **2011**, *6*, 888.

[55] a) K. L. Aillon, Y. Xie, N. El-Gendy, C. J. Berkland, M. L. Forrest, *Adv. Drug Delivery Rev.* **2009**, *61*, 457; b) M. A. Dobrovolskaia, S. E. McNeil, *Nat. Nanotechnol.* **2007**, *2*, 469; c) B. S. Zolnik, Á. González-Fernández, N. Sadrieh, M. A. Dobrovolskaia, *Endocrinology* **2010**, *151*, 458; d) A. Chompoosor, K. Saha, P. S. Ghosh, D. J. Macarthy, O. R. Miranda, Z.-J. Zhu, K. F. Arcaro, V. M. Rotello, *Small* **2010**, *6*, 2246.

[56] a) W. J. Stark, *Angew. Chem. Int. Ed.* **2011**, *50*, 1242; b) M. L. Schipper, G. Iyer, A. L. Koh, Z. Cheng, Y. Ebenstein, A. Aharoni, S. Keren, L. A. Bentolila, J. Q. Li, J. H. Rao, X. Y. Chen, U. Banin, A. M. Wu, R. Sinclair, S. Weiss, S. S. Gambhir, *Small* **2009**, *5*, 126.

[57] a) W. H. De Jong, W. I. Hagens, P. Krystek, M. C. Burger, A. Sips, R. E. Geertsma, *Biomaterials* **2008**, *29*, 1912; b) P. Aggarwal, J. B. Hall, C. B. McLeland, M. A. Dobrovolskaia, S. E. McNeil, *Adv. Drug Delivery Rev.* **2009**, *61*, 428.

[58] a) R. R. Arvizo, O. R. Miranda, M. A. Thompson, C. M. Pabelick, R. Bhattacharya, J. D. Robertson, V. M. Rotello, Y. S. Prakash, P. Mukherjee, *Nano Lett.* **2010**, *10*, 2543; b) E. B. Dickerson, E. C. Dreaden, X. Huang, I. H. El-Sayed, H. Chu, S. Pushpanketh, J. F. McDonald, M. A. El-Sayed, *Cancer Lett.* **2008**, *269*, 57; c) J. Chen, C. Glaus, R. Laforest, Q. Zhang, M. Yang, M. Gidding, M. J. Welch, Y. Xia, *Small* **2010**, *6*, 811; d) A. M. El Badawy, R. G. Silva, B. Morris, K. G. Scheckel, M. T. Suidan, T. M. Tolaymat, *Environ. Sci. Technol.* **2010**, *45*, 283; e) M. Lundqvist, J. Stigler, G. Elia, I. Lynch, T. Cedervall, K. A. Dawson, *Proc. Natl. Acad. Sci. USA* **2008**, *105*, 14265; f) C. M. Goodman, C. D. McCusker, T. Yilmaz, V. M. Rotello, *Bioconjugate Chem.* **2004**, *15*, 897.

[59] a) T.-H. Chung, S.-H. Wu, M. Yao, C.-W. Lu, Y.-S. Lin, Y. Hung, C.-Y. Mou, Y.-C. Chen, D.-M. Huang, *Biomaterials* **2007**, *28*, 2959; b) S. E. A. Gratton, P. A. Ropp, P. D. Pohlhaus, J. C. Luft, V. J. Madden, M. E. Napier, J. M. DeSimone, *Proc. Natl. Acad. Sci. USA* **2008**, *105*, 11613; c) A. L. Martin, L. M. Bernas, B. K. Rutt, P. J. Foster, E. R. Gillies, *Bioconjugate Chem.* **2008**, *19*, 2375; d) E. C. Cho, J. Xie, P. A. Wurm, Y. Xia, *Nano Lett.* **2009**, *9*, 1080.

[60] P. R. Leroueil, S. Hong, A. Mecke, J. R. Baker, B. G. Orr, M. M. Banaszak Holl, *Acc. Chem. Res.* **2007**, *40*, 335.

[61] P. R. Leroueil, S. A. Berry, K. Duthie, G. Han, V. M. Rotello, D. Q. McNerny, J. R. Baker, B. G. Orr, M. M. Banaszak Holl, *Nano Lett.* **2008**, *8*, 420.

[62] E. C. Dreaden, M. A. Mackey, X. Huang, B. Kang, M. A. El-Sayed, *Chem. Soc. Rev. 40*, 3391.

[63] A. Albanese, E. A. Sykes, W. C. W. Chan, *ACS Nano* **2010**, *4*, 2490.

[64] a) S. L. Harper, J. L. Carriere, J. M. Miller, J. E. Hutchison, B. L. S. Maddux, R. L. Tanguay, *ACS Nano* **2011**, *5*, 4688;

b) R. Duncan, L. Izzo, *Adv. Drug Delivery Rev.* **2005**, *57*, 2215; c) N. A. Stasko, C. B. Johnson, M. H. Schoenfisch, T. A. Johnson, E. L. Holmuhamedov, *Biomacromolecules* **2007**, *8*, 3853.
[65] J. Lin, H. Zhang, Z. Chen, Y. Zheng, *ACS Nano* **2010**, *4*, 5421
[66] T. Xia, M. Kovochich, M. Liong, J. I. Zink, A. E. Nel, *ACS Nano* **2007**, *2*, 85.
[67] K. Menzel, M. Hausmann, F. Obermeier, K. Schreiter, N. Dunger, F. Bataille, W. Falk, J. Scholmerich, H. Herfarth, G. Rogler, *Clin. Exp. Immunol.* **2006**, *146*, 169.
[68] J. Speshock, L. Braydich-Stolle, E. Szymanski, S. Hussain, *Nanoscale Res. Lett.* **2011**, *6*, 1.
[69] Z. J. Deng, M. Liang, M. Monteiro, I. Toth, R. F. Minchin, *Nat. Nanotechnol.* **2011**, *6*, 39.
[70] D. E. Owens III, N. A. Peppas, *Int. J. Pharm.* **2006**, *307*, 93.
[71] A. Beduneau, Z. Ma, C. B. Grotepas, A. Kabanov, B. E. Rabinow, N. Gong, R. L. Mosley, H. Dou, M. D. Boska, H. E. Gendelman, *PLoS One* **2009**, *4*, e4343.
[72] S.-Y. Seong, P. Matzinger, *Nat. Rev. Immunol.* **2004**, *4*, 469.
[73] S. Lin, Y. Zhao, T. Xia, H. Meng, Z. Ji, R. Liu, S. George, S. Xiong, X. Wang, H. Zhang, S. Pokhrel, L. Mädler, R. Damoiseaux, S. Lin, A. E. Nel, *ACS Nano* **2011**, *5*, 7284.
[74] P. G. Etchegoin, E. C. Le Ru, in *Surface Enhanced Raman Spectroscopy*, Wiley-VCH, Weinheim, Germany **2010**, pp. 1–37.
[75] E. C. Le Ru, J. Grand, I. Sow, W. R. C. Somerville, P. G. Etchegoin, M. Treguer-Delapierre, G. Charron, N. Félidj, G. Lévi, J. Aubard, *Nano Lett.* **2011**, *11*, 5013.
[76] K. Willets, *Anal. Bioanal. Chem.* **2009**, *394*, 85.
[77] a) H.-W. Tang, X. B. Yang, J. Kirkham, D. A. Smith, *Appl. Spectrosc.* **2008**, *62*, 1060; b) K. Kneipp, A. S. Haka, H. Kneipp, K. Badizadegan, N. Yoshizawa, C. Boone, K. E. Shafer-Peltier, J. T. Motz, R. R. Dasari, M. S. Feld, *Appl. Spectrosc.* **2002**, *56*, 150.
[78] a) J. Yang, Y. Cui, S. Zong, R. Zhang, C. Song, Z. Wang, *Mol. Pharm.* **2012**, *9*, 842; b) K. Ock, W. I. Jeon, E. O. Ganbold, M. Kim, J. Park, J. H. Seo, K. Cho, S.-W. Joo, S. Y. Lee, *Anal. Chem.* **2012**, *84*, 2172.
[79] a) J. Kneipp, H. Kneipp, B. Wittig, K. Kneipp, *J. Phys. Chem. C* **2010**, *114*, 7421; b) K. Nowak-Lovato, B. Wilson, K. Rector, *Anal. Bioanal. Chem.* **2010**, *398*, 2019; c) S. Zong, Z. Wang, J. Yang, Y. Cui, *Anal. Chem.* **2011**, *83*, 4178.
[80] L. Xu, H. Kuang, C. Xu, W. Ma, L. Wang, N. A. Kotov, *J. Am. Chem. Soc.* **2011**, *134*, 1699.
[81] D. Zhang, S. M. Ansar, K. Vangala, D. Jiang, *J. Raman Spectrosc.* **2010**, *41*, 952.
[82] R. A. Alvarez-Puebla, A. Agarwal, P. Manna, B. P. Khanal, P. Aldeanueva-Potel, E. Carbó-Argibay, N. Pazos-Pérez, L. Vigderman, E. R. Zubarev, N. A. Kotov, L. M. Liz-Marzán, *Proc. Natl. Acad. Sci. USA* **2011**, *108*, 8157.
[83] U. Resch-Genger, M. Grabolle, S. Cavaliere-Jaricot, R. Nitschke, T. Nann, *Nat. Meth.* **2008**, *5*, 763.
[84] S. V. Dezhurov, I. Y. Volkova, M. S. Wakstein, *Bioconjugate Chem.* **2011**, *22*, 338.
[85] S. Jiang, Y. Zhang, *Langmuir* **2010**, *26*, 6689.
[86] C. Xu, B. Xing, J. Rao, *Biochem. Biophys. Res. Commun.* **2006**, *344*, 931.
[87] W. R. Algar, D. Wegner, A. L. Huston, J. B. Blanco-Canosa, M. H. Stewart, A. Armstrong, P. E. Dawson, N. Hildebrandt, I. L. Medintz, *J. Am. Chem. Soc.* **2012**, *134*, 1876.
[88] M. Levy, S. F. Cater, A. D. Ellington, *ChemBioChem* **2005**, *6*, 2163.
[89] I. L. Medintz, H. Mattoussi, *Phys. Chem. Chem. Phys.* **2009**, *11*, 17.
[90] a) V. Bagalkot, L. Zhang, E. Levy-Nissenbaum, S. Jon, P. W. Kantoff, R. Langer, O. C. Farokhzad, *Nano Lett.* **2007**, *7*, 3065; b) K.-Y. Pu, Z. Luo, K. Li, J. Xie, B. Liu, *J. Phys. Chem. C* **2011**, *115*, 13069; c) H. Lee, I.-K. Kim, T. G. Park, *Bioconjugate Chem.* **2010**, *21*, 289.
[91] K. Boeneman, J. B. Delehanty, K. Susumu, M. H. Stewart, I. L. Medintz, *J. Am. Chem. Soc.* **2010**, *132*, 5975.

Received: June 3, 2012
Published online: October 30, 2012

Elsevier Editorial System(tm) for Biotechnology Advances
Manuscript Draft

Manuscript Number:

Title: Interaction of stable colloidal nanoparticles with cellular membranes

Article Type: SI:Biotech in Nanomed- Review Paper

Keywords: Nanoparticle; Colloid; Cell Membrane; Receptor; Protein corona; Targeted delivery

Corresponding Author: Prof. Subramanian Tamil Selvan,

Corresponding Author's Institution: Institute of Materials Research and Engineering

First Author: Morteza Mahmoudi

Order of Authors: Morteza Mahmoudi ; Subramanian Tamil Selvan; Jie Meng; Xue Xue; Xing Jie Liang; Massoud Rahman; Christian Pfeiffer; Raimo Hartmann; Pilar Rivera Gil; Beatriz Pelaz; Wolfgang J Parak; Pablo del Pino; Susana Carregal-Romero; Antonios G. Kanaras

Abstract: Due to their ultra-small size, inorganic nanoparticles (NPs) have distinct properties compared to the bulk form. The unique characteristics of NPs are broadly exploited in biomedical sciences in order to develop various methods of targeted drug delivery, novel biosensors and new therapeutic pathways. However, relatively little is known in the negotiation of NPs with complex biological environments. Cell membranes (CMs) in eukaryotes have dynamic structures, which is a key property for cellular responses to NPs. In this review, we discuss the current knowledge of various interactions between advanced types of NPs and CMs.

Suggested Reviewers: Karthikeyan Narayanan
Senior Research Scientist, Stem Cells, Institute of Bioengineering & Nanotechnology
karthikeyan@ibn.a-star.edu.sg
http://www.ibn.a-star.edu.sg/research_areas_7.php?expandable=1&id=238&section=publications

Sophie Laurent
Prof, NMR and Molecular Imaging Laboratory, Université de Mons
Sophie.LAURENT@umons.ac.be
http://www.cost.eu/domains_actions/cmst/Actions/eufen?address=1&db=mangement&back=management&anchor=participants

http://www.innovons.be/portail/site/innovons/lang/en/accueil/resultat_entite;jsessionid=7830A2BFEF9DA969389E64053CE7974A?entpub=SCGOBRIMOLEC6a6

Ramasamy Paulmurugan
Prof, School of Medicine, Stanford University
paulmur8@stanford.edu
http://med.stanford.edu/profiles/Ramasamy_Paulmurugan/

Paul Mulvaney

Prof, Bio21 Institute, The University of Melbourne
mulvaney@unimelb.edu.au
http://www.findanexpert.unimelb.edu.au/display/person1947

Xiaoyuan Chen
Prof., National Institute of Biomedical Imaging and Bioengineering , National Institutes of Health
chen@nih.gov
http://www.nibib.nih.gov/Research/Intramural/XChen

Valeria Grazu
Researcher , Biofunctionalization of Nanoparticles and Surfaces (bioNANOsurf), Instituto de Nanociencia de Aragón (INA), Zaragoza, Spain
vgrazu@unizar.es
http://www.bionanosurf.info/members/grazu

Andreas Riedinger
Research fellow , Nanochemistry group , IIT Genova
andreas.riedinger@iit.it
http://www.iit.it/en/people/nanochemistry-biology/fellow-phd/andreas-riedinger.html

Martin Oheim
Research Director, Neurophysiology, CNRS, Paris, France
martin.oheim@parisdescartes.fr
http://www.biomedicale.univ-paris5.fr/neurophysiologie/labo/oheim.php

Cover Letter

Institute of Materials Research and Engineering
3 Research Link,
Singapore 117602
Tel: +65-6874-5249
Fax: +65-6774-4657

July 24, 2013

Professor M. Moo-Young
Editor, Biotechnology Advances

Dear Prof. Moo-Young,

Please find our Review entitled "Interaction of stable colloidal nanoparticles with cellular membranes", which we would like to submit for publication in *Biotechnology Advances*. This review is submitted to the special issue on "SI: Biotech in nanomedicine".

Thank you for your consideration of this Review for publication in *Biotechnology Advances*. Please feel free to contact me if you have any questions or need additional information.

Sincerely,

Dr. Subramanian Tamil Selvan
Adjunct Associate Professor, Bioengineering, National University of Singapore
Research Scientist, Institute of Materials Research and Engineering, Singapore
Email: subramaniant@imre.a-star.edu.sg

Interaction of stable colloidal nanoparticles with cellular membranes

Morteza Mahmoudi[1,2], Jie Meng[3], Xue Xue[3], Xing Jie Liang[3], Massoud Rahman[4], Christian Pfeiffer[5], Raimo Hartmann[5], Pilar Rivera Gil[5], Beatriz Pelaz[5], Wolfgang J. Parak[5,6], Pablo del Pino[5], Susana Carregal-Romero[5,7], Antonios G. Kanaras[8], Subramanian Tamil Selvan[9,10]*

Conflict of Interest

We declare that there is no conflict of interest.

Competing financial interests: The authors declare no competing financial interests.

Interaction of stable colloidal nanoparticles with cellular membranes

Morteza Mahmoudi[1,2], Jie Meng[3], Xue Xue[3], Xing Jie Liang[3], Massoud Rahman[4], Christian Pfeiffer[5], Raimo Hartmann[5], Pilar Rivera Gil[5], Beatriz Pelaz[5], Wolfgang J. Parak[5,6], Pablo del Pino[5], Susana Carregal-Romero[5,7], Antonios G. Kanaras[8], Subramanian Tamil Selvan[9,10]*

[1]Department of Nanotechnology, Faculty of Pharmacy, Tehran University of Medical Sciences, Tehran, Iran

[2] Nanotechnology Research Center, Faculty of Pharmacy, Tehran University of Medical Sciences, Tehran, Iran

[3]Key Laboratory for Biomedical Effects of Nanomaterials and Nanosafety National Center for Nanosciences and Technology of China, Beijing 100190, China.

[4]Department of Chemical Engineering and Materials Science, University of California Davis, CA 95616, USA

[5]Fachbereich Physik, Philipps University of Marburg, Renthof 7, D-35037 Marburg, Germany

[6]CIC biomaGUNE, Paseo Miramón 182, 20009 San Sebastián, Spain

[7]Andalusian Center for Nanomedicine and Biotechnology (BIONAND), Andalusian Technological Park. C/ Severo Ochoa, 35, 29590 Campanillas, Málaga, Spain.

[8]Institute for Life Sciences, Physics and Astronomy, Faculty of Physical and Applied Sciences, University of Southampton, Highfield, Southampton SO17, 1BJ, United Kingdom.

[9]A*STAR Institute of Materials Research and Engineering (IMRE), 3 Research Link, Singapore 117602.

[10]National University of Singapore, Division of Bioengineering, Faculty of Engineering, 7 Engineering Drive 1 Singapore 117576.

[*]Corresponding author. Tel: +65 6874 5249; Fax: +65 6774 4657.
E-mail addresses: subramaniant@imre.a-star.edu.sg; biests@nus.edu.sg

Keywords:
Nanoparticle;
Colloid
Cell membrane
Receptor
Protein corona
Targeted delivery

Abstract

Due to their ultra-small size, inorganic nanoparticles (NPs) have distinct properties compared to the bulk form. The unique characteristics of NPs are broadly exploited in biomedical sciences in order to develop various methods of targeted drug delivery, novel biosensors and new therapeutic pathways. However, relatively little is known in the negotiation of NPs with complex biological environments. Cell membranes (CMs) in eukaryotes have dynamic structures, which is a key property for cellular responses to NPs. In this review, we discuss the current knowledge of various interactions between advanced types of NPs and CMs.

1. Introduction

The cell membrane (CM) is a biological barrier that separates the interior of cells or organelles from the outside environment, preserving the local chemical composition and most importantly, playing an active role in the negotiation with foreign macromolecules including nanoparticles (NPs) and other biologically relevant components. It is a lipid-based sheath that envelops the cell, encloses the cytoplasm, and creates a selectively permeable barrier. The CM, also known as the plasma membrane, has a crucial significance to life of cells (Zhang et al., 2012a). The CM must retain molecules such as DNA, RNA and a variety of proteins from dissipating away, while keeping out foreign molecules that might damage or destroy the cell's contents, including molecules that are essential for life. On the other hand, it must be selectively permeable to certain ions (such as Na^+ and K^+ for the creation of action potentials in electrically excitable cells) or organic molecules such as nutrients. In this way, the CM is involved in many important cellular processes such as signal transduction, molecular transportation, and cell communication (Anitei and Hoflack, 2012). The first interaction of NPs with cells occurs at the CM and is critically dependent on the physicochemical properties of the NPs (*e.g.* composition, size, shape, charge, surface roughness/smoothness, and surface chemistry) (Fischer and Chan, 2007; Rauch et al., 2013; Zhao et al., 2011). Importantly, the surface of NPs (*e.g.* charge, hydrophobicity, curvature, and stiffness) ultimately determines how NPs interact with physiological

macromolecules from the physiological pool (largely dependent on the local bio-environment) and with the CM. The effect of protein corona on the biological fate of NPs is discussed in detail (Mahmoudi et al., 2011a).

In physiological environments, the outer shell of NPs can be greatly modified by the adsorption of proteins, *i.e.* the protein corona, which typically will form the interface between NPs and the CM (Walkey and Chan, 2012). Thus, for a detailed study of these interactions, highly defined NPs (Rivera-Gil et al., 2012) and well characterized CMs are needed. Herein, unless otherwise specified, we will refer to different NPs, which encompass an inorganic core and a hydrophilic coating layer, purposely derivatized to avoid non-specific interactions with proteins, for instance. We also highlight the concept of typical hybrid NPs, while addressing the topic of the interaction of inorganic NPs and CMs, wherein the inorganic NPs are functionalized with biocompatible coatings and/or serum biomolecules.

1.1. Importance of the physicochemical properties of NPs and their interaction with CMs

The interaction of NPs with CMs is indispensable for many applications in imaging, diagnostics, drug delivery, and therapy. The interplay between NPs and CMs is mainly governed by nanoengineering of the outermost hydrophilic shell of NPs. Nowadays, many synthetic routes have been established towards the design of NPs (Parak, 2011) with controlled composition, size, shape, charge, and surface functionalization (Cortie and McDonagh, 2011; Day et al., 2010; Goesmann and Feldmann, 2010; Ibanez et al., 2012, Perrault and Chan, 2010; Sau and Rogach, 2010; Xia and Halas, 2005) with excellent colloidal stability and biocompatibility (Bartczak and Kanaras, 2010; Kanaras et al., 2002; Liu et al., 2008; Zhang et al., 2011a). However, under physiological conditions, the inorganic NP core may undergo corrosion leading to the release of toxic ions (*e.g.* due to the insufficient shielding of coating materials). Also, coatings can detach from the NP´s surface. These two examples can impede the potential bio-applications of certain NPs (Pelaz et al., 2012).

The size of NPs has a significant effect on cellular interaction and uptake.(Rejman et al. , 2004) NPs whose sizes are smaller than the thickness of the lipid bilayer (~5 nm) may exhibit bilayer insertion, leading to the disruption of the membrane.(Yang and Ma, 2010) While the size of NPs is critical for pore formation in the CM, the shape (*i.e.* aspect ratio, curvature radius, etc.) can also play an important role as it defines the contact surface between NPs and the CM. The properties of the organic coating of NPs (*e.g.* charge, hydrophobicity, and structure) can be also critical towards defining their interplay with CMs. Ultimately, the hydrophilic coating on NPs determines the colloidal stability and reactivity with biomacromolecules or components of the CM. A superior colloidal stability of the NPs can be achieved by different coating methods, which is highly indispensable for a variety of applications. The most common functionalization methods of NPs include the coating by biocompatible silica (Fischer and Chan, 2007; Rauch et al., 2013; Selvan et al., 2010; Zhao et al., 2011), oligomers or polymers such as DNA, polyethylene glycol (PEG), oligopeptide, phospholipid, poly(maleic anhydride), poly(dextran) and poly(acrylic acid) (Bartczak and Kanaras, 2011; Cutler et al., 2012; Nikolic et al., 2006; Yen et al., 2013; Zhang et al., 2011a). In most cases, the biocompatible polymers adsorb on the surface or attach covalently to the NPs *via* anchoring groups.

Despite continuous efforts to formulate the interactions of NPs with the CM based on their physicochemical properties, a straightforward correlation has not yet been achieved. This is partly due to the fact that most physicochemical parameters of NPs are entangled (Rivera-Gil et al., 2013). Any NP aimed for biological application, has to be well characterized so that it can be used as a diagnostic or sensing tool based on their fluorescence, magnetic contrast, surface enhanced Raman scattering (SERS) and Förster resonance energy transfer (FRET) properties (Dawson, 2013; Mahmoudi et al., 2011b; Mahmoudi and Shokrgozar, 2012). Recently, the importance of the characterization of NPs in physiological fluids has been well addressed (Pelaz et al., 2013). For instance, although gold (Au) colloids are typically referred to as “biocompatible” NPs, their size and organic coating on the surface can have a dramatic cytotoxicity effects on the cells. Current synthetic methods can produce different sizes and shapes of Au NPs, as for other inorganic NPs. Nevertheless, it is important to understand the performance of structurally equivalent Au NPs (having the same core size, shape and charge) in physiological environments, which can be very different, depending on their surface capping, *i.e.* thickness of the organic coating, and adsorbed protein corona or covalently attached coatings. Finally, this understanding can greatly influence the suitability of NPs for desired applications. For instance, while Au nanorods coated with cetyltrimethylammonium bromide (CTAB) are perfectly stable in aqueous solution, when these are dispersed in physiological fluids, CTAB molecules can detach, leading to unwanted effects such as NP agglomeration and CTAB toxicity (Alkilany et al., 2009), limiting their suitability. It is therefore a

key to guarantee the integrity and performance of NPs in their working environment, as otherwise conclusions from poorly characterized systems can be misleading (Pelaz et al., 2013).

1.2. The composition and thickness of the cell membrane

The basic structure of the CM is a phospholipid bilayer comprising two layers of fatty acids organized in two sheets. The hydrophobic fatty acyl tails of the phospholipids form the middle of the bilayer. The hydrophilic head groups interact with the aqueous medium on the two opposing sheets (leaflets) of the bilayer. Within the lipid structure various types of molecules such as proteins and carbohydrates are trapped. All of them play critical roles in the cellular functions (Figure 1). The composition of the CM clearly influences the thickness and stiffness of the cellular bilayer (Lewis and Engelman, 1983). Nevertheless, the membrane bilayers are typically 7.5–10 nm thick (Hine, 1999).

Cells are highly heterogenic and the composition of the CM varies significantly for different cell types and for different organelles of a cell. For example, the plasma membranes of human red blood cells contain nearly equal amounts of proteins and lipids. Myelin contains 18% protein and 76% lipid, but the mitochondrial inner membrane contains 76% protein and only 24% lipid. Also the lipid composition of the CM is highly diverse. The proportion of cholesterol in the CM of mammalian cells varies from <15% in the endoplasmic reticulum to 20−50% in the plasma membrane (Mitra et al., 2004; van Meer et al., 2008). The fluid lipid composition in CMs is dynamic and undergoes changes in response to various developmental and environmental stimuli (Rauch et al., 2013). Moreover, the local composition of the CM is dynamic and ordered structures can arise such as lipid rafts or immunological synapses (Dustin and Long, 2010). For example, in the progress of the cell cycle of hepatocytes or during the differentiation of neuroblastoma cells, the fluidity of the CM changes by modifying the ratio of cholesterol and phospholipid (Cheng and Levy, 1979; Gulaya et al., 1989).

Besides lipids, proteins are also key components of the CM. The diverse role of proteins ranges from catalysis of reactions and signal transduction to molecular transportation across the CM. The content of proteins in CMs varies for different classes of cells, but the typical amount is ca. 50% of the total mass of the membrane (Bretscher, 1973).

The structures of membrane proteins are significantly influenced by interactions with the environment (Cross et al., 2011). There are integral and peripheral membrane proteins, and lipid-anchored proteins, which assemble in an oriented way in the CM (Daley, 2008). Integral membrane proteins such as cell adhesion proteins (*e.g.* integrins, cadherins or selectins) traverse the lipid bilayer and connect the extracellular with the intracellular space of the cells. The sticking of NPs to the CM can be facilitated by these proteins. Other examples are pore-forming proteins such as ion channels that controls the permeability of the CM. Oligosaccharides are part of the CM because most proteins and lipids are indeed glycoproteins and glycolipids.

The interaction of NPs with CMs, in particular the uptake of NPs and defense mechanism of cells are considerably different according to the cell type (*i.e.* more specifically on CM composition and charge) (Laurent et al., 2013; Mahmoudi et al., 2012; Ojea-Jimenez et al., 2012). Various approaches for evaluation of cell life cycle and the effects of various nanomaterials on the cell-life cycle were reviewed (Mahmoudi et al., 2011c). For instance, when the same amounts of superparamagnetic NPs were incubated with various cell lines including immune cells (Jurkat), pancreas (Panc-1 and Capan-2), and cervix (HeLa), significant different toxicity results were observed (Laurent, Burtea, 2013). It is noteworthy to mention that in this work, the predetermined cell lines were selected from non-phagocytes cells, and therefore, their behaviors were restricted to differences in cell surface charge and in particular composition (*i.e.* negative surface for Capan-2 and Panc-1 in addition to presence of mucin; surface rich in fucose (not charged) for HeLa cells; positively charged surface for Jurkat T cells). The results confirmed that each cell type responded differently to the same NPs, as a result of significant differences in the composition of the CMs. There remains, of course, the fundamental question regarding the CM composition of various cell lines and to what degree they are able to control the uptake and toxicity of NPs (Laurent et al., 2012; Mahmoudi et al., 2011d; Mahmoudi et al., 2012). Also, fine tuning of the surface composition of NPs will surely allow for controlling the CM's response to a particular type of cell. The answer to such questions will greatly influence the future roadmap of nanomedicine and nanosafety (Krol et al., 2012; Krug and Wick, 2011; Mahmoudi et al., 2011e; Rauch et al., 2013).

1.3. The importance of protein corona

Besides the physicochemical properties of NPs, the protein corona has a crucial role in the cellular uptake of NPs. The composition and quantity of associated proteins in the corona are strongly dependent on the physicochemical properties of the NPs (Mahmoudi et al., 2011a), protein source (Laurent et al., 2013), and incubating temperature (Mahmoudi et al., 2013). In order to lower the free energy of the NPs surface, the NPs strongly interact nonspecifically with the CM. However, if a protein corona is present, the free energy is already lowered. As a result, the adhesion to the CM and uptake are reduced (Lesniak et al., 2013). This is especially true for bare NPs with high surface energy. Since the composition of the corona is variable and dynamic (Chou et al., 2011; Milani et al., 2012; Tenzer et al., 2011), there must be a delicate equilibrium between the surface energy of the NPs, adhesion to the CM, and uptake. The proteins incorporated in the NPs molecular corona can directly influence the endocytosis and exocytosis of NPs through the CM (Walkey et al., 2012). Furthermore, the formation of the protein corona increases the size of the NPs and can trigger agglomeration and sedimentation of NPs (Cho et al., 2011; Safi et al., 2011), if the NPs are not adequately stabilized. In a very recent study, it has been shown that the presence of the protein corona can strongly reduce the adhesion of the NPs to the CM due to possible specific interactions between the NP-corona complex and the CM, resulting in decreased uptake, despite the presence of the physiological ligands (Lesniak et al., 2013). This report raised an important point, *i.e.* in addition to common physicochemical characterizations of nanomaterials (*e.g.* size, charge and colloidal stability). An evaluation of the adhesion properties of the NPs in physiological medium (probably carrying a protein corona) to relevant CMs is very important. Recently, the topic of influence of the net charge of polymer coated NPs on the formation of the protein corona and cellular internalization (in different cell lines) was addressed in detail (Hühn et al., 2013). Interestingly, although positively charged NPs are more readily internalized, the net charge does not significantly influence the number of proteins adsorbed. Furthermore, the authors pointed out that while having the same protein corona in terms of number of proteins, the conformation of these proteins might vary depending on the net charge of the NPs.

In summary, although the number of studies on the interactions of cells and NPs are steadily increasing, our understanding of the biological mechanisms involved in this process is still limited and perhaps, one of the areas where future studies should be focused. Moreover, there are several new factors, *e.g.* slight temperature changes (Mahmoudi et al., 2013), variation of protein concentrations in complex medium (Monopoli et al., 2011), and gradient protein concentrations (Ghavami et al., 2013) should be considered in detail for achieving better understanding of the NP-CM interactions *in vivo* and elucidating the safety considerations for biomedical applications, resulting in nano-biomaterials that are "safe by design". The "reward" might be critical to establish a long lasting stable bridge between nanotechnology and life sciences. We should, however, acknowledge that giving solid messages regarding the interplay between engineered NPs and CMs represents a challenge due to the complexity inherent to biological systems, as well as the large variation of experimental conditions between different studies.

2. The internalization patterns of NPs through physiological barriers such as the CMs depend on their physicochemical properties

Molecules, including NPs, can in principle pass the cell membrane in several ways (see Figure 2) (Luccardini et al., 2007): (i) diffusion of membrane-permeable molecules (such as O_2), (ii) transport through ion channels (such as Na^+), (iii) endocytotic processes involving an invagination of the cell membrane, leaving the most NPs in a pinched-off vesicle (Dahan et al., 2001; Parak et al., 2002; Yang et al., 2005), and (iv) reversible local disruption of the CM (Lin et al., 2010; Wang et al., 2012) by electroosmotic shock or electroporation. It is noteworthy to mention that these pathways are not recognized for nucleus-free cells (*e.g.* red blood cells), where diffusion is the dominant NP entrance mechanism (Rothen-Rutishauser et al., 2006).

Direct traversing of the CM by NPs is believed to be *via* the reversible formation of small pores (Lin et al., 2010; Wang et al., 2012). These NPs are (at least for some time, considering autophagocytosis) free in the cytosol. A proof of such non-endocytotic pathway is the internalization of NPs by red blood cells, which are incapable of endocytosis (Wang et al., 2012). In the case of NPs with at least a few nm hydrodynamic diameter, direct diffusion to the cytosol or transport through ion channels can be excluded, as these mechanisms are designed only for very small molecules (such as O_2 or Na^+). Conversely, NPs are too large and are known to enter cells *via* endocytotic pathways (Chan and Nie, 1998, Chithrani, 2010; Derfus et al., 2004; Fercher et al., 2011; Mailander and Landfester, 2009; Nam et al., 2009; Parak, et al., 2002; Sée et al., 2009). In most cases, after uptake, these NPs are not free in the cytosol, but are inside endocytotic vesicles surrounded by membranes.

Endocytosis-free model membrane systems such as giant unilamellar vesicles and giant plasma membrane vesicles were used to study the penetration of amphiphilic thiolated PEG-stabilized quantum dots (QDs) (CdTe@mPEG-SH) and hydrophilic CdTe@TGA QDs. The amphiphilic QDs were found to penetrate live cell plasma membranes and escape the endocytic pathway and distributed over the entire interior of cells with partial entrapment in endosomes, whereas hydrophilic CdTe@TGA QDs were solely accumulated in endosomes. This was caused by the agglomeration of hydrophilic QDs on the CM. The less or non-agglomerated amphiphilic QDs could penetrate the CM (Canton and Battaglia, 2012, Dubavik et al., 2012). In another study, the hydrophobic interaction between surface-tailored QDs and CMs was used for the labeling of CMs (Figure 3) (Selvan et al., 2007). These examples illustrate how derivatizing the surface of NPs (while retaining other structural parameters such as size and shape) enables the tailoring of the NP interaction with physiological entities such as the CM.

Table 1. Some delivery approaches available for NPs.

Internalization Pathway[a]	Mediated by	Comments	Ref.
Using ligands	i) Cell penetrating peptides (CPP)	Up to 100-fold more uptake than equivalent "bare" NPs	Child et al., 2011; Dejardin et al., 2011; Chaudhary et al., 2013; de la Fuente and Berry, 2005.
	ii) Polycation ligands	Used typically for gene transfection	Kievit et al., 2009; Mykhaylyk et al., 2012; Howard et al., 2009.
	iii) Coated NPs	Endocytosis; Pinocytosis (receptor independent) in macrophages	Buono et al., 2009; Walkey et al., 2012.
Magnetofection	Magnetic fields	Magnetic force is used to pull magnetic NPs inside cells	del Pino et al., 2010; Child et al., 2011.
Electroporation	Permeabili-zation of CM using electric fields	In vitro method for transforming cells	Lin et al., 2009.
Microinjection	Micro-needle assisted delivery	Single cell studies	Candeloro et al., 2011.
Photothermal nanoblade delivery	Polymeric imidazole	High throughput delivery into live cell cytoplasm	Lee et al., 2012.
Microfluidic Device	Tubulin	Tubulin-QD conjugates delivered into the cytoplasm of HeLa cells	Xu et al., 2012.

[a] List of common techniques used for facilitating the internalization of NPs inside cells.

Clearly, it would be desirable to correlate these uptake mechanisms to the physicochemical properties of the NPs (Rivera Gil et al., 2010; Rivera-Gil et al., 2013). Some of the general correlations will be discussed in the following sections.

2.1. Size

Size is certainly a key parameter (Chithrani and Chan, 2007, Chithrani et al., 2006, Jin et al., 2009). Despite their "small" size, NPs are not able to diffuse freely through the CM. The semi-permeable nature of the CM allows for free diffusion of small and non-polar molecules. However, "bigger" objects such as NPs cannot enter the CM and require specific uptake mechanisms such as endocytosis or pore formation (except for nucleus-free cells such as red blood cells) (Chou et al., 2011). In the case of endocytotic uptake, the capability of the CM to wrap around adhered extracellular NPs strongly influences their uptake efficiency. It is strongly affected by the elasticity of the bilayer (Reynwar et al., 2007), the number of free biding sites (*i.e.* receptors), and the size, shape and charge of the nanomaterials (Nel et al., 2009). Concerning the last aspect, several mathematical and experimental approaches were realized to clarify the dependence of NP size, shape and charge on the internalization efficiency (Albanese and Chan, 2011; Deserno, 2004; Deserno and Gelbart, 2002; Nangia and Sureshkumar, 2012). For spherical NPs, optimal NP radii for membrane wrapping were calculated by either using a kinetic model describing receptor diffusion combined with energetic analysis (Bao

and Bao, 2005; Decuzzi and Ferrari, 2007) or approaches motivated by thermodynamic considerations (Zhang et al., 2009). Despite different fundamental assumptions, two conclusions can be drawn from both theoretical approaches. The efficient uptake of spherical NP radius is found in the size regime of around 20-30 nm. When the size of NP radius is smaller than 20 nm, the capability of membrane wrapping is strongly reduced (NP agglomerates can trigger internalization). Both findings are in good agreement with the experimental data (Chithrani and Chan, 2007; Chithrani et al., 2006; Jiang et al., 2008). The uptake efficiency of 50 nm citrate-coated Au NPs in HeLa cells was found to be higher than that of spherical Au NPs of sizes of 14 and 74 nm (Chithrani et al., 2006). Transferrin-coated 14 nm Au NPs were exocytosed faster in HeLa cells than larger particles of 100 nm diameter (Chithrani and Chan, 2007). The Au NPs with ultra-small size (1.2 -1.4 nm) coated with phosphine ligands exhibited cytotoxicity in cancer cells. The cytotoxicity of the Au NPs depended primarily on their size and not on their ligand chemistry (Pan et al., 2007). Larger 15 nm Au colloids were comparatively nontoxic in comparison to 1-2 nm NPs, irrespective of the cell type used. The authors suggested that the toxicity of NPs could originate from interactions at the CM, despite endocytosis. In a recent study, 4 nm poly(methacrylic acid) coated Au NPs induced cytotoxicity on neural progenitor and human vein endothelial cells especially at a higher concentration (50-200 nM), due to the induction of reactive oxygen species (ROS), which caused the deformation of actin and tubulin filaments of the cell cytoskeleton, inhibiting cell proliferation and differentiation (Soenen et al., 2012). In another study, the NPs caused the DNA damage to the cultured cells without crossing the cellular barrier (Bhabra et al., 2009). It has been revealed later that the indirect DNA damage is dependent on the thickness of the cellular barrier and mediated by signaling through gap junction proteins, following the generation of mitochondrial free radicals (Sood et al., 2011).

The hydrodynamic size of inorganic core NPs in aqueous solution can be larger, depending on the organic coating (Rivera-Gil et al., 2013). Obviously, this has to be considered while taking assumptions from previous studies, as NPs with the same inorganic core can be derivatized with different organic coatings (*e.g.* charge and thickness of the organic coating). This can have an important impact on the selective accumulation of NPs in kidney cells, *in vivo* (Choi et al., 2011). Interestingly, in contrast to other reports (Chithrani and Chan, 2007; Chithrani et al., 2006; Jiang et al., 2008), the effects of size, shape and surface derivatization on the cellular uptake of nanospheres and nanocages were studied (Cho et al., 2010). The authors found that "small" 15 nm NPs were more readily internalized by cells than larger 45 nm NPs. They compared directly the size of inorganic cores without explicitly taking into account the organic layer. In particular, PEG layer of 5 kDa might triplicate the hydrodynamic size of their "small" 15 nm NPs, which can be estimated using previously reported experimental equations for the determination of hydrodynamic radii of PEGylated NPs (Doane et al., 2010). Thus, what appears as contradictory is in fact in perfect agreement with the work of Chan and coworkers (Chithrani and Chan, 2007; Chithrani et al., 2006; Jiang et al., 2008). Lastly, particles with the same surface charge and hydrodynamic radii can be made with different stiffness (hard and soft), which is an ultimate key for *in vivo* prolonged circulation, avoiding interaction and following macrophage's sequestration (Zhang et al., 2012a).

2.2. Shape

Besides the size of NPs, their shape and geometry plays a pivotal role. For example, in a systematic computational analysis on how carbon nanotubes interact with a CM, it was found that carbon nanotubes prefer to orient horizontally inside the internal hydrophobic layer of the CM (Hofinger et al., 2011; Shi et al., 2011). These theoretical studies discussed the basic dynamics underlying the insertion process and explained the accumulation of short carbon nanotubes in the hydrophobic domain of the CM. Another more general and recent computational study shed light on the effects of shape and charge on translocation through the membrane. Using advanced molecular dynamics simulations, the authors found that the penetration rate through the membrane varied for pyramid-, rod-, rice-, sphere-, and cube-shaped NPs (Nangia and Sureshkumar, 2012). Though these computational results illustrate very well the complexity of the interaction of CM and the shape of NPs, they should be taken with caution, as they do not take into account physiological macromolecules, which add further complexity to the "big" picture. In another experimental study, the interactions between endothelial cells and Au NPs of different morphologies but with the same ligand capping were investigated. The authors (Bartczak et al., 2012a) found that hollow Au NPs of a size around 90 nm were taken up lower than 15 nm spherical NPs and rod-shape NPs (17 nm x 47 nm). Also, Au nanorods with different aspect ratios and surface coating were found to be less readily internalized than their spherical counterparts (Chithrani and Chan, 2007, Chithrani et al., 2006). Equivalently, Au nanostars were found to be less efficiently internalized than the corresponding Au spheres (Rodriguez-Lorenzo et al., 2011). Again, one

should not draw general conclusions from these results, as physicochemical properties of NPs can be interconnected. For instance, the authors (Chithrani et al., 2006) hypothesized the poor uptake of Au nanorods (compared to nanospheres) and higher degree of exocytosis. While they acknowledged the interaction with serum proteins as the main parameter dictating the interaction with the CM, the shape and remaining CTAB-sticking to nanorods (it is difficult to fully exchange CTAB by other molecules) might also play a role in the interaction of NPs with the CM and/or serum proteins (Chithrani and Chan, 2007; Chithrani et al., 2006). In another example, Xia and coworkers (Cho et al., 2010) pointed out that the surface modification of NPs could influence the uptake differences, while comparing nanocages and nanospheres.

2.3. Charge

The recent developments in surface functionalization techniques have enabled the researchers to introduce different charges and charge densities on the surface of NPs. For example, NPs can be synthesized to have positive (cationic) or negative (anionic) surface. It is broadly accepted that highly positively charged NPs may interact electrostatically with the negatively charged glycocalyx on the CM. As predicted above by theory, this leads to faster internalization rates of positively charged NPs than negatively charged NPs (Asati et al., 2010; Ojea-Jiménez et al., 2012; Schweiger et al., 2012; Soenen et al., 2011; Soenen et al., 2012; Tanguay et al., 2011). However, the translocation rate of positively charged NPs can critically disrupt the CM, enhancing toxicity (Goodman et al., 2004). It was also shown that NPs with different charges migrated selectively to different locations of tumor cylindroids, which in turn modulated their uptake (Kim et al., 2010). However, the whole image is more complex. Recently, the effects of various parameters such as the surface charge of NPs, the presence of surface functional groups on NPs, the presence of receptors on the CM, NP-CM interaction, and the cellular uptake route were investigated (Gu et al., 2011). In this work, the authors employed Au nanorods (NRs) as a model for a drug delivery vector and monitored their rotational motion upon adsorption on the CM. Using this NR rotation imaging technique, they were able to obtain some information about the nature and strength of the NR-CM bond. By attaching various functional groups such as PEG, carboxyl-terminated PEG (PEG-CO_2^{2-}), transferrin, trans-activating transcriptional (TAT) peptides, and polyethylenimine (PEI) on the surface of Au NRs, they studied the effect of each parameter. The study of rotational dynamics of Au NRs on live CMs also showed the fate of these functionalized vectors. PEI-modified NRs with high positive surface charge were attracted to the negatively charged CMs through electrostatic interaction and lost their rotation immediately. In contrast to PEI, negatively charged NRs barely adsorbed to the CM and even after non-specific binding to the cationic sites, many of them detached from the CM on the time scale of seconds to minutes. These negatively charged PEG-NRs rarely attached to the CM and even after adsorption, they showed lateral movement and high-speed rotation, and eventually no uptake to the cell interior was observed. This study indicates that positively charged NPs can attach preferentially to the CM and therefore have the highest chance of uptake. In contrast, the negatively charged NPs have the least chance of CM adsorption, resulting in lower uptake probability.

Most importantly, electrostatic interactions can cause membrane deformations of the contacting domains. The interaction of strongly charged or hydrophilic NPs with the zwitterionic head-groups of the phospholipids can result in transient membrane leakage or rupture (Deserno and Gelbart, 2002; Smith et al., 2007), caused by the forming of energetically favorable hybrid micelles (colloids formed by a NP core surrounded by a phospholipid shell). In this way, the surface charge polarity and density of Au NPs can influence the level of CM penetration and disruption (Lin et al., 2010). Positively charged NPs have in some cases increased the above two factors during their internalization into cells, bypassing endocytosis. Thus, charge is an important factor which can influence whether NPs enter cells *via* endocytotic processes or membrane poration. In another work, it has been shown that superparamagnetic iron oxide NPs with different surface charges (*i.e.* negative, plain, and positive) can differentially affect signal transduction pathways, after interaction with CMs (Rauch et al., 2012). Using isogenic pairs of breast and colon derived cell lines, the stimulation of ERK and AKT signaling pathways were occurred by the NPs, which was selectively dependent on the types of cell and NPs. In general, cells with Ras mutations respond better than their non-mutant counterparts. The negatively charged NPs activated ERK to a similar extent as epidermal growth factor (EGF), and used the same upstream signaling components including activation of the EGF receptor. Importantly, negatively charged NPs stimulated the proliferation of Ras transformed breast epithelial cells as efficiently as EGF, suggesting that NPs can mimic physiological growth factors (Rauch et al., 2012; 2013).

Obviously, the effect of charge alone cannot be taken into consideration, as for example, the size of cationic NPs can derive into different results. In an experimental work involving highly charged polyelectrolyte-based

materials, large micrometer-sized positively charged NPs were shown to be taken up more efficiently than equivalent negatively charged NPs, but both types were endocytosed (Muñoz Javier et al., 2006). In this study, atomic force microscopy (AFM) and confocal microscopy were used to address and correlate the adhesion forces between particles and CMs of different cell lines and internalization of particles. Equivalently, amine terminated magnetic NPs (larger than 100 nm) were internalized through endocytosis processes, which might vary (involving different CM proteins such as clathrin, caveolin, *etc.*) depending on the size and surface of the NPs (Chaudhary et al., 2013; Child et al., 2011; Dejardin et al., 2011).

2.4. Surface Chemistry

Appropriate surface coating can lower the energy barrier exerted during translocation across the CM and thus switch from uptake *via* endocytosis to uptake through pores. In this regard, the group of Stellacci (Jewell et al., 2011; Verma et al., 2008; Verma and Stellacci, 2010) showed that the structural organization of chemical groups on the surface of the NPs can dictate their interaction with the CM. 5 nm Au NPs coated with a pattern of hydrophobic and anionic ligands could pass through the CM of dendritic cells at 4°C without permanently disrupting it (Verma et al., 2008). The authors claimed that the pattern is formed by ligands, which are regularly arranged in ribbon-like domains of alternating composition. Conversely, the same sized Au NPs with structural disorder in the ligand shell did not penetrate CMs. However, the incorporation of these hydrophobic NPs into the membrane bilayer was associated with membrane swelling (Verma and Stellacci, 2010). The patterned NPs with anisotropic ligands encountered the lowest energy barrier when passing through the hydrophobic core of bilayer, as demonstrated by dissipative NP dynamics simulations (Li et al., 2012).

Phospholipid (as in the CM) binding to Au NPs enabled the immobilization on the surface of living cells, and were delivered to the CM *via* rather slow diffusion of lipid coated NPs, avoiding non-specific binding (Ba et al., 2010). Peptides can also change NP uptake from endocytosis to penetration *via* transient pores. Cell penetrating peptides are an important example in this direction (Josephson et al., 1999; Nativo et al., 2008). The type of peptide conjugation can play a critical role on the interaction of NPs with the CM, but it can also influence the cellular behavior. For example, Au NPs of the same size and charge but different peptides on their surface showed a substantially different exocytosis rate in endothelial cells (Bartczak et al., 2012b).

3. Strategies for crossing CMs to improve targeted NP delivery

NPs have been used as carriers for several anti-cancer drugs including paclitaxel, doxorubicin, and 5-fluorouracil. Various types of designs have been tested as drug delivery vehicles (Yoo et al., 2011). The most widely employed ones are: (i) entrapping the drug inside a nano-cavity such as liposomes or hollow NPs (Al-Jamal and Kostarelos, 2011), (ii) entrapping it inside mesoporous NPs (Bringas et al., 2012; Kim et al., 2008; Zhang et al., 2011b), and (iii) attaching the drug to the surface of the NPs. Although, the interaction between the NP and the CM determines the successful entry of the NP into the cell, this is not the only critical factor for delivering the drugs to the targeted organelles. The non-specific interactions between the endocellular biological molecular cocktail and the particles as well as the target selectivity, period of drug release, and exocytosis of the carrier play an equal critical role on the successful drug delivery. Nevertheless, two of the main advantages of delivering drugs using NP carriers are the highest localized drug reactivity, and the targeting of specific types of cells. Amphotericin B (AMB), an antifungal drug often used for fungal infections, can bind to sterol-containing CMs, resulting in the formation of holes in the CM, which decreases the CM integrity and eventually results in cell death. A primary sterol in fungal membranes is ergosterol which can be attacked by AMB. Although AMB has a lower effect on cholesterol-containing CMs, it has a toxic effect on some mammalian cells. It was reported that the side effect of AMB on other cells could be decreased by packing the AMB into a nanosized delivery vehicle based on phospholipid and apolipoprotein A-I (Burgess et al., 2010). In the same study, it was noticed that the nanocarriers can even restore the CM integrity of previously AMB-exposed cells.

The appropriate bioconjugation of NPs (with biological ligands, such as peptides/proteins (Chan and Nie, 1998; Pinaud et al., 2004) or sugars (Luo et al., 2011; Moros et al., 2012; Qiu et al., 2010) leads to their targeting to the specific CMs. This results in receptor-mediated endocytosis (Goldstein et al., 1979; Tekle et al., 2008; Yang et al., 2005). For example, QDs that were conjugated with specific targeting ligands such as Cholera Toxin B and polyarginine conjugates labeled vesicles and perinuclear endosomes (Chakraborty et al., 2007). Besides their intrinsic properties, NPs are also modified by their environment, which in turn influences their interaction with CMs. The attachment of cell-penetrating peptides (CPP) to NPs has also been reported to

enable direct permeation of NPs through the CM, bypassing endocytosis. For example, arginine conjugated iron oxide NPs loaded with siRNA permeated across the CM for direct access to the cytoplasm (Veiseh et al., 2011). Avoiding endocytosis and the corresponding NPs entrapment in endocytic vesicles would be highly beneficial for myriad bioapplications. However, other reports on the internalization of NPs derivatized with penetratin or TAT (two of the most studied peptides among CPPs) have pointed out that the internalization occurs *via* endocytosis (Chaudhary et al., 2013; Child et al., 2011; Dejardin et al., 2011, Yuan et al., 2012). These studies illustrate that CPPs can improve the internalization of NPs more than 100-fold (Josephson et al., 1999).

Nevertheless, the classical way of targeting is *via* receptor-mediated endocytosis (Parton and Simons, 2007). The receptors on the CM, which are responsible for membrane recycling pathways, can be employed as targeting points (Farokhzad and Langer, 2009). The use of doxorubicin-polyethylene glycol-folate (DOX-PEG-FOL) conjugated NPs (containing the hydrophobic DOX in the center of the nanoconjugate and FOL on the NP surface) was also reported (Yoo and Park, 2004). In this study, the higher intracellular uptake by FOL-receptor-positive cancer cells in comparison with FOL-receptor-negative cells was observed, due to FOL-receptor-mediated endocytosis uptake mechanism. In another example, RGD peptides were conjugated to the PEG coating of NPs, which enhanced the cellular uptake and targeting efficiency of the NPs (Hak et al., 2012).

Cell surface receptor specific ligands such as RGD peptides conjugated to the PEG coating in order to obtain specificity for the integrin, can enhance the cellular uptake and targeting efficiency of NPs (Hak et al., 2012). This study confirmed that RGD nanoemulsions were mainly internalized through a caveolae-dependent pathway, which was consistent with the reports that αvβ3-integrin can be internalized *via* caveolae-mediated endocytosis (Caswell and Norman, 2008). QDs conjugated with receptor-mediated endocytosis signaling peptides were shown to directly access the cell nucleus through interaction with the nuclear pore complex. It was found that approximately 28% of nuclear localization signaling (NLS) peptide-coated QDs and 25% of Tat-NLS peptide coated QDs could be delivered into the cell nucleus (Kuo et al., 2011). Very recently, one of our groups (Narayanan et al., 2013) have shown that a higher nucleus targeting of over 60% can be achieved by mimicking the cellular transport pathway using a combined NLS and microtubule-associated sequence (MTAS) peptide-coated CdSe/ZnS QDs. The authors have used biotinylated peptides with NLS and MTAS for conjugation with streptavidin-coated QDs, and have found that these bioconjugated QDs enhance the endosomal escape and promote targeted delivery into the nucleus of human mesenchymal stem cells via microtubules.

NPs can be used to target EGF receptor and cell adhesion molecules such as integrins, cadherins and selectins to control the disease progression (Moghimi et al., 2005; Suri et al., 2007). Carbon nanotubes (CNTs) are a very comprehensive example, which shows the effect of carrier geometry (Hilder and Hill, 2008) and surface chemistry. Pristine CNTs are insoluble in many solvents. Therefore, functionalization is used to make them dispersible. It has been shown that functionalized single wall CNTs can cross the CM (Pantarotto et al., 2004a), and also enter both non-adherent and adherent cell lines *via* endocytosis (Shi Kam et al., 2004). In this case, multiple proteins, which cannot enter the cells individually, can be transported inside the cell by simultaneous adsorption on the surface of oxidized single wall CNTs. The CNT-protein conjugates pass through the CM by endocytosis and reach the cytoplasm after releasing from endosomes (Kam and Dai, 2005). In addition, single wall CNTs showed comparable exocytosis and endoytsosis rates (Jin et al., 2008). Attachment of multiple molecules and functional groups provide facile opportunities for targeted drug delivery applications. The binding between EGF and EGF-receptors on the cancer cells was achieved by functionalizing the CNT with cisplatin, an anticancer drug and EGF (Bhirde et al., 2009). The above studies showed that the functional groups on the CNT surface and their interaction with the CM played an important role on the uptake mechanism and delivery pathways (Bianco et al., 2005). However, there are other reports which indicate the endosome-independent penetration of CNT-DNA complexes (Pantarotto et al., 2004a). All these examples show how the CNTs can interact with CMs and deliver cargo into the cell *via* specific and unspecific uptake mechanisms. An additional approach is based on mechanical force. Functionalized CNTs immobilized on an atomic force microscopy (AFM) tip can be used to deliver cargo molecules into cells (Chen et al., 2007). In this particular case, after penetration of the CM by force, molecules from the CNT surface were released into the cytosol *via* reductive cleavage of disulfide bonds. In a similar approach, multi-walled CNTs were pumped to cross the CM and released into the cytosol and organelles using a glass pipette (Singhal et al., 2011).

4. Applications of regulated NP-CM interactions

4.1. Gene therapy

Transfection and gene delivery have been equally targeted to alter the cellular behavior. Mesoporous silica NPs, QDs, chitosan, polylactic/glycolic acid (PLGA) and PLGA-based NPs have been used for *in vitro* ribonucleic acid interference (RNAi) delivery (Hom et al., 2010; Meng et al., 2010; Meng et al., 2013; Xia et al., 2009). The optimized NPs for transfection should have targeting properties for the specific type of target cells/tissues, high cellular uptake probability, and a delivery mechanism to the desired intracellular location. For achieving these criteria, the interaction of NPs with the CM is crucial. NPs can contribute to gene delivery in different directions. First, by tuning the geometry of the NPs, different interaction mechanisms with the CM can be achieved. In this case, CNTs have shown to be promising agents for gene delivery (Liu et al., 2011). More specifically, by employing ionic interaction, plasmid DNA was attached to the surface of functionalized CNTs. These supramolecular complexes showed an endosome-independent cell penetration (Pantarotto et al., 2004b). As mentioned previously in the case of drug delivery, the penetration of CNTs through the CM can be facilitated, by using the needle shaped CNTs and by the application of a magnetic field (Cai et al., 2005). This approach is called spearing. It starts by a rotating magnetic field to pierce the CM, followed by a constant magnetic field. Since DNA delivery inside the cell through endosomal or lysosomal pathways results in the hydrolyzation of DNA, the spearing penetration of CNTs into the nucleus, is considered as a promising method for genetic transduction of DNA. Second, NPs may reduce cytotoxic effects, which may normally occur during gene delivery. An approach to deliver DNA to the cytosol is by its complexation with PEI. By altering the pH in the endosomes, PEI is able to create an osmotic effect that leads to the rupture of the endosome, facilitating the release of DNA to the cytosol (Wagner, 2012). However, PEI may be toxic to the cellular membrane. More sophisticated NP formulations help to reduce cytotoxicity. For example, gene delivery by ultrasound mediated nano-bubbles has recently become an attractive system, both from application as well as research point of view (Suzuki et al., 2011). In another study, albumin microbubbles were used but resulted in low conjugation with plasmid DNA, due to the negative surface potential of albumin (Dang et al., 2011). On the other hand, PEI coated albumin microbubbles (PAMB) with positive surface charge showed the same transgene effect but with a lower toxicity, in comparison with Lipofectamine 2000. The ultrasound-mediated destruction of microbubbles and formation of cavitation facilitates gene entry into the cell. Cavitation can disrupt the capillaries inside the CM and therefore increases the cell permeability. The permeability of CMs can alter the oscillation of microbubbles due to ultrasound stimulation. As an alternative to PEI, photochemical disruption of endosomal membranes has also been demonstrated (de Bruin et al., 2008). Third, NPs allow for integration of several functionalities into one carrier system (Peteiro-Cartelle et al., 2009; Rivera-Gil and Parak, 2008). A multifunctional envelop type nanodevice (MEND) was reported for gene delivery into tumors (Hatakeyama et al., 2011). MEND was constructed by a core of nucleic acid covered with a lipid envelope. Various functional groups were added to the lipid membrane: PEG to enhance blood circulation times, cell penetrating peptides to enhance cellular uptake, and fusogenic lipids for endosomal escape.

The magnetically assisted transfection (magnetofection) is an elegant method of increasing the transfection efficiency of non-viral vectors (Scherer et al., 2002). It was hypothesized that the lipospheres functionalized with magnetic NPs could greatly enhance the release siRNA to the cytosol *via* either magnetic field gradient pulling across the CM or fusion with the lipidic components of the CM or *via* endocytosis and degradation of lipospheres in endosomes (del Pino, et al., 2010).

4.2. Hyperthermia therapy

The cell can be sensitive to environmental variations. For example, a small increase in the local temperature (even a few degrees) or a high production of free radicals can result in the damage of the cellular membrane (Laurent et al., 2011). Nowadays, with the facilitation of new methods to synthesize and functionalize inorganic NPs, advanced types of NPs can deliberately cause such type of variations to the surrounding environment of a cell. For example, metal NPs can be irradiated with lasers, generating a temperature increase at their vicinity or a high volume of free radicals (Bardhan et al., 2009; O'Neal et al., 2004). These effects are strongly dependent on the laser power and the NP morphological characteristics. On the other hand, magnetic NPs can induce a temperature increase with the application of strong magnetic fields (Gazeau et al., 2008; Lévy et al., 2011; Lévy et al., 2008). Recent studies showed that under mild laser conditions involving NPs

bound to the cellular membrane of endothelial cells, the cellular membrane can be temporarily damaged and recovered without promoting cellular death (Bartczak et al., 2011). This method could open up new directions in cellular nanosurgery, where the cellular membrane could be deliberately opened, facilitating the easy delivery of drugs to cells. Ag NPs decorated on magnetic beads served as photothermal agents upon near-infrared (NIR) irradiation and caused the cell death of cancerous cells (*e.g.* HeLa and KB) (Di Corato et al., 2012; Huang et al., 2008). It is known that cancerous cells are more sensitive to temperature variations in comparison to healthy cells (Gordon et al., 1979; Jordan et al., 2006; Jordan et al., 1993; Kong et al., 2000; Wust et al., 2002).

The surface functionalization methods for NPs need to be judiciously designed in order to target only malignant cells, avoiding the uptake of NPs by non-malignant cells. The presence of overexpressed epidermal growth factor receptor (EGFR) on the CM of malignant cells provides an opportunity for targeting these cells. Bifunctional Au NRs functionalized with anti-EGFR were employed as agents for both labeling and photothermal cancer therapy (Huang et al., 2006). The size of the NRs was designed to be active in the NIR region, which is an optical window for biological tissue. The light absorption is minimum in the NIR and hence the light penetration inside the tissue is maximum (Smith et al., 2009). The imaging properties of these NRs were related to their strong light scattering in the NIR region using dark field microscopy. The EGFR targeting and cellular uptake resulted in the increase of the NRs concentration inside malignant cells. Therefore, upon exposure to 800 nm continuous laser light, the surface plasmon resonance of the NRs increased their temperature inside the cells. Due to the higher concentration of NRs inside malignant cells, the required energy for their destruction was about half the laser energy required for the destruction of non-malignant cells (Dickerson et al., 2008). More details on the Au NR-CM interaction, the cellular uptake, and the mechanism of Au NR-assisted hyperthermia (HT) were described (Fernandez Cabada et al. , 2012). The uptake of Au NRs by glioblastoma cells revealed that following the uptake, the NRs were bound inside the membrane and not freely dispersed in the cytoplasm. These membrane-bound compartments were compatible with endosomes and/or lysosomes. Cell viability tests (as evaluated by a lactate dehydrogenase release assay) after laser irradiation, showed that NRs compromised the integrity of the CM (necrosis). However, no evidence of the process of programmed cell death (apoptosis) was noticed. In fact, a higher HT effect was noticed for NRs located on the CM, which implied that the CM was the most effective component for the thermal damage.

4.3. Strategies to penetrate the blood brain barrier

The blood brain barrier (BBB) separates the circulating blood from brain extracellular fluid. The tight junction between the BBB endothelial cells prevents the diffusion of large objects to the central nervous system (CNS). Treatments of various neurodegenerative diseases rely on the delivery of the drug to the brain. However, due to restriction of diffusion of most of the drug molecules from blood capillaries to the BBB, the fast and efficient delivery of the drug is a big challenge (Krol et al., 2012). In this case, NPs with modified surface properties that can interact with CMs of the barrier are recognized as promising candidates (Bhaskar et al., 2010). The most widely employed method for the transport of NPs is *via* receptor-mediated transcytosis (Ulbrich et al., 2009). For instance, Tween 80 (T-80) coated PLGA NPs were employed as estradiol carrier. T-80 enhanced the targeting of NPs to the brain through the endocytosis-mediated transportation across CM barriers. Apolipoprotein E and/or B (which are present inside the blood stream) were attached to the surface of NPs by T-80. These coated NPs interacted with lipoprotein receptors on the CM of the brain capillary endothelial cells, stimulating endocytotic uptake.

4.4. Limitations of the nano-targeting approach

It has been claimed that the decoration of protein corona can cover/eliminate the targeting moieties on the surface of NPs and therefore, strongly reduce the recognition of the targeting ligands by the CM receptors (Laurent and Mahmoudi, 2011).

In agreement with the claim, it has been recently shown that the targeting ability of transferrin-conjugated NPs was significantly reduced, after interaction of NPs with serum proteins. More specifically, protein corona shielded transferrin from binding to its targeted receptors on the CM (Salvati et al., 2013). Furthermore, to simulate the protein corona's effects on reducing targeting capability, a copper-free click reaction between NPs functionalized with a strained cycloalkyne, bicyclononyne (BCN) and an azide on a silicon substrate as the model targeting reaction, was employed (Figure 4) (Mirshafiee et al., 2013).

The conjugation of pristine BCN-NPs to those of BCN-NPs exposed to protein media that mimic *in vitro* culture conditions (*i.e.* medium with 10% serum) and the biological fluids present *in vivo* (*i.e.* 100% serum) were compared. The fluorescence microscopy images confirmed a high number of the pristine BCN-NPs conjugated to the azide-functionalized substrate, whereas there were a few 10% or 100% serum corona BCN-NPs attached to the azide-functionalized substrates. Using quantitative analysis, it was found that the number of conjugated NPs, and therefore the targeting efficiencies for the 10% and 100% serum corona BCN-NPs were lower than that of the pristine BCN-NPs by 94 and 99%, respectively (see Figure 4 for details) (Mirshafiee et al., 2013).

The conformational changes of the adsorbed proteins on the surface of NPs can lead to exposing the buried sequences (hydrophobic/charged) of specific proteins, which alter the way how the adsorbed proteins interact with CMs. For example, it was shown that negatively charged poly (acrylic acid)-conjugated Au NPs induce unfolding of the fibrinogen protein, which leads to exposing the normally buried sequence (C-terminus of γ chain) to the CMs (Deng et al., 2011). In this case, the unfolded fibrinogen interacted with the integrin receptor, Mac-1, of CM of human acute monocytic leukemia cell line. Activation of this receptor increased the NF-κB signalling pathway, resulting in the release of inflammatory cytokines. It is noteworthy to mention that not all NPs (*e.g.* SiO_2, TiO_2, and ZnO) that bind to fibrinogen demonstrated the Mac-1 activation effect (due to the fact that the C-terminus of γ chain of fibrinogen was not exposed to the CM). Thus, one can expect that the binding of certain NPs to fibrinogen in plasma offers an alternative mechanism to the more commonly described role of ROS (Park and Park, 2009; Xia et al., 2006; Yang et al., 2009) in the inflammatory response to NPs. In summary, the protein corona of NPs can interfere with the targeting strategy, which makes the rational design of specificity more difficult.

5. Summary and Outlook

This review highlights the central role of the CM for the delivery of NPs inside cells. We have given extensive examples of NPs with different functionalities made from a wide variety of materials with different charge, geometry and surface functionalization, and discussed their interactions with the CM, involving potential applications. Due to the varieties of cell types, biological environments and NPs, there are still many questions to be answered. We expect that more scientists will engage in research to reveal the nature of interactions between the CM, protein corona, and the different types of advanced NPs. This knowledge pool will be critical to realize the full potential of nanomaterials for either *in vitro* or *in vivo* applications. The better understanding of cellular functions and dynamics will shed more light on the design of NPs-in-demand for different applications, by considering toxicological issues.

Declaration of interest

The authors do not have any conflicts of interest to declare.

Acknowledgement

A part of this work was funded by HSFP (project RGP0052/2012 to WJP). WJP acknowledges the support from the Chinese Academy of Sciences (visiting professorship for senior international scientists, grant No. 2012T1J0021). BP acknowledges the Alexander von Humboldt Foundation for a Postdoctoral fellowship. AGK would like to thank the EU COST actions MP1202, MP1005 and TD1003 for networking opportunities associated to this work. STS acknowledges the funding from the Agency for Science, Technology and Research (A*STAR) Joint Council Office, JCO (Grant: JCOAG03_FG03_2009), Singapore.

References

Al-Jamal WT, Kostarelos K. Liposomes: from a clinically established drug delivery system to a nanoparticle platform for theranostic nanomedicine. Acc Chem Res 2011;44:1094-104.

Albanese A, Chan WCW. Effect of gold nanoparticle aggregation on cell uptake and toxicity. ACS Nano 2011;5:5478-89.

Alkilany AM, Nagaria PK, Hexel CR, Shaw TJ, Murphy CJ, Wyatt MD. Cellular uptake and cytotoxicity of gold nanorods: molecular origin of cytotoxicity and surface effects. Small 2009;5:701-8.

Anitei M, Hoflack B. Bridging membrane and cytoskeleton dynamics in the secretory and endocytic pathways. Nat Cell Biol 2012;14:11-9.
Asati A, Santra S, Kaittanis C, Perez JM. Surface-charge-dependent cell localization and cytotoxicity of cerium oxide nanoparticles. ACS Nano 2010;4:5321-31.
Ba HJ, Rodríguez-Fernández J, Stefani, FD, Feldmann J. Immobilization of gold nanoparticles on living cell membranes upon controlled lipid binding. Nano Lett 2010;10:3006-12.
Bao G, Bao XR. Shedding light on the dynamics of endocytosis and viral budding. Proc Natl Acad Sci U S A 2005;102:9997-8.
Bardhan R, Chen W, Perez-Torres C, Bartels M, Huschka RM, Zhao LL, et al. Nanoshells with targeted simultaneous enhancement of magnetic and optical imaging and photothermal therapeutic response. Adv Funct Mater 2009;19:3901-9.
Bartczak D, Kanaras A. Preparation of peptide-functionalized gold nanoparticles using one pot EDC/sulfo-NHS coupling. Langmuir 2011;27:10119-23.
Bartczak D, Kanaras AG. Diacetylene-containing ligand as a new capping agent for the preparation of water-soluble colloidal nanoparticles of remarkable stability. Langmuir 2010;26:7072-7.
Bartczak D, Muskens OL, Millar TM, Sanchez-Elsner T, Kanaras AG. Laser-induced damage and recovery of plasmonically targeted human endothelial cells. Nano Lett 2011;11:1358-63.
Bartczak D, Muskens OL, Nitti S, Sanchez-Elsner T, Millar TM, Kanaras AG. Interactions of human endothelial cells with gold nanoparticles of different morphologies. Small 2012a;8:122-30.
Bartczak D, Nitti S, Millar TM, Kanaras AG. Exocytosis of peptide functionalized gold nanoparticles in endothelial cells. Nanoscale 2012b; 4:4470-2.
Bhabra G, Sood A, Fisher B, Cartwright L, Saunders M, Evans WH, et al. Nanoparticles can cause DNA damage across a cellular barrier. Nature Nanotechnol 2009;4:876-83.
Bhaskar S, Tian FR, Stoeger T, Kreyling W, de la Fuente JM, Grazu V, et al. Multifunctional nanocarriers for diagnostics, drug delivery and targeted treatment across blood-brain barrier: perspectives on tracking and neuroimaging. Particle and Fibre Toxicology 2010;7:3.
Bhirde AA, Patel V, Gavard J, Zhang G, Sousa AA, Masedunskas A, et al. Targeted killing of cancer cells in vivo and in vitro with EGF-directed carbon nanotube-based drug delivery. ACS Nano 2009;3:307-16.
Bianco A, Kostarelos K, Prato M. Applications of carbon nanotubes in drug delivery. Curr Opin Chem Biol 2005;9:674-9.
Bretscher MS. Membrane structure: some general principles. Science 1973;181:622 - 9.
Bringas E, Koysuren O, Quach DV, Mahmoudi M, Aznar E, Roehling JD, et al. Triggered release in lipid bilayer-capped mesoporous silica nanoparticles containing SPION using an alternating magnetic field. Chem Commun 2012;48:5647-9.
Buono C, Anzinger JJ, Amar M, Kruth HS. Fluorescent pegylated nanoparticles demonstrate fluid-phase pinocytosis by macrophages in mouse atherosclerotic lesions. Journal of Clinical Investigation 2009;119:1373-81.
Burgess BL, Cavigiolio G, Fannucchi MV, Illek B, Forte TM, Oda MN. A phospholipid-apolipoprotein A-I nanoparticle containing amphotericin B as a drug delivery platform with cell membrane protective properties. Int J Pharm 2010;399:148-55.
Cai D, Mataraza JM, Qin ZH, Huang Z, Huang J, Chiles TC, et al. Highly efficient molecular delivery into mammalian cells using carbon nanotube spearing. Nat Methods 2005;2:449-54.
Candeloro P, Tirinato L, Malara N, Fregola A, Casals E, Puntes V, et al. Nanoparticle microinjection and Raman spectroscopy as tools for nanotoxicology studies. Analyst 2011;136:4402-8.
Canton I, Battaglia G. Endocytosis at the nanoscale. Chem Soc Rev 2012;41:2718-39.
Caswell P, Norman J. Endocytic transport of integrins during cell migration and invasion. Trends Cell Biol 2008;18:257-63.
Chakraborty SK, Fitzpatrick JAJ, Phillippi JA, Andreko S, Waggoner AS, Bruchez MP, et al. Cholera Toxin B conjugated quantum dots for live cell labeling. Nano Lett 2007;7:2618-26.
Chan WCW, Nie S. Quantum dot bioconjugates for ultrasensitive nonisotopic detection. Science 1998;281:2016-8.
Chaudhary S, Smith C, del Pino P, de la Fuente J, Mullin M, Hursthouse A, et al. Elucidating the function of penetratin and a static magnetic field in cellular uptake of magnetic nanoparticles. Pharmaceuticals 2013;6:204-22.

Chen X, Kis A, Zettl A, Bertozzi CR. A cell nanoinjector based on carbon nanotubes. Proc Natl Acad Sci U S A 2007;104:8218-22.
Cheng S, Levy D. The effects of cell proliferation on the lipid composition and fluidity of hepatocyte plasma membranes. Arch Biochem Biophys 1979;196:424-9.
Child HW, Del Pino PA, De La Fuente JM, Hursthouse AS, Stirling D, Mullen M, et al. Working together: the combined application of a magnetic field and penetratin for the delivery of magnetic nanoparticles to cells in 3D. ACS Nano 2011;5:7910-9.
Chithrani BD, Ghazan AA, Chan CW. Determining the size and the shape dependence of gold nanoparticle uptake into mammalian cells. Nano Lett 2006;6:662-8.
Chithrani BD, Chan WCW. Elucidating the mechanism of cellular uptake and removal of protein-coated gold nanoparticles of different sizes and shapes. Nano Lett 2007;7:1542-50.
Chithrani DB. Intracellular uptake, transport, and processing of gold nanostructures. Mol Membr Biol 2010;27:299-311.
Cho EC, Au L, Zhang Q, Xia Y. The effects of size, shape, and surface functional group of gold nanostructures on their adsorption and internalization by cells. Small 2010;6:517-22.
Cho EC, Zhang Q, Xia YN. The effect of sedimentation and diffusion on cellular uptake of gold nanoparticles. Nat Nanotechnol 2011;6:385-91.
Choi CHJ, Zuckerman JE, Webster P, Davis ME. Targeting kidney mesangium by nanoparticles of defined size. Proc Natl Acad Sci U S A 2011;108:6656-61.
Chou LY, Ming K, Chan WC. Strategies for the intracellular delivery of nanoparticles. Chem Soc Rev 2011;40:233-45.
Cortie MB, McDonagh AM. Synthesis and optical properties of hybrid and alloy plasmonic nanoparticles. Chem Rev 2011;111:3713-35.
Cross TA, Sharma M, Yi M, Zhou HX. Influence of solubilizing environments on membrane protein structures. Trends Biochem Sci 2011;36:117-25.
Cutler JI, Auyeung E, Mirkin CA. Spherical Nucleic Acids. J Am Chem Soc 2012;134:1376-91.
Dahan M, Laurence T, Pinaud F, Chemla DS, Alivisatos AP, Sauer M, et al. Time-gated biological imaging by use of colloidal quantum dots. Opt Lett 2001;26:825-7.
Daley DO. The assembly of membrane proteins into complexes. Curr Opin Struct Biol 2008;18:420-4.
Dang SP, Wang RX, Qin MD, Zhang Y, Gu YZ, Wang MY, et al. A novel transfection method for eukaryotic cells using polyethylenimine coated albumin microbubbles. Plasmid 2011;66:19-25.
Dawson KA. Leave the policing to others. Nat Nanotechnol 2013;8:73-3.
Day HA, Bartczak D, Fairbairn N, Mcguire E, Ardakani M, Porter AE, et al. Controlling the three-dimensional morphology of nanocrystals. CrystEngComm 2010;12:4312-6.
de Bruin KG, Fella C, Ogris M, Wagner E, Ruthardt N, Brauchle C. Dynamics of photoinduced endosomal release of polyplexes. J Control Release 2008;130:175-82.
de la Fuente JM, Berry CC. Tat peptide as an efficient molecule to translocate gold nanoparticles into the cell nucleus. Bioconjugate Chem 2005;16:1176-80.
Decuzzi P, Ferrari M. The role of specific and non-specific interactions in receptor-mediated endocytosis of nanoparticles. Biomaterials 2007;28:2915-22.
Dejardin T, de la Fuente J, del Pino P, Furlani EP, Mullin M, Smith CA, et al. Influence of both a static magnetic field and penetratin on magnetic nanoparticle delivery into fibroblasts. Nanomedicine 2011;6:1719-31.
del Pino P, Munoz-Javier A, Vlaskou D, Rivera Gil P, Plank C, Parak WJ. Gene silencing mediated by magnetic lipospheres tagged with small interfering RNA. Nano Lett 2010;10:3914-21.
Deng ZJ, Liang M, Monteiro M, Toth I, Minchin RF. Nanoparticle-induced unfolding of fibrinogen promotes Mac-1 receptor activation and inflammation. Nat Nanotechnol 2011;6:39-44.
Derfus AM, Chan WCW, Bhatia SN. Intracellular delivery of quantum dots for live cell labeling and organelle tracking. Adv Mater 2004;16:961-6.
Deserno M. When do fluid membranes engulf sticky colloids? J Phys: Condens Matter 2004;16:1-10.
Deserno M, Gelbart WM. Adhesion and wrapping in colloid-vesicle complexes. J Phys Chem B 2002;106:5543-52.
Di Corato R, Palumberi D, Marotta R, Scotto M, Carregal-Romero S, Rivera_Gil P, et al. Magnetic nanobeads decorated with silver nanoparticles as cytotoxic agents and photothermal probes. Small 2012;8:2731-42.

Dickerson EB, Dreaden EC, Huang X, El-Sayed IH, Chu H, Pushpanketh S, et al. Gold nanorod assisted near-infrared plasmonic photothermal therapy (PPTT) of squamous cell carcinoma in mice. Cancer Lett 2008;269:57-66.
Doane TL, Cheng Y, Babar A, Hill RJ, Burda C. Electrophoretic mobilities of PEGylated gold NPs. J Am Chem Soc 2010;132:15624-31.
Dubavik A, Sezgin E, Lesnyak V, Gaponik N, Schwille P, Eychmüller A. Penetration of amphiphilic quantum dots through model and cellular plasma membranes. ACS Nano 2012;6:2150-6.
Dustin ML, Long EO. Cytotoxic immunological synapses. Immunological Reviews 2010;235:24-34.
Farokhzad OC, Langer R. Impact of nanotechnology on drug delivery. ACS Nano 2009;3:16-20.
Fercher A, Borisov SM, Zhdanov AV, Klimant I, Papkovsky DB. Intracellular O_2 sensing probe based on cell-penetrating phosphorescent nanoparticles. ACS Nano 2011;5:5499-508.
Fernandez Cabada T, de Pablo CS, Serrano AM, Guerrero Fdel P, Olmedo JJ, Gomez MR. Induction of cell death in a glioblastoma line by hyperthermic therapy based on gold nanorods. International Journal of Nanomedicine 2012;7:1511-23.
Fischer HC, Chan WCW. Nanotoxicity: the growing need for in vivo study. Curr Opin Biotechnol 2007;18:565-71.
Gazeau F, Lévy M, Wilhelm C. Optimizing magnetic nanoparticle design for nanothermotherapy. Nanomedicine 2008;3:831-44.
Ghavami M, Saffar S, Abd Emamy B, Peirovi A, Shokrgozar MA, Serpooshan V, et al. Plasma concentration gradient influences the protein corona decoration on nanoparticles. RSC Advances 2013;3:1119-26.
Goesmann H, Feldmann C. Nanoparticulate functional materials. Angew Chem Int Ed 2010;49:1362-95.
Goldstein JL, Anderson RG, Brown MS. Coated pits, coated vesicles, and receptor-mediated endocytosis. Nature 1979;279:679-85.
Goodman CM, McCusker CD, Yilmaz T, Rotello VM. Toxicity of gold nanoparticles functionalized with cationic and anionic side chains. Bioconjugate Chem 2004;15:897-900.
Gordon RT, Hines JR, Gordon D. Intracellular hyperthermia a biophysical approach to cancer treatment via intracellular temperature and biophysical alterations. Med Hypotheses 1979;5:83-102.
Gu Y, Sun W, Wang G, Fang N. Single particle orientation and rotation tracking discloses distinctive rotational dynamics of drug delivery vectors on live cell membranes. J Am Chem Soc 2011;133:5720-3.
Gulaya NM, Volkov GL, Klimashevsky VM, Govseeva NN, Melnik AA. Changes in lipid composition of neuroblastoma C1300 N18 cell during differentiation. Neuroscience 1989;30:153-64.
Hak S, Helgesen E, Hektoen HH, Huuse EM, Jarzyna PA, Mulder WJM, et al. The effect of nanoparticle polyethylene glycol surface density on ligand-directed tumor targeting studied in vivo by dual modality imaging. ACS Nano 2012;6:5648-58.
Hatakeyama H, Akita H, Harashima H. A multifunctional envelope type nano device (MEND) for gene delivery to tumours based on the EPR effect: a strategy for overcoming the PEG dilemma. Adv Drug Deliv Rev 2011;63:152-60.
Hilder TA, Hill JM. Carbon nanotubes as drug delivery nanocapsules. Current Applied Physics 2008;8:258-61.
Hine R. The facts on file dictionary of biology. New York: Facts On File; 1999.
Hofinger S, Melle-Franco M, Gallo T, Cantelli A, Calvaresi M, Gomes JA, et al. A computational analysis of the insertion of carbon nanotubes into cellular membranes. Biomaterials 2011;32:7079-85.
Hom C, Lu J, Liong M, Luo H, Li Z, Zink JI, et al. Mesoporous silica nanoparticles facilitate delivery of siRNA to shutdown signaling pathways in mammalian cells. Small 2010;6:1185-90.
Howard KA. Delivery of RNA interference therapeutics using polycation-based nanoparticles. Advanced Drug Delivery Reviews 2009;61:710-20.
Huang X, El-Sayed IH, Qian W, El-Sayed MA. Cancer cell imaging and photothermal therapy in the near-infrared region by using gold nanorods. J Am Chem Soc 2006;128:2115-20.
Huang X, Jain PK, El-Sayed IH, El-Sayed MA. Plasmonic photothermal therapy (PPTT) using gold nanoparticles. Lasers in Medical Science 2008;23:217-28.
Hühn D, Kantner K, Geidel C, Brandholt S, De Cock I, Soenen SJH, et al. Polymer-coated nanoparticles interacting with proteins and cells: focusing on the sign of the net charge. ACS Nano 2013; 7:3253-63.
Ibanez M, Zamani R, Li WH, Shavel A, Arbiol J, Morante JR, et al. Extending the nanocrystal synthesis control to quaternary compositions. Crystal Growth & Design 2012;12:1085-90.
Jewell CM, Jung JM, Atukorale PU, Carney RP, Stellacci F, Irvine DJ. Oligonucleotide delivery by cell-penetrating "striped" nanoparticles. Angew Chem Int Ed 2011;50:12312-5.

Jiang W, Kim BYS, Rutka JT, Chan WCW. Nanoparticle-mediated cellular response is size-dependent. Nat Nanotechnol 2008;3:145-50.
Jin H, Heller DA, Sharma R, Strano MS. Size-dependent cellular uptake and expulsion of single-walled carbon nanotubes: single particle tracking and a generic uptake model for nanoparticles. ACS Nano 2009;3:149-58.
Jin H, Heller DA, Strano MS. Single-particle tracking of endocytosis and exocytosis of single-walled carbon nanotubes in NIH-3T3 cells. Nano Lett 2008;8:1577-85.
Jordan A, Scholz R, Maier-Hauff K, van Landeghem FKH, Waldoefner N, Teichgraeber U, et al. The effect of thermotherapy using magnetic nanoparticles on rat malignant glioma. J Neurooncol 2006;78:7-14.
Jordan A, Wust P, Fahling H, John W, Hinz A, Felix R. Inductive heating of ferrimagnetic particles and magnetic fluids: physical evaluation of their potential for hyperthermia. Int J Hyperthermia 1993;9:51-68.
Josephson L, Tung C-H, Moore A, Weissleder R. High-efficiency intracellular magnetic labeling with novel superparamagnetic-Tat peptide conjugates. Bioconjugate Chem 1999;10:186-91.
Kam NW, Dai H. Carbon nanotubes as intracellular protein transporters: generality and biological functionality. J Am Chem Soc 2005;127:6021-6.
Kanaras AG, Kamounah FS, Schaumburg K, Kiely CJ, Brust M. Thioalkylated tetraethylene glycol: a new ligand for water soluble monolayer protected gold clusters. Chem Commun 2002;2002:2294-5.
Kievit FM, Veiseh O, Bhattarai N, Fang C, Gunn JW, Lee D, et al. PEI–PEG–chitosan-copolymer-coated iron oxide nanoparticles for safe gene delivery: synthesis, complexation, and transfection. Adv Func Mater 2009;19:2244-51.
Kim B, Han G, Toley BJ, Kim CK, Rotello VM, Forbes NS. Tuning payload delivery in tumour cylindroids using gold nanoparticles. Nature Nanotechnol 2010;5:465-72.
Kim J, Kim HS, Lee N, Kim T, Kim H, Yu T, et al. Multifunctional uniform nanoparticles composed of a magnetite nanocrystal core and a mesoporous silica shell for magnetic resonance and fluorescence imaging and for drug delivery. Angew Chem Int. Ed 2008;120:8566-9.
Kong G, Braun RD, Dewhirst MW. Hyperthermia enables tumor-specific nanoparticle delivery: effect of particle size. Cancer Res. 2000;60:4440-5.
Krol S, Macrez R, Docagne F, Defer G, Laurent S, Rahman M, et al. Therapeutic benefits from nanoparticles: the potential significance of nanoscience in diseases with compromise to the blood brain barrier. Chem Rev 2012a; 113:1877-903.
Krug HF, Wick P. Nanotoxicology: an interdisciplinary challenge. Angewandte Chemie International Edition. 2011;50:1260-78.
Kuo C-W, Chueh D-Y, Singh N, Chien F-C, Chen P. Targeted Nuclear Delivery using Peptide-Coated Quantum Dots. Bioconjugate Chem. 2011;22:1073-80.
Laurent S, Burtea C, Thirifays C, Häfeli UO, Mahmoudi M. Crucial Ignored Parameters on Nanotoxicology: The Importance of Toxicity Assay Modifications and "Cell Vision". PLoS ONE. 2012;7:e29997.
Laurent S, Burtea C, Thirifays C, Rezaee F, Mahmoudi M. Significance of cell "observer" and protein source in nanobiosciences. J Colloid Interface Sci. 2013;392:431-45.
Laurent S, Dutz S, Häfeli UO, Mahmoudi M. Magnetic fluid hyperthermia: focus on superparamagnetic iron oxide nanoparticles. Advances in Colloid and Interface Science. 2011;166:8-23.
Laurent S, Mahmoudi M. Superparamagnetic iron oxide nanoparticles: promises for diagnosis and treatment of cancer. Int J Mol Epidemiol Genet. 2011;2:367-90.
Lee J, Sharei A, Sim WY, Adamo A, Langer R, Jensen KF, et al. Nonendocytic Delivery of Functional Engineered Nanoparticles into the Cytoplasm of Live Cells Using a Novel, High-Throughput Microfluidic Device. Nano Lett 2012;12:6322-7.
Lesniak A, Salvati A, Santos-Martinez MJ, Radomski MW, Dawson KA, Åberg C. Nanoparticle Adhesion to the Cell Membrane and Its Effect on Nanoparticle Uptake Efficiency. J Am Chem Soc 2013;135:1438-44.
Lévy M, Quarta A, Espinosa A, Figuerola A, Wilhelm C, García-Hernández M, et al. Correlating magneto-structural properties to hyperthermia performance of highly monodisperse iron oxide nanoparticles prepared by a seeded-growth route. Chemistry of Materials. 2011;23:4170-80.
Lévy M, Wilhelm C, Siaugue J-M, Horner O, Bacri J-C, Gazeau F. Magnetically induced hyperthermia: size-dependent heating power of γ-Fe_2O_3 nanoparticles. Journal of Physics: Condensed Matter. 2008;20:204133.
Lewis BA, Engelman DM. Lipid bilayer thickness varies linearly with acyl chain length in fluid phosphatidylcholine vesicles. J Mol Biol 1983;166:211-7.

Li Y, Li X, Li Z, Gao H. Surface-structure-regulated penetration of nanoparticles across a cell membrane. Nanoscale 2012;4:3768.
Lin J, Zhang H, Chen Z, Zheng Y. Penetration of Lipid Membranes by Gold Nanoparticles: Insights into Cellular Uptake, Cytotoxicity, and Their Relationship. ACS Nano 2010;4:5421-9.
Lin JQ, Chen R, Feng SY, Li YZ, Huang ZF, Xie SS, et al. Rapid delivery of silver nanoparticles into living cells by electroporation for surface-enhanced Raman spectroscopy. Biosensors & Bioelectronics 2009;25:388-94.
Liu M, Chen B, Xue Y, Huang J, Zhang L, Huang S, et al. Polyamidoamine-grafted multiwalled carbon nanotubes for gene delivery: synthesis, transfection and intracellular trafficking. Bioconjugate Chem 2011;22:2237-43.
Liu W, Howarth M, Greytak AB, Zheng Y, Nocera DG, Ting AY, et al. Compact Biocompatible Quantum Dots Functionalized for Cellular Imaging. J Am Chem Soc 2008;130:1274-84.
Luccardini C, Yakovlev A, Gaillard S, Hoff Mvt, Alberola AP, Mallet J-M, et al. Getting Across the Plasma Membrane and Beyond: Intracellular Uses of Colloidal Semiconductor Nanocrystals. J Biomed Biotechnol 2007;2007:Article ID 68963.
Luo JT, Xiao K, Li YP, Lee JS, Xiao WW, Gonik AM, et al. The effect of surface charge on in vivo biodistribution of PEG-oligocholic acid based micellar nanoparticles. Biomaterials 2011;32:3435-46.
Mahmoudi M, Lynch I, Ejtehadi MR, Monopoli MP, Bombelli FB, Laurent S. Protein-nanoparticle interactions: opportunities and challenges. Chem Rev. 2011a;111:5610-37.
Mahmoudi M, Amiri H, Shokrgozar MA, Sasanpour P, Rashidian B, Laurent S, et al. Raman active jagged-shaped gold-coated magnetic particles as a novel multimodal nanoprobe. Chem Commun 2011b;47:10404-6.
Mahmoudi M, Azadmanesh K, Shokrgozar MA, Journeay WS, Laurent S. Effect of nanoparticles on the cell life cycle. Chem Rev 2011c;111:3407-32.
Mahmoudi M, Dutz S, Behzadi S, Ejtehadi MR, Rezaei M, Shokrgozar MA, et al. Temperature - the ignored factor at the nanobio interface. ACS Nano. 2013;Under revision.
Mahmoudi M, Hofmann H, Rothen-Rutishauser B, Petri-Fink A. Assessing the in vitro and in vivo toxicity of superparamagnetic iron oxide nanoparticles. Chem Rev 2011d;112:2323-38.
Mahmoudi M, Laurent S, Shokrgozar MA, Hosseinkhani M. Toxicity evaluations of superparamagnetic iron oxide nanoparticles: cell "vision" versus physicochemical properties of nanoparticles. ACS Nano 2011e;5:7263-76.
Mahmoudi M, Saeedi-Eslami SN, Shokrgozar MA, Azadmanesh K, Hassanlou M, Kalhor HR, et al. Cell "vision": complementary factor of protein corona in nanotoxicology. Nanoscale 2012;4:5461-8.
Mahmoudi M, Shokrgozar MA. Multifunctional stable fluorescent magnetic nanoparticles. Chem Commun 2012;48:3957-9.
Mailander V, Landfester K. Interaction of Nanoparticles with Cells. Biomacromolecules. 2009;10:2379-400.
Meng H, Liong M, Xia T, Li Z, Ji Z, Zink JI, et al. Engineered design of mesoporous silica nanoparticles to deliver doxorubicin and p-glycoprotein siRNA to overcome drug resistance in a cancer cell line. ACS Nano 2010;4:4539-50.
Meng H, Mai WX, Zhang H, Xue M, Xia T, Lin S, et al. Codelivery of an optimal drug/siRNA combination using mesoporous silica nanoparticles to overcome drug resistance in breast cancer in vitro and in vivo. ACS Nano 2013;7:994-1005.
Milani S, Baldelli Bombelli F, Pitek AS, Dawson KA, Rädler J. Reversible versus Irreversible Binding of Transferrin to Polystyrene Nanoparticles: Soft and Hard Corona. ACS Nano 2012;6:2532-41.
Mirshafiee V, Mahmoudi M, Lou K, Cheng J, Kraft ML. Protein corona significantly reduces active targeting yield. Chem Commun 2013;49:2557-9.
Mitra K, Ubarretxena-Belandia I, Taguchi T, Warren G, Engelman DM. Modulation of the bilayer thickness of exocytic pathway membranes by membrane proteins rather than cholesterol. Proc Natl Acad Sci U S A 2004;101:4083-8.
Moghimi SM, Hunter AC, Murray JC. Nanomedicine: current status and future prospects. The FASEB Journal 2005;19:311-30.
Monopoli MP, Walczyk D, Campbell A, Elia G, Lynch I, Baldelli Bombelli F, et al. Physical−chemical aspects of protein corona: relevance to in vitro and in vivo biological impacts of nanoparticles. J Am Chem Soc 2011;133:2525-34.

Moros M, Hernáez B, Garet E, Dias JT, Sáez B, Grazú V, et al. Monosaccharides versus PEG-functionalized NPs: Influence in the cellular uptake. ACS Nano 2012; 6:1565-77.
Muñoz Javier A, Kreft O, Piera Alberola A, Kirchner C, Zebli B, Susha AS, et al. Combined atomic force microscopy and optical microscopy measurements as a method to investigate particle uptake by cells. Small 2006;2:394-400.
Mykhaylyk O, Sobisch T, Almstätter I, Sanchez-Antequera Y, Brandt S, Anton M, et al. Silica-iron oxide magnetic nanoparticles modified for gene delivery: a search for optimum and quantitative criteria. Pharmaceutical Research 2012;29:1344-65.
Nam HY, Kwon SM, Chung H, Lee SY, Kwon SH, Jeon H, et al. Cellular uptake mechanism and intracellular fate of hydrophobically modified glycol chitosan nanoparticles. J Controlled Release 2009;135:259-67.
Nangia S, Sureshkumar R. Effects of nanoparticle charge and shape anisotropy on translocation through cell membranes. Langmuir 2012;28:17666-71.
Narayanan K, et al. Mimicking cellular transport mechanism in stem cells through endosomal escape of newpeptide-coated quantum dots. Sci Rep 2013;3:2184;DOI:10.1038/srep02184.
Nativo P, Prior IA, Brust M. Uptake and intracellular fate of surface-modified gold nanoparticles. ACS Nano 2008;2:1639-44.
Nel AE, Madler L, Velegol D, Xia T, Hoek EMV, Somasundaran P, et al. Understanding biophysicochemical interactions at the nano-bio interface. Nat Mater 2009;8:543-57.
Nikolic MS, Krack M, Aleksandrovic V, Kornowski A, Forster S, Weller H. Tailor-made ligands for biocompatible nanoparticles. Angew Chem Int Ed 2006;45:6577-80.
O'Neal DP, Hirsch LR, Halas NJ, Payne JD, West JL. Photo-thermal tumor ablation in mice using near infrared-absorbing nanoparticles. Cancer Lett 2004;209:171-6.
Ojea-Jiménez I, García-Fernández L, Lorenzo J, Puntes VF. Facile preparation of cationic gold nanoparticle-bioconjugates for cell penetration and nuclear targeting. ACS Nano 2012;6:7692-702.
Ojea-Jiménez I, Tort O, Lorenzo J, Puntes VF. Engineered nonviral nanocarriers for intracellular gene delivery applications. Biomedical Materials 2012;7:054106.
Pan Y, Neuss S, Leifert A, Fischler M, Wen F, Simon U, et al. Size-dependent cytotoxicity of gold nanoparticles. Small 2007;3:1941-9.
Pantarotto D, Briand JP, Prato M, Bianco A. Translocation of bioactive peptides across cell membranes by carbon nanotubes. Chem Commun 2004a:16-7.
Pantarotto D, Singh R, McCarthy D, Erhardt M, Briand JP, Prato M, et al. Functionalized carbon nanotubes for plasmid DNA gene delivery. Angew Chem Int Ed 2004b;43:5242-6.
Parak WJ. Complex colloidal assembly. Science 2011;334:1359-60.
Parak WJ, Boudreau R, Gros ML, Gerion D, Zanchet D, Micheel CM, et al. Cell motility and metastatic potential studies based on quantum dot imaging of phagokinetic tracks. Adv Mater 2002;14:882-5.
Park E-J, Park K. Oxidative stress and pro-inflammatory responses induced by silica nanoparticles in vivo and in vitro. Toxicol Lett 2009;184:18-25.
Parton RG, Simons K. The multiple faces of caveolae. Nat Rev Mol Cell Biol 2007;8:185-194.
Pelaz B, Charron G, Pfeiffer C, Zhao Y, de la Fuente JM, Liang X-J, et al. Interfacing engineered nanoparticles with biological systems: anticipating adverse nano–bio interactions. Small 2013;9:1573-84.
Perrault SD, Chan WCW. Synthesis and surface modification of highly monodispersed, spherical gold nanoparticles of 50-200 nm. J Am Chem Soc 2009;131: 17042-3.
Peteiro-Cartelle J, Rodríguez-Pedreira M, Zhang F, Rivera_Gil P, del_Mercato LL, Parak WJ. One example on how colloidal nano- and microparticles could contribute to medicine. Nanomedicine. 2009;4:967-79.
Pinaud F, King D, Moore H-P, Weiss S. Bioactivation and cell targeting of semiconductor CdSe/ZnS nanocrystals with phytochelatin-related peptides. J Am Chem Soc 2004;126:6115-23.
Qiu Y, Liu Y, Wang LM, Xu LG, Bai R, Ji YL, et al. Surface chemistry and aspect ratio mediated cellular uptake of Au nanorods. Biomaterials 2010;31:7606-19.
Rauch J, Kolch W, Mahmoudi M. Cell Type-specific activation of AKT and ERK signaling pathways by small negatively-charged magnetic nanoparticles. Sci Rep 2012;2:868.
Rauch J, Kolch W, Laurent S, Mahmoudi M. Big Signals from Small Particles: Regulation of cell signaling pathways by nanoparticles. Chem Rev 2013;113:3391-3406.
Rejman J, Oberle V, Zuhorn IS, Hoekstra D. Size-dependent internalization of particles via the pathways of clathrin- and caveolae-mediated endocytosis. Biochem J 2004;377:159-69.

Reynwar BJ, Illya G, Harmandaris VA, Muller MM, Kremer K, Deserno M. Aggregation and vesiculation of membrane proteins by curvature-mediated interactions. Nature 2007;447:461-4.
Rivera-Gil P, Oberdörster G, Elder A, Puntes V, Parak WJ. Correlating physico-chemical with toxicological properties of nanoparticles: the present and the future. ACS Nano 2010;4:5527-31.
Rivera-Gil P, Parak WJ. Composite nanoparticles take aim at cancer. ACS Nano 2008;2:2200-5.
Rivera-Gil P, Jimenez De Aberasturi D, Wulf V, Pelaz B, Del Pino P, Zhao Y, et al. The challenge to relate the physicochemical properties of colloidal nanoparticles to their cytotoxicity. Acc Chem Res 2013;46:743-9.
Rodriguez-Lorenzo L, Krpetic Z, Barbosa S, Alvarez-Puebla RA, Liz-Marzan LM, Prior IA, et al. Intracellular mapping with SERS-encoded gold nanostars. Integrative Biology 2011;3:922-6.
Rothen-Rutishauser BM, Schürch S, Haenni B, Kapp N, Gehr P. Interaction of fine particles and nanoparticles with red blood cells visualized with advanced microscopic techniques. Environmental science & technology 2006;40:4353-9.
Safi M, Courtois J, Seigneuret M, Conjeaud H, Berret JF. The effects of aggregation and protein corona on the cellular internalization of iron oxide nanoparticles. Biomaterials 2011;32:9353-63.
Salvati A, Pitek AS, Monopoli MP, Prapainop K, Bombelli FB, Hristov DR, et al. Transferrin-functionalized nanoparticles lose their targeting capabilities when a biomolecule corona adsorbs on the surface. Nat Nanotechnol 2013;8:137-43.
Sau TK, Rogach AL. Nonspherical Noble Metal Nanoparticles: Colloid-chemical synthesis and morphology control. Adv Mater 2010;22:1781-804.
Scherer F, Anton M, Schillinger U, Henke J, Bergemann C, Kruger A, et al. Magnetofection: enhancing and targeting gene delivery by magnetic force in vitro and in vivo. Gene Ther 2002;9:102-9.
Schweiger C, Hartmann R, Zhang F, Parak W, Kissel T, Rivera_Gil P. Quantification of the internalization patterns of superparamagnetic iron oxide nanoparticles with opposite charge. Journal of Nanobiotechnology 2012;10:28.
Sée V, Free P, Cesbron Y, Nativo P, Shaheen U, Rigden D, et al. Cathepsin L digestion of nanobioconjugates upon endocytosis. ACS Nano 2009;3:2461-8.
Selvan ST, Patra PK, Ang CY, Ying JY. Synthesis of silica-coated semiconductor and magnetic quantum dots and their use in the imaging of live cells. Angew Chem Int Ed 2007;46:2448-52.
Selvan ST, Tan TTY, Yi DK, Jana NR. Functional and multifunctional nanoparticles for bioimaging and biosensing. Langmuir 2010;26:11631-41.
Shi Kam NW, Jessop TC, Wender PA, Dai H. Nanotube molecular transporters: internalization of carbon nanotube-protein conjugates into Mammalian cells. J Am Chem Soc 2004;126:6850-1.
Shi X, von Dem Bussche A, Hurt RH, Kane AB, Gao H. Cell entry of one-dimensional nanomaterials occurs by tip recognition and rotation. Nature Nanotechnol 2011;6:714-9.
Singhal R, Orynbayeva Z, Sundaram RVK, Niu JJ, Bhattacharyya S, Vitol EA, et al. Multifunctional carbon-nanotube cellular endoscopes. Nature Nanotechnol 2011;6:57-64.
Smith AM, Mancini MC, Nie SM. Bioimaging: Second window for in vivo imaging. Nature Nanotechnol 2009;4:710-1.
Smith KA, Jasnow D, Balazs AC. Designing synthetic vesicles that engulf nanoscopic particles. J Chem Phys 2007;127:084703.
Soenen SJH, Brisson AR, Jonckheere E, Nuytten N, Tan S, Himmelreich U, et al. The labeling of cationic iron oxide nanoparticle-resistant hepatocellular carcinoma cells using targeted magnetoliposomes. Biomaterials 2011;32:1748-58.
Soenen SJ, Manshian B, Montenegro JM, Amin F, Meermann B, Thiron T, et al. Cytotoxic effects of gold nanoparticles:a multiparametric study. ACS Nano 2012;6:5767–83.
Sood A, Salih S, Roh D, Lacharme-Lora L, Parry M, Hardiman B, et al. Signalling of DNA damage and cytokines across cell barriers exposed to nanoparticles depends on barrier thickness. Nature Nanotechnol 2011;6:824-33.
Suri SS, Fenniri H, Singh B. Nanotechnology-based drug delivery systems. J Occup Med Toxicol 2007;2:16.
Suzuki R, Oda Y, Utoguchi N, Maruyama K. Progress in the development of ultrasound-mediated gene delivery systems utilizing nano- and microbubbles. J Control Release 2011;149:36-41.
Tanguay RL, Harper SL, Carriere JL, Miller JM, Hutchison JE, Maddux BLS. Systematic evaluation of nanomaterial toxicity: utility of standardized materials and rapid assays. ACS Nano 2011;5:4688-97.

Tekle C, van Deurs B, Sandvig K, Iversen TG. Cellular trafficking of quantum dot-ligand bioconjugates and their induction of changes in normal routing of unconjugated ligands. Nano Lett 2008;8:1858-65.
Tenzer S, Docter D, Rosfa S, Wlodarski A, Kuharev J, Rekik A, et al. Nanoparticle size is a critical physicochemical determinant of the human blood plasma corona: a comprehensive quantitative proteomic analysis. ACS Nano 2011;5:7155-67.
Ulbrich K, Hekmatara T, Herbert E, Kreuter J. Transferrin- and transferrin-receptor-antibody-modified nanoparticles enable drug delivery across the blood-brain barrier (BBB). Eur J Pharm Biopharm 2009;71:251-6.
van Meer G, Voelker DR, Feigenson GW. Membrane lipids: where they are and how they behave. Nat Rev Mol Cell Biol. 2008;9:112-24.
Veiseh O, Kievit FM, Mok H, Ayesh J, Clark C, Fang C, et al. Cell transcytosing poly-arginine coated magnetic nanovector for safe and effective siRNA delivery. Biomaterials 2011;32:5717-25.
Verma A, Uzun O, Hu Y, Hu Y, Han H-S, Watson N, et al. Surface-structure-regulated cell-membrane penetration by monolayer-protected nanoparticles. Nat Mater 2008;7:588-95.
Verma A, Stellacci F. Effect of surface properties on nanoparticle–cell interactions. Small 2010;6:12-21.
Wagner E. Polymers for siRNA Delivery: Inspired by viruses to be targeted, dynamic, and precise. Acc Chem Res 2012;45:1005-13.
Walkey CD, Chan WCW. Understanding and controlling the interaction of nanomaterials with proteins in a physiological environment. Chem Soc Rev 2012a;41:2780-99.
Walkey CD, Olsen JB, Guo H, Emili A, Chan WCW. Nanoparticle size and surface chemistry determine serum protein adsorption and macrophage uptake. J Am Chem Soc 2012b;134:2139-47.
Wang T, Bai J, Jiang X, Nienhaus GU. Cellular uptake of nanoparticles by membrane penetration: a study combining confocal microscopy with FTIR spectroelectrochemistry. ACS Nano 2012;6:1251-9.
Wust P, Hildebrandt B, Sreenivasa G, Rau B, Gellermann J, Riess H, et al. Hyperthermia in combined treatment of cancer. Lancet Oncology 2002;3:487-97.
Xia T, Kovochich M, Brant J, Hotze M, Sempf J, Oberley T, et al. Comparison of the abilities of ambient and manufactured nanoparticles to induce cellular toxicity according to an oxidative stress paradigm. Nano Lett 2006;6:1794-807.
Xia T, Kovochich M, Liong M, Meng H, Kabehie S, George S, et al. Polyethyleneimine coating enhances the cellular uptake of mesoporous silica nanoparticles and allows safe delivery of siRNA and DNA constructs. ACS Nano 2009;3:3273-86.
Xia YN, Halas NJ. Shape-controlled synthesis and surface plasmonic properties of metallic nanostructures. MRS Bull 2005;30:338-44.
Xu J, Teslaa T, Wu T-H, Chiou P-Y, Teitell MA, Weiss S. Nanoblade delivery and incorporation of quantum dot conjugates into tubulin networks in live cells. Nano Lett 2012;12:5669-72.
Yang H, Liu C, Yang D, Zhang H, Xi Z. Comparative study of cytotoxicity, oxidative stress and genotoxicity induced by four typical nanomaterials: the role of particle size, shape and composition. J Appl Toxicol 2009;29:69-78.
Yang K, Ma Y-Q. Computer simulation of the translocation of nanoparticles with different shapes across a lipid bilayer. Nat Nanotechnol 2010;5:579.
Yang P-H, Sun X, Chiu J-F, Sun H, He Q-Y. Transferrin-mediated gold nanoparticle cellular uptake. Bioconjugate Chem 2005;16:494-6.
Yen SK, Jańczewski D, Lakshmi JL, Dolmanan SB, Tripathy S, Ho VHB, et al. Design and synthesis of polymer-functionalized NIR fluorescent dyes–magnetic nanoparticles for bioimaging. ACS Nano 2013; DOI 10.1021/nn401734t.
Yoo HS, Park TG. Folate-receptor-targeted delivery of doxorubicin nano-aggregates stabilized by doxorubicin-PEG-folate conjugate. J Control Release 2004;100:247-56.
Yoo JW, Irvine DJ, Discher DE, Mitragotri S. Bio-inspired, bioengineered and biomimetic drug delivery carriers. Nat Rev Drug Discov 2011;10:521-35.
Yuan H, Fales AM, Vo-Dinh T. TAT Peptide-Functionalized Gold Nanostars: Enhanced intracellular delivery and efficient NIR photothermal therapy using ultralow irradiance. J Am Chem Soc 2012;134:11358-61.
Zhang F, Lees E, Amin F, Rivera-Gil P, Yang F, Mulvaney P, et al. Polymer-coated nanoparticles: a universal tool for biolabelling experiments. Small 2011a;7:3113-27.
Zhang F, Braun GB, Pallaoro A, Zhang Y, Shi Y, Cui D, et al. Mesoporous multifunctional upconversion luminescent and magnetic “nanorattle” materials for targeted chemotherapy. Nano Lett 2011b;12:61-7.

Zhang L, Cao Z, Li Y, Ella-Menye J-R, Bai T, Jiang S. Softer zwitterionic nanogels for longer circulation and lower splenic accumulation. ACS Nano 2012a;6:6681-6.
Zhang S, Li J, Lykotrafitis G, Bao G, Suresh S. Size-dependent endocytosis of nanoparticles. Adv Mater 2009;21:419-24.
Zhang X, Servos MR, Liu J. Ultrahigh nanoparticle stability against salt, pH, and solvent with retained surface accessibility via depletion stabilization. J Am Chem Soc 2012b;134:9910-3.
Zhao F, Zhao Y, Liu Y, Chang X, Chen C, Zhao Y. Cellular uptake, intracellular trafficking, and cytotoxicity of nanomaterials. Small 2011;7:1322-37.

Figure Captions

Fig. 1. (Left): Diagram of the CM, which comprises of mainly a lipid bilayer and (glyco)proteins. (Right): A schematic of protein corona and the interaction of nanoparticle (NP) with the CM.

Fig. 2. Schematic representation of different scenarios involved in the interplay between NPs and CMs.

Fig. 3. A cartoon depicting the CM interaction with –oleyl group anchored silica-coated CdSe QDs (left) and confocal image of HepG2 cancer cells labeling (right) (Selvan et al., 2007).

Fig. 4. (A) A copper-free click reaction between the BCN moieties on the NPs and the azides on the modified silicon substrate was selected as the model targeting reaction. (B) simplified schematic of protein corona-induced screening of NP targeting ligands, which reduces targeted NP delivery; the protein corona covers the targeting ligands on the NP, preventing the ligands from binding to their targets on the CM. (C) fluorescence microscopy images of 5 mm by 5 mm silicon substrates after incubation with pristine BCN-NPs and those coated with a protein corona. (a) Little non-specific binding of pristine BCN-NPs to the azide-free substrate occurred. (b) Numerous pristine BCN-NPs were conjugated to the azide-functionalized substrate. (c and d) A few 10% (c) or 100% (d) corona BCN-NPs were visible on the azide-functionalized substrates. Arrows designate individual NPs (Mirshafiee et al., 2013).

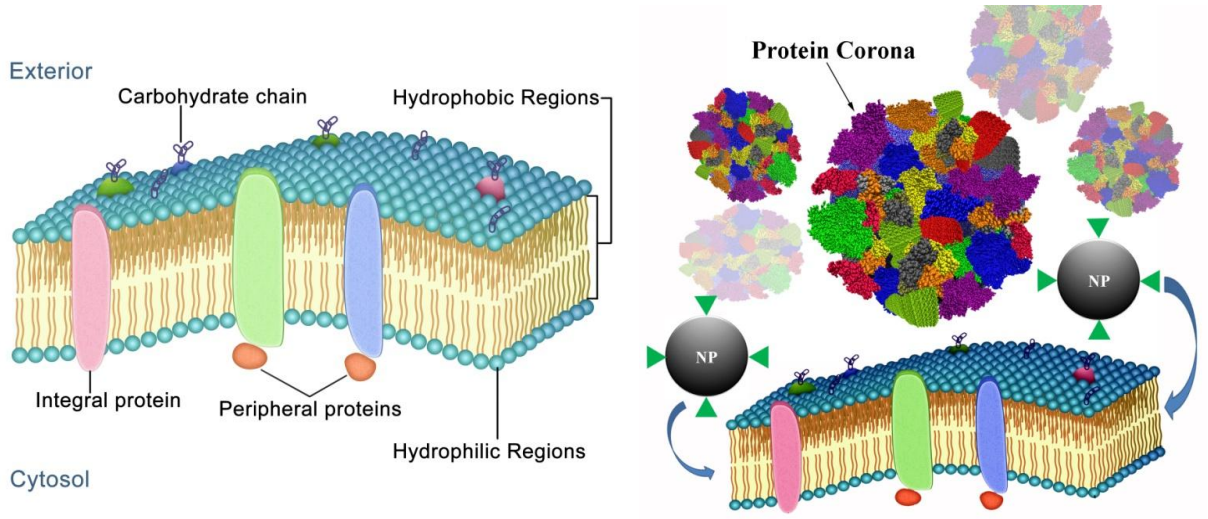

Figure 1

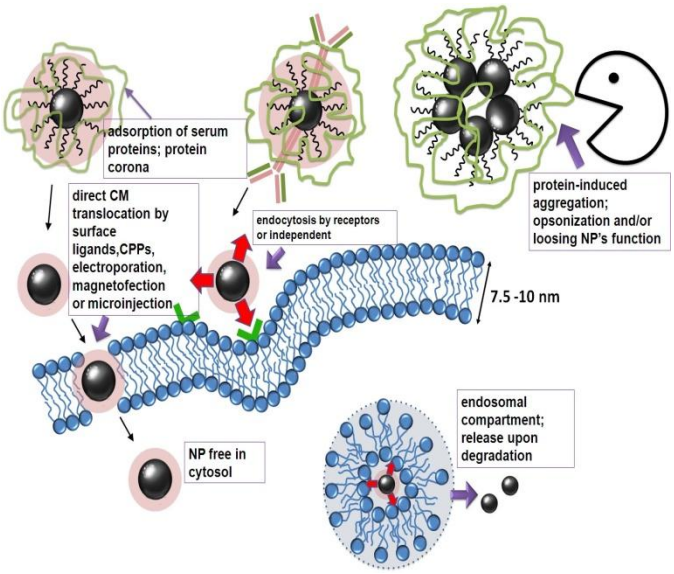

Figure 2

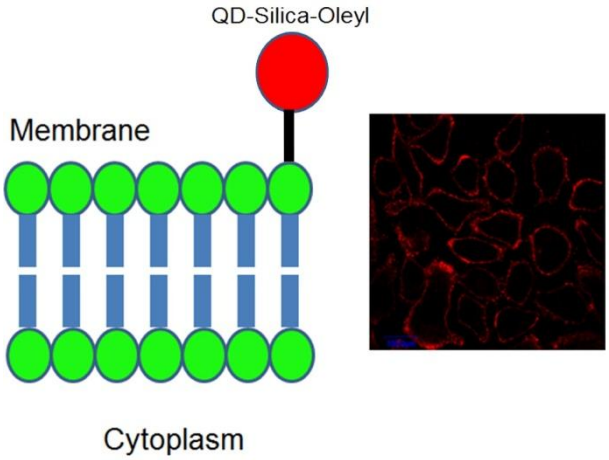

Figure 3

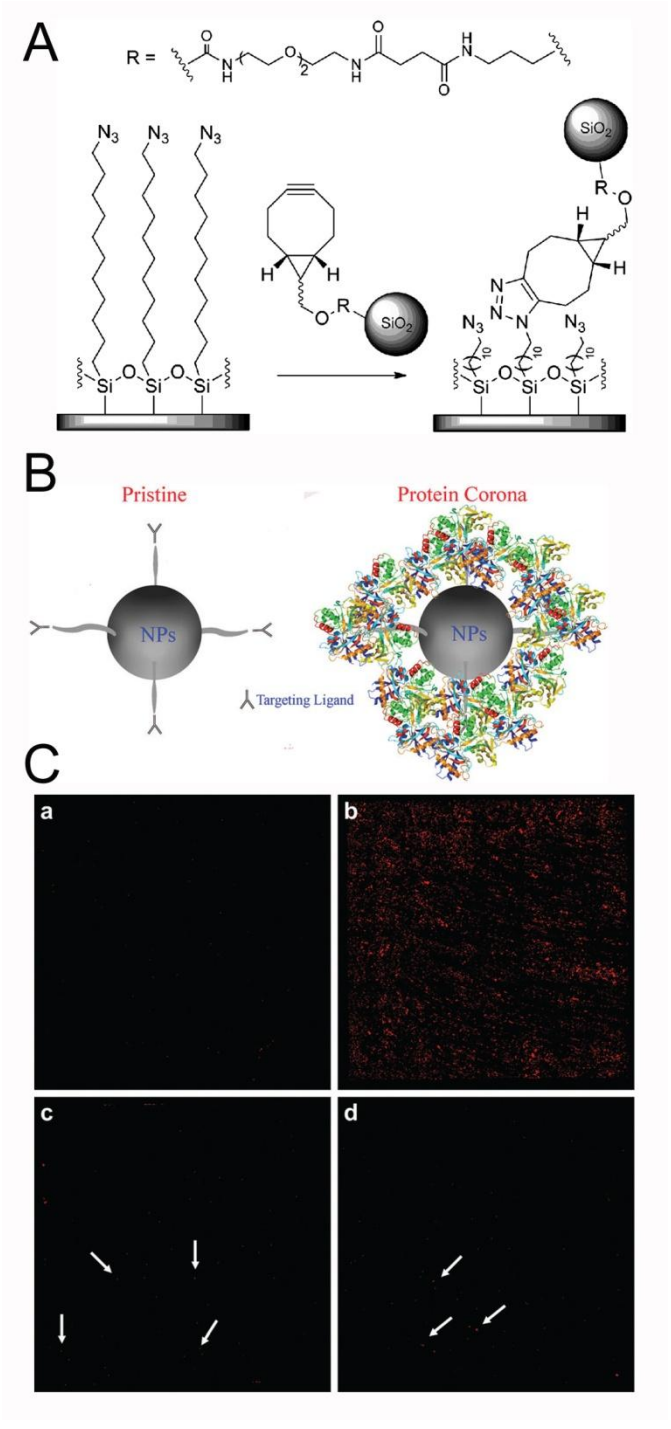
A
R =
SiO2
B
Pristine
Protein Corona
NPs
NPs
Targeting Ligand
C
a
b
c
d

Figure 4

Interaction of colloidal nanoparticles with their local environment - the (ionic) nanoenvironment around nanoparticles is different from bulk and determines the physico chemical properties of the nanoparticles

Christian Pfeiffer[1#], Christoph Rehbock[2#], Dominik Hühn[1], Carolina Carrillo[1], Dorleta Jimenez de Aberasturi[1], Vivian Merk[2], Stephan Barcikowski[2,*], Wolfgang J. Parak[1,3,*]

[#]both authors contributed equally to this work
[*]corresponding authors: stephan.barcikowski@uni-due.de, wolfgang.parak@physik.uni-marburg.de

Abstract

The physicochemical properties of colloidal nanoparticles (NPs) are influenced by their local environment, as in turn the local environment influences the physicochemical properties of the NPs. In other words, the local environment around NPs has profound impact on the NPs, and it is different from bulk due to interaction with the NP surface. The vicinity of NPs can be sensitively influenced by local ions and ligands, with effects already occurring at extremely low concentrations. NPs in the Hückel regime are more sensitive against fluctuations in the ionic environment, because of larger Debye length. The local ion concentration hereby affects the colloidal stability of the NPs, as it is different from bulk due to Debye Hückel screening caused by the charge of the NPs. This can have subtle effects, now caused by the environment to the performance of the NP, such as for example a buffering effect caused by surface reaction on ultrapure nanogold, a size quenching effect in the presence of specific ions, and a significant impact on fluorophore-labelled NPs acting as ion sensors.

Introduction

The potential impact of colloidal nanoparticles (NPs) towards the environment is debate of ongoing discussion {Pelaz, 2013 #24459}. The scenario of intended exposure (*e.g*. fertilizers {Singh, 2012 #23779; Corradini, 2010 #23780; Khodakovskaya, 2012 #24465}, antimicrobial agents {Perelshtein, 2013 #24482; Chernousova, 2013 #23670; Hajipour, 2012 #23330}, removal of contaminants {Ojea-Jimenez, 2012 #23567; Venkatanarasimhan, 2013 #23782; Zhu, 2010 #23783}, and clinical use {Arvizo, 2012 #20871; Parveen, 2012 #20084; Garcia-Bennett, 2011 #24137; Al-Jamal, 2011 #20968; Peteiro-Cartelle, 2009 #14869}), as well as unintended exposure (*e.g.* contamination {Batley, 2013 #23781} and general uptake by all types of organisms {Peters, 2012 #24466; Zhang, 2012 #24467; Hernandez-Viezcas, 2013 #24462; Van_Hoecke, 2013 #20526}) has been analyzed in a large body of work. These studies clearly point out that in fact NPs have impact on the environment, be it intended or unintended. However, besides such global impact of NPs on their environment, in a less spectacular way they also influence the physicochemical properties of their local environment. Likewise, the local environment impacts the physicochemical properties of the NPs. In this way there is a subtle interaction between the surface of NPs and their local environment, which affects the physicochemical properties of both. Important

physicochemical paramters of NP surfaces are for example charge, and hydrophobicity {Rivera Gil, 2013 #20645}. They are influenced by the local environment (*e.g.* the surface charge of NPs may depend on the local pH), as the NPs influence themselves the local environment (*e.g.* accumulations of ions and proteins from bulk due to local charge and hydrophobicity patterns). In the following this will be explained with the example of two major compounds of biological fluids: salt and proteins.

Since many proteins are charged, repulsive interaction between proteins and NPs (for like-charged NPs and proteins) or electrostatic adsorption (for oppositely charged NPs and proteins) can occur {Fu, 1993 #23804; Peng, 2004 #23805. NP surfaces also may contain local hydrophilic / hydrophobic patterns which cause protein adsorption {Verma, 2008 #15576; Hung, 2011 #18434}. This layer of adsorbed proteins to the surface of NPs has been termed protein corona {Cedervall, 2007 #11283; Linse, 2007 #11431}. Continuing our aforementioned argument, the formation of the protein corona (*i.e.* interaction between NPs and proteins {Lynch, 2008 #23810}) affects both, the NPs, as well as their local environment. Adsorbed proteins clearly change two key parameters of NPs, their hydrodynamic diameter {Röcker, 2009 #14229; Jiang, 2010 #14231}, as in many cases also their colloidal stability {Rehbock, 2013 #24302; Gebauer, 2012 #23676; Kittler, 2010 #23675}. On the other hand also the NPs may affect (some types of) adsorbed proteins, in particular *via* structural changes, which may lead to disfuntion of the proteins {Shemetov, 2012 #24181; Deng, 2012 #24425; Goy-Lopez, 2012 #23564}. In addition, due to local charge and hydrophobicity {Amin, 2012 #21003} effects associated with the NP surface there is a higher local protein concentration present on the NP surface (the corona) than in bulk, and thus high NP concentrations can deplete bulk solutions from protein. Adsorption of proteins to NPs can be experimentally assessed with a variety of different methods, some of which are specific to the NP nature. One example are size measurements of the NPs {Fatin-Rouge, 2004 #23807; Sperling, 2007 #11244; Bell, 2012 #21190}. The more protein molecules are adsorbed on the NP surface, the bigger the size of each NP becomes {Lees, 2008 #13229; Monopoli, 2011 #19428; Röcker, 2009 #14229}. In the case of highly colloidally stable NPs with narrow size distribution it was shown that in solutions with only one type of protein (such as for example human bovine serum {Röcker, 2009 #14229; Maffre, 2011 #18520}, or transferrin {Jiang, 2010 #14231; Mahmoudi, 2013 #24418}) adsorbed proteins under saturation conditions form a monolayer on top of the NP surface. Often interaction of proteins with NPs is unwanted and thus needs to be circumvented. Protein adsorption to surfaces is for example reduced by controlled preincubation of the surface with the serum albumine, which blocks adsorption spots and thus reduces adsorption of other proteins. The PEGylation (PEG: poly(ethyleneglycol)) of NPs is also used as a general and effective approach to reduce nonspecific binding of proteins to NPs {He, 2010 #23806}.

Also interaction of salt and NPs has an effect as well on the NPs, as on the local concentraion of the ions (from the dissociated salt). The surface charge of NPs plays also an important role in stabilizing NPs. In order to be colloidally stable, NPs need to be stabilized either by electrostatic or by steric repulsion {Pellegrino, 2005 #9686; Zhang, 2012 #23799}, otherwise they would start agglomerating driven by van der Waals interaction {Ravikumar, 2012 #23784}. In the case of electrostatically stabilized NPs the NPs with likewise charged surface repel each other and thus are dispersed. Salt in solution screens the charge on the NP surface (basically in first order the Debye-Hückel effect {Debye, 1923 #602}), and thus typically leads at high concentrations to colloidal instability, followed by agglomeration {Huynh, 2011 #23801; Li,

2012 #23800; Gebauer, 2011 #23677; Hühn, 2013 #20527}. While this screening effect (*e.g.* the effect of the local ion concentration on the colloidal stability of NPs) is reported plentiful in literature, another consequence of the same effect is less widely reported, but not less relevant. In case the charge on the surface of the NPs is screened by counter ions, there is a higher and lower concentration of ions with the opposite and the same sign of charge around the NPs compared to bulk, respectively. Thus the NPs change their local environment, and ion concentrations at the NP surface are different from bulk {Zhang, 2010 #14235; Riedinger, 2010 #15205; Zhang, 2011 #18339}. Local ion concentration around NP surfaces can be for example measured using ion-sensitive fluorophores {Zhang, 2010 #14235; Riedinger, 2010 #15205; Zhang, 2011 #18339}. The theoretical analysis however is not as straightforward. When interactions of ions with the curved nanoenvironment of NPs are generally discussed, most applied models, *e.g.* the DLVO theory {Derjaguin, 1941 #36; Verwey, 1948 #37}, are based on continuum effects considering ions as point charges {Ninham, 1999 #24274}. However, effects considering the nature of the used ions, namely *specific* ion effects, are often disregarded, though they may be of high importance for example for the colloidal stability of the NPs. These effects have long been known for example in biological systems, where they are responsible for the well-known Hofmeister effect {P. Bauduin, 2006 #24291; Hofmeister, 1888 #24290; Medda, 2012 #24280; Vrbka, 2006 #24279}, describing stabilization and precipitation tendencies in proteins. Another example is the well-known fact that specific adsorption and monolayer formation of anions occurs in flat charged gold surfaces dipped in electrolytes {Gao, 1986 #24278; Magnussen, 1996 #24277; Magnussen, 1995 #24276; Biggs, 1994 #24275; Boer, 1936 #24292}. Hence ion specific effects must not be ignored when the nanoenvironment of NPs is studied, particularly at low salinities when the previously discussed screening of charges described by continuum models is not dominant. Changes in the ion concentration around the surface of NPs have for example profound effect on ion-sensitive NPs, as instead of the bulk ion concentraion the local ion concentration is determined {Zhang, 2010 #14235; Riedinger, 2010 #15205; Zhang, 2011 #18339}.

Thus interaction of ions and proteins with NPs, effect both the ions and proteins, as the NPs. In the following we will focus on the case of ions.

Non-specific effects of ion-induced nanoenvironments on the synthesis and stability of ligand-free metal NPs

The nanoenvironment of charged NPs has been extensively studied for a long time. Generally, the model of the electrochemical “double layer” by Stern {Stern, 1924 #347; Rhee, 1998 #24265} which describes a fixed layer of surface charges (the Helmholtz model {Helmholtz, 1879 #233}) and a continuous diffuse layer of counterions (the Gouy-Chapman model {Chapman, 1913 #164; Gouy, 1909 #222; Gouy, 1910 #223}) is used in this context. The thickness of this diffuse layer, and hence the nanoscopic vicinity of the NPs, is highly dependent on the solution´s ionic strength and may be characterized by the Debye parameter (κ) or its reciprocal value, the Debye screening length (κ^{-1}). In a classical DLVO model {Verwey, 1948 #24269; Derjaguin, 1941 #24266}, which considers dissolved ions as point charges, κ^{-1} decreases with increasing ionic strength (I [M], which is defined as concentration of all ions: $I = \frac{1}{2}\sum_i z_i^2 c_i$, whereby z_i is the charge number of ions of species i, and c_i [M] the respective concentration of these ions). This

leads to a screening of the electrostatic stabilization and induces NP agglomeration due to dominant van-der-Waals attractions. Next to these frequently described effects, the nanoenvironment also affects the electrophoretic mobility (μ [$m^2V^{-1}s^{-1}$]) of NPs and hence related values, such as the the ξ-potential (ξ [V]), a parameter of the outmost importance when judging NP stabilities in colloidal science {Doane, 2012 #23744}. Main parameters in this context are the ionic strength, influencing the Debye parameter (κ [m^{-1}]), and the NP radius (r_c [m]). Based on these values the best representation of the correlation between μ and ξ may be given by the Smoluchowski formula {Smoluchowski, 1921 #24270} for the nanoenvironment of larger NPs at high ionic strengths ($\kappa \cdot r_c >> 1$) and by the Hückel equation {Hückel, 1924 #24268} for low ionic strengths and small NPs ($\kappa \cdot r_c << 1$). In the intermediate regime, the Henry-function $f_H(\kappa \cdot r_c)$ may be used {Henry, 1931 #24271}. Please note that we are refering to (geometric) particle radii d_c, not to hydrodynamic radii r_h {Rivera Gil, 2013 #20645}. A more detailed discussion of the different models can be found in a review article recently published by Doane *et al.* {Doane, 2012 #24272}. Figure 1 shows the different regimes dependent on NP radius r_c and ionic strength I. With the potential ξ being inversely proportional to the Henry-Factor, ξ-potentials of a NP at a given mobility μ are up to 50% higher (f_H = 1.5) in the Hückel regime. NPs synthesized by wet chemistry methods typically bear charge and mobility properties in the intermediate regime (marked in Figure 1) between Smoluchowski and Hückel {Doane, 2012 #24272}, whereas colloids with low ionic strength, *e.g.* physically prepared colloidal NPs, are often located in the Hückel regime, being more sensitive for local changes or fluctuations in the ionic environment as a result of the larger Debye length κ^{-1}. Note that ion adsorption to the surface of NPs results in a non-continuum ionic strength regime around the NPs, causing a gradient in the Henry factor. In ideal conditions (no drag force, very low or very high fluid Reynold numbers), the 2D distribution of the Henry factor around the NP is symmetric.

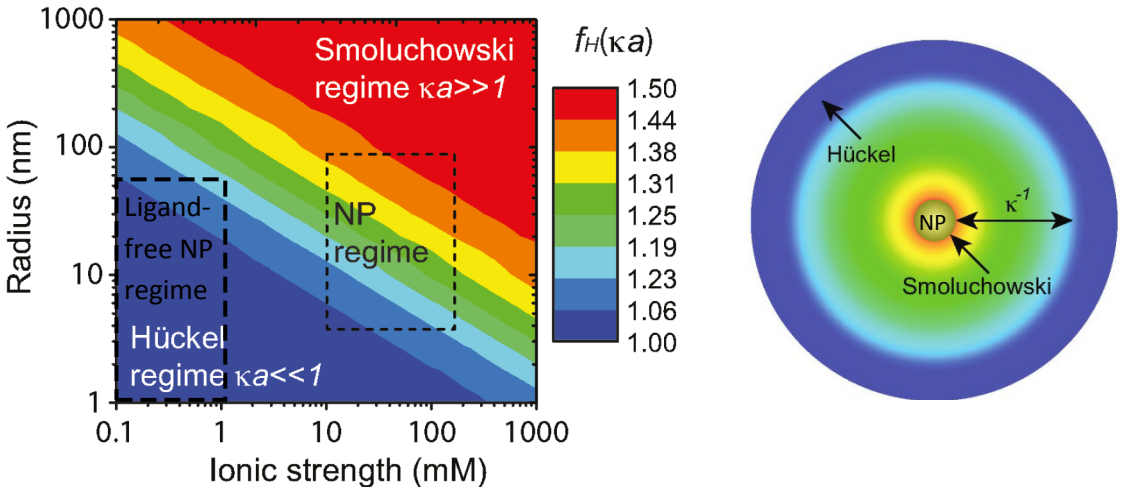

Figure 1: A) Scheme showing different models for the determination of the electrophoretic mobility of bare NPs (with geometric radius of the inorganic NP material of r_c) for different ionic strengths I and NP radii r_c (refering to the geometric radii of the inorganic NP materials). The colour indicates the Henry factor f_H,which defines the relationship between the bare mobility μ and resulting zeta-potential ξ, with higher zeta-potentials at given mobility in the Hückel regime. Note that f_H changes with the distance

from the NP surface. B) The image shows the 2D distribution of the Debye layer thickness κ^{-1} (adapted from Doane *et al.* {Doane, 2012 #24272}).

Next to external electrical fields, the symmetric vicinity of a NP may also be altered by gravitational forces as they are found during centrifugation. A detailed understanding of this process and its correlation with ionic strength, g-force and zeta potential may help to elucidate the sedimentation process and might contribute to controlling agglomeration processes occurring during centrifugation. Recent simulation experiments conducted by Keller *et al.* {Keller, 2010 #24273} revealed that the counter-ion cloud found in the vicinity of the NPs is deformed at high g-forces (Figure 2A). This leads to a local electric field which causes a reduction of the sedimentation velocity v_S [m/s] This process is highly dependent on the applied zeta potential ξ involving the factor ($\xi e/k_BT$), and the ionic strength I, which is illustrated in Figure 2B. Hereby e is the elemental charge, k_B the Boltzman factor, and T [K] the temperature of the solution.

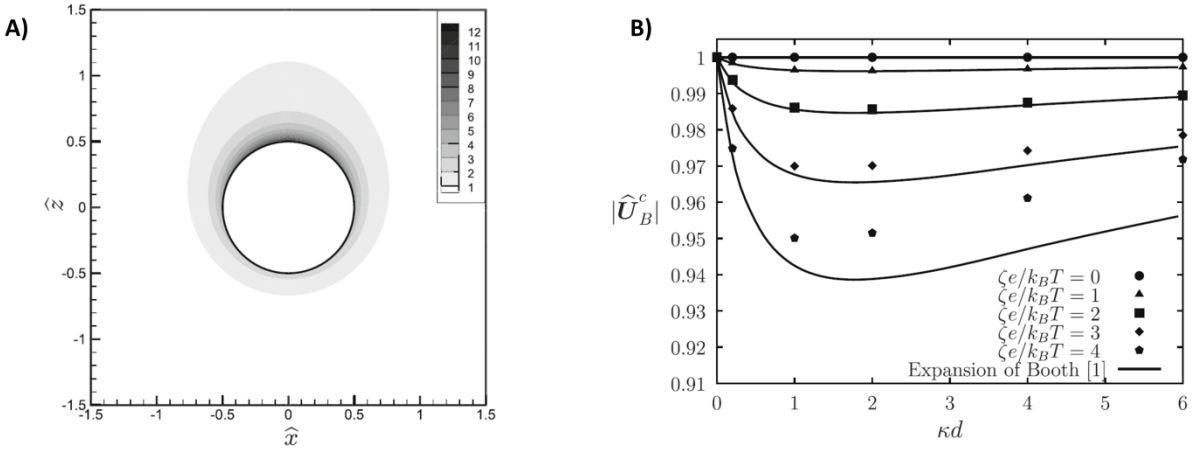

Figure 2: Distortion of the ionic nanoenvironment during centrifugation and effect on the sedimentation velocity v_S at different zeta potentials ξ. A) Distribution of counter-ions around a NP at $\kappa \cdot r_c = 2$, $\xi = 3$, and a fluidic Reynolds number of $Re_f = 4.45 \cdot 10^{-2}$. B) normalized sedimentation velocity v_S/v_{Smax} at different $\kappa \cdot r_c$ and ($\xi e/k_BT$) values (adapted from Keller *et al.* {Keller, 2010 #24273})

The preceding examples clearly demonstrate that the continuous, ion-induced nanoenvironment can dramatically alter the physical properties of NPs and may have a severe influence on colloidal chemistry. However, in the above described effects the ions were only considered as point charges and ion specific effects were not yet considered {Ninham, 1999 #24274}. The point of ion specifity is further addressed in the following paragraph.

Specific effects of ion-induced nanoenvironments on the synthesis and stability of ligand-free metal NPs

The specific impact of ions on bare noble metal surfaces has been widely studied for decades e.g. for gold electrodes in the presence of different electrolytes. A significant accumulation and adsorption of

the halides Cl^-, Br^- and I^- and hence changes of the nanoenvironment have been reported and verified by several methods including atomic force microscopy (AFM) {Biggs, 1994 #24275}, X-ray diffraction (XRD) - analysis {Magnussen, 1995 #24276}, scanning tunneling microscopy (STM) {Magnussen, 1996 #24277}, and surface enhanced Raman scattering (SERS) {Gao, 1986 #24278}. Additionally, it has been known for a very long time that bare gold surfaces dipped in pure water suppositionally collect a negative surface charge due to accumulation of OH^- ions on their surface {Boer, 1936 #24292}. Another well-known example of specific ion interactions is the Hofmeister effect, which has been known since the 19^{th} century {Hofmeister, 1888 #24290}. It was first discovered in the field of protein precipitation {P. Bauduin, 2006 #24291; Medda, 2012 #24280; Vrbka, 2006 #24279} but was successfully applied to other fields, ranging from simple physical effects on electrolytes to colloidal dispersions and macromolecules {Lo Nostro, 2012 #24281}. This effect is based on the fact that ions may be classified into chaotropic (soft) and cosmotropic (hard) based on their stabilization of biomolecules and their interactions with surfaces. The nature of these effects is not yet fully understood but it is believed that it may be related to the polarizability of the ions {F. W. Tavares, 2004 #24318; dos Santos, 2012 #24283}. While chaotropic anions have a more diffused charge distribution they may interact with hydrophobic surfaces, while cosmotropic ions with a high surface charge density are repelled by them. Other findings seem to indicate that the structure of the water molecules found on their surface may be of paramount importance. While water molecules on cosmotropic ions are highly ordered, chaotropic ions are known to alter their surrounding water shell {Collins, 1997 #24284; Collins, 2004 #24320; Manciu, 2003 #24319}. Hence, ions may lose their hydrate shell and become chemisorbed on hydrophobic surface, which is not possible for densely hydrated cosmotropic anions {Kolb, 1989 #6}. Even though ion specific effects have been discussed for a very long time, a detailed examination and transfer of these effects to the nanoenvironment of NPs has long been neglected due to the unavailability of appropriate testing systems. NPs obtained from gas-phase synthesis are barely available in colloidal state due to their strong agglomeration tendencies and hence undefined surface areas {Gutsch, 2005 #24287; Kruis, 1998 #24286}. On the other hand ion-induced interactions with metal surfaces are screened in the presence of surface ligands like *e.g.* citrate {Thompson, 1992 #24288} negating a study of these effects with chemically synthesized NPs. In this case ion-NP interactions in the nanoenvironment are dominated by the nature of the organic ligands, which is thoroughly discussed in the next paragraph. Most recently, the availability of ligand-free colloidal NPs synthesized by the quickly emerging field {Menendez-Manjon, 2011 #24300; Barcikowski, 2013 #24293} of pulsed laser ablation in liquid {Zeng, 2012 #24297; Amendola, 2009 #24296; Semaltianos, 2010 #24295; Amendola, 2013 #24294}, has significantly stimulated this research, while particularly gold colloids were extensively studied {Menendez-Manjon, 2011 #24300; Tilaki, 2007 #24299; Kabashin, 2003 #24298}. Due to this emerging synthesis route, ultrapure curved NP surfaces are nowadays available which enable studies of NP-ion interactions in the Hückel-regime at extremely low ionic strengths {Rehbock, 2013 #24302; V. R. Merk, 2013 #24309}. These effects will be thoroughly reviewed in the following and complemented by some recent findings. Basically these effects can be subdivided into i) ion effects and ii) pH-effects though in many experiments this influence cannot be clearly distinguished.

Ion effects. When it comes to interactions of NPs with electrolytes, generally a destabilization due to the well known screening of surface charges is predominantly discussed in literature {Pellegrino, 2005

#9686}. However, when totally ligand-free gold and silver NPs were first laser-synthesized in the presence of electrolytes a stabilization occurred in the presence of NaCl {Siskova, 2008 #24304; Sylvestre, 2004 #24303}. More extensive studies with different electrolytes at varying salinities revealed that these effects are anion specific, occurring only with chaotropic anions (Cl^-, Br^-, I^-, SCN^-) while cosmotropic anions (F^-, SO_4^{2-}) did not induce a stabilizing effect. For NO_3^- the findings in literature are inconsistent. While generally a destabilizing effect is reported for gold {Sylvestre, 2004 #24303; Thompson, 1992 #24288}, at lower ionic strengths {V. R. Merk, 2013 #24309} and for silver {Siskova, 2008 #24304}, however, stabilization was found. It is believed that this ion adsorption significantly alters the NP´s nanoenvironment, as the ions transfer their charges to the NP surface and hence increase electrostatic stabilization (Figure 3A). These findings seem to indicate that Hofmeister effects, thoroughly described in the preceeding paragraph, may also appear on curved gold interfaces. A Hofmeister series of anions for this system could be deferred, by successfully correlating the stability of gold colloids to the polarisability of the anions present during synthesis {V. R. Merk, 2013 #24309} (Figure 3B). Interestingly, these effects already occur in highly diluted electrolytes in a micromolar to-millimolar concentration range {V. R. Merk, 2013 #24309; Siskova, 2008 #24304; Rehbock, 2013 #24302}. Specific accumulation of chaotropic anions in the nanoenvironment of NPs does not only affect colloidal stability, it also interferes with the growth mechanism of ligand-free NPs. As a result these ions induce a size quenching effect during NP growth which was reported for gold {Sylvestre, 2004 #24303; Rehbock, 2013 #24302; Amendola, 2009 #24296} and silver NPs {Srnova, 1998 #24307; Bae, 2002 #24306; Prochazka, 1997 #24305; Siskova, 2008 #24304}. This means that in a micromolar concentration regime increasing ionic strengths significantly reduce NP size and their NP size distribution. It was recently proposed that size reduction in highly diluted electrolytes is directly related to the NP surface area, which can be electrostatically stabilized by the available anions {Rehbock, 2013 #24302}. A summary of the different anions and their stabilizing and size quenching effects on ligand-free gold and silver NPs is summarized in Table 1.

Ion	**Stabilization**	**Size quenching**	**References**
F^-	-	-	Au {V. R. Merk, 2013 #24309}
Cl^-	(+)/(-) concentration	(+)/(-) concentration	Au {V. R. Merk, 2013 #24309; Sylvestre, 2004 #24303; Rehbock, 2013 #24302; Amendola, 2013 #24294; Thompson, 1992 #24288} Ag {Srnova, 1998 #24307; Bae, 2002 #24306; Prochazka, 1997 #24305; Siskova, 2008 #24304}
Br^-	++	+	Au {V. R. Merk, 2013 #24309; Rehbock, 2013 #24302}
I^-	(++) NP etching	+	Au {V. R. Merk, 2013

			#24309; Thompson, 1992 #24288}
SCN^-	++	+	Au {V. R. Merk, 2013 #24309}
NO_3^-	(-)/(+) Concentration	(-)/(+) concentration	Au {V. R. Merk, 2013 #24309; Sylvestre, 2004 #24303; Thompson, 1992 #24288} Ag {Siskova, 2008 #24304}
SO_4^{2-}	-	-	Au {V. R. Merk, 2013 #24309; Rehbock, 2013 #24302}
PO_4^{3-}	+	+	Au {Rehbock, 2013 #24302}
NaH_2PO_4/ Na_2HPO_4	+	+	Au {Rehbock, 2013 #24302}
OH^-	+	(+)/(-) concentration	Au {Sylvestre, 2004 #24303}
HCl	(-)/(+) concentration, material	(-)/(+) concentration, material	Au {Sylvestre, 2004 #24303} Ag {Siskova, 2008 #24304}
$S_2O_3^{2-}$	-	-	Ag {Siskova, 2008 #24304}

Table 1: Specific effects of different ions on the stability and size quenching of ligand-free Au and Ag NPs. (Signs in brackets indicate limitations or ambivalent effects found by different researchers including comments as to possible reasons)

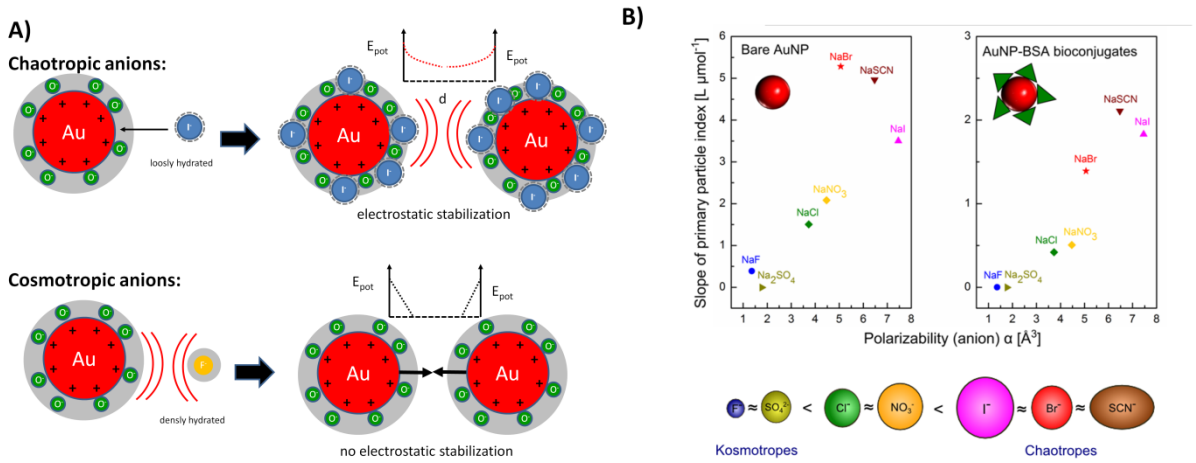

Figure 3: A) Ion-specific interactions of chaotropic and cosmotropic anions in the nanoenvironment of gold NPs. The graph shows the dependence of the repulsive potential energy Epot in dependence of the surface-to-surface distance 2R between adjacent NPs. B) Colloidal stability as indicated by the slope S of the polydispersity index from UV-Vis spectroscopy, in dependence of the polarizability α of the anion, for

bare Au NPs without ligand and Au NPs coated with bovine serum albumine (BSA). The resulting Hofmeister series for gold NPs is shown. The image is adopted from Merk et. al. {V. R. Merk, 2013 #24309}, to which we also refer for more details.

pH-effects. The influence of the pH on the nanoenvironment of ligand-free colloidal metal (M) NPs is mostly due to oxidation of surface atoms and a pH-dependent equilibrium between M-O^-/M-OH and M-OH/MOH_2^+ species, respectively. This has been quantitatively described in the case of SiO_2 and Al_2O_3 surfaces by the site-binding model used for solid-state based ion-sensitive sensors {Bousse, 1983 #153; Bousse, 1991 #24; Raiteri, 1996 #1398; van_Hal, 1995 #1500; Healy, 1980 #2387}. At low pH the surface can be charged positively by the adsorption of protons (MOH_2^+), whereas it will be negatively charged at high pH due to depletion of protons (M-O^-). The equilibrium of the reaction M-O^- + 2 H^+ ↔ M-OH + H^+ ↔ MOH_2^+ is described by the law of mass action by the respective pK_a (= -log(K_a)) values K_{a1} = c(M-O^-)·c(H^+)/c(M-OH) and K_{a2} = c(M-OH)·c(H^+)/c(MOH_2^+). Both equilibria depend on the pH (= -log(c(H^+)). In this way the surface charge and hence the electrostatic stability reaches a minimum close to the isoelectric point at pH = pI {Parks, 1965 #24308}. This effect was frequently observed for metal oxide NPs like ZnO {S. Liufu, 2004 #24316; He, 2007 #24310}, TiO_2 {M. Sugiyama, 2002 #24317}, and Al_2O_3 {Al-Mamun, 2013 #24311}, where larger NPs due to agglomeration were predominantly formed close to the pI value of the respective NP species. It is important to note that with metal oxides, *e.g.* for Al_2O_3, different hydroxide species may form dependent on the pH the NPs were equilibrated in and hence different pI values may be found {J. J. Gulicovski, 2008 #24315}. The pI values of exemplary NP species are shown in Table 2. As the presence of surface hydroxide is obvious in metal oxides they are also found in the case of gold NPs obtained from physical synthesis routes like laser ablation in liquid. X-ray photoelectrom spectroscopy (XPS) measurements confirmed that these NPs possess partially oxidized surfaces (3.3 – 6.6 % of Au^+ and Au^{3+}) {Muto, 2007 #24312; V. R. Merk, 2013 #24309}. Fourier transformed infrared spectroscopy (FTIR)-measurements verified the presence of Au-O bonds on the surface {Sylvestre, 2004 #24303}. An indirect verification of an pI value in ligand-free noble metal systems was recently found for $Au_{50}Pt_{50}$-alloy NPs which had been laser-ablated at different pH. Here a steep increase in NP size due to agglomeration processes was found at pH < 7 {Zhang, 2012 #24313}. A titration of ligand-free gold NPs in order to determine the pI value was performed for NPs obtained from gas phase synthesis {Thompson, 1992 #24288} and laser ablation in liquid {Petersen, 2011 #24314; Sylvestre, 2004 #24303} by monitoring of the zeta-potential at different pH-values. In all cases stabilization was found for more alkaline pH. The results from 3 different references and recently obtained experimental data are summarized in Figure 4. In our experiments, totally additive-free gold NPs were titrated with HCl, fitted with a 4^{th} order polynomial, while linear extrapolation was used in order to determine the pI value. Note that Thompson *et al.* {Thompson, 1992 #24288} originally measured the electrophoretic motility, which was transferred to the zeta-potential for better comparability, applying Smoulochowski´s equation {Smoluchowski, 1921 #24270}.

NP species	**pI**	**reference**
TiO_2	6	{M. Sugiyama, 2002 #24317}
ZnO	9	{S. Liufu, 2004 #24316}
Al_2O_3	8.6 (acidic equilibration) 5.3 (alkaline equilibration)	{J. J. Gulicovski, 2008 #24315}

AuPt	(7) indirect method	{Zhang, 2012 #24313}
Au	2-2.5 (4.5)	{Petersen, 2011 #24314; Sylvestre, 2004 #24303; Thompson, 1992 #24288}

Table 2: Charge equilibrium in the nanoenvironment (pH at the isoelectric points (pI)) of exemplary ligand-free colloidal NPs

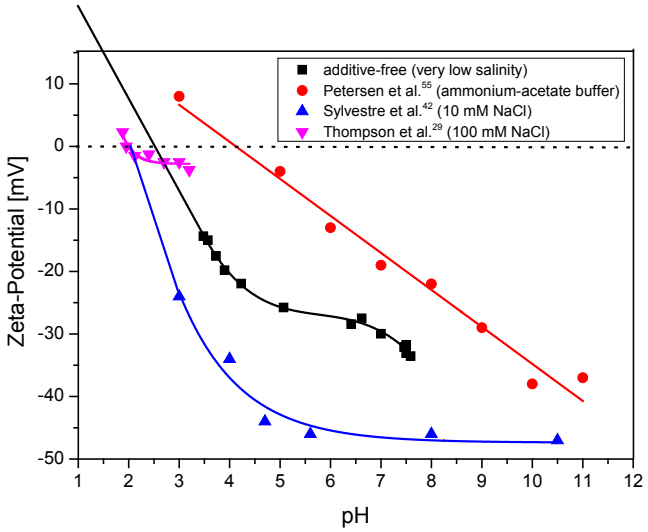

Figure 4: Ion effects on the isoelectric points of metal NPs. Zeta-potential ξ of ligand-free NPs at different pH-values for the determination of the isoelectric point, as adapted from references {Petersen, 2011 #24314; Sylvestre, 2004 #24303; Thompson, 1992 #24288} as well as unpublished data.

These data clearly show, that additive-free gold NPs possess an isoelectric point at pH = 2.5. These findings slightly deviate from pI-values reported in literature by Thompson *et al.* {Thompson, 1992 #24288} (pI = 2) and Sylvestre *et al.* {Sylvestre, 2004 #24303} (pI = 2.2). These differences may be due to high concentrations of chloride (100 mM and 10 mM) present during their experiments, while in the additive-free sample chloride solutions with 3 orders of magnitude lower salinities (93 µM) were applied. As it was described in the preceeding paragraph, chloride may specifically adsorb to gold NP surfaces, which increases the negative surface charge of the NPs. Naturally, in these samples more protons are necessary for charge compensation and the isoelectric point is reached at a more acidic pH. Completely different results were obtained by Petersen *et al.* {Petersen, 2011 #24314} where an pI of 4.5 was found. These deviations may be due to the fact that a system of CH_3COOH/NH_3 was used for pH adjustment. On the one hand side this approach eliminates ion effects but on the other hand another organic ligand is added and a CH_3COO^-/CH_3COOH buffer system is formed, influencing the solution´s pH. This high diversity of findings clearly illustrates that to further examine the influence of varying pH on the nanoenvironment of ligand-free gold NPs, additional ion effects need to be minimized and hence the ionic strength has to be reduced. To this end we recently prepared NPs by pulsed laser ablation in liquid in the presence of NaOH and HCl at concentrations from 1 – 500 µM. In both cases a significant growth quenching causing size reduction of the NPs was found compared to products synthesized in water. In

case of HCl this is most likely due to the stabilizing effect of Cl^-, blocking the gold seed´s crystal growth preventing further growth. In the observed concentration regime this effect seems to compensate the destabilization by protons reported for higher HCl concentrations {Sylvestre, 2004 #24303}. For NaOH the deprotonation of surface Au-OH groups and the increased abundance of surface charges is the most probable cause for reduced NP size and stabilization, which is in accordance with data from literature {Sylvestre, 2004 #24303}. The most interesting effect, however, was observed when the pH of the stock solution (just diluted HCl or NaCl) and the NP-containing solution were monitored during this experiment (Figure 5). It was found that the pH of both NP-containing solutions synthesized in the presence of HCl and NaOH remained stable at around 6.5 up to a concentration of 30 µM, leading to a significant deviation from pH-values found in the stock solution. For higher concentrations the pH significantly deviated from the value of 6.5, though the measured values were still considerably different from the stock solutions. These findings seem to indicate that ligand-free gold Nps work as a buffer in highly diluted electrolytes, totally stabilizing the pH at 6.5 up to a proton surplus, as well as a proton deficiency of 30 µM. Apparently, the nanoenvironment of the gold NPs accumulates protons from acidic solutions and emits protons to an alkaline environment probably by changing the $Au\text{-}O^-$/ Au-OH ratio, significantly affecting the pH of the bulk solution. This fundamental effect, that the NPs themselves and their nanoenvironment work as a buffer system, significantly affecting the bulk solution is often neglected when working with NPs. The underlying concept is illustrated in Figure 6. As a result, in 1 mL of the examined gold NP solution with an average NP core radius r_c of 4 nm and a mass concentration of 100 µg/mL there are roughly $2.2 \cdot 10^{17}$ gold surface atoms present, which can accumulate and emit about 30 nmols of H^+, which is equal to $1.8 \cdot 10^{16}$ H^+ ions. Consequently, about 8% of the surface atoms take part in this buffering reaction, which is in good accordance with literature stating that up to 6.6 % of the gold surface is oxidized {Muto, 2007 #24312; V. R. Merk, 2013 #24309} and hence may carry a Au-OH, AuO^- or $AuOH_2^+$ group. In conclusion, a buffer capacity of 0.77 nmol $(H^+)/cm^2$(gold NP surface) is reached, which is very low compared to conventional buffers, though such this comparison only considers pure continuum states of the environment. In contrast, the observed buffer effect is directly caused by the Gouy-Chapman layer in the nanoscopic vicinity of the NPs. Hence such effects might be relevant in highly pH-sensitive reactions at low concentrations.

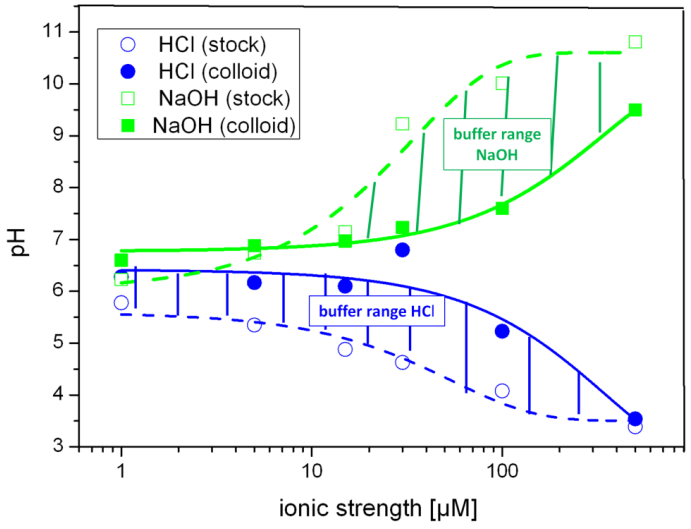

Figure 5: The buffer effect of charged NP surfaces. The pH-values of ligand-free gold NP solutions as synthesized in the presence of NaOH and HCl at varying concentrations of the respective acid (HCl) and base (NaOH; solid lines) are plotted versus the ionic strength I of the solution. As comparison the pH of the NaOH and HCl stock solutions was monitored as well (dashed lines).

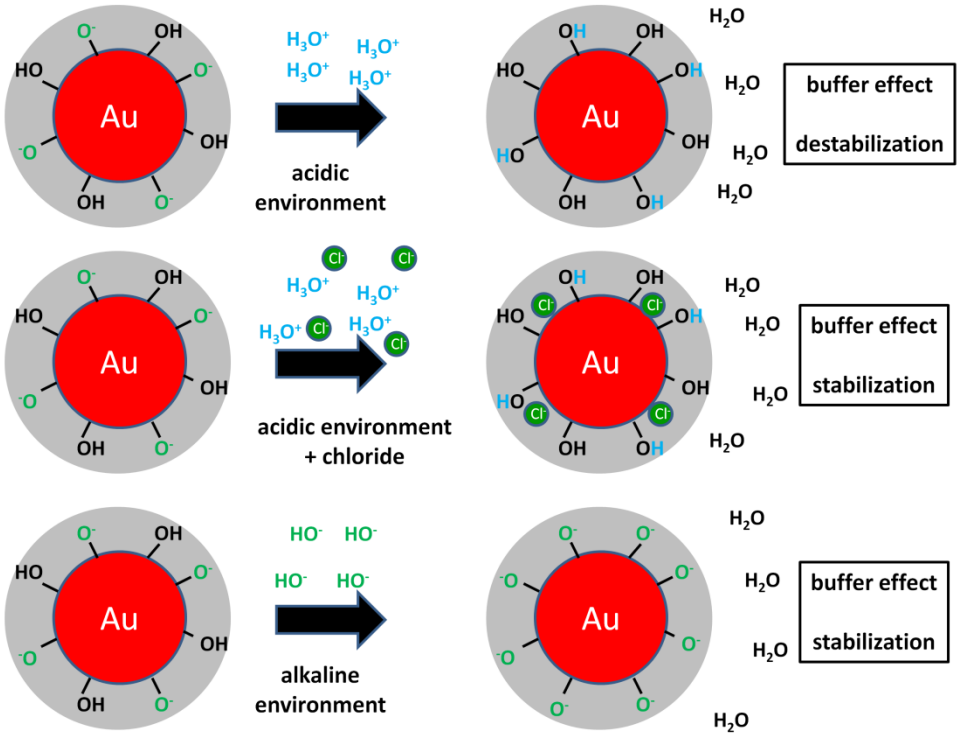

Figure 6: Buffer effect caused by the nanoenvironment of gold NPs in acidic and alkaline bulk environment.

Effects of ion-induced nanoenvironments on the stability and the nanoenvironment of ligand-coated NPs

While the concepts as described above for ligand-free metal NPs in general are true also for ligand-coated NPs, the situation becomes more complex. This is due to the hybrid nature of ligand-coated NPs, which besided the inorganic core also comprise an organic (ligand-) coating {Rivera Gil, 2013 #20645}. Now ions in solution will be in equilibrium with several entities, not only with the originally bare NP surface of the ionorganic but, as in particular also with the ligand shell, which itself can comprise different parts. In the important case of carboxylic acids as ligand, there will be the pH-dependend equilibrium $-COO^- + H^+ \leftrightarrow -COOH$ with $K_a = c(-COO^-)\cdot(H^+)/c(-COOH)$. In case of complex carboxylic acids several pK_a values can exist, which can be determined by titration experiments {Charron, 2012 #23478}. In case the pH is smaller than the pK_a value, the NP surface is loosing its charge and predominantly comprises -COOH groups , as pK_a - pH = $-\log(c(-COO^-)/c(-COOH))$. Thus the NPs loose their colloidal stability and start to agglomerate. At alkaline solution pH >> pK_a the NPs surface on the other hand is saturated with negative charge $c(-COO^-)$ and the NPs are colloidally stable. The situation can change with

other ligands, for example with positively charged ones {Geidel, 2011 #19314}. In case of amino terminated ligands $-NH_2 + H^+ \leftrightarrow -NH_3^+$ the NPs are charged at low, acid pH ($-NH_3^+$, pH << pK_a), as pK_a - pH = $-\log(c(-NH_2)/c(-NH_3^+)$. In the case of high pH >> pK_a the NPs are uncharged ($-NH_2$) and thus will loose their colloidal stability. Thus as described before for ligand free NPs also in the case of ligand-coated NPs the local pH can (though not automatically) determine the surface charge of the NPs, whereby the dependence is given by the nature of the ligand. In contrast to ligand-free NPs, ligand-coated NPs can be also made with ligands comprising a permanent charge (*e.g.* ammonium salts, which are fully dissociated and thus permanently charged), which then have a pH-independent surface charge {Hühn, 2013 #20527}. Most important, these NPs can be stabilized also with macromolecular ligands, such as polyethylenglycol (PEG), which provides colloidal stability *via* steric repulsion. In this way ligands on the NP surface introduce higher flexibility in achieving (pH-independent) colloidal stability, in particular *via* permanently charged ligands and / or ligands providind steric repulsion. As for ligand-free NP, besides the charge directly associated with the NP surface (now here in particular to the ligand shell), also ligand-coated NPs comprise a diffusive cloud of charge by attracted counter ions according to the Gouy-Chapman model. Thus in a similar way the use of charged NPs produces changes in the concentration of charged species in a solution. For negatively charged NP surfaces (*e.g.* COO^- stabilized NPs) there is a local depletion of negatively charged analytes (*i.e.* anions such as OH^- or Cl^-), and a local accumulation of positively charged analytes (*i.e.* cations such as H^+), see Figure 7A. The opposite scenario will happen when working with positively charged NPs. Coming back to our main statement this means that the local ion concentration close to the NP surface will be different from thebulk concentration (Figure 7B), *i.e.* NPs influence their environment. This fact has severe effects on sensing with NPs, which will be discussed later. In the same way this screening effect due to the adsorption of counter-ions, together with the pH-dependent surface charge of the ligand shell, determines the colloidal stability of the NPs, *i.e.* the nanoenvironment affects the physico-chemical properties of the NP surface.

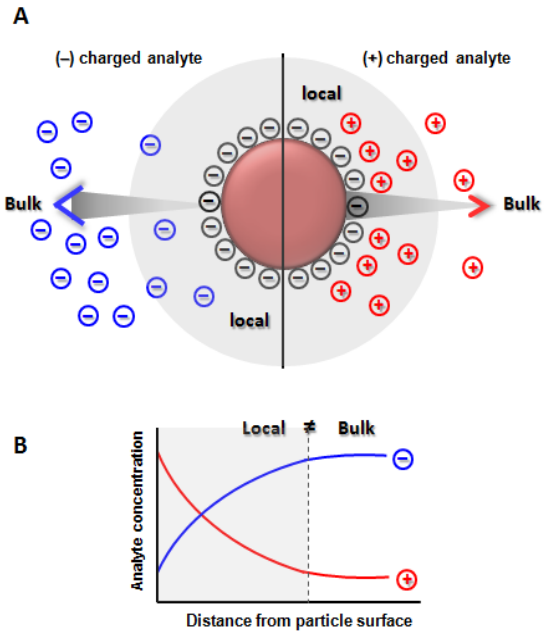

Figure 7: The concentration of a ions at the surface of a NP is different from the respective bulk concentration. A) in the case of negatively charged NPs (*e.g.* NPs with -COO^- ligands) due to Debye-Hückel screening there will be a local depletion and accumulation of anions and cations, respectively, close to the NPs surface. B) This demonstrates that the concentration c_i of ions of different species depends on the distance R from the NP surface, and is different from bulk close to NP surfaces.

Unfortunately a detailed theoretical description of the ion distribution around ligand-coated NPs is not as straight forward as for ligand-free NPs. This is due to their hybrid nature. Already the question where the NP surface begins can't be clearly answered {Rivera Gil, 2013 #20645}. The ligand shell in general is not homogeneous. A practical system for example can comprise hydrophobic surfactant molecules, surrounded by an amphiphilic polymer, with an addition shell of PEG {Zhang, 2011 #18339}. This ligand shell is not completely rigid, *i.e.* one can't exactly determine where the transition from one layer to the next layer (*e.g.* the polymer PEG interface) is located. Even the final hydrodynamic radii r_h underly much larger distributions than the original core radius r_c. Thus models describing the different parts of the ligand shell would need to consider distributions of respective different layers. Fortunately distributions are not as smeared out as one may expect, as for example indicated by fluorescence resonance energy transfer (FRET) measurements which revealed relatively narrow distribution of fluorophores attached to the polymer shell around fluorescent NPs {Yakovlev, 2009 #13413}. Different layers of the ligand shell also can interact in different ways with ions. Long PEG chains for example chelate ions such as Na^+ or K^+, and thus change the surface charge of the NPs {Sperling, 2006 #10309}. All the effects make theoretical predictions about the quantitative ion distribution around ligand-coated NPs complicated.

From an experimental approach ion-sensitive fluorophores attached to the NPs are a feasible strategy to probe ion concentration close to NP surfaces. Such fluorophores change their emission, most frequently the intensity of emission, dependent on the concentration of the respective ion. However, most convenient are ion sensitive fluorophores with ratiometric detection schemes, in which not absolute intensities need to be detected, but where the intensities of the emissions at two different wavelengths are compared {Arduini, 2007 #23791; Riedinger, 2010 #15205}. This can be achieved either by fluorophores with two emission peaks {Page, 2011 #23792}, or by combing an ion sensitive fluorophore which emits at one wavelength with a reference fluorophore which emits at another wavelength {Doussineau, 2009 #14108; Riedinger, 2010 #15205; Ali, 2011 #17340}. Thus, in order to determine the ion concentration profile around NPs, ion-sensitive fluorophores (and the reference fluorophores) need to be immobilized at different distances R to the NP surface. This can be conveniently done by using molecular spacers such as DNA {Obliosca, 2012 #23785; Diaz, 2012 #23786; Chhabra, 2009 #23788} or polyethyleneglcol (PEG) {Riedinger, 2010 #15205; Zhang, 2010 #14235; Zhang, 2011 #18339}. In order to obtain spacers providing controlled distances R the trick lies in saturating the NP surface. In this way the spacers are stretched (instead of forming statistical coils) and thus have defined conformation {Pellegrino, 2007 #10589}. The confirmation of only a few spacer molecules per NP is in general not known. In case of flexible spacers they might be partly wrapped around the NP surface, or they might be dangling in solution {Pellegrino, 2007 #10589}. However, in the case the NP surface is saturated with attached spacer molecules, they all will adopt similar geometry and thus lead to defined distances R. Fluorophores can be linked to the end of the spacer molecules {Shenoy, 2006 #23802; Liu, 2008 #12946},

and by using spacers with different molecular weight the average distance between fluorophores and the NP surface can be tuned {Dulkeith, 2005 #9845; Nagatoishi, 2007 #23803; Obliosca, 2012 #23785}. This principle has been applied to sense lokal H^+ {Zhang, 2010 #14235; Zhang, 2011 #18339} and Cl^- {Riedinger, 2010 #15205} concentrations. According to Figures 7 and 8 for negatively charged NPs higher H^+ and lower Cl^- concentrations were found close to the NP surface as compared to bulk. Thus the response curves of the ion-sensitive fluorescence read-out are shifted in case the fluorophores are attached close to the NP surface. In case of long enough spacers the fluorophores are sufficiently far away from the NP surface and thus bulk read-out is obtained. This implicates that for all NP-based sensing applications one must consider that the actual environment of the NPs where the measurement takes place is different from bulk, *e.g.* ion concentrations at the NP surface are different from bulk values. While the fact that the local environment around NPs is different from the bulk can be potentially seen as a potential drawback or source of complication in the field of sensors based on NPs, is also could be potentially harnessed for improving sensitivity. Here, we will suggest possible ways of exploiting this effect. One advantage of getting a higher concentration of an analyte (here in particular ions) close to the NP surface is that the NP can act not only as detector but also as preconcentration system. When the concentration of an ion species in the bulk is extremely low it is hard to detect it. However, the sensitivity is increased if the ions can be preconcentrated on the surface of the NP playing with the charge density of the NP. Several articles have already been reported showing this potential use. For example, tetraalkylammonium bromide coated silver NPs have been successfully applied as electrostatic affinity probes to preconcentrate peptide mixtures in biological samples {Sudhir PR et al. Rapid Commun Mass Spectrom. 2008 22(19):3076-86}. In another example detection limits as low as nanomolar concentrations were achieved using positively charged poly-L-lysine-coated silver NPs {Marsich L et al. Langmuir. 2012 28(37):13166-71}. Local concentration at the NP surface hereby was achieved by the strong interaction of these NPs with the anionic bilirubin molecules . In the case of working with ion-sensitive fluorophores, the strategy would be to locate the fluorophore on the NP surface (*e.g.* b<integrating the fluorophore directly in the polymer shell) for measuring the local concentration (of oppositely charged ions), which wouled be much higher than the bulk concentration due to the preconcentration effect. Using appropriate calibration curves then could be used to calculate the preconcentration factor achieved with the particular configuration in order to finally determine the bulk concentration of the target ions.

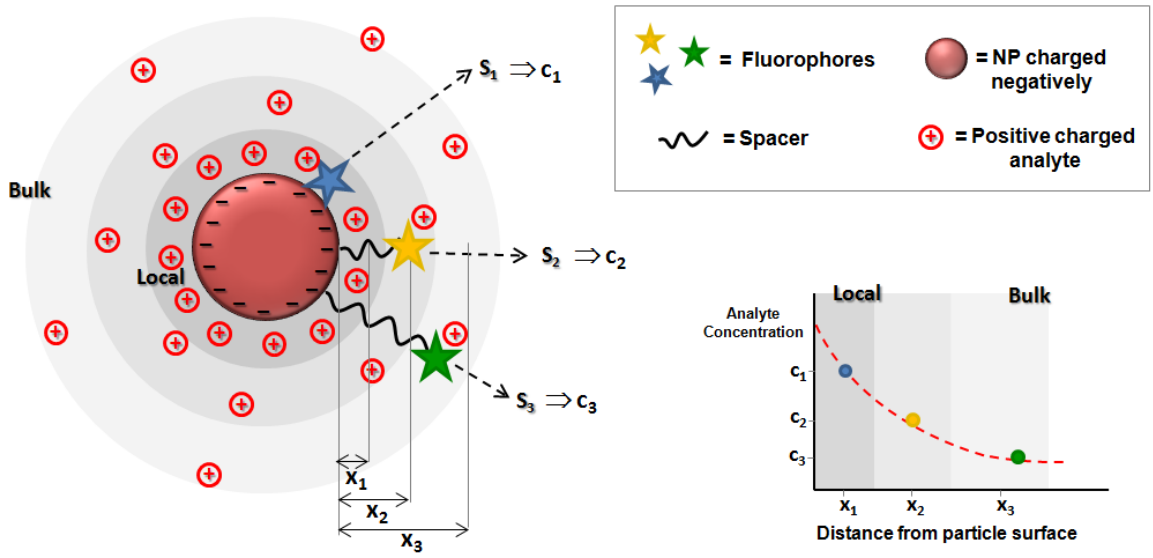

Figure 8. Scheme for measuring the distribution of ions with concentration c(R) in dependens from the distance R to the NP surface.

Conclusions

The local enviroment of NPs has profound interaction with the surface of NPs, in which the physico-chemical properties of both, the environment and the surface can be mutually altered. The surface of NPs creates a special local environment, with different properties compared to bulk. Due to different repulsion / adsorption effects local molecular concentrations around the NP surface can be quite different from bulk concentrations. This has strong effects on NP-based sensors, as those probe concentrations of the local environment, and not from bulk. In the other direction the surface charge of NPs is determined by the presence of ions in the local nanoenvironment. *Via* reaction with ligands or even with the bare NP surface this regulates the surface charge of NPs and thus also their colloidal stability.

Acknowledgements: This work was supported by the DFG (graduate research school 1782 to WJP and the project REPROTOX within priority program SPP1313 to SB). CC acknowledges a postdoctoral fellowship from the Alexander von Humboldt Foundation. DJ acknowledges a PhD fellowship for the Basque Country, Spain.

References:

small NANO MICRO

Nanoparticles

A General Synthetic Approach for Obtaining Cationic and Anionic Inorganic Nanoparticles via Encapsulation in Amphiphilic Copolymers

C. Geidel, S. Schmachtel, A. Riedinger, C. Pfeiffer, K. Müllen, M. Klapper, and W. J. Parak**

***A** series of amphiphilic copolymers with variable charge densities on their backbone is synthesized. Positively charged N,N,N-trimethylammonium-2-ethyl methacrylate iodide or negatively charged 2-(methacryloyloxy)ethylphosphonic acid and lauryl methacrylate are used as building blocks. When wrapped around hydrophobically capped inorganic nanoparticles (NPs), the latter are able to disperse in aqueous solutions. Using this method, positively as well as negatively charged colloidal NPs can be synthesized in a reliable way. The method presented herein allows the charge on the NPs to be adjusted to different negative and positive values by using polymers with a variable ratio of charged monomers and lauryl methacrylate. Virtually all kinds of hydrophobic inorganic NPs could be coated with these amphiphilic polymers. The coating procedure is demonstrated for Au particles as well as for CdSe/ZnS quantum dots. To date, wrapping amphiphilic polymers around NPs has led only to anionic NPs. The polymers synthesized in this work allow for positively charged NPs with a high colloidal stability.*

1. Introduction

The colloidal stabilization of nanoparticles (NPs) in aqueous solutions can be provided by electrostatic or steric repulsion.[1] In the case of electrostatic repulsion, the repulsion is provided by (typically negative) charges on the NP surface in the form of an organic ligand shell. However, the undesirable agglomeration of NPs and subsequent changes to their properties in aqueous media can be caused by several events. First, ions in salt-containing solutions screen the surface charge of the NPs.[2] Second, in biological media, proteins can adsorb to the NP surface.[3] Third, corrosion of the inorganic NP cores and loss of the organic ligand shell are observed in aqueous environments, which is accentuated in acidic or alkaline media.[4] These issues highlight the role of the charged organic ligand shell around the inorganic NP for obtaining colloidally stable NPs. The other option, steric stabilization, is not affected by ionic screening in salt-containing solutions, as the problem associated with vanishing surface charges at certain pH values does not apply. The other two events also apply for sterically stabilized NPs. In the present work, we focus explicitly on electrostatically stabilized NPs.

One way of realising robust, electrostatically colloidally stable NPs with a narrow size distribution is wrapping them with an amphiphilic polymer.[5,6] Hydrophobic inorganic NPs are embedded in a micelle formed by amphiphilic polymers whose hydrophilic moiety points towards the solution. This method has proven to be very versatile since it works for virtually any type of NP.[6] However, so far only negatively charged NPs have been reported using this method. The synthesis of positively charged NPs remains an interesting challenge as they are considered to be superior for several applications. One example is nanoprinting, which is typically performed on a slightly negatively charged paper.[7] Positively

C. Geidel,[†] Prof. K. Müllen, Dr. M. Klapper
Max Planck Institute for Polymer Research
Ackermannweg 10, 55128 Mainz, Germany
E-mail: klapper@mpip-mainz.mpg.de
S. Schmachtel,[†] A. Riedinger, C. Pfeiffer, Prof. W. J. Parak
Fachbereich Physik und Wissenschaftliches Zentrum für Materialwissenschaften
Philipps Universität Marburg
Marburg, Germany
E-mail: wolfgang.parak@physik.uni-marburg.de
[†]These authors contributed equally to this work.

DOI: 10.1002/smll.201100509

charged NP systems would improve immobilization on paper due to charge interactions. A second example is the study of NP uptake by cells, for which cationic NPs have shown an improved membrane transition.[8]

It should be mentioned that for sterically stabilized NPs, as well negatively[9] and positively charged NPs[10] have been reported. The classical way of sterically stabilizing NPs is providing them with a shell of polyethylene glycol (PEG).[11] As PEG with different terminal groups can be used, and as PEG also chelates cations from solution, negatively and positively charged PEG-coated NPs have been reported.[12,13]

In the present work, the synthesis of a series of amphiphilic copolymers with variable positive and negative charge densities based on the same polymer backbone is reported. Using these polymers, it is possible to obtain colloidally stable, positively and negatively charged NPs with a surface charge that can be adjusted independent of NP size.

2. Results and Discussion

The amphiphilic copolymers used in this approach consist of *N,N,N*-trimethylamonium-2-ethyl methacrylate iodide (TMAEMA) and lauryl methacrylate (LMA) units for providing positively charged NP shells (PTMAEMA–*stat*–PLMA). The monomers 2-(*N,N*-dimethylamino) ethyl methacrylate (DMAEMA) and LMA were copolymerized via free radical polymerization in the presence of azobisisobutyronitrile (AIBN). The structure and composition of these copolymers were determined by ^{1}H-NMR spectroscopy (see Supporting Information (SI)). Comparison of the relative signal intensities at $\delta = 2.3$ ppm, representing the six dimethylamino protons, with that of the oxymethylene group of LMA at $\delta = 3.9$ ppm, allowed the definition of the copolymer composition. Quaternization of the dimethylamino groups was carried out in dichloromethane (DCM) using methyl iodide (MeI) (**Scheme 1**a). The quantitative degree of quaternization was determined by ^{1}H-NMR spectroscopy. The absence of any unquarternized dimethylamino protons at $\delta = 2.3$ ppm indicates a 100% quaternization for PTMAEMA–*stat*–PLMA. Furthermore, a new peak at $\delta = 3.6$ ppm appeared, which may be attributed to the quaternary methyl groups.

For the formation of negatively charged NP shells, copolymers containing 2-(dimethoxyphosphoryl)ethyl methacrylate (MAPHOS(OMe)$_2$) and LMA monomers were synthesized via free-radical polymerization (PMAPHOS(OMe)$_2$–*stat*–PLMA). The amount of MAPHOS(OMe)$_2$ and LMA units in the copolymers was evaluated in a similar way to that of the positively charged copolymers. In this case, the integration of the doublet at $\delta = 3.8$ ppm, assigned to the methoxy groups of MAPHOS(OMe)$_2$, was compared with the signal at 3.9 ppm, representing the oxymethylene group of LMA. The esters were converted into the corresponding acids ($pK_{a1} = 2.4$, $pK_{a2} = 8.1$) by a reported cleavage method using trimethylsilyl bromide (TMSBr) followed by methanolysis at room temperature (Scheme 1b).[14] The hydrolysis was quantitative shown by ^{1}H-NMR spectroscopy. The absence of the doublet at $\delta = 3.8$ ppm corresponding to the ester groups indicated 100% hydrolysis for PMAPHOS-*stat*-PLMA. Furthermore, a new peak at $\delta = 8.5$ ppm appeared due to the phosphonic diacid moiety. Copolymers were chosen based only on methacrylate-type monomers, as they have similar copolymerization parameters due to their similar electronic structures.[15] This similarity guaranteed a statistical but homogeneous distribution of the hydrophilic and hydrophobic monomer units throughout the copolymers. A selection of polymers (Scheme 1) with different molecular weights (M_n) and ratios of charged (x) to uncharged (y) monomer units (positive species **P1(+)–P5(+)** and negative species **N1(-)–N3(-)**) is listed in **Table 1**. The molecular weights (Table 1) were kept in the range 5000–40 000 g mol^{-1} as, during polymer absorption onto inorganic nanoparticles, longer polymer chains are likely to result in aggregation as a consequence of bridging effects between nanoparticles. As a reference, the negatively charged amphiphilic polymer

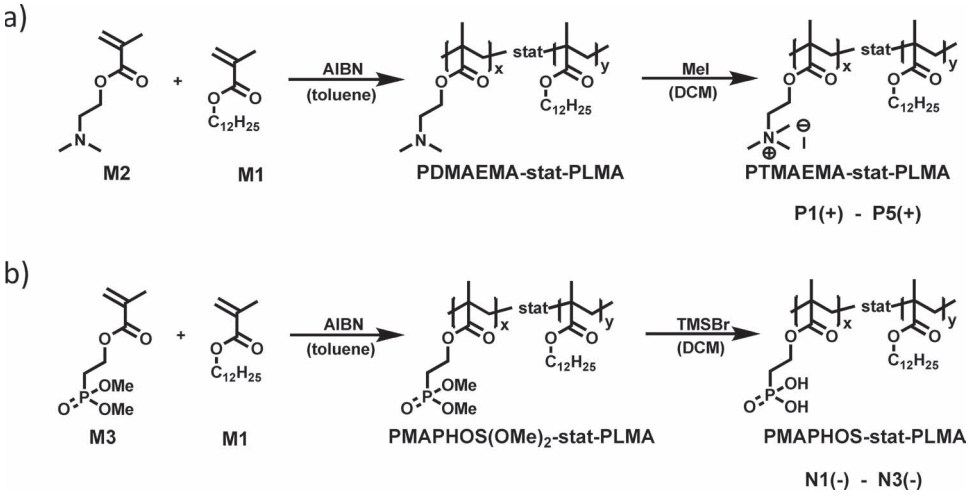

Scheme 1 Scheme of the synthesis of the amphiphilic copolymers used: a) Synthesis of the PTMAEMA–*stat*–PLMA polymer using LMA (**M1**) and DMAEMA (**M2**) followed by quaternization of the amine. b) Synthesis of the PMAPHOS–*stat*–PLMA type polymer using LMA (**M1**) and MAPHOS(OMe)$_2$ (**M3**) followed by deprotection of the phosphonate.

NANO MICRO small

Table 1. The selected polymers used in this study. Polymers **P1(+)–P5(+)** are of the PTMAEMA–*stat*–PLMA type and polymers **N1(-)–N3(-)** are of the PMAPHOS–*stat*–PLMA type. **PMA–g–D(-)** is used as a reference polymer.[16] The ratio x:y corresponds to the ratio of charged to uncharged monomer units in the polymer, as determined by ^{1}H-NMR spectroscopy. M_n is the molecular weight of the polymer and PDI the measured polydispersity index. Both were determined using the precursor copolymers PDMAEMA–*stat*–PLMA and PMAPHOS(OMe)$_2$–*stat*–PLMA.

Amphiphilic copolymers	x:y [mol%]	M_n [g mol^{-1}]	PDI	
P1(+)	19:81	11000	1.9	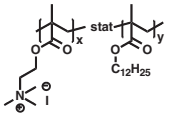 P1(+) - P5(+)
P2(+)	38:62	9500	1.6	
P3(+)	51:49	47000	2.2	
P4(+)	53:47	11000	1.8	
P5(+)	76:24	7000[a)]	1.6[a)]	
N1(-)	25:75	8000	1.9	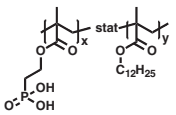 N1(-) - N3(-)
N2(-)	35:65	11800	2.1	
N3(-)	40:60	9500	2.0	
PMA–*g*-D(-)	68:32[b)]	6000	NA	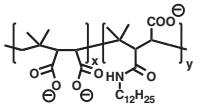 PMA-g-D(-)

[a)] M_n was determined for polymer **P5(+)** in dimethylformamide (DMF). In all other cases, M_n was determined with the polymer dissolved in tetrahydrofurane (THF); [b)]Charge distribution. The monomer ratio was 25:75 mol% (see SI).

poly(isobutylene–*alt*–maleic anhydride)–*graft*–dodecyl (**PMA–*g*–D(-)**), as previously used in our group,[16] was chosen. The negative charge on this polymer originates from carboxylic acid groups ($pK_a = 4.3$) generated by hydrolysis of the anhydride rings.[16] For this reference polymer, the ratio of charged to uncharged units was estimated to be around 68:32 mol% (see SI).

The coating procedure with these polymers was tested on hydrophobic Au NPs (≈4 nm core diameter), which had been synthesized in an organic solvent (in this case, toluene) according to standard procedures (see SI),[2,17] and on commercial hydrophobic CdSe/ZnS NPs (≈4 nm core diameter, Plasmachem, see SI). The NPs were coated with amphiphilic copolymers as described previously,[6,16] or with slight modifications to the procedure (see SI). Briefly, the polymer dissolved in chloroform was added to NPs dispersed in chloroform. The chloroform was then evaporated and the NPs were redissolved in aqueous solution and colloidally stabilized by the charges on the polymer, as shown in **Figure 1**. The critical step was the phase transfer, in which NPs were redispersed in aqueous solution.

For the highly charged, chloroform insoluble polymer (**P5(+)**, PTMAEMA–*stat*–PLMA), an alternative protocol was needed, based on a method proposed by Stelzig et al.[18] The water phase (polymer) and the organic phase (NPs) were merged using ethanol as co-solvent to close the miscibility gap between both phases. This allowed the NPs to be redispersed in water of after evaporation of all solvents.

In order to characterize in particular the colloidal properties of the polymer-coated NPs, analyses utilizing UV–vis spectroscopy, size-exclusion chromatography (SEC), gel electrophoresis, dynamic light scattering (DLS), transmission electron microscopy (TEM), and zeta-potential measurements were performed.[19]

Amphiphilic copolymers were composed as described in Table 1. Polymers with different ratios of hydrophilic (x) and hydrophobic (y) monomer units were synthesized via free-radical polymerization (Scheme 1). The compositions ranged from x:y = 11:89–76:24 mol% (positive charge) and 21:79–40:60 mol% (negative charge). A detailed list of all compositions obtained as well as the M_n and PDI values can be found in the SI. By varying the amount of hydrophilic monomer units the charge densities of the polymers could be tuned. For positively charged polymers, charge was provided by quaternary ammonium groups. A negative charge on the other hand was introduced by a phosphonic acid group ($pK_{a1} = 2.4$, $pK_{a2} = 8.1$).

By applying our previously described protocol,[16] hydrophobic Au NPs as well as green fluorescent CdSe/ZnS NPs were transferred to an aqueous solution by coating with the polymers listed above. The properties of the hydrophobic NPs have already been extensively described in the literature.[17,20] These NPs have been chosen as examples. Based predominantly on hydrophobic interactions, the polymer coating procedure, as utilized with our reference polymer **PMA–g–D(-)**, has been previously demonstrated to be applicable to a wide range of hydrophobically capped NP materials of various sizes[6,16] and is thus not limited to a certain type of inorganic material.

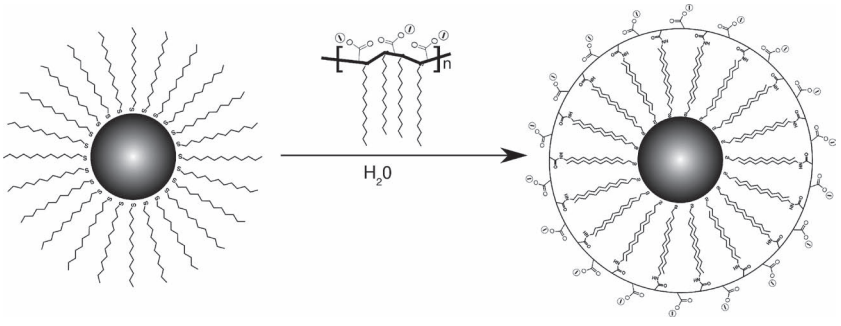

Figure 1. Sketch of the coating process of hydrophobic inorganic Au or CdSe/ZnS NPs, which are wrapped in amphiphilic polymers and thereby rendered water-soluble.

The performance of the polymer coating procedure depended on the type

of polymer used. As expected, polymers with high molecular weights (e.g., PTMAEMA–*stat*–PLMA, **P3(+)**, x:y = 51:49 mol%; M_n = 47 000 g mol^{-1}) redissolved very slowly in an aqueous medium (see the SI for buffers used for the different polymers), resulting in **NP3(+)** agglomerates after the coating procedure. All other polymers were therefore synthesized with lower molecular weights on the order of $M_n \approx 10\,000$ g mol^{-1}. For these polymers, the x:y ratio, and thus the charge density, were varied. NPs (**NP1(+)**, **NP1(-)**) wrapped in polymers with very low charge densities (positive charge, **P1(+)**, x:y = 19:81 mol% or negative charge, **N1(-)**, x:y = 25:75 mol%) could not be redissolved in aqueous solution. In these cases, the polymers were neither soluble in aqueous medium nor did they form soluble polymer-coated NPs. NPs (**NP2(+)**, **NP2(-)**) coated with polymers of slightly higher charge densities (PTMAEMA–*stat*–PLMA, **P2(+)**, x:y = 38:62 mol%; PMAPHOS–*stat*–PLMA, **N2(-)**, x:y = 35:65 mol%) could be dissolved in aqueous solution, although DLS measurements demonstrated the presence of some agglomerates. The best results were obtained for positively charged polymers (PTMAEMA–*stat*–PLMA, **P4(+)**) with x:y of 53:47 mol% and negatively charged polymers (PMAPHOS–*stat*–PLMA, **N3(-)**) with x:y of 40:60 mol%. Copolymers with higher charge densities such as PTMAEMA–*stat*–PLMA, **P5(+)**, (x:y = 76:24 mol%) turned out to be problematic as they were no longer soluble in chloroform. In this case, ethanol had to be used as mediator to bring the polymers, which were only soluble in water but not in chloroform, together with the hydrophobic NPs dispersed in chloroform.[18] As ethanol reduces the polarity of the mixture, the tendency of the NPs to agglomerate increased. These results suggest that the charge density (as controlled and estimated by the x:y ratio) of the polymer needs to be high enough to provide water solubility but low enough to maintain solubility in chloroform. This is in accordance with our negatively charged reference polymer, **PMA–*g*–D(-)**,[16] with an estimated x:y ratio of 68:32 mol%, which dissolves well in both water and chloroform.

Based on these initial findings, the NPs coated with polymers that possessed sufficient solubility in water were then studied in greater detail, namely PTMAEMA–*stat*–PLMA **P2(+)** x:y = 38:62 mol%, **P4(+)** x:y = 53:47 mol%, and **P5(+)** x:y = 76:24 mol%, and PMAPHOS–*stat*–PLMA(-) **N2(-)** x:y = 35:65 mol% and **N3(-)** x:y = 40:60 mol%. Purification of the polymer-coated NPs was crucial, as in the case of our reference polymer (**PMA–*g*–D(-)**) both empty polymer micelles and aggregates without NPs inside have been demonstrated to be a side product of the polymer coating procedure.[21] In this study, the charged NPs were purified using SEC and when possible gel electrophoresis. As small molecules, and thus also empty polymer aggregates, elute last during SEC, they could be separated to ensure the isolation of pure polymer coated NPs.[19]

Gel electrophoresis is a convenient method to separate water soluble charged NPs by size and charge.[12,22,23] This technique was also applied for the purification of negatively charged, polymer-coated Au and CeSe/ZnS NPs, which migrated in the applied electric field towards the positive pole as expected (see SI). However, migration of the positively charged Au and CeSe/ZnS NPs towards the negative pole was not observed, as they stuck in the loading-wells of the gel (see SI). There have been reports of positively charged NPs migrating towards the negative pole in gels.[12,23,24] In these cases, however, the surface of the NPs was additionally coated with PEG molecules, which provided colloidal stability through steric interactions instead of electrostatic repulsion. The fact that the positively charged NPs used in the present study get stuck in the gel might indicate NP agglomeration. However, this possibility could be disproved by DLS and UV–vis measurments. It was assumed that electrostatic interactions with the matrix are the cause; this has been observed before for glucose, which has been reported to stick inside chromatography columns equipped with quaternary ammonium groups.[25]

Transmission electron microscopy analysis (**Figure 2**b) of purified Au NPs demonstrated that the polymer coating procedure did not change the size distribution of the Au cores and that no obvious agglomeration of NPs occurred (note that the polymer shell is not visible in TEM).

Further analysis of the colloidal properties of the NPs was carried out in solution (see the SI for the buffers used). In the case of Au NPs, severe agglomeration can in principle be detected with UV–vis absorption spectroscopy (Figure 2c), as the surface plasmon peak of agglomerated Au NPs becomes broader, shifts to longer wavelengths, and shows scattering in the near-IR.[26] As these indicators were not observed for our purified, polymer-coated Au NPs, a significant presence of larger NP agglomerates in solution could be ruled out. However, the UV–vis data does indicate differences in the robustness of the polymer coating procedure. For the positively charged polymer, an x:y ratio of 53:47 mol% worked best, while in some coatings polymer ratios of 76:24 mol% caused a shift of the surface plasmon peak to higher wavelengths (see SI). This again points out the importance of tuning the x:y ratio to within a suitable range. Au NPs wrapped with the negatively charged PMAPHOS–*stat*–PLMA polymers showed high quality UV–vis spectra for x:y ratios of 35:65 and 40:60 mol%.

In order to quantify the amount of smaller NP agglomerates, DLS experiments were performed to determine the hydrodynamic diameter of the purified Au NPs (Figure 2d). The presence of agglomerates would cause broader distributions or additional peaks at larger hydrodynamic diameters. The DLS data (**Table 2**) indicates that the majority of the NPs were well dispersed. These data confirmed quantitatively what was measured by UV–vis: for positively charged polymers, the best dispersion of NPs was obtained with an x:y ratio of 53:47 mol%. The average hydrodynamic diameter of these NPs was the smallest of all the samples investigated. As indicated above, NPs coated with a polymer with an x:y ratio of 76:24 mol% were slightly aggregated, as can be seen from the increase in their average hydrodynamic diameter. The same applies to NPs with x:y of 38:62 mol%. Results for the NPs coated with negatively charged polymers **N2(-)** and **N3(-)** show that there was no agglomeration for all polymer compositions used. However, with regard to reproducibility, our reference polymer (**PMA–*g*–D(-)**) turned out to be the most robust. This can be seen from the very low standard deviation in the hydrodynamic diameters, as detected for NPs in several batches. Positively charged Au particles

small NANO MICRO

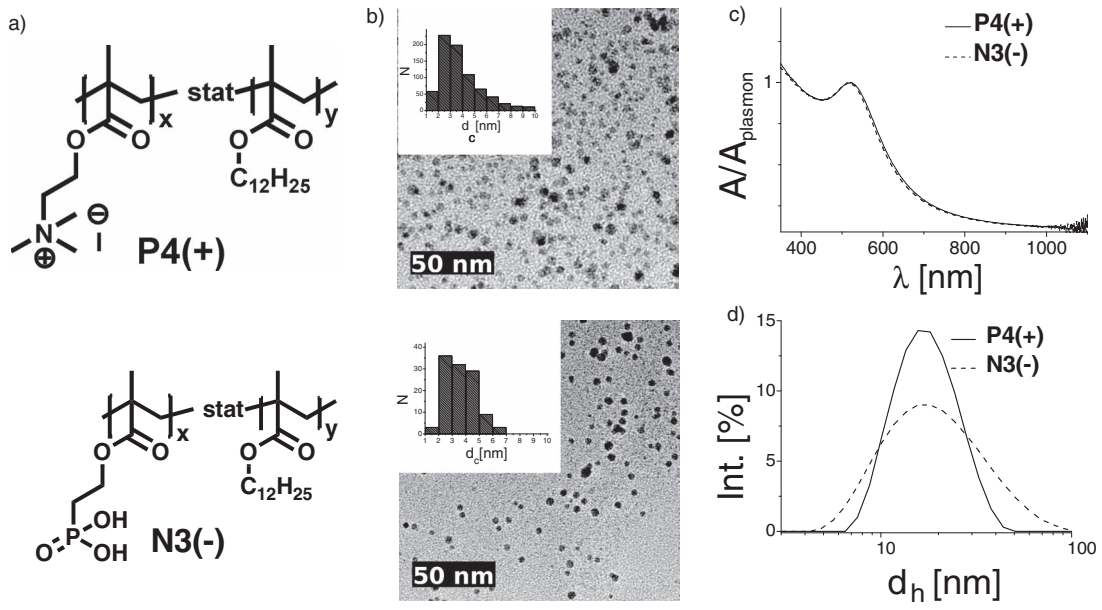

Figure 2. Examples of amphiphilic polymers (**P4(+)** and **N3(-)**) for creating positively (upper lane, sample **NP4(+)**) and negatively charged (lower lane, sample **NP3(-)**) Au NPs. a) Structural formulae of the amphiphilic polymers used. b) TEM micrographs of Au NPs. The scale bars correspond to 50 nm. The insets show the size distribution of the NPs, whereby ***N*** is the occurrence of NPs with a core diameter d_c (i.e., without the polymer shell). c) UV–vis absorption spectra (normalized to the surface plasmon peak) of the polymer-coated Au NPs in water. d) DLS data as obtained from polymer-coated Au NPs in water. The intensity-weighted distribution of hydrodynamic diameters is shown.

NP4(+) with hydrodynamic diameters of ≈7 nm were slightly smaller than the negatively charged ones (**NP2(-)**, **NP3(-)**, NP(-)) with hydrodynamic diameters of ≈11 nm (Table 2). As this difference clearly did not originate from NP agglomeration, we speculate that it might be due to different clouds of counter ions. Furthermore, these results are highly reproducibile. NPs coated with similar polymers (sample **NP2(-)** versus sample **NP3(-)**) lead to similar colloidal properties, Table 2.

As our NPs were stabilized by charge, the zeta potential Φ is an important factor for the determination of their colloidal stability. The Φ of Au NPs (an indicator of their surface charge) was verified using a Malvern Zetasizer (Table 2). All negatively charged, polymer-coated NPs showed sufficiently negative zeta potentials (<-20 mV), and all positively charged NPs showed sufficiently positive zeta potentials (>+25 mV), which is a prerequisite for good colloidal stability. The colloidal stability of the NPs was further challenged by adding salt to the solution (100 mM NaCl). As the NPs (in particular samples **NP4(+)** and **NP3(-)**) barely agglomerated under these conditions (see SI), it was concluded that these NPs have good colloidal stability.

Table 2. Hydrodynamic diameters, d_h, and zeta-potentials, Φ, for Au NPs coated with amphiphilic polymers with the given ratios of charged to uncharged units. Polymers **P2(+)–P5(+)** are of the PTMAEMA–*stat*–PLMA type and polymers **N2(-)** and **N3(-)** are of the PMAPHOS–*stat*–PLMA type. **PMA–*g*–D(-)** is used as a reference polymer.[16] Experimental errors correspond to the standard deviation between the values as obtained for five different batches of NPs.

Coated gold nanoparticles	Amphiphilic copolymers	x:y [mol%]	d_h [nm]	Zeta potential, Φ [nV]
NP2(+)	**P2(+)**	38:62	22.2 ± 12.8	+28.1 ± 14.8
NP4(+)	**P4(+)**	53:47	7.3 ± 1.8	+30.0 ± 13.7
NP5(+)	**P5(+)**	76:24	28.3 ± 21.5	+30.9 ± 5.6
NP2(-)	**N2(-)**	35:65	12.6 ± 2.7	−24.6 ± 4.9
NP3(-)	**N3(-)**	40:60	11.5 ± 3.6	−20.8 ± 8.7
NP(-)	**PMA–*g*–D(-)**	68:32[a)]	10.6 ± 0.7	−24.1 ± 4.5

[a)]Charge distribution: the monomer ratio was 25:75 mol%.

3. Conclusion

We have described a versatile approach to transfer hydrophobically capped NPs, such as Au or CdSe/ZnS NPs, to an aqueous solution by embedding them in a shell of negatively or positively charged amphiphilic copolymers. Importantly, in this way it was possible to synthesize positively charged colloidal NPs with excellent colloidal stability. Due to the hydrophobic interactions between the original NP capping ligands and the hydrophobic side chains of the amphiphilic polymer, this method can be applied to NPs of different sizes and core materials. Positively and negatively charged NPs were prepared, which had the same properties (e.g., size, core material, surface morphology) except for the charge. The ratio between charged and uncharged groups of the polymer proved to be crucial to achieve a successful coating. We were able to tune the charge ratio (hydrophilic:hydrophobic) in a range of approx. 35:65–75:25 mol%. However, the best results were obtained for x:y of around 50:50 mol%. One can assume that based on similar copolymers even more complex positively and negatively charged polymer-shell-coated NPs will become accessible.

The approach outlined here makes NPs available for use in many different studies designed to investigate

charge-dependent processes, in particular, cellular uptake, which is dependent on the surface charge of NPs. The interaction of cells with nanoparticulate objects is governed by specific receptor-ligand-mediated recognition, but also by basic physicochemical properties such as size and charge.[27] Recent simulations suggest, for example, that it is possible to gain control over the interactions of NPs with cell membranes by carefully tuning their surface-charge densities.[8] Precise probes with a well-defined size and charge are required for experimental verification. Anionized and cationized derivatives of peptides, such as ferritin[28] or hemeundecapeptides,[29] have been used to investigate charge dependence. Size dependence has been examined using colloidal NPs with sizes covering the whole nanometer range.[30] In particular, studies in which charge and size could be independently tuned in parallel would be of great interest. One approach in this direction are PEG-coated NPs with PEG molecules that have different terminal groups. We suggest that the polymer coating procedure described in this report, which leads to positively as well as negatively charged NPs, may lead to alternative probes for investigating charge-dependent cellular uptake. In contrast to PEG-coated NPs, these NPs are just stabilized by charge, which may lead to different effects as compared to PEG-coated NPs, which are sterically stabilized.

Supporting Information

Supporting Information is available from the Wiley Online Library or from the author.

Acknowledgements

This work was funded by the German Research Foundation (DFG, grant PA794/11-1 to WJP) and the European Union (grant NANOGNOSTICS to WJP). The authors are grateful to Dr. Feng Zhang, Dr. Jose Maria Montenegro Martos, Dr. Ali Zulqurnain, and Faheem Amin for helpful technical discussions.

[1] T. Pellegrino, S. Kudera, T. Liedl, A. M. Javier, L. Manna, W. J. Parak, *Small* **2005**, *1*, 48.
[2] F. Zhang, Z. Ali, F. Amin, A. Feltz, M. Oheim, W. J. Parak, *ChemPhysChem* **2010**, *11*, 730.
[3] a) T. Cedervall, I. Lynch, S. Lindman, T. Berggård, E. Thulin, H. Nilsson, K. A. Dawson, S. Linse, *Proc. Natl. Acad. Sci. USA* **2007**, *104*, 2050; b) C. Röcker, M. Pötzl, F. Zhang, W. J. Parak, G. U. Nienhaus, *Nat. Nanotechnol.* **2009**, *4*, 577.
[4] S. Kittler, C. Greulich, J. Diendorf, M. Koller, M. Epple, *Chem. Mater.* **2010**, *22*, 4548.
[5] a) M. X. Wu, H. Liu, J. Liu, K. N. Haley, J. A. Treadway, J. P. Larson, N. Ge, F. Peale, M. P. Bruchez, *Nat. Biotechnol.* **2003**, *21*, 41; b) R. E. Anderson, W. C. W. Chan, *ACS Nano* **2008**, *2*, 1341; c) B. W. Muir, B. A. Moffat, P. Harbour, G. Coia, G. L. Zhen, L. Waddington, J. Scoble, D. Krah, S. H. Thang, Y. K. Chong, P. Mulvaney, P. Hartley, *J. Phys. Chem. C* **2009**, *113*, 16615.
[6] T. Pellegrino, L. Manna, S. Kudera, T. Liedl, D. Koktysh, A. L. Rogach, S. Keller, J. Rädler, G. Natile, W. J. Parak, *Nano Lett.* **2004**, *4*, 703.
[7] B. Alince, P. Arnoldova, R. Frolik, *J. Appl. Polym. Sci.* **2000**, *76*, 1677.
[8] J. Lin, H. Zhang, Z. Chen, Y. Zheng, *ACS Nano* **2010**, *4*, 5421.
[9] W. W. Yu, E. Chang, J. C. Falkner, J. Zhang, A. M. Al-Somali, C. M. Sayes, J. Johns, R. Drezek, V. L. Colvin, *J. Am. Chem. Soc.* **2007**, *129*, 2871.
[10] F. Chen, G. Xu, T.S. Andy Hor, *Mat. Lett.* **2003**, *57*, 3282.
[11] A. Karakoti, S. Das, S. Thevuthasan, S. Seal, *Angew. Chem., Int. Ed.* **2011**, *50*, 1980.
[12] R. A. Sperling, T. Pellegrino, J. K. Li, W. H. Chang, W. J. Parak, *Adv. Funct. Mater.* **2006**, *16*, 943.
[13] a) B. C. Mei, K. Susumu, I. L. Medintz, J. B. Delehanty, T. J. Mountziaris, H. Mattoussi, *J. Mater. Chem.* **2008**, *18*, 4949; b) A. Eisenberg, T. Azzam, L. Bronstein, *Langmuir* **2008**, *24*, 6521; c) L. M. Bronstein, E. V. Shtykova, A. Malyutin, J. C. Dyke, E. Gunn, X. F. Gao, B. Stein, P. V. Konarev, B. Dragnea, D. I. Svergun, *J. Phys. Chem. C* **2010**, *114*, 21900; d) E. V. Shtykova, A. Malyutin, J. Dyke, B. Stein, P. V. Konarev, B. Dragnea, D. I. Svergun, L. M. Bronstein, *J. Phys. Chem. C* **2010**, *114*, 21908.
[14] C. E. McKenna, M. T. Higa, N. H. Cheung, M. C. McKenna, *Tetrahedron Lett.* **1977**, *18*, 155.
[15] D. Bloch, in *Polymer Handbook*, Vol. *4* (Eds: J. Brandrup, E. Immergut, E. A. Grulke, A. Abe, D. Bloch), John Wiley & Sons Inc., New York, **1999**, 2336.
[16] C.-A. J. Lin, R. A. Sperling, J. K. Li, T.-Y. Yang, P.-Y. Li, M. Zanella, W. H. Chang, W. J. Parak, *Small* **2008**, *4*, 334.
[17] M. Brust, J. Fink, D. Bethell, D. J. Schiffrin, C. Kienly, *J. Chem. Soc., Chem. Commun.* **1995**, 1655.
[18] S. H. Stelzig, M. Klapper, K. Müllen, *Adv. Mater.* **2008**, *20*, 929.
[19] R. A. Sperling, T. Liedl, S. Duhr, S. Kudera, M. Zanella, C.-A. J. Lin, W. Chang, D. Braun, W. J. Parak, *J. Phys. Chem. C* **2007**, *111*, 11552.
[20] P. Reiss, J. Bleuse, A. Pron, *Nano Lett.* **2002**, *2*, 781.
[21] M. T. Fernández-Argüelles, A. Yakovlev, R. A. Sperling, C. Luccardini, S. Gaillard, A. S. Medel, J.-M. Mallet, J.-C. Brochon, A. Feltz, M. Oheim, W. J. Parak, *Nano Lett.* **2007**, *7*, 2613.
[22] C. J. Loweth, W. B. Caldwell, X. G. Peng, A. P. Alivisatos, P. G. Schultz, *Angew. Chem., Int. Ed.* **1999**, *38*, 1808.
[23] W. J. Parak, D. Gerion, D. Zanchet, A. S. Woerz, T. Pellegrino, C. Micheel, S. C. Williams, M. Seitz, R. E. Bruehl, Z. Bryant, C. Bustamante, C. R. Bertozzi, A. P. Alivisatos, *Chem. Mater.* **2002**, *14*, 2113.
[24] M. Hanauer, S. Pierrat, I. Zins, A. Lotz, C. Sonnichsen, *Nano Lett.* **2007**, *7*, 2881.
[25] D. R. Buhler, R. C. Thomas, B. E. Christensen, C. H. Wang, *J. Am. Chem. Soc.* **1955**, *77*, 481.
[26] I. Hussain, Z. Wang, A. I. Cooper, M. Brust, *Langmuir* **2006**, *22*, 2938.
[27] E. Chang, W. W. Yu, V. L. Colvin, R. Drezek, *J. Biomed. Nanotechnol.* **2005**, *1*, 397.
[28] a) S. Mutsaers, J. Papadimitriou, *J. Leukocyte Biol.* **1988**, *44*, 17; b) L. Ghitescu, A. Fixman, *J. Cell Biol.* **1984**, *99*, 639; c) M. Williams, *Proc. Natl. Acad. Sci. USA* **1984**, *81*, 6054.
[29] N. Ghinea, N. Simionescu, *J. Cell Biol.* **1985**, *100*, 606.
[30] a) B. D. Chithrani, W. C. W. Chan, *Nano Lett.* **2007**, *7*, 1542; b) B. D. Chithrani, A. A. Ghazan, C. W. Chan, *Nano Lett.* **2006**, *6*, 662; c) F. Lu, S. H. Wu, Y. Hung, C. Y. Mou, *Small* **2009**, *5*, 1408.

Received: March 15, 2011
Revised: April 24, 2011
Published online: August 29, 2011

Langmuir

Article

pubs.acs.org/Langmuir

Synthesis and Characterization of Colloidal Fluorescent Silver Nanoclusters

Sherry Huang,[†,‡,§,∥] Christian Pfeiffer,[‡,∥] Jana Hollmann,[‡] Sebastian Friede,[‡] Justin Jin-Ching Chen,[§] Andreas Beyer,[‡] Benedikt Haas,[‡] Kerstin Volz,[‡] Wolfram Heimbrodt,[‡] Jose Maria Montenegro Martos,*[,‡] Walter Chang,[§] and Wolfgang J. Parak*[,‡]

[†]Institute of Polymer Science and Engineering, National Taiwan University, Taipei, Taiwan

[‡]Fachbereich Physik and WZMW, Philipps Universität Marburg, Marburg, Germany

[§]Department of Biomedical Engineering, Chung Yuan Christian University, Chungli, Taiwan

Supporting Information

ABSTRACT: Ultrasmall water-soluble silver nanoclusters are synthesized, and their properties are investigated. The silver nanoclusters have high colloidal stability and show fluorescence in the red. This demonstrates that like gold nanoclusters also silver nanoclusters can be fluorescent.

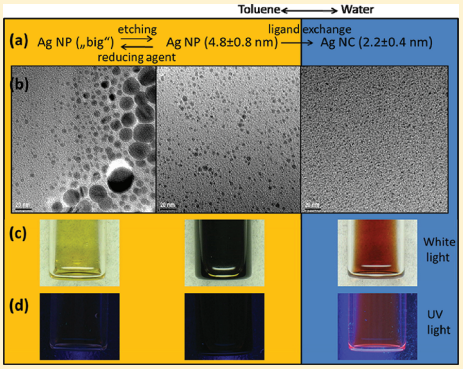

INTRODUCTION

Recently, it has been demonstrated by a variety of groups that gold nanoclusters (NCs) are fluorescent.[1−7] Though colloidal gold nanoparticles (NPs) have been in use over decades of time,[8,9] this feature has been only popularized recently. While fluorescence of bigger gold NPs (bigger than ≈5 nm) is at maximum very low, smaller gold NPs (smaller than ≈3 nm), which are also often termed as gold NCs, show a remarkable fluorescence with quantum yields (QY) up to a few percent (diameter, QY: 2 nm, 3.5%; ≤1 nm, 5%; ≤1 nm, 3.7%;[10] 0.92 nm, 0.07%;[11] 2 nm, 2%;[12] 1.4 nm, 0.6%;[13] 1.8 nm, 8%.[14]) This fact is interesting in two directions. First, the possibility of having well-defined Au NCs allows for detailed investigation of their photophysical properties and thus it is an interesting model system for investigating size-dependent optical properties of materials. In this way, besides colloidal quantum dots,[15−19] also Au NCs show size-dependent fluorescence, that is, effects on downscaling materials from bulk to nanometer dimensions, though the photophysical mechanisms are different. Second, due to their small size, Au NCs are potentially useful for labeling of biological structures.[2,5,11,12] Compared to semiconductor NPs (quantum dots), their lower quantum yield is compensated by the fact that they do not contain any intrinsically toxic material, as, for example, cadmium. Thus, Au NCs could be used for labeling of small biological structures which they are still able to penetrate, such as, for example, the synaptic cleft.

Though in the last years several reports have been published around fluorescent Au NCs, studies for similar Ag NCs are still scarce.[20−31] Silver is another noble metal, which similar to gold exhibits plasmonic properties on the nanometer scale. Next to Au NPs, Ag NPs are the most studied system of colloidal metal NPs. Initially, interest in Au NPs mainly arose from their high electron density, which has been used for immunostaining with Au NPs as marker for transmission electron based imaging.[32] Later on, the plasmonic properties of Au NPs have been widely used for colorimetric detection of biological molecules.[33,34] In contrast, Ag NPs have been initially considered because of their antibacterial activity.[35−42] Different pathways about the cytotoxicity of Ag NPs have been observed.[43−46] It is generally believed that release of Ag^+ from the Ag NPs surface upon corrosion[47] is a major source for cytotoxicity, though it is still under discussion if Ag NPs are more or less toxic compared to an equivalent amount of Ag^+ ions.[45,48]

Similarity between Au and Ag NPs motivated us to transfer a recent synthetic route for fluorescent Au NCs[2] to produce Ag NCs. The synthetic approaches to obtain Ag NCs previously reported follow two major synthetic routes.[49] The stabilization of the Ag NCs can be made using polymers or dendrimers as

Special Issue: Colloidal Nanoplasmonics

Received: January 31, 2012
Revised: March 22, 2012
Published: March 26, 2012

dx.doi.org/10.1021/la300346t | Langmuir 2012, 28, 8915−8919

ligand and/or scaffold,[50] using DNA/oligonucleotides,[51] or proteins[24] for stabilization. Methods using an inorganic scaffold such as zeolites[52,53] have also been reported. The Ag NCs in the current report are not stabilized by one of these methods, but by using small organic molecules. This methodology is scarcely present in the literature,[26] but has the advantage that the Ag NCs are separated because of their electrostatic repulsion. However, the use of small molecules for stabilization usually leads to weaker fluorescence emission in comparison with other molecules such as proteins. All the synthetic methods start from an Ag^+ precursor that must be reduced to Ag^0. This reduction can be done chemically,[23,24,26] or by visible light,[22] UV-light,[54,55] microwaves,[25] or sonochemically.[56] The reduction of the Ag NCs synthesized in this work is done chemically, but by changing the commonly used sodium borohydride ($NaBH_4$) for tetrabutylammonium borohydride (TBAB), which is not such a strong reducing agent such as $NaBH_4$.

Thus, in this work, we want to demonstrate an easy synthesis route for colloidally stable Ag NCs in aqueous solutions. These NCs are fluorescent, though their quantum yield is arguably relatively small.

RESULTS AND DISCUSSION

Recently, a protocol for the synthesis of fluorescent Au NCs has been published by our research group.[2] The same synthetic strategy can be also applied for making Ag NCs. Synthesis started with the reduction of a Ag^+ precursor (AgCl) complexed by didodecyldimethylammonium bromide and decanoic acid, dissolved in toluene to Ag^0 by addition of tetrabutylammonium borohydride as reducing agent. Reduction leads to the formation of Ag NPs capped with didodecyldimethylammonium bromide and decanoic acid dissolved in toluene.[57] These Ag NPs displayed the typical surface plasmon peak around 430 nm. The inorganic Ag core diameters (i.e., the NP diameters without organic ligand capping) had a broad size distribution as determined by transmission electron microscopy (TEM), though many NPs had diameters around 4 nm (cf. Figure 1 and the Supporting Information). The size distribution was improved by further dropwise addition of Ag^+ precursor solution. Hereby, the bigger NPs were etched to smaller sizes. Narrowing of the size distribution was monitored by the increased intensity of the surface plasmon peak (cf. Supporting Information), which finally led to a mean Ag NP diameter of 4.8 ± 0.8 nm. In a subsequent step, phase transfer to aqueous solution was performed. The Ag NPs dissolved in toluene were precipitated by the addition of freshly prepared lipoic acid and didodecyldimethylammonium bromide, followed by heating and UV-light exposure. Following several purification steps, the precipitate was dissolved in aqueous solution (SBB9, 50 mM sodium borate buffer, pH 9). The phase transfer step led to two important changes. First, the size of the Au NPs was further decreased, leading to Ag NCs with an average Ag core diameter (as determined with TEM) of 2.2 ± 0.4 nm (cf. Figure 1 and the Supporting Information). High-resolution TEM (HR-TEM) using fast Fourier transform (FFT) experiments was carried out (cf. Figure 2). In the FFT image, one can observe two distinct rings which can be attributed to two main diffracting planes, the {111} and the {002} planes of Ag, which theoretically appear at 4.319 and 4.988 nm^{-1} respectively. The theoretical position of the Ag diffraction is indicated as red half rings. Possible byproducts such as silver chloride (AgCl) and silver oxide (Ag_2O) do not show any diffraction in this range;

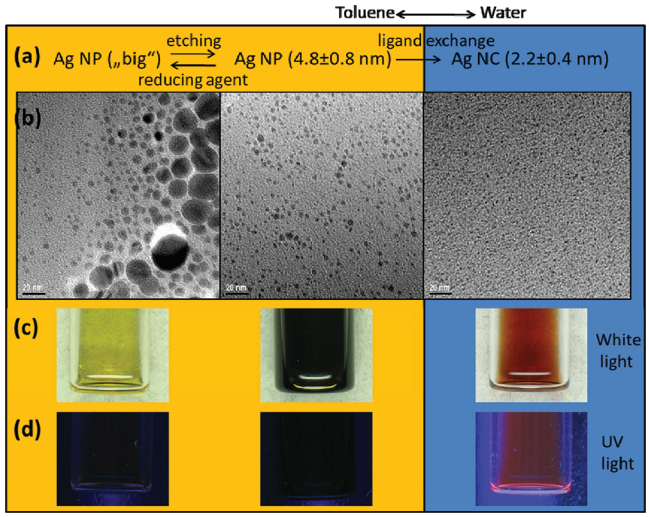

Figure 1. (a) General procedure for the synthesis of Ag nanoclusters (Ag NCs). Big and not well-defined silver nanoparticles (Ag NPs) stabilized by DDAB were etched to well-defined smaller Ag NP by addition of more silver precursor. The hydrophobic Ag NPs were etched to very small hydrophilic Ag NCs upon ligand exchange with dihydrolipoic acid (DHLA). (b) TEM pictures of the three different NPs/NCs. The diameter of the small Ag NPs was determined to be 4.8 ± 0.8 nm and for the Ag NCs 2.2 ± 0.4 nm. The scale bar correspond to 20 nm. (c) Pictures of the different samples under white light illumination. The big Ag NP solution is yellow up to brown in color, the solution of the small Ag NPs is almost black, and the solution of the Ag NCs shows a red-brown color. (d) Pictures of the same solutions under UV light excitation. The Ag NCs show a red fluorescence, whereas the Ag NPs show no fluorescence.

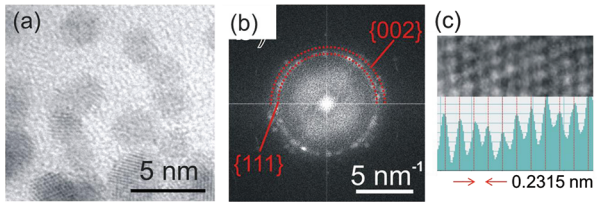

Figure 2. (a) TEM image of several of the Ag nanoclusters. The average diameter of the clusters is between 2 and 3 nm. (b) FFT of the entire image. Two distinct rings can be observed in the FFT, which can be attributed to two main diffracting planes, the {111} and the {002} planes of Ag, which are theoretically at 4.319 and 4.988 nm^{-1}, respectively (red half-rings). (c) High-resolution TEM section of a single NC and corresponding linescan.

hence, it can unambiguously be concluded that the NCs are pure silver. This result is also confirmed examining one single NC, which shows lattice resolution in two directions (cf. Figure 2). The measurement of the lattice spacing from this image shows a regular spacing of planes, with a distance in good agreement with the Ag {111} lattice plane spacing of 0.2315 nm (red dashed lines in the linescan). As well as before, neither AgCl nor Ag_2O has lattice planes in this spacing range, proving the purity of the Ag NCs.[58,59]

The overall hydrodynamic diameter (as determined with dynamic light scattering, cf. the Supporting Information) was 2.7 nm. This demonstrates the presence of lipoic acid on the surface of the Ag NCs, leading to a negative zeta potential of −30 ± 2 mV. Due to this negative charge, the Ag NCs are well dispersed in aqueous solution. Most important, their high colloidal stability allowed for vigorous purification by gel

dx.doi.org/10.1021/la300346t | Langmuir 2012, 28, 8915−8919

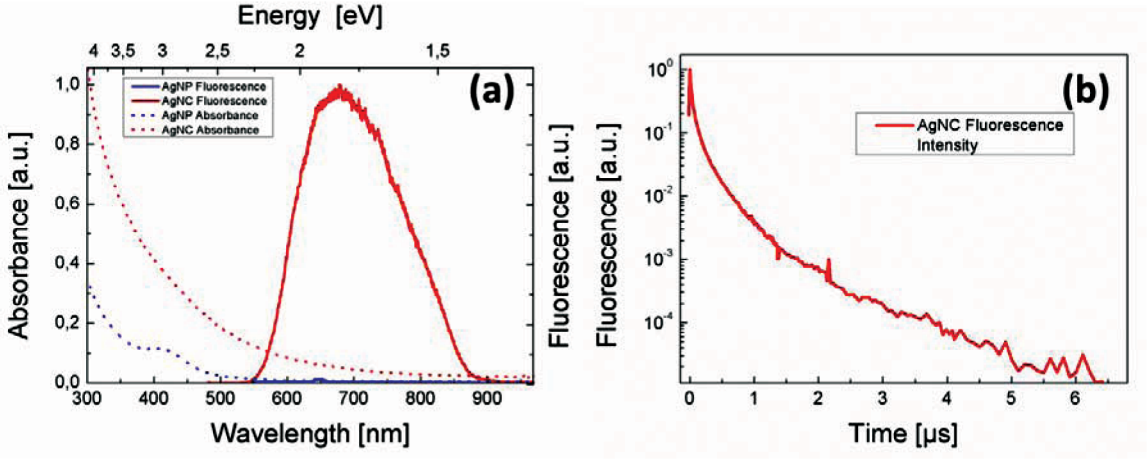

Figure 3. (a) Absorbance (dotted lines) and fluorescence (full lines) spectra of silver nanoparticles (Ag NP) and silver nanoclusters (Ag NC). (b) Transient of the Ag NC fluorescence.

electrophoresis and size exclusion chromatography. These methods warrant for highly purified samples, in which only the Ag NCs but no excess precursors, excess ligands, or intermediated reaction products are present.[60] As second effect, upon phase transfer and capping with lipoic acid, the Ag NCs became fluorescent. It is important to note that fluorescence originating from other compounds in solution but the Ag NCs (such as from not removed precursors) can be excluded due to the vigorous purification.

The fluorescence of the Ag NCs is in the red spectral range, with a broad maximum centered around 680 nm (cf. Figure 3). The quantum yield of the Ag NCs was calculated by the method described by Lakowicz[61] and was determined to be 0.024% (cf. the Supporting Information). Despite this very small value, the fluorescence was clearly above the signal-to-noise-ratio and was even clearly visible by the naked eye. It should be mentioned that, with highly sensitive detectors also for the larger Ag NPs secondary photons, for example, scattered photons can be detected. A comparison is depicted in Figure 3a. It is obvious that the measured intensity of the NCs (which is due to fluorescence) is orders of magnitude stronger. In Figure 3a also the absorption spectra of the NPs and NCs (dotted lines) are depicted. For the NPs, a distinct absorption band can be seen at about 415 nm, which is caused by the surface plasmon of the NPs. This plasmon absorption band is not detectable for the Ag NCs. Such damping of the plasmon absorption with respective weak and broadened absorption is typical for NC sizes around 2 nm.[62,63] Eventually, the question rises from which physical mechanism the fluorescence may occur. It is known that for metal NPs quantum size effects are observable if the diameter is below 2 nm and the NC is made up of just a few atoms.[1,64] For a gold NC of 28 atoms, an intersubband splitting of about 1.7 eV was found.[65] To reveal the physical origin of the red band from the Ag NCs, we performed fluorescence decay measurements. The transient of the red fluorescence is depicted in Figure 3b. The curve exhibits a strong nonexponential decay with decay times in the microsecond range. Such long lifetimes are typical for transitions with rather weak dipole matrix elements. This corresponds well to the fact, that we did not measure a respective absorption band. We therefore conclude that the luminescence is caused by the spatially indirect charge transfer excitons with the electron in the organic shell and the hole in the Ag NC. The conduction band level splitting and shift is obviously large enough to enable a quick transfer of the excited electrons from the NC to the organic shell, namely, the lipoic acid at the surface of the Ag NCs. Only in case of a spatially type II level alignment such electron transfer can compete with intercluster relaxation. It is important to note that Ag NCs and lipoic acid independently and well separated did not show any fluorescence.

It clearly has to be stated that the quantum yield of the Ag NCs is poor. Nevertheless, we performed cellular labeling experiments (cf. Supporting Information). Signal intensity however turned out to be not enough to clearly spatially resolve location of the Ag NCs. Though certainly this indicates that the use of Ag NCs as prepared in this report for fluorescence labeling of cells is limited, in particular due to intrinsic cytotoxicity and low quantum yield, these NCs still provide interesting features. Due to their small hydrodynamic size, they might penetrate in tissue locations where bigger NPs could not enter. They are a complementary material to Au NCs, and in particular to semiconductor NCs, which may help for multiplexed detection. At any rate, due to their high purity and good size distribution, they allow for detailed photophysical characterization, which will help for further understanding of the consequences of downscaling solid state materials on their optical properties. Thus, in case the quantum yield could be improved in the future (such as it has improved for Au NCs upon progressing synthesis protocols), Ag NCs might become applicable for cellular imaging in the future.

■ CONCLUSIONS

We developed ultrasmall water-soluble fluorescent Ag NCs based on a simple wet chemical synthetic route. These Ag NCs possess high colloidal stability and are fluorescent in the red. The Ag NCs are incorporated by cells via nonspecific pathways, and cytotoxic effects are tolerable.

■ SYNTHESIS AND CHARACTERIZATION

The synthesis of Ag NCs has been derived from a previous protocol for the production of fluorescent Au NCs.[2] All the details can be found in the Supporting Information. In brief, first Ag NPs capped with didodecyldimethylammonium bromide (DDAB) were synthesized in toluene and etched down to a size of 4.8 ± 0.8 nm by adding AgCl precursor. During this process, the typical plasmon absorption peak at 430 nm decreased but was still slightly present (see the Supporting

dx.doi.org/10.1021/la300346t | Langmuir 2012, 28, 8915−8919

Information). The peak got lost during the ligand exchange with freshly prepared dihydrolipoic acid (DHLA). Therefore, lipoic acid was reduced by tetrabutylammoniumborohydride (TBAB) in toluene in a molar ratio of 1:4 and added directly to the Ag NP solution. By adding the DHLA in toluene into the Ag NP solution, the dark brown particles started to agglomerate. This mixture was exposed to 336 nm UV light until the agglomerates stuck to the glass walls. After discarding the toluene, the Ag NCs could be dissolved in basic aqueous solution (pH 9). During this ligand exchange, the Ag NPs were etched down to a size of 2.2 ± 0.4 nm, and by replacing the DDAB by DHLA the resulting Ag NCs became water-soluble. Before using the Ag NCs, they were purified from bigger agglomerates and excess ligands first by gel electrophoresis and afterward by high performance liquid chromatography (HPLC). Additionally, the Ag NCs were characterized by UV−vis absorption, fluorescence spectroscopy, time-resolved photoluminescence (trPL), TEM, and dynamic light scattering (DLS).

■ ASSOCIATED CONTENT

Supporting Information

Synthetic and characterization details. Interaction of silver nanoclusters and cells. This material is available free of charge via the Internet at http://pubs.acs.org.

■ AUTHOR INFORMATION

Corresponding Author

*E-mail: wolfgang.parak@physik.uni-marburg.de (W.J.P.); jose.montenegromartos@physik.uni-marburg.de (J.M.M.M.).

Author Contributions

‖Both authors contributed equally to this study.

Notes

The authors declare no competing financial interest.

■ ACKNOWLEDGMENTS

This project has been funded by BMBF Germany (Project UMSICHT to W.J.P.) and NSC Taiwan (NSC 99-2120-M-038-001 and NSC 99-2911-I-033-003-2)

■ REFERENCES

(1) Zheng, J.; Nicovich, P. R.; Dickson, R. M. Highly Fluorescent Noble-Metal Quantum Dots. *Annu. Rev. Phys. Chem.* **2007**, *58*, 409−431.

(2) Lin, C. A. J.; Yang, T. Y.; Lee, C. H.; Huang, S. H.; Sperling, R. A.; Zanella, M.; Li, J. K.; Shen, J. L.; Wang, H. H.; Yeh, H. I.; Parak, W. J.; Chang, W. H. Synthesis, Characterization, and Bioconjugation of Fluorescent Gold Nanoclusters toward Biological Labeling Applications. *ACS Nano* **2009**, *3*, 395−401.

(3) Jin, R. Quantum sized, thiolate-protected gold nanoclusters. *Nanoscale* **2010**, *2*, 343−362.

(4) Scolari, M.; Mews, A.; Fu, N.; Myalitsin, A.; Assmus, T.; Balasubramanian, K.; Burghard, M.; Kern, K. Surface enhanced Raman scattering of carbon nanotubes decorated by individual fluorescent gold particles. *J. Phys. Chem. C* **2008**, *112*, 391−396.

(5) Wu, X.; He, X.; Wang, K.; Xie, C.; Zhou, B.; Qing, Z. Ultrasmall near-infrared gold nanoclusters for tumor fluorescence imaging in vivo. *Nanoscale* **2010**, *2*, 2244−2249.

(6) Lin, Y. H.; Tseng, W. L. Ultrasensitive sensing of Hg(2+) and CH(3)Hg(+) based on the fluorescence quenching of lysozyme type VI-stabilized gold nanoclusters. *Anal. Chem.* **2010**, *82*, 9194−9200.

(7) Xie, J.; Zheng, Y.; Ying, J. Y. Protein-directed synthesis of highly fluorescent gold nanoclusters. *J. Am. Ceram. Soc.* **2009**, *131*, 888−889.

(8) Whetten, R. L.; Khoury, J. T.; Alvarez, M. M.; Murthy, S.; Vezmar, I.; Wang, Z. L.; Stephens, P. W.; Cleveland, C. L.; Luedtke, W. D.; Landman, U. Nanocrystal gold molecules. *Adv. Mater.* **1996**, *8*, 428−433.

(9) Whetten, R. L.; Shafigullin, M. N.; Khoury, J. T.; Schaaff, T. G.; Vezmar, I.; Alvarez, M. M.; Wilkinson, A. Crystal Structures of Molecular Gold Nanocrystal Arrays. *Acc. Chem. Res.* **1999**, *32*, 397−406.

(10) Kawasaki, H.; Hamaguchi, K.; Osaka, I.; Arakawa, R. ph-Dependent Synthesis of Pepsin-Mediated Gold Nanoclusters with Blue Green and Red Fluorescent Emission. *Adv. Funct. Mater.* **2011**, *21*, 3508−3515.

(11) Liu, C. L.; Wu, H. T.; Hsiao, Y. H.; Lai, C. W.; Shih, C. W.; Peng, Y. K.; Tang, K. C.; Chang, H. W.; Chien, Y. C.; Hsiao, J. K.; Cheng, J. T.; Chou, P. T. Insulin-directed synthesis of fluorescent gold nanoclusters: preservation of insulin bioactivity and versatility in cell imaging. *Angew. Chem., Int. Ed.* **2011**, *50*, 7056−7060.

(12) Wang, H.-H.; Lin, C.-A. J.; Lee, C.-H.; Lin, Y.-C.; Tseng, Y.-M.; Hsieh, C.-L.; Chen, C.-H.; Tsai, C.-H.; Hsieh, C.-T.; Shen, J.-L.; Chan, W.-H.; Chang, W. H.; Yeh, H.-I. Fluorescent Gold Nanoclusters as a Biocompatible Marker for In Vitro and In Vivo Tracking of Endothelial Cells. *ACS Nano* **2011**, *5*, 4337−4344.

(13) Shang, L.; Azadfar, N.; Stockmar, F.; Send, W.; Trouillet, V.; Bruns, M.; Gerthsen, D.; Nienhaus, G. U. One-pot synthesis of near-infrared fluorescent gold clusters for cellular fluorescence lifetime imaging. *Small* **2011**, *7*, 2614−2620.

(14) Liu, H.; Zhang, X.; Wu, X.; Jiang, L.; Burda, C.; Zhu, J. J. Rapid sonochemical synthesis of highly luminescent non-toxic AuNCs and Au@AgNCs and Cu (II) sensing. *Chem. Commun.* **2011**, *47*, 4237−4239.

(15) Katzschmann, R.; Rehfeld, A.; Kranold, R. Optical anomaly of small particles in glasses. *Phys. Status Solidi A* **1977**, *40*, K161.

(16) Spanhel, L.; Haase, M.; Weller, H.; Henglein, A. Photochemistry of Colloidal Semiconductors. 20. Surface Modification and Stability of Strog Luminescing CdS Particles. *J. Am. Chem. Soc.* **1987**, *109*, 5649−5655.

(17) Bawendi, M. G.; Steigerwald, M. L.; Brus, L. E. The quantum mechanics of large semiconductor clusters ("quantum dots"). *Annu. Rev. Phys. Chem.* **1990**, *41*, 477−496.

(18) Ekimov, A. I.; Efros, A. L.; Onushchenko, A. A. Quantum size effect in semiconductor microcrystals. *Solid State Commun.* **1993**, *88*, 947−50.

(19) Alivisatos, A. P. Semiconductor Clusters, Nanocrystals, and Quantum Dots. *Science* **1996**, *271*, 933−937.

(20) Vosch, T.; Antoku, Y.; Hsiang, J.-C.; Richards, C. I.; Gonzalez, J. I.; Dickson, R. M. Strongly emissive individual DNA-encapsulated Ag nanoclusters as single-molecule fluorophores. *Proc. Natl. Acad. Sci. U.S.A.* **2007**, *104*, 12616−12621.

(21) Guo, C.; Irudayaraj, J. Fluorescent Ag Clusters via a Protein-Directed Approach as a Hg(II) Ion Sensor. *Anal. Chem.* **2011**, *83*, 2883−2889.

(22) Diez, I.; Pusa, M.; Kulmala, S.; Jiang, H.; Walther, A.; Goldmann, A. S.; Muller, A. H.; Ikkala, O.; Ras, R. H. Color tunability and electrochemiluminescence of silver nanoclusters. *Angew. Chem., Int. Ed.* **2009**, *48*, 2122−2125.

(23) Li, T.; Zhang, L.; Ai, J.; Dong, S.; Wang, E. Ion-Tuned DNA/Ag Fluorescent Nanoclusters As Versatile Logic Device. *ACS Nano* **2011**, *5*, 6334−6338.

(24) Le Guével, X.; Hötzer, B.; Jung, G.; Hollemeyer, K.; Trouillet, V.; Schneider, M. Formation of Fluorescent Metal (Au, Ag) Nanoclusters Capped in Bovine Serum Albumin Followed by Fluorescence and Spectroscopy. *J. Phys. Chem. C* **2011**, *115*, 10955−10963.

(25) Liu, S.; Lu, F.; Zhu, J. J. Highly fluorescent Ag nanoclusters: microwave-assisted green synthesis and Cr3+ sensing. *Chem. Commun.* **2011**, *47*, 2661−2263.

(26) Adhikari, B.; Banerjee, A. Facile Synthesis of Water-Soluble Fluorescent Silver Nanoclusters and HgII Sensing. *Chem. Mater.* **2010**, *22*, 4364−4371.

(27) Sharma, J.; Yeh, H.-C.; Yoo, H.; Werner, J. H.; Martinez, J. S. A complementary palette of fluorescent silver nanoclusters. *Chem. Commun.* **2010**, *46*, 3280−3282.

(28) Sharma, J.; Yeh, H. C.; Yoo, H.; Werner, J. H.; Martinez, J. S. Silver nanocluster aptamers: in situ generation of intrinsically fluorescent recognition ligands for protein detection. *Chem. Commun.* **2011**, *47*, 2294−2296.
(29) Yeh, H.-C.; Sharma, J.; Han, J. J.; Martinez, J. S.; Werner, J. H. A DNA-Silver Nanocluster Probe That Fluoresces upon Hybridization. *Nano Lett.* **2010**, *10*, 3106−3110.
(30) Yuan, X.; Luo, Z. T.; Zhang, Q. B.; Zhang, X. H.; Zheng, Y. G.; Lee, J. Y.; Xie, J. P. Synthesis of Highly Fluorescent Metal (Ag, Au, Pt, and Cu) Nanoclusters by Electrostatically Induced Reversible Phase Transfer. *ACS Nano* **2011**, *5*, 8800−8808.
(31) Shang, L.; Dong, S.; Nienhaus, G. U. Ultra-small fluorescent metal nanoclusters: Synthesis and biological applications. *Nano Today* **2011**, *6*, 401−418.
(32) Sperling, R. A.; Rivera_Gil, P.; Zhang, F.; Zanella, M.; Parak, W. J. Biological Applications of Gold Nanoparticles. *Chem. Soc. Rev.* **2008**, *37*, 1896−1908.
(33) Leuvering, J. H. W.; Thal, P. J. H. M.; Waart, M. v. d.; Schuurs, A. H. W. M. Sol Particle Agglutination Immunoassay For Human Chorionic-Gonadotropin. *Fresenius' J. Anal. Chem.* **1980**, *301*, 132.
(34) Elghanian, R.; Storhoff, J. J.; Mucic, R. C.; Letsinger, R. L.; Mirkin, C. A. Selective Colorimetric Detection of Polynucleotides Based on the Distance-Dependent Optical Properties of Gold Nanoparticles. *Science* **1997**, *277*, 1078−1081.
(35) Morones, J.; Elechiguerra, J.; Camacho, A.; Holt, K.; Kouri, J.; Ram, J.; Yacaman, M. The bactericidal effect of silver nanoparticles. *Nanotechnology* **2005**, *16*, 2346−2352.
(36) Baker, C.; Pradhan, A.; Pakstis, L.; Pochan, D. J.; Shah, S. I. Synthesis and antibacterial properties of silver nanoparticles. *J. Nanosci. Nanotechnol.* **2005**, *5*, 244−249.
(37) Sondi, I.; Salopek-Sondi, B. Silver nanoparticles as antimicrobial agent: a case study on E. coli as a model for Gram-negative bacteria. *J. Colloid Interface Sci.* **2004**, *275*, 177−182.
(38) Choi, O.; Deng, K. K.; Kim, N. J.; Ross, L. Jr.; Surampalli, R. Y.; Hu, Z. The inhibitory effects of silver nanoparticles, silver ions, and silver chloride colloids on microbial growth. *Water Res.* **2008**, *42*, 3066−3074.
(39) Fu, J.; Ji, J.; Fan, D.; Shen, J. Construction of antibacterial multilayer films containing nanosilver via layer-by-layer assembly of heparin and chitosan-silver ions complex. *J. Biomed. Mater. Res., Part A* **2006**, *79*, 665−674.
(40) Lok, C. N.; Ho, C. M.; Chen, R.; He, Q. Y.; Yu, W. Y.; Sun, H.; Tam, P. K.; Chiu, J. F.; Che, C. M. Proteomic analysis of the mode of antibacterial action of silver nanoparticles. *J. Proteome Res.* **2006**, *5*, 916−924.
(41) Gogoi, S. K.; Gopinath, P.; Paul, A.; Ramesh, A.; Ghosh, S. S.; Chattopadhyay, A. Green fluorescent protein-expressing Escherichia coli as a model system for investigating the antimicrobial activities of silver nanoparticles. *Langmuir* **2006**, *22*, 9322−9328.
(42) Rastogi, S. K.; Rutledge, V. J.; Gibson, C.; Newcombe, D. A.; Branen, J. R.; Branen, A. L. Ag colloids and Ag clusters over EDAPTMS-coated silica nanoparticles: synthesis, characterization, and antibacterial activity against Escherichia coli. *Nanomed. Nanotechnol. Biol. Med.* **2011**, *7*, 305−314.
(43) Tarantola, M.; Schneider, D.; Sunnick, E.; Adam, H.; Pierrat, S.; Rosman, C.; Breus, V.; Sonnichsen, C.; Basche, T.; Wegener, J.; Janshoff, A. Cytotoxicity of Metal and Semiconductor Nanoparticles Indicated by Cellular Micromotility. *ACS Nano* **2009**, *3*, 213−222.
(44) Eom, H.-J.; Choi, J. p38 MAPK Activation, DNA Damage, Cell Cycle Arrest and Apoptosis As Mechanisms of Toxicity of Silver Nanoparticles in Jurkat T Cells. *Environ. Sci. Technol.* **2010**, *44*, 8337−8342.
(45) Piao, M. J.; Kang, K. A.; Lee, I. K.; Kim, H. S.; Kim, S.; Choi, J. Y.; Choi, J.; Hyun, J. W. Silver nanoparticles induce oxidative cell damage in human liver cells through inhibition of reduced glutathione and induction of mitochondria-involved apoptosis. *Toxicol. Lett.* **2011**, *201*, 92−100.
(46) Díaz, B.; Sánchez-Espinel, C.; Arruebo, M.; Faro, J.; de Miguel, E.; Magadán, S.; Yagüe, C.; Fernández-Pacheco, R.; Ibarra, M. R.; Santamaría, J.; González-Fernández, Á. Assessing Methods for Blood Cell Cytotoxic Responses to Inorganic Nanoparticles and Nanoparticle Aggregates. *Small* **2008**, *4*, 2025−2034.
(47) Kittler, S.; Greulich, C.; Diendorf, J.; Koller, M.; Epple, M. Toxicity of Silver Nanoparticles Increases during Storage Because of Slow Dissolution under Release of Silver Ions. *Chem. Mater.* **2010**, *22*, 4548−4554.
(48) Li, P.-W.; Kuo, T.-H.; Chang, J.-H.; Yeh, J.-M.; Chan, W.-H. Induction of cytotoxicity and apoptosis in mouse blastocysts by silver nanoparticles. *Toxicol. Lett.* **2010**, *197*, 82−87.
(49) Diéz, I.; Ras, R. H. A. Fluorescent silver nanoclusters. *Nanoscale* **2011**, *3*, 1963−1970.
(50) Li, G.; Luo, Y.; Lu, W.; Li, J.; Jin, Y.; Guo, S. Dependence of Property of Silver Nanoparticles within Dendrimer-template on Molar Ratios of Ag+ to PAMAM Dendrimers. *Chin. J. Chem.* **2010**, *28*, 633−638.
(51) Gwinn, E. G.; O Neill, P.; Guerrero, A. J.; Bouwmeester, D.; Fygenson, D. K. Sequence-Dependent Fluorescence of DNA-Hosted Silver Nanoclusters. *Adv. Mater.* **2008**, *20*, 279−283.
(52) Cremer, G. D.; Antoku, Y.; Roeffaers, M. B. J.; Sliwa, M.; Noyen, J. V.; Smout, S.; Hofkens, J.; Vos, D. E. D.; Sels, B. F.; Vosch, T. Photoactivation of Silver-Exchanged Zeolite A. *Angew. Chem., Int. Ed.* **2008**, *47*, 2813−2816.
(53) Ozln, G. A.; Hugues, F.; Mattar, S. M.; McIntosh, D. F. Low Nuclearlty Sllver Clusters in Faujasite-Type Zeolites: Optical Spectroscopy, Photochemistry, and Relationship to the Photodlmerization of Alkanes. *J. Phys. Chem.* **1983**, *87*, 3445−3450.
(54) Zhang, H.; Huang, X.; Li, L.; Zhang, G.; Hussain, I.; Li, Z.; Tan, B. Photoreductive synthesis of water-soluble fluorescent metal nanoclusters. *Chem. Commun.* **2012**, *48*, 567−569.
(55) Shang, L.; Dong, S. Facile preparation of water-soluble fluorescent silver nanoclusters using a polyelectrolyte template. *Chem. Commun.* **2008**, 1088−90.
(56) Xu, H.; Suslick, K. S. Sonochemical Synthesis of Highly Fluorescent Ag Nanoclusters. *ACS Nano* **2010**, *6*, 3209−3214.
(57) Jana, N. R.; Peng, X. Single-phase and gram-scale routes toward nearly monodisperse Au and other noble metal nanocrystals. *J. Am. Chem. Soc.* **2003**, *125*, 14280−14281.
(58) Hull, S.; Keen, D. A. Pressure-induced phase transitions in AgCl, AgBr, and AgI. *Phys. Rev. B: Condens. Matter* **1999**, *59*, 750−761.
(59) Niggli, P. The crystal structure of several oxides. *Z. Kristallogr.* **1922**, *57*, 253−299.
(60) Sperling, R. A.; Liedl, T.; Duhr, S.; Kudera, S.; Zanella, M.; Lin, C.-A. J.; Chang, W.; Braun, D.; Parak, W. J. Size determination of (bio-) conjugated water-soluble colloidal nanoparticles - a comparison of different techniques. *J. Phys. Chem. C* **2007**, *111*, 11552−11559.
(61) Lakowicz, J. R. *Principles of Fluorescence Spectroscopy*; 3rd ed.; Springer: New York, 2006; p 954.
(62) Alvarez, M. M.; Khoury, J. T.; Schaaff, T. G.; Shafigullin, M. N.; Vezmar, I.; Whetten, R. L. Optical Absorption Spectra of Nanocrystal Gold Molecules. *J. Phys. Chem. B* **1997**, *101*, 3706−3712.
(63) Schaaff, T. G.; Shafigullin, M. N.; Khoury, J. T.; Vezmar, I.; Whetten, R. L.; Cullen, W. G.; First, P. N. Isolation of Smaller Nanocrystal Au Molecules: Robust Quantum Effects in Optical Spectra. *J. Phys. Chem. B* **1997**, *101*, 7885−7891.
(64) de Heer, W. A. The physics of simple metal Clusters: experimantal aspects and simple models. *Rev. Mod. Phys.* **1993**, *65*, 611−676.
(65) Schaaff, T. G.; Knight, G.; Shafigullin, M. N.; Borkman, R. F.; Whetten, R. L. Isolation and Selected Properties of a 10.4 kDa Gold: Glutathione Cluster Compound. *J. Phys. Chem. B* **1998**, *102*, 10643−10646.

Colloids and Surfaces B: Biointerfaces 102 (2013) 511–518

Contents lists available at SciVerse ScienceDirect

Colloids and Surfaces B: Biointerfaces

journal homepage: www.elsevier.com/locate/colsurfb

Protein-mediated synthesis, pH-induced reversible agglomeration, toxicity and cellular interaction of silver nanoparticles

Sumaira Ashraf[a,c], Azhar Zahoor Abbasi[b], Christian Pfeiffer[b], Syed Zajif Hussain[c], Zafar Mahmood Khalid[a], Pilar Rivera Gil[b], Wolfgang J. Parak[b], Irshad Hussain[c,*]

[a] National Institute for Biotechnology and Genetic Engineering (NIBGE), Jhang road, Faisalabad, Pakistan
[b] Department of Physics and WZMW, Philipps University of Marburg, Marburg, Germany
[c] Department of Chemistry, School of Science & Engineering (SSE), Lahore University of Management Sciences (LUMS), DHA, Lahore Cantt 54792, Pakistan

ARTICLE INFO

Article history:
Received 7 June 2012
Received in revised form
15 September 2012
Accepted 17 September 2012
Available online 25 September 2012

Keywords:
Casein
Silver nanoparticles
Reversible agglomeration
Toxicity
Cellular uptake

ABSTRACT

Casein, a milk protein, is used to produce biotolerable and highly stable silver nanoparticles with a fair control over their size without using any additional reducing agent. These silver nanoparticles undergo reversible agglomeration to form protein–silver nanoparticle composite agglomerates as pH approaches to the isoelectric point of casein protein (p*I* = 4.6). These agglomerates can then easily be re-dispersed in alkaline aqueous media with no obvious change in their optical properties. The nanoparticles can withstand high salt concentration (~0.5 M), and can also be freeze-dried, stored as dry powder and then dispersed in aqueous media whenever required. More interestingly, by controlling the concentration of casein protein and pH, it was also possible to control the self-assembly of silver nanoparticles to produce fairly uniform spherical agglomerates. The nanoparticles and their agglomerates were thoroughly characterized using UV–visible and FTIR spectroscopy, TEM, SEM and DLS, etc. Cytotoxicity of the hybrid materials was examined using a Resazurin based cytotoxicity assay. After determining the LD_{50} using NIH/3T3 fibroblast cells, the cellular interaction of these hybrid nanoparticles was studied to examine the behavior of casein-coated nanoparticles for their potential bio-applications.

1. Introduction

Metal nanoparticles, especially gold and silver, are currently among the most attractive nanomaterials due to their applications in electronics [1], photonics [2], optoelectronics [3], sensing [4], catalysis [5,6], antimicrobial products [7,8], pharmaceuticals [9] and therapeutics [10–12]. Currently, the nanosilver-containing products are fairly common in the consumer products due to their relatively low cost and antimicrobial activity against a wide range of bacteria and fungi. For example, silver nanoparticles are being incorporated into clothes, bandages, coatings, and food containers as deodorizers and disinfectants [13,14]. In addition studies have been conducted to explore the use of silver nanoparticles for the disinfection of drinking water and more recently as an insecticide to control the attack of pest on various crops [15].

Most of the above-mentioned applications of silver nanoparticles are due to their size and shape-dependent unique chemical and physical properties [6,16–21]. Several protocols already exist to prepare silver nanoparticles, the reproducible production, stability and control over their size, shape and surface chemistry is still less established compared to gold nanoparticles. This is probably due to easier oxidation of reduced silver and its complex interaction with a variety of currently used stabilizers for such nanomaterials. Therefore, it is still desired to develop more efficient, reproducible, sustainable, environmental friendly and economically viable protocols not only for the production of size and shape-controlled silver nanoparticles but also to achieve a fair control over their surface chemistry for subsequent applications. The common pathways to produce silver nanoparticles include borohydride reduction [22], acrylate/citrate reduction [23–26], polyol process [27,28], microwave irradiation [29–32], the use of plant extracts and vegetable oils [33–38], photoreduction [39], amino acids [30] and vitamins, etc. [40]. However, the synthesis of silver nanoparticles in pure protein system is less explored, and requires exquisite crystal growth control. Recently, a few proteins such as bovine serum albumin (BSA) and lysozyme have been reported to produce subnanometer gold/silver clusters which are fluorescent [41–44]. In those cases, the "surface wrapping" model is considered to play an important role in controlling the formation of these nanomaterials [45]. The formation of metal nanoclusters/nanoparticles in protein system is very complex and depends much on the nature of the amino acids and their sequence, and size, conformation and charge of the protein in the system. A systematic study on the synthesis of silver nanoparticles using various proteins with different

* Corresponding author. Tel.: +92 42 3560 8133; fax: +92 42 3560 8314.
E-mail addresses: ihussain@lums.edu.pk, irshadnibge@gmail.com (I. Hussain).

0927-7765/$ – see front matter © 2012 Elsevier B.V. All rights reserved.
http://dx.doi.org/10.1016/j.colsurfb.2012.09.032

structures is still lacking and, if properly explored, may lead not only to the clues on how to control the shape and size of the resulting nanoparticles, but also contribute to the understanding of the mechanism of the growth process of such nanomaterials.

Casein proteins are the most economical and readily available globular proteins which are major components of milk proteins (~38% of bovine caseins) [46]. These are proline-rich, open-structured rheomorphic proteins (i.e. they assume any one of several energetically favorable conformations in solution), which have distinct hydrophobic and hydrophilic domains [47]. Due to these hydrophobic and hydrophilic domains, casein proteins are naturally self-assembled into casein micelles, which are spherical colloidal particles, 50–500 nm (average 150 nm) in diameter [47]. They comprise about 94% protein and 6% low molecular weight compounds collectively called colloidal calcium phosphate. They are extremely well adapted to their evolutionary tasks of concentrating, stabilizing and delivering calcium, phosphate and protein from the mammalian mother to its neonate. Moreover, the open structure of the caseins, due to their high proline content, makes them readily accessible for proteolytic cleavage. This along with the acid-soluble calcium-phosphate bridging, provides an excellent target-activated release mechanism for unloading the cargo in the stomach. The casein micelle is indeed a remarkable example of a natural nano-vehicle for nutrient delivery. In addition, the supramolecular assembly of casein proteins offers multifunctional properties and is influenced by the change in pH, salt, temperature, and the solvent in which these proteins are dispersed [48–52]. Casein micelles can also be cross-linked chemically to produce thermally responsive proteinaceous nanoparticles [46]. Moreover, casein proteins have many structural properties and functionalities which make them highly suitable as vehicles or as components for the construction of vehicles for delivering various bioactives [47,53,54]. Despite these applications and easy availability, casein proteins have not been much explored to produce metal nanoparticles, which, in addition to being biotolerable, stable, and chemically diverse, may also possess stimuli responsive properties.

Here we report the use of casein proteins to produce biotolerable and highly stable silver nanoparticles with a fair control over their size without using any additional reducing agent. The stable silver particles formed under alkaline conditions undergo reversible agglomeration at acidic pH. pH-induced agglomeration of primary silver nanoparticles can be controlled to produce fairly spherical aggregates. Cytotoxicity of these hybrid materials was examined using a Resazurin based cytotoxicity assay, which is based on mitochondrial activity of the living cells. After determining the LD_{50} (lethal dose toxic to 50% of cells under given experimental conditions) using NIH/3T3 fibroblast cells, the cellular interaction of these hybrid nanoparticles was studied to examine their potential bio-applications.

2. Materials and methods

Casein (molecular weight 75–100 kDa) used in this work was of Hammerstein grade purchased from MP Biomedicals. Tris (hydroxymethyl) amino methane-, phosphate buffers and silver nitrate were purchased from Sigma–Aldrich. All solutions of casein were prepared in 50 mM Tris buffer and pH adjusted using 1 M $NaOH/H_2SO_4$. The Resazurin based toxicology kit, TOX-8, was purchased from Sigma–Aldrich to determine the LD_{50} of the silver nanoparticles. NIH/3T3 fibroblast cells were obtained from LGC Promochem Cell Biology Collection. ATCC complete growth medium, Dulbecco's Modified Eagle's medium, was used for the cultivation of cells. WGA-Alexa from Molecular Probes was used for staining the membranes of the cells while observing them under confocal laser scanning microscope. Ultrapure water with a resistivity of 18.2 MΩ cm was used as the solvent in all preparations.

3. Synthesis of silver nanoparticles

In a typical experiment to prepare silver nanoparticles, a given volume of a warm (50–60 °C) suspension of casein (Ideally, 10 mL, 1%) in Tris-buffer, set at a desired pH (Ideally 13), was added quickly to a boiling aqueous solution of $AgNO_3$ (25 mL, 1 mM) under vigorous stirring. The color of the reaction mixture gradually changed from colorless to light yellow to yellow to brown depending on the reaction conditions (pH and casein concentration) within 5–10 min. The reflux was continued for one hour to ensure complete reaction resulting in the formation of a brownish silver nanoparticles suspension. The nanoparticle suspension was then filter purified to remove excess casein proteins and other impurities using centrifuge filters (Amicon® Ultra Centrifugal Filters by Millipore Corporation) having a molecular weight cut off value of 100 kDa, and then stored at room temperature for further analysis and use in subsequent experiments.

4. Characterization

Transmission electron microscopy (TEM) of silver nanoparticles was carried out using a high resolution transmission electron microscope (JEOL, JEM-3010) operating at 300 kV. Scanning electron microscopy (SEM) of casein–silver nanoparticle agglomerates was carried out using a field emission scanning electron microscope (JEOL, JSM-7500F). Nanoparticle specimens for inspection by transmission electron microscopy were prepared by slow evaporation of one drop of a dilute aqueous solution of the particles on a carbon coated copper mesh grid. Image J software was used to calculate the particle size distribution from transmission electron micrographs. For analysis by field emission scanning electron microscopy the samples of casein–silver nanoparticle agglomerates were loaded onto copper stubs, without further conductive coating. The particle size distribution and surface potential of nanoparticles was determined using a Zetasizer Nano ZS (Malvern Instruments). The surface chemistry of silver nanoparticles was investigated with a Bruker Alpha-P FTIR with a diamond ATR attachment. UV–visible spectra of silver nanoparticles suspension were recorded using an Agilent 8453 UV–visible spectrophotometer. The approximate concentration of silver nanoparticles was determined using a fast sequential atomic absorption spectrometer (AA240FS) by VARIAN.

5. Determination of the LD_{50} of silver nanoparticles

A Resazurin based cytotoxicity assay, based on mitochondrial activity of the living cells, was performed to determine the LD_{50} of the silver nanoparticles. For this purpose NIH/3T3 fibroblast cells were seeded in a 96 well plate (15,000 cells/well) in 100 μL of growth medium and incubated at 37 °C with a constant supply of CO_2 at 5% for 24 h. After 24 h the cells were washed with PBS buffer and incubated, in triplicate, in growth media containing varying concentrations of silver nanoparticles (serial dilution of silver nanoparticles was used to examine the cytotoxicity effect of a broad range of nanoparticles, i.e. $1.25–2.04 \times 10^{-9}$ μg/mL from maximum to minimum concentrations, respectively) and a positive control containing no silver nanoparticles. After 24 h of incubation of the cells with silver nanoparticles (as used in experiments), growth media was aspirated, the cells were washed with PBS buffer and finally 100 μL of 10% Resazurin solution in growth media was added into each well. Resazurin solution alone was added in the last 3 wells which served as a negative control and the assay plate was incubated for 3 h under the same conditions as described above. After 3 h of incubation, the fluorescence of each well of the assay plate was measured using an excitation wavelength of 560 nm and the emission spectra were recorded from 572 to 650 nm.

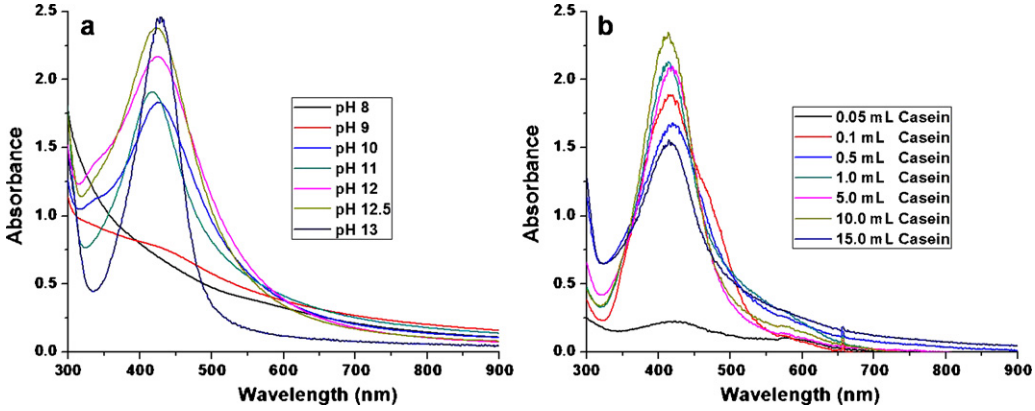

Fig. 1. UV–visible absorption spectra showing the effect of pH (a) and concentration of casein (b) on the formation of silver nanoparticles.

Fluorescence detection was performed with a fluorescence spectrometer, a Fluorolog®-3 spectrofluorometer with FluorEscence™ by HORIBA JOBIN YVON. For plate reading a Micromax 384 microwell-plate reader compatible with FluoroMax® and Fluorolog® was used. For plotting a non-linear curve derived from the fluorescence intensity measurements, a mean of the maximum fluorescence value for each concentration was used (as each concentration of silver nanoparticles was used in triplicate) and calculated their standard deviation. The LD_{50} of silver nanoparticles was then calculated from the sigmoidal curve (logistic dose response fit) by plotting the concentrations of silver nanoparticles against their normalized fluorescence intensity values.

6. Cellular uptake of silver nanoparticles

After determining the LD_{50} of silver nanoparticles, their cellular uptake by NIH/3T3 fibroblast cells was examined. For this purpose cells were grown at a density of 25,000 cells per well on an ibidi cell culture plate (http://www.ibidi.com/) having 8 wells. After one day, when it was confirmed that all cells have properly been attached to the surface/bottom of the plate wells, the growth media was removed, the cells washed with PBS and then incubated with silver nanoparticles using a concentration (0.025 μg/mL) lower than the LD_{50} value (0.314 ± 0.073 μg/mL). Some wells were left without adding silver nanoparticles to serve as control for the experiment. The period of incubation with silver nanoparticles was varied from 24 h to 48 h depending upon the experiment. After incubation with silver nanoparticles, the cells were washed with PBS and their cellular/nuclear membranes were stained with WGA-Alexa 594. A CLSM 5 PASCAL confocal laser scanning microscope (Carl Zeiss) was used for live cellular imaging using the zeta scanning/stacking option. Samples were observed through a 100x/1.45 NA oil-immersion PLAN-FLUOR objective. Excitation wavelengths of 488 nm (Ar/Kr laser) and 543 nm (He/Ne laser) were used to measure the reflectance signal from silver nanoparticles in the range of 470–500 nm and the fluorescence from WGA-Alexa labeled cellular membranes respectively.

7. Results and discussion

Various proteins have previously been used to functionalize metal nanoparticles to generate specific interaction of nanoparticles with anti-proteins. In most of the cases, protein functionalization of metal nanoparticles was either achieved by electrostatic and non-specific adsorption of proteins or by covalent interaction through cysteine residues or by conjugating the proteins by the formation of amide bonds between the proteins and already bound organic molecules at the nanoparticle's surface. Once the proteins are on the nanoparticle surface, protein chemistry can then be exploited to use the nanoparticles for a variety of bio-applications. In order to produce biocompatible metal nanoparticles, we have explored the potential of casein proteins to produce silver nanoparticles, observed the influence of pH-driven assembly of casein molecules on nanoparticles agglomeration, evaluated their cytotoxicity and finally examined their uptake by living cells.

Casein proteins are known to form micelles in the pH ranges from 2 to 3 and 5.5 to 12 [52]. The casein molecules in these micelles are held together by calcium ions and hydrophobic interactions rendering their surface hydrophilic in polar solvents [55,56]. Due to significant effect of pH on casein micelles structure, we initially investigated the effect of pH on the formation of the silver nanoparticles. For this purpose, the effect of pH on nanoparticle formation was examined beyond pH 8, because casein proteins form fairly clear suspension in Tris-buffer in this pH range (For optical images of silver nanoparticles formed at pH 10–14, see the Supporting Information Fig. S1). Though particle formation can be observed at pH 9, their yield and monodispersity increases with an increase in pH up to 13 as was evident from the surface Plasmon resonance (SPR) band of these nanoparticles. The SPR band, which is due to collective oscillation of electrons at the nanoparticle surface, is a characteristic of silver nanoparticles. It becomes more intense and narrower as the pH increases from 9 to 13 (Fig. 1a) indicating a higher yield and narrower dispersion of nanoparticles, respectively. We assume that tyrosine and histidine residues of casein may be responsible for the reduction of ionic silver (Ag^+) to zerovalent silver. The reduction potential of several carboxyl group containing molecules is already known to be improved at higher pH, and that is why the most of the hydrosols of gold and silver are produced using sodium salts of carboxylic acids. The optimum pH for the formation of fairly uniform silver nanoparticles was found to be 13 and all the nanoparticles for further characterization and applications were produced at this pH.

After optimizing the pH, the effect of concentration of casein on the formation of silver nanoparticles was explored by adding 0.02–15 mL of 1% casein suspension in Tris-buffer to 25 mL of silver salt solution (for optical images of silver nanoparticle suspensions formed by using different casein concentrations, see the Supporting Information, Fig. S2). No particle formation was observed when the amount of casein suspension was less than 0.05 mL/25 mL of silver salt solution. The SPR band, however, started appearing when the amount of casein suspension was 0.05 mL/25 mL silver salt solution and became more prominent, intense and narrower (Fig. 1b), as the concentration of casein was increased up to 10 mL casein suspension/25 mL of silver salt solution, indicating the formation of higher concentration and fairly uniform silver nanoparticles under these conditions. Further increase in casein concentration resulted

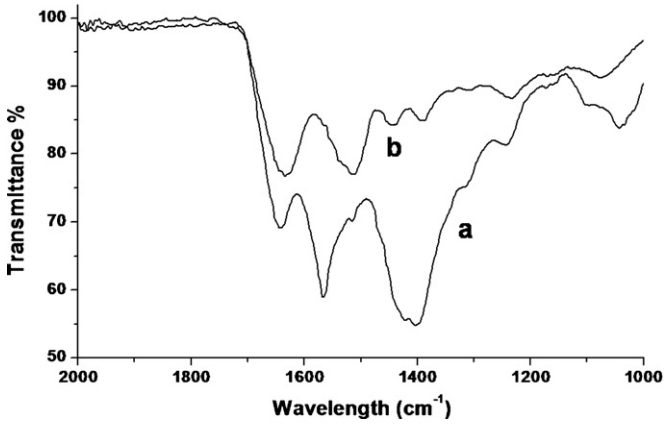

Fig. 2. FTIR spectra of casein (a) and casein stabilized silver nanoparticles (b).

in low yield and polydisperse particles. The fairly uniform nanoparticles, produced at pH 13 and at optimum concentration of casein (10 mL casein suspension/25 mL silver salt solution), are probably due to the formation of fairly uniform micelles of casein in aqueous media under these conditions. Due to the hydrophilic nature of these micelles, the so-formed silver nanoparticles were also soluble in other polar solvents such as methanol, ethanol, tetrahydrofuran, and pyridine, etc. These silver nanoparticles were also found to be highly stable and can be centrifuged and re-dispersed in water for several times and do not show any significant change in SPR band, even upon the addition of 0.5 M sodium chloride solution. This indicates strong interaction of casein with silver nanoparticles, which can prevent them from agglomeration under electrostatic imbalance. These nanoparticles can also be freeze-dried, stored as dry powder and then re-dispersed in aqueous media whenever required.

FTIR spectroscopy is a valuable tool to monitor the secondary structural nature of proteins in various environments [57]. The positions of the amide I (C=O stretch, 1600–1700 cm^{-1}) and the amide II (C—N stretch and N—H deformation, 1530–1560 cm^{-1}) band frequencies can be easily correlated to the structure of proteins. The specific stretching and bending vibrations of the peptide backbone in amide I, II, and III bands provide information about different types of secondary structures such as α-helix, β-sheets, turns, and unordered structures. Of all the amide bands of the peptide group, amide I has proven to be the most sensitive probe of protein secondary structure. FTIR spectra (Fig. 2) of native casein and that bound to the nanoparticle surface show obvious changes in both the shape and the peak position, which suggest the changes in the secondary structure of casein after nanoparticle formation. The appearance of a band at 1644 cm^{-1} in casein indicates the unordered structures of the protein because of the high content of proline residues. However, in case of casein–silver nanoparticle conjugates this band is shifted, indicating a content of α-helix structure. The secondary amide peak, centered at 1514 cm^{-1} in case of native casein, is also shifted in the case of casein stabilized

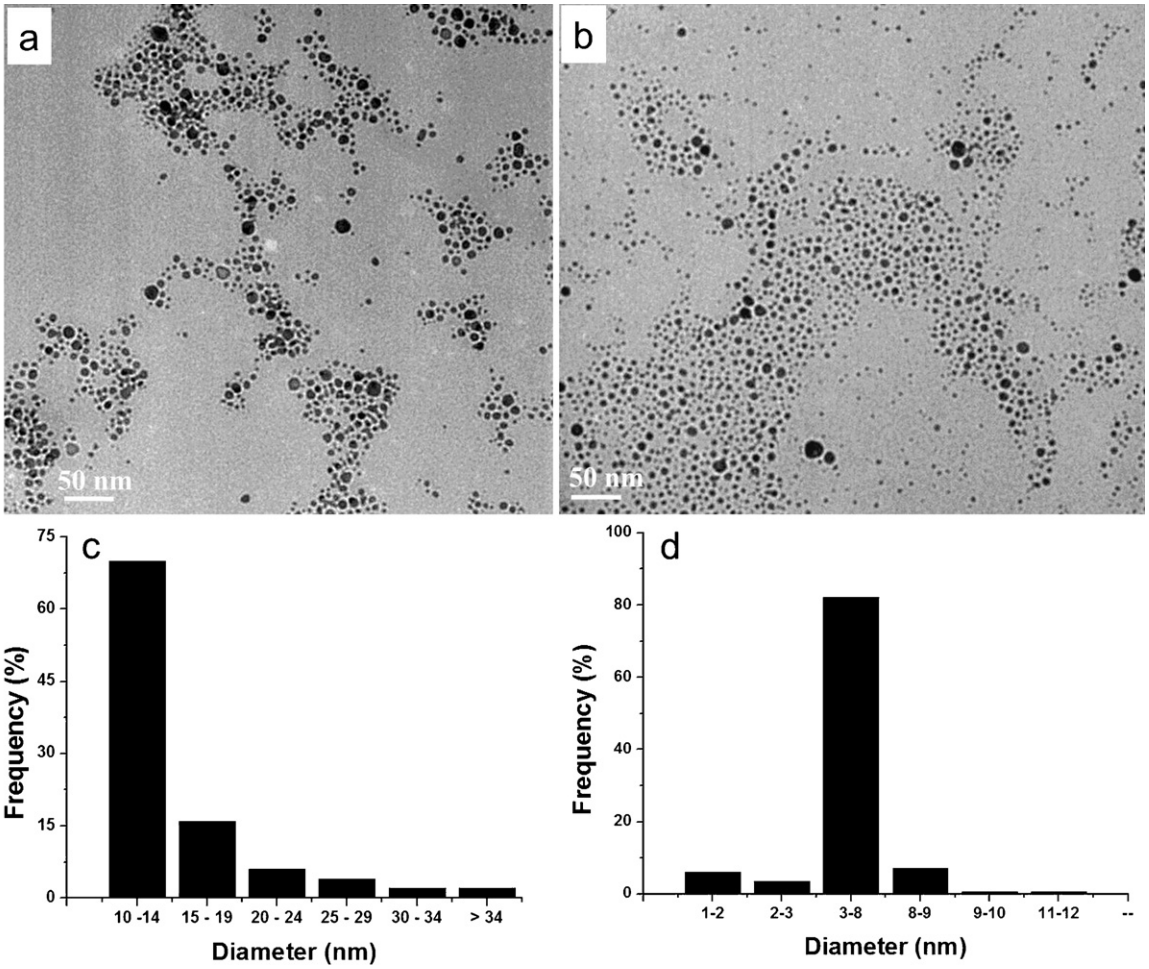

Fig. 3. Transmission electron micrographs of silver nanoparticles formed using 1 mL (a) and 10 mL (b) of 1% casein per 25 mL of $AgNO_3$. Histograms showing size distribution of silver nanoparticles formed using 1 mL (c) and 10 mL (d) of 1% casein per 25 mL of $AgNO_3$ respectively.

silver nanoparticles. This strongly suggests that the lone pair of the electrons present on nitrogen of amide I and II region may have an important role in the formation/stabilization of silver nanoparticles. A band centered at 1445 cm^{-1}, due to the presence of $^{\delta}CH$ of CH_2 group in native protein, also disappeared in casein stabilized silver nanoparticles. From these results it can be inferred that the hydrophobic part and amide functionality of casein is involved in the stabilization of silver nanoparticles, which might be encapsulated in the core of micelles with negatively charged carboxylic exterior under alkaline conditions. This was further confirmed by measuring the zeta potential of these nanoparticles, using the ZetaSizer nano ZS, which was found to be -25 mV (see the Supporting Information, Fig. S3), thus confirming the presence of negatively charged groups extending out from the surface of silver nanoparticles.

In order to analyze the morphology of silver nanoparticles, they were characterized using transmission electron microscopy. The size and size distribution of the nanoparticles was measured using the program Image J while measuring at least 300 particles to get representative data. The transmission electron microscopic analysis data were in close agreement with the information obtained using UV–visible spectroscopy, showing the formation of fairly uniform silver nanoparticles under optimum conditions (i.e. using 10 mL casein suspension/25 mL silver salt solution at pH 13). Transmission electron micrographs (Fig. 3a and b) show that the size of nanoparticles decreases with an increase in the concentration of casein until its optimum concentration, beyond which the polydispersity of nanoparticles increases. Fig. 3c and d show the histograms of nanoparticles produced by using 1 mL and 10 mL of casein suspension respectively. The particles formed by using 1 mL of casein suspension were mostly in the size regime of ca. 10–15 nm and comparatively more polydisperse as compared to those formed by using 10 mL of casein suspension; in that case the majority of the particles were in the size regime of ca. 3–8 nm and fairly uniform in size. These results were also in consistent with the size distribution data obtained while analyzing the hydrodynamic diameter of these nanoparticles using dynamic light scattering (see the Supporting Information, Fig. S4).

Casein is a globular protein and its globular nature becomes more prominent when its pH approaches towards its isoelectric point (p*I* 4.6) at which it has least solubility in aqueous media and thus precipitates out. The agglomeration behavior of casein-stabilized silver nanoparticles was studies by systematically lowering the pH from 13, the pH at which the nanoparticles were formed, to 2, which is well below its p*I*. The nanoparticles remained suspended in aqueous media until pH 8, without any significant change in their UV–visible spectrum, below which the nanoparticle suspensions become slightly cloudy due to agglomeration of nanoparticles as indicated by the broadening and decrease in the intensity of SPR band (Fig. 4). The nanoparticles started precipitating at pH 5.7, as indicated by the intense turbidity of nanoparticles suspension, and were almost completely precipitated at pH 4.8 and thus settled down at the bottom of the container. The agglomeration of silver nanoparticles started at pH 7, got more intense at pH 5.7, and even more intense agglomeration was observed up to pH 2. This agglomeration of nanoparticles is probably due to hydrogen bonding, cation–π interaction and hydrophobic interaction among casein molecules. The agglomeration of nanoparticles was also monitored using UV–visible spectroscopy. Fig. 4 shows a decrease in the intensity and broadening of the SPR band with decrease in pH. The appearance of a shoulder at pH 5 and below shows a clear agglomeration of these nanoparticles. The pH-induced agglomeration of silver nanoparticles was reversible and they can be re-suspended in aqueous media by increasing the pH to 9 and higher. (For optical images of agglomeration and dispersion

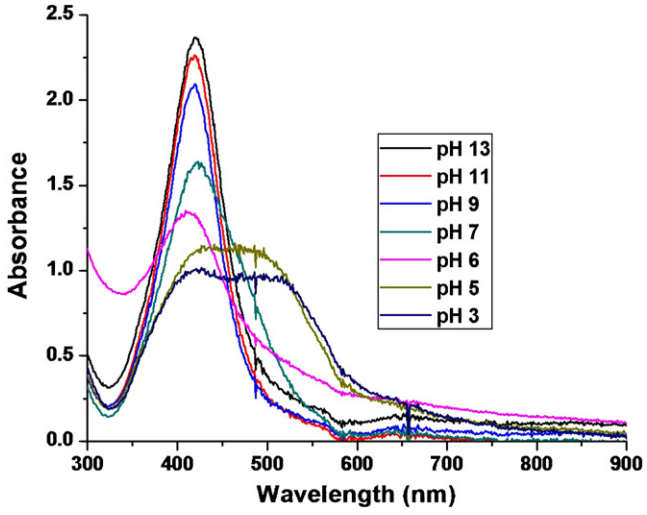

Fig. 4. UV–visible absorption spectra showing the effect of decreasing pH of silver nanoparticles formed under optimum conditions using 10 mL of 1% casein per 25 mL of $AgNO_3$ at pH 13.

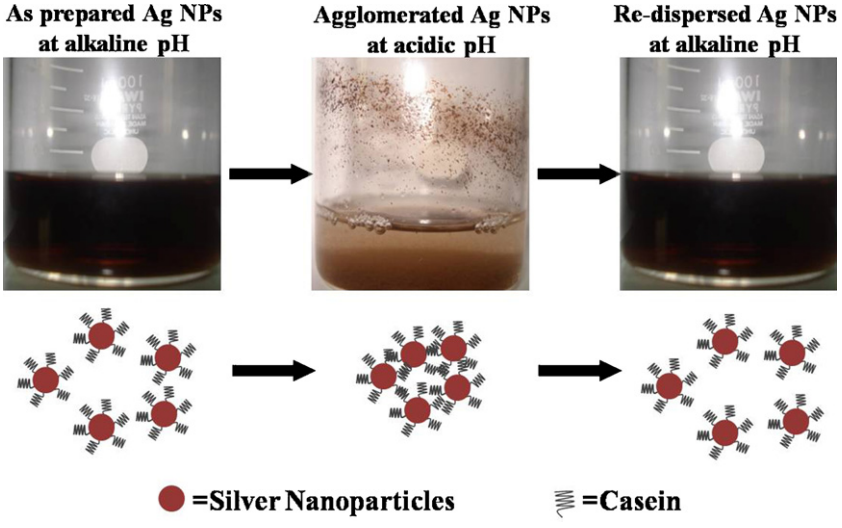

Fig. 5. Scheme showing the pH-induced reversible agglomeration and dispersion of silver nanoparticles.

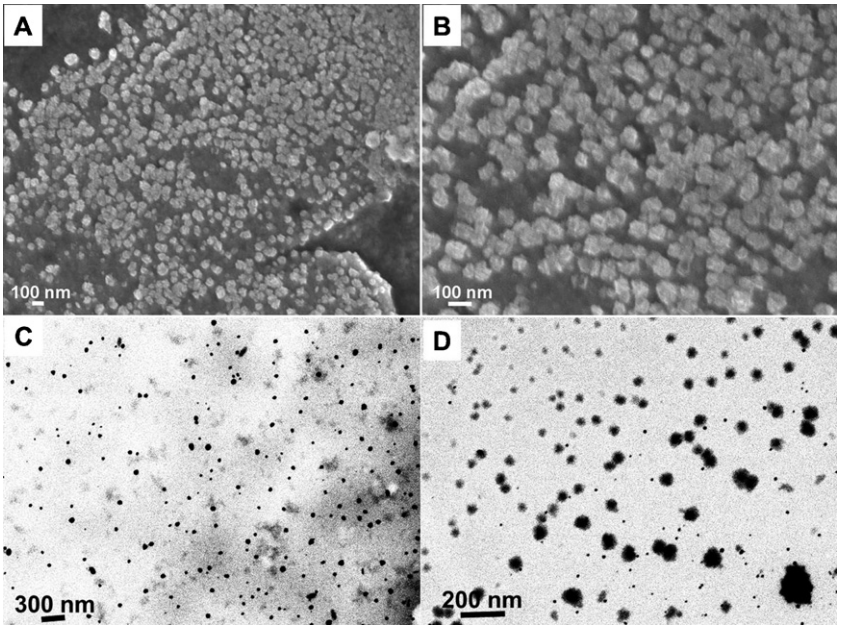

Fig. 6. Scanning (a, b) and transmission (c, d) electron micrographs of spherical agglomerates formed by carefully decreasing the pH to 3.32. These silver nanoparticles were formed using 0.1 mL of 1 % casein per 25 mL of $AgNO_3$.

of silver nanoparticles at different pH, see the Supporting Information, Fig. S5, a schematic description of the process is also given in Fig. 5.) The agglomeration of silver nanoparticles with a decrease in pH was also confirmed by analyzing the selected samples using transmission electron microscopy (see the Supporting Information, Fig. S6-I and S6-II). It was possible to assemble silver nanoparticles using lower concentration of casein (0.1 mL of 1% casein/25 mL of silver salt solution) into fairly uniform and spherical assemblies by lowering the pH down to 3.32 as shown in scanning and transmission electron micrographs in Fig. 6. The average diameter of these spherical agglomerates was 60–80 nm as shown in the histogram prepared by measuring the size of over 200 agglomerates using image J software (see the Supporting Information, Fig. S7). Such assemblies were, however, not formed by the nanoparticles produced using higher concentration of casein. At the isoelectric point of casein, the silver nanoparticles produced at higher concentration of casein were completely agglomerated and can be clearly observed on the assemblies of globular casein as shown in the scanning electron micrographs (see the Supporting Information Fig. S8). All these casein–silver nanoparticle agglomerates can be easily dispersed by increasing the pH beyond 9. Due to pH-induced reversible agglomeration of these nanoparticles, casein-coated nanoparticles may be potentially useful for the controlled delivery and release of drugs. But the known toxicity of silver nanoparticles due to their corrosion/oxidation and subsequent release of silver ions may, however, restrict the use of silver nanoparticles for any such applications [58–60]. Current findings show that casein proteins are bound strongly to the silver nanoparticles, as is evident from their stability against electrostatic imbalance and freeze-drying, and may resist the oxidation/corrosion of silver nanoparticles. Thus more study is certainly required to evaluate the potential and fate of casein-stabilized silver nanoparticles for any such applications.

In order to evaluate the potential of casein-stabilized silver nanoparticles, we conducted a simple experiment to observe the uptake of these nanoparticles by NIH/3T3 fibroblast cells. Before conducting cellular uptake studies, it was important to determine the toxicity and LD_{50} of these nanoparticles under the given experimental conditions (i.e. the time of incubation with nanoparticles, conditions of incubation, etc.). For this purpose, cytotoxicity measurements were performed on the basis of metabolic activity of living cells using a Resazurin based assay [61,62]. For this purpose, the cells were incubated with the nanoparticles for 24 h. Resazurin was then added and samples were analyzed to count viable cells, using a fluorescence spectrophotometer, immediately after 3 h to avoid further conversion of fluorescent resorufin to non-fluorescent hydroresorufin. Silver nanoparticles were tested for their cytotoxicity in the concentration range of $1.25–2.04 \times 10^{-9}$ μg/mL. The LD_{50} of the nanoparticles was then measured from the sigmoidal curve (logistic dose response fit) shown in Fig. 7 and was found to be 0.314 ± 0.073 μg/mL.For all subsequent experiments to study cellular uptake of casein-stabilized silver nanoparticles, the nanoparticles dose was chosen to be 0.025 μg/mL, which was well below their LD_{50} value. In order to prevent potential artifacts associated with cell fixation, the living cells were imaged using CLSM. As shown in the CLSM image in Fig. 8, the silver nanoparticles (red) were found inside the cells after 24 h. The particles were imaged on

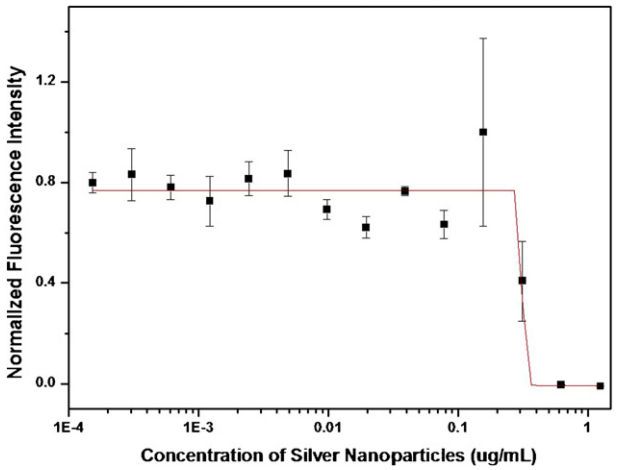

Fig. 7. A graph showing the LD_{50} of casein-stabilized silver nanoparticles measured from a logistic dose response fit in log scale after normalization.

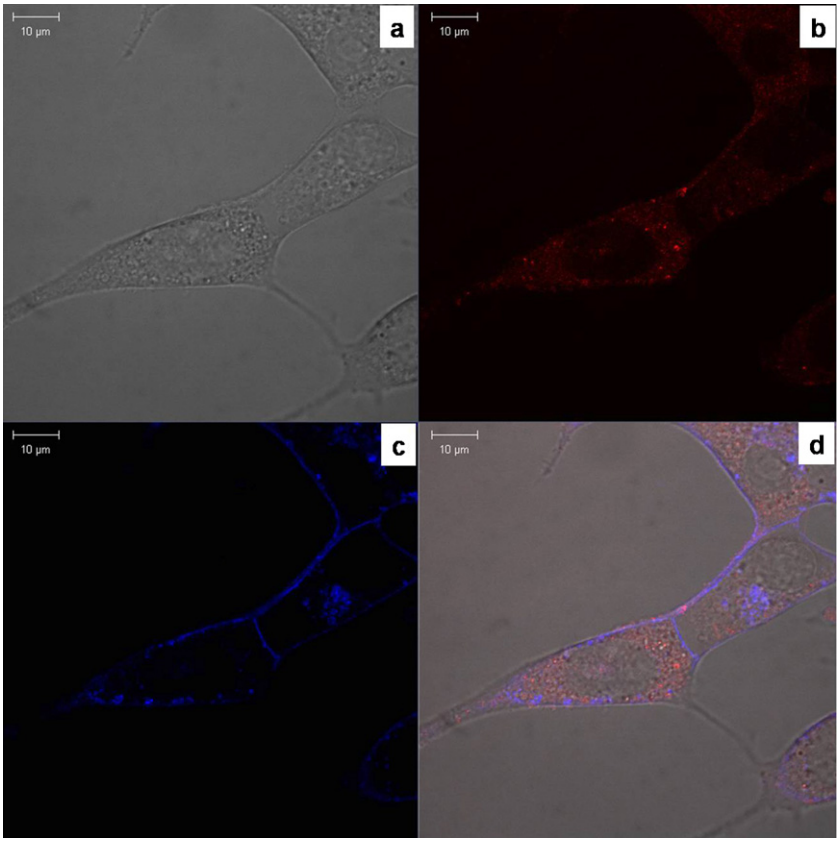

Fig. 8. Confocal laser microscope image showing cellular uptake of silver nanoparticles in the cytoplasm after 24 h based on the reflectance of silver nanoparticles. (a) Transmission channel, (b) red channel (silver nanoparticles), (c) blue channel (membrane stained), and (d) overlay of all three channels. (For interpretation of the references to color in this figure legend, the reader is referred to the web version of the article.)

the basis of their reflectance based on their light scattering properties [63]. These results are in consistent with the previous findings in which casein hollow nano-spheres were found to be accumulated in the cytoplasm of live cells [53]. In order to visualize silver nanoparticles more clearly inside the cells, the cellular and nuclear membranes were stained with WGA-Alexa 594, with blue emission, and imaged after 30 min by illuminating with a He/Ne laser (543 nm). A control experiment was performed to verify that the distribution of silver nanoparticles inside the cells is really based on their reflectance measurements/light scattering properties and not due to imaging artifacts. By means of control experiments in which no nanoparticles were given to the cells and only the membranes of the cells were labeled, only blue colored emission from the labeled cellular membranes was observed without any red light scattering due to silver nanoparticles (see the Supporting Information Fig. S9). The images of the silver nanoparticles inside the cells after 48 h of incubation with cells (see the Supporting Information, Fig. S10) revealed that the particles were fairly distributed inside the cells. We believe that the casein protein at the surface of nanoparticles plays an important role to keep these nanoparticles dispersed in the cytoplasm.

8. Conclusion

The use of casein proteins is demonstrated to produce biotolerable and highly stable silver nanoparticles with a fair control over their size without using any additional reducing agent. The particles were formed by boiling alkaline aqueous solution of casein proteins. Under these conditions, the casein proteins undergo significant structural changes and then self assemble on cooling on nanoparticles surface to produce highly stable silver nanoparticles. The silver nanoparticles undergo reversible agglomeration to form protein–silver nanoparticle composite agglomerates as the pH approaches to the isoelectric point of casein protein (pI = 4.6). By controlling the concentration of casein protein and pH, it was also possible to control the assembly of silver nanoparticles to produce fairly uniform spherical agglomerates. Cytotoxicity and the cellular uptake of these hybrid nanoparticles was also studied to explore their potential bio-applications.

Authors contribution

SA and IH conceived and designed all the experiments. SA performed all experiments. AZA and CF captured TEM micrographs. SZH carried out FTIR analysis. ZMK co-supervised SA along with IH during all studies. PRG guided SA while studying cellular interaction of Casein AgNPs. SA, WJP and IH discussed the interpretation of results. SA and IH co-wrote the draft paper. SA, WJP and IH were involved in all revision process. Correspondence and requests for materials should be addressed to IH.

Acknowledgements

We gratefully acknowledge Higher Education Commission (HEC), Govt. of Pakistan, for financial support to Sumaira Ashraf during her PhD studies. We are also thankful to National Commission on Nanoscience and Technology (NCNST) and Ministry of Science and Technology (MoST), Govt. of Pakistan, for financial support to initiate nano-biotechnology research at NIBGE. IH thanks LUMS School of Science & Engineering (SSE), Lahore, Pakistan for start-up funds to initiate nanomaterials research at LUMS. This project was also partially supported by BMBF Germany (project UMSICHT to

WJP). The authors are also thankful to Saif-ur-Rehman for capturing FESEM images.

Appendix A. Supplementary data

Supplementary data associated with this article can be found, in the online version, at http://dx.doi.org/10.1016/j.colsurfb.2012.09.032.

References

[1] G. Tripathi, J. Am. Chem. Soc. 125 (2003) 1178.
[2] W. Wang, S.A. Asher, J. Am. Chem. Soc. 123 (2001) 12528.
[3] Y. Cui, C.M. Lieber, Science 291 (2001) 851.
[4] A.D. McFarland, R.P. Van Duyne, Nano Lett. 3 (2003) 1057.
[5] N.R. Jana, T.K. Sau, T. Pal, J. Phys. Chem. B 103 (1999) 115.
[6] Z.J. Jiang, C.Y. Liu, L.W. Sun, J. Phys. Chem. B 109 (2005) 1730.
[7] V.K. Sharma, R.A. Yngard, Y. Lin, Adv. Colloid Interface Sci. 145 (2009) 83.
[8] I. Sondi, B. Salopek-Sondi, J. Colloid Interface Sci. 275 (2004) 177.
[9] E. Ülkür, O. Oncul, H. Karagoz, E. Yeniz, B. Celiköz, Burns 31 (2005) 874.
[10] Y. Li, K. Hindi, K.M. Watts, J.B. Taylor, K. Zhang, Z. Li, D.A. Hunstad, C.L. Cannon, W.J. Youngs, K.L. Wooley, Chem. Commun. 46 (2010) 121.
[11] C. Shao, B. Yuan, H. Wang, Q. Zhou, Y. Li, Y. Guan, Z. Deng, J. Mater. Chem. 21 (2011) 2863.
[12] J. Jain, S. Arora, J.M. Rajwade, P. Omray, S. Khandelwal, K.M. Paknikar, Mol. Pharm. 6 (2009) 1388.
[13] T.M. Benn, P. Westerhoff, Environ. Sci. Technol. 42 (2008) 4133.
[14] J. Gensel, T. Borke, N.P. Perez, A. Fery, D.V. Andreava, E. Betthausen, A.H.E. Muller, H. Mohwald, E.V. Skorb, Adv. Mater. 24 (2012) 985.
[15] Q. Li, S. Mahendra, D.Y. Lyon, L. Brunet, M.V. Liga, D. Li, P.J.J. Alvarez, Water Res. 42 (2008) 4591.
[16] F. Kiss, R. Miotto, A. Ferraz, Nanotechnology 22 (2011) 275708.
[17] Y. Yang, S. Matsubara, L.M. Xiong, T. Hayakawa, M. Nogami, J. Phys. Chem. C 111 (2007) 9095.
[18] S. Panigrahi, S. Praharaj, S. Basu, S.K. Ghosh, S. Jana, S. Pande, T. Vo-Dinh, H. Jiang, T. Pal, J. Phys. Chem. B 110 (2006) 13436.
[19] W. Luo, W. Hu, S. Xiao, J. Phys. Chem. C 112 (2008) 2359.
[20] Y.A. Krutyakov, A.A. Kudrinskiy, A.Y. Olenin, G.V. Lisichkin, Russ. Chem. Rev. 77 (2008) 233.
[21] D.D. Evanoff Jr., G. Chumanov, ChemPhysChem 6 (2005) 1221.
[22] Y. Qu, R. Porter, F. Shan, J.D. Carter, T. Guo, Langmuir 22 (2006) 6367.
[23] I. Hussain, M. Brust, A.J. Papworth, A.I. Cooper, Langmuir 19 (2003) 4831.
[24] H. Xia, S. Bai, J. Hartmann, D. Wang, Langmuir 26 (2009) 3585.
[25] G.P. Lee, L.J. Bignell, T.C. Romeo, J.M. Razal, R.L. Shepherd, J. Chen, A.I. Minett, P.C. Innis, G.G. Wallace, Chem. Commun. 46 (2010) 7807.
[26] X. Dong, X. Ji, H. Wu, L. Zhao, J. Li, W. Yang, J. Phys. Chem. C 113 (2009) 6573.
[27] P.Y. Silvert, R. Herrera-Urbina, K. Tekaia-Elhsissen, J. Mater. Chem. 7 (1997) 293.
[28] B. Wiley, T. Herricks, Y. Sun, Y. Xia, Nano Lett. 4 (2004) 1733.
[29] B. Baruwati, V. Polshettiwar, R.S. Varma, Green Chem. 11 (2009) 926.
[30] B. Hu, S.B. Wang, K. Wang, M. Zhang, S.H. Yu, J. Phys. Chem. C 112 (2008) 11169.
[31] F. Gao, Q. Lu, S. Komarneni, Chem. Mater. 17 (2005) 856.
[32] M. Nishioka, M. Miyakawa, H. Kataoka, H. Koda, K. Sato, T.M. Suzuki, Nanoscale 3 (2011) 2621.
[33] A. Kumar, P.K. Vemula, P.M. Ajayan, G. John, Nat. Mater. 7 (2008) 236.
[34] M.N. Nadagouda, R.S. Varma, Green Chem. 10 (2008) 859.
[35] S. Li, Y. Shen, A. Xie, X. Yu, L. Qiu, L. Zhang, Q. Zhang, Green Chem. 9 (2007) 852.
[36] D.M. Ali, N. Thajuddin, K. Jeganathan, M. Gunasekaran, Colloids Surf. B 85 (2011) 360.
[37] S.P. Chandran, M. Chaudhary, R. Pasricha, A. Ahmad, M. Sastry, Biotechnol. Prog. 22 (2006) 577.
[38] C. Krishnaraj, E. Jagan, S. Rajasekar, P. Selvakumar, P. Kalaichelvan, N. Mohan, Colloids Surf. B 76 (2010) 50.
[39] J. Marignier, J. Belloni, M. Delcourt, J. Chevalier, Nature 317 (1985) 344.
[40] M.N. Nadagouda, R.S. Varma, Cryst. Growth Des. 7 (2007) 2582.
[41] C. Guo, J. Irudayaraj, Anal. Chem. 83 (2011) 2883.
[42] H. Wei, Z. Wang, L. Yang, S. Tian, C. Hou, Y. Lu, Analyst 135 (2010) 1406.
[43] J. Xie, Y. Zheng, J.Y. Ying, J. Am. Chem. Soc. 131 (2009) 888.
[44] C.A.J. Lin, T.Y. Yang, C.H. Lee, S.H. Huang, R.A. Sperling, M. Zanella, J.K. Li, J.L. Shen, H.H. Wang, H.I. Yeh, W.J. Parak, W.H. Chang, ACS Nano 3 (2009) 395.
[45] J. Xie, J.Y. Lee, D.I.C. Wang, J. Phys. Chem. C 111 (2007) 10226.
[46] N. Kamiya, Y. Shiotari, M. Tokunaga, H. Matsunaga, H. Yamanouchi, K. Nakano, M. Goto, Chem. Commun. (2009) 5287.
[47] Y.D. Livney, Curr. Opin. Colloid Interface Sci. 15 (2010) 73.
[48] P.X. Qi, E.D. Wickham, H.M. Farrell, Protein J. 23 (2004) 389.
[49] V.N. Uversky, Y. Goto, Curr. Protein Pept. Sci. 10 (2009) 447.
[50] K.M. Alkaabi, A. Yafea, S.S. Ashraf, Appl. Biochem. Biotechnol. 126 (2005) 149.
[51] M. Weijers, P.A. Barneveld, M.A. Cohen Stuart, R.W. Visschers, Protein Sci. 12 (2003) 2693.
[52] Y. Liu, R. Guo, Biophys. Chem. 136 (2008) 67.
[53] C. Liu, W. Yao, L. Zhang, H. Qian, W. Wu, X. Jiang, Chem. Commun. 46 (2010) 7566.
[54] A. Shapira, Y.G. Assaraf, D. Epstein, Y.D. Livney, Pharm. Res. 27 (2010) 2175.
[55] D.G. Dalgleish, P.A. Spagnuolo, H. Douglas Goff, Int. Dairy J. 14 (2004) 1025.
[56] P. Walstra, Int. Dairy J. 9 (1999) 189.
[57] Y. Liu, R. Guo, Mater. Chem. Phys. 126 (2011) 619.
[58] S. Kittler, C. Greulich, J. Gebauer, J. Diendorf, L. Treuel, L. Ruiz, J. Gonzalez-Calbet, M. Vallet-Regi, R. Zellner, M. Köller, J. Mater. Chem. 20 (2009) 512.
[59] P.V. AshaRani, G. Low Kah Mun, M.P. Hande, S. Valiyaveettil, ACS Nano 3 (2009) 279.
[60] S. Shrivastava, T. Bera, S.K. Singh, G. Singh, P. Ramachandrarao, D. Dash, ACS Nano 3 (2009) 1357.
[61] J. O'Brien, I. Wilson, T. Ortaon, F. Pognan, Toxicology 164 (2001) 132.
[62] J. O'Brien, I. Wilson, T. Orton, F. Pognan, Eur. J. Biochem. 267 (2000) 5421.
[63] K. Sokolov, M. Follen, J. Aaron, I. Pavlova, A. Malpica, R. Lotan, R. Richards-Kortum, Cancer Res. 63 (2003) 1999.

Temperature: The "Ignored" Factor at the NanoBio Interface

Morteza Mahmoudi,[†,*] Abuelmagd M. Abdelmonem,[‡,¶] Shahed Behzadi,[†] Joachim H. Clement,[§] Silvio Dutz,[⊥] Mohammad R. Ejtehadi,[∥] Raimo Hartmann,[‡] Karsten Kantner,[‡] Uwe Linne,[‡] Pauline Maffre,[#] Scott Metzler,[△] Mojhgan K. Moghadam,[⊗] Christian Pfeiffer,[‡] Meisam Rezaei,[∥] Pilar Ruiz-Lozano,[△] Vahid Serpooshan,[△] Mohammad A. Shokrgozar,[⊗] G. Ulrich Nienhaus,[∞,#,*] and Wolfgang J. Parak[‡,▽,*]

[†]Nanotechnology Research Center and Department of Nanotechnology, Faculty of Pharmacy, Tehran University of Medical Sciences, Tehran, Iran, [‡]Fachbereich Physik/Chemie, Philipps-Universität Marburg, Marburg, Germany, [§]Department of Hematology/Oncology, University Hospital Jena, Friedrich-Schiller University Jena, Jena, Germany, [⊥]Department Nano Biophotonics, Institute of Photonic Technology, Jena, Germany, [∥]Department of Physics, Sharif University of Technology, Tehran, Iran, [∞]Department of Physics, University of Illinois at Urbana-Champaign, Urbana, Illinois, United States, [#]Institute of Applied Physics and Center for Functional Nanostructures (CFN) and Institute of Toxicology and Genetics (ITG), Karlsruhe Institute of Technology (KIT), Karlsruhe, Germany, [△]Department of Pediatrics, Division of Cardiology, School of Medicine, Stanford University, Stanford, California, United States, [⊗]National Cell Bank, Pasteur Institute of Iran, Tehran, Iran, and [▽]CIC Biomagune, San Sebastian, Spain. [¶]Contributing authors in alphabetic order.

ABSTRACT Upon incorporation of nanoparticles (NPs) into the body, they are exposed to biological fluids, and their interaction with the dissolved biomolecules leads to the formation of the so-called protein corona on the surface of the NPs. The composition of the corona plays a crucial role in the biological fate of the NPs. While the effects of various physicochemical parameters on the composition of the corona have been explored in depth, the role of temperature upon its formation has received much less attention. In this work, we have probed the effect of temperature on the protein composition on the surface of a set of NPs with various surface chemistries and electric charges. Our results indicate that the degree of protein coverage and the composition of the adsorbed proteins on the NPs' surface depend on the temperature at which the protein corona is formed. Also, the uptake of NPs is affected by the temperature. Temperature is, thus, an important parameter that needs to be carefully controlled in quantitative studies of bionano interactions.

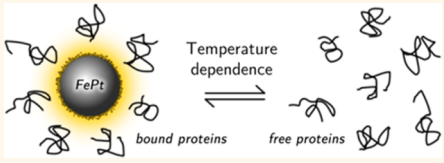

KEYWORDS: colloidal magnetic nanoparticles · protein corona · temperature dependence · uptake by cells · protein adsorption

Nanoparticles (NPs) are presently being employed in a wide variety of biomedical and biotechnological applications. In some applications, such as targeted drug delivery, researchers aim to develop NPs such that they are selectively incorporated by specific cell types in living tissue. In other applications, such as NP-based contrast agents for magnetic resonance imaging, NPs should stay in the bloodstream and subsequently be cleared by the kidneys, but not be internalized by cells. It is known that cellular NP uptake is strongly influenced by the NP size as well as their surface properties, including decoration by functional groups and biomolecules. A detailed understanding of the interactions between NPs and different cell types is key to understanding and controlling cellular uptake mechanisms.[1−4]

NPs entering the human body first come in contact with a biological fluid, *e.g.*, blood or lung-lining fluid. They interact with the dissolved biomacromolecules, in particular proteins, and an adsorption layer of proteins, the so-called "protein corona", forms around the NPs.[5−7] While protein adsorption onto planar surfaces has been investigated for decades, detailed studies of NP−protein interactions have only started recently.[8−13] Studies have especially focused on the effects of physicochemical parameters of NPs (*e.g.*, size, shape, composition, surface roughness, porosity, surface charge) on the formation of the protein corona.[14] The temperature, however, at which the NPs and the protein are maintained in solution likewise should be an important factor influencing the corona composition. For example, it has been shown that the composition of the protein corona formed upon NP exposure to heat-inactivated proteins (preheating at 56 °C) and non-heat-inactivated proteins is different.[15] As a result, significant differences were observed in the amounts of NPs taken up by cells. However, temperature effects close to physiological temperature (*i.e.*, not involving denaturation) on the

* Address correspondence to Mahmoudi-M@TUMS.ac.ir; uli@uiuc.edu; wolfgang.parak@physik.uni-marburg.de.

Received for review November 16, 2012 and accepted June 30, 2013.

Published online July 01, 2013
10.1021/nn305337c

protein corona have not yet been studied in detail. Those effects may be relevant for *in vivo* applications of NPs because body temperature can vary significantly. The mean human body temperature ranges from 35.8 to 37.2 °C and varies for different parts of the body.[16] It decreases during sleep and increases by up to 2 °C during physical activities and can even climb to 41 °C in the case of fever.[17] It is also known that the temperature in peripheral parts of the body (*e.g.*, skin) during exposure to cold weather can drop to 28 °C.[18] Very recently, even the intracellular temperature of living cells was shown to be inhomogeneous.[19,20]

If protein adsorption onto the surface of NPs depends on the body temperature, it may also result in a significant effect on the cellular uptake of NPs *in vivo*. Therefore, we have studied the influence of near-physiological temperature variation on the formation of the protein corona, using superparamagnetic NPs synthesized from different materials with different surface coatings and thus different ζ-potentials as model NPs. Magnetic NPs enable effective magnetic washing and separation, which is beneficial for handling of small amounts of NP sample. Precisely defined and well-characterized polymer-coated FePt NPs were incubated with human serum albumin (HSA) and apo-transferrin (apo-Tf) at different concentrations and temperatures, and the monolayer formation of adsorbed proteins was quantified by using fluorescence correlation spectroscopy (FCS). Moreover, larger FeO_x NPs (superparamagnetic iron oxide NPs, SPIONs) with positive and negative charge and also with neutral surfaces were incubated in fetal bovine serum (FBS) at different temperatures, and the compositions of the resulting coronae were analyzed as a function of the incubation temperature. We have also assessed the effect of the temperature-dependent corona composition on cellular uptake.

RESULTS AND DISCUSSION

Temperature Dependence of HSA and apo-Tf Monolayer Formation on FePt NPs. For our protein adsorption studies we used fluorescently labeled, negatively charged polymer-coated FePt NPs. The inorganic core diameter, d_c, was determined by transmission electron microscopy (TEM). The hydrodynamic diameter, d_h, was measured by dynamic light scattering (DLS, *cf.* Table 1) and fluorescence correlation spectroscopy (FCS, *cf.* Table 2) at room temperature in phosphate-buffered saline (PBS). Results obtained with the FCS method (d_h = 12.0 ± 0.2 nm and 10 ± 0.4 nm for two different batches at room temperature) are very precise and reproducible and have been verified in several independent studies.[21−24] The DLS data on bare NPs without proteins (d_h = 10 ± 5 nm) are—within experimental error—in agreement with the FCS data but have larger margins of error.[21,24] Furthermore, the FCS data (*cf.* Table 2) indicate that temperature variation between 9 and 43 °C does not affect the hydrodynamic diameter of the bare FePt NPs. Thus, the polymer surface of these NPs can be considered to be stable in this temperature range. In a previous study, we also demonstrated that the polymer shell of the NPs dissolved in PBS remains stable over time.[14]

TABLE 1. Core (d_c) and Hydrodynamic (d_h) Diameters of NPs As Determined with TEM and DLS (at room temperature in PBS)

NP material	charge	d_c [nm]	d_h [nm]
FePt	Negative	3.5 ± 0.6	10 ± 5
FeO_x	Negative	15 ± 5	33 ± 8
FeO_x	Neutral	22 ± 7	33 ± 10
FeO_x	Positive	17 ± 5	79 ± 7

TABLE 2. Temperature-Dependent Protein Adsorption onto FePt NPs As Derived from FCS Measurements in PBS[a]

	HSA				
T [°C]	$r_h(0)$ [nm]	$r_h(N_{max})$ [nm]	K'_D [μM]	n	N_{max}
13	5.5 ± 0.3	9.2 ± 0.4	10 ± 4	0.6 ± 0.1	31 ± 5
23	6.0 ± 0.1	9.3 ± 0.2	6.3 ± 2.2	0.9 ± 0.2	30 ± 3
43	6.0 ± 0.1	8.8 ± 0.2	0.8 ± 0.4	0.7 ± 0.2	23 ± 2
	Apo-Tf				
T [°C]	$r_h(0)$ [nm]	$r_h(N_{max})$ [nm]	K'_D [μM]	n	N_{max}
9	5.1 ± 0.2	15.1 ± 0.8	13 ± 4	0.6 ± 0.1	47 ± 7
22	5.0 ± 0.2	14.3 ± 0.7	16 ± 6	0.7 ± 0.1	40 ± 6
43	5.3 ± 0.1	11 ± 0.4	5 ± 1	0.7 ± 0.1	17 ± 2

[a] $r_h(0)$ and $r_h(N_{max})$ are the hydrodynamic radii of NPs without adsorbed proteins and upon saturation of the NP surface with proteins, respectively; n is the Hill coefficient, which controls the steepness of the binding curve, N_{max} is the maximum number of proteins adsorbing onto a single NP, and K'_D represents the concentration of protein molecules at half coverage. Data for two different proteins are shown, HSA and apo-Tf.

Protein adsorption was quantified in terms of changes in hydrodynamic radius, $r_h = d_h/2$, of the NPs by using FCS. We studied the adsorption of HSA and apo-Tf, two important serum proteins, onto polymer-coated FePt NPs. Please note that, due to the small size of the NPs and due to the thin protein shell (which provides only little contrast), TEM turned out not to be the method of choice for the analysis of the protein corona (*cf.* Supporting Information). FCS analysis was performed directly on NP solutions with varying protein concentrations. Because the fluorescent labels reside in the polymer shell of the FePt NPs and not on the proteins, there was no need for purification steps to remove unbound proteins, which may introduce errors in the quantitative assessment of protein−NP interactions. Thus, FCS measurements allow for the direct analysis of the proteins forming the protein corona *in situ*. Because the surface of our polymer-coated FePt NPs is homogeneous, a spherical shape will be maintained under saturating conditions, *i.e.*, when the whole NP surface is covered with protein. In the other limit, *i.e.*, upon binding of only one or two

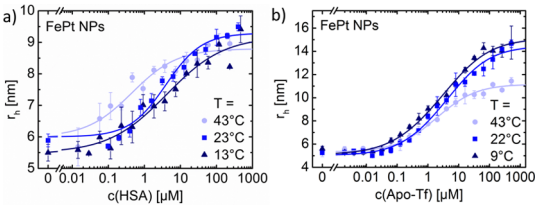

Figure 1. Change of the hydrodynamic radius, r_h, of negatively charged FePt NPs as a function of (a) HSA and (b) apo-Tf concentration in the solution due to protein adsorption at different temperatures *T*.

protein molecules per NP, the resulting shape is aspherical. However, FCS is not sensitive to small deviations from a spherical shape. In fact, in the analysis, we have made the approximation that the shape of the NPs remains spherical upon protein binding.

In accordance with our previous study[21] at room temperature HSA adsorption increases with protein concentration in the solution up to the formation of a protein monolayer, as we have observed *in situ* by using FCS. In Figure 1a, we show HSA monolayer formation for a set of three temperatures (13, 23, 43 °C), as inferred from (i) the observed saturation behavior, *i.e.*, the NP size does not continue to increase beyond a certain HSA concentration, and (ii) the increase in NP size due to HSA binding, which corresponds to the physical size of the HSA molecules. The structure of HSA can be modeled as a 3 nm thick equilateral triangle with sides that are 8 nm long. At 13 and 23 °C the thickness of the protein corona is in agreement with our previous results taken at room temperature, $r_h \approx 3.3$ nm.[21,24] The measured protein corona thickness of 3.3 nm indicates that the HSA molecules adsorb with their triangular surface facing the NPs, supposedly *via* the big, positively charged patch on the surface of one of the two triangular faces, which binds to the negatively charged NPs *via* Coulomb interactions.[24] At 43 °C, the radius increase upon HSA binding is slightly smaller, which may result from an enhanced flexibility of the polymer shell wrapping the FePt core of the NPs at higher temperature, so that the adsorbed HSA proteins may partially penetrate the shell, leading to an overall radius increase just slightly below 3.3 nm. Most remarkable, however, is the finding that the binding affinity displays a marked temperature dependence, as seen from the values of K'_D, the concentration at half coverage (Table 2). Surprisingly, K'_D decreases with temperature, so the highest protein binding affinity is found at the highest temperature. Usually, one would expect that a system tends to dissociate into its individual components at higher temperature so as to increase the overall translational entropy. The observed stronger binding of HSA to the NPs at 43 °C, however, may arise from structural fluctuations of the proteins and/or the polymer shell around the NPs, which will be enhanced at higher temperature. These could induce structural changes that lead to a free energy-optimized binding interface.

We also note that the maximum number, N_{max}, of HSA molecules per NP appears to decrease at 43 °C (Table 2). The N_{max} values, however, should be taken with a grain of salt. They are based on a geometrical model that assumes (1) that the NPs have a smooth spherical surface and (2) that the added volume due to protein adsorption, which we infer from the change in r_h, is homogeneously filled with protein. At 43 °C, N_{max} will be underestimated if HSA molecules partially enter the polymer shell, as we expect from the smaller thickness of the protein corona. At 23 or 13 °C, N_{max} may be overestimated if the monolayer formed is not completely densely packed.

The binding of apo-Tf onto the FePt NPs was studied at 9, 22, and 43 °C (*cf.* Figure 1b). The data indicate formation of a monolayer of apo-Tf around each NP under saturating conditions.[22] As for HSA, the affinity of apo-Tf toward the FePt NPs is greater at 43 °C than at room temperature, as indicated by the smaller ligand concentration producing half occupation K'_D at 43 °C (*cf.* Table 2). The affinities of Apo-Tf toward the NPs are identical within experimental error at 22 °C and at 9 °C. The measured protein corona thickness is also very similar at 22 and 9 °C, *i.e.*, 9.3 and 10 nm. The overall size of apo-Tf protein is around $4.2 \times 10 \times 7$ nm^3. It consists of two identical subunits each having dimensions of $4.2 \times 5 \times 7$ nm^3.[25] Because the thickness of the protein corona correlates with one dimension of the protein, Apo-Tf presumably binds to the NPs with the 4.2×7 nm^2 face. We note that, in earlier experiments,[22] we had observed an apo-Tf corona of 7 nm, which suggests that apo-Tf binds to the NP surface with the 4.2×10 nm^2 face. Considering the surface charge and the structure of apo-Tf (*cf.* the Supporting Information) and assuming that apo-Tf binds to the negatively charged NPs *via* positive patches on its surface, apo-Tf may be able to adsorb to the NPs with the 4.2×7 nm^2 as well as with the 4.2×10 nm^2 face. In fact, we have observed different corona thicknesses on apo-Tf with different protein batches purchased from the same supplier. For the same batch of apo-Tf, however, the results were always reproducible. At 43 °C, the experiments revealed a 3 to 4 nm reduced thickness of the protein corona as compared with 22 or 9 °C. Therefore, the added volume due to apo-Tf adsorption is significantly smaller, which results in only 17 apo-Tf molecules attached per NP under saturation conditions in our analysis (*cf.* Table 2). As for HSA, this may be due to conformational changes of the proteins upon binding, which could involve changes in how the positive patches on the surface of the proteins are exposed to the solvent. Consequently, the overall orientation of the proteins on the surface may also change. Another possible scenario is that the proteins

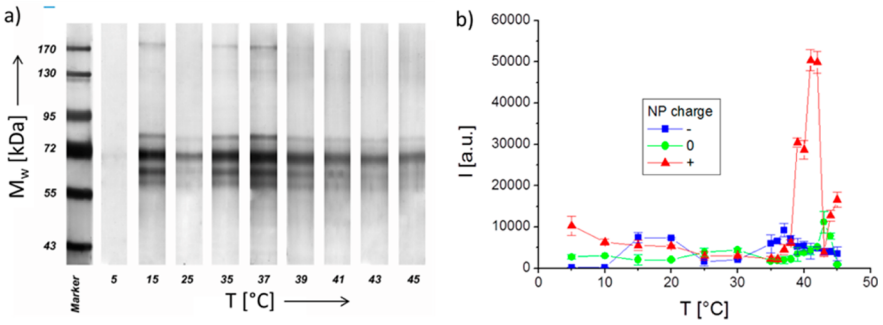

Figure 2. (a) SDS-PAGE gel of proteins adsorbed onto the surfaces of negatively charged FeO_x NPs after 1 h incubation in FBS at different temperatures. The molecular weights M_w of the proteins in the marker lane on the left are reported for reference. (b) Quantification of the amount of adsorbed proteins on negatively charged (−), neutral (0), and positively charged (+) NPs as derived from the total band intensities of proteins on the SDS-PAGE gels.

partially penetrate the polymer shell, which may be more flexible at this temperature.

Compound-Specific Adsorption of FBS onto FeO_x NPs. Because magnetic separation of the small, colloidally stable, and highly defined FePt NPs was not feasible due to their small size, data involving removal of unbound protein were carried out with the bigger FeO_x NPs. Structural and colloidal properties of dextran-coated FeO_x NPs were investigated with TEM and DLS. The diameter d_c of the inorganic FeO_x core and the hydrodynamic diameter d_h (as determined in PBS), respectively, are included in Table 1. Due to their larger size, these NPs allow for convenient magnetic separation and, thus, removal of unbound proteins. However, the NP cores have a relatively large size distribution and were partly agglomerated (especially the positively charged NPs), as indicated by hydrodynamic diameters much bigger than the diameters of the inorganic cores (*cf.* the Supporting Information). After incubation of the NPs in protein solution (10% FBS + 90% PBS) for 1 h at different temperatures, unbound or loosely bound proteins were removed by two washing steps in succession, during which the magnetic NPs were trapped in a strong magnetic field, while the eluted washing solutions were discarded. All washing steps were performed using prewarmed/-cooled washing solutions of the same temperature as during incubation. Only strongly attached proteins are retained on the NP surface after washing.

The proteins were afterward extracted from the NPs and then run on SDS-PAGE. The amount of protein was inferred from the integrated intensities along each line in the gel. An example of a gel with proteins that had adsorbed onto negatively charged NPs (incubated at different temperatures) is shown in Figure 2a (further data and details are included in the Supporting Information). The temperature dependence of the total amount of adsorbed proteins is reported in Figure 2b for the three types of FeO_x NPs. Our data indicate that even a slight temperature increase can already cause remarkable changes in the band intensities and, consequently, the composition of the protein adsorption layer. In order to challenge these findings, control experiments were performed to study the influence of possible sources of error. (i) As FeO_x NPs were found to be partly agglomerated, batch-to-batch variations were probed. (ii) During the washing steps, some NPs might get lost and the amount of the detached proteins might also vary. Thus, variations among different purification runs were probed. (iii) SDS-PAGE and the subsequent quantification of protein may introduce errors: therefore, also these variations were also examined. The observed peak variations were below 10%, which in addition to the smooth connection between the data points indicates that the peaks in the amount of detected corona proteins (Figure 2b) are real. The amount of adsorbed proteins was highest around 40 °C. Also, for neutral and negatively charged NPs, less pronounced maxima exist around 43 and 37 °C, respectively.

The contribution of individual proteins to the corona under conditions of varying NP functionalization and incubation temperature was investigated with liquid chromatography/mass spectrometry (LC-MS/MS) (Figure 3). Significant differences were found between the protein profiles at various temperatures. In particular, we focused on the adsorption of three important serum proteins, for which association to FePt NPs has been previously investigated by using FCS: serum albumin (M_w = 66 kDa),[21,24] serotransferrin (M_w = 76 kDa),[22] and apolipoprotein A-I (M_w = 28 kDa).[24] In addition, we also studied alpha-2-HS-glycoprotein (M_w = 49 kDa). The contributions of serum albumin, serotransferrin, apolipoprotein A-I, and alpha-2-HS-glycoprotein demonstrate a temperature-dependent corona. Noticeably, increased protein adsorption can be seen around 40 °C, in particular for positively charged NPs and for alpha-2-HS-glycoprotein. The significance of this peak, which also appears in the SDS-PAGE data (Figure 2), is further strengthened by the fact that it extends consistently over several data points. However, due to the large error bars (*cf.* the Supporting Information) and also due to limited quality of the FeO_x NPs concerning size distribution

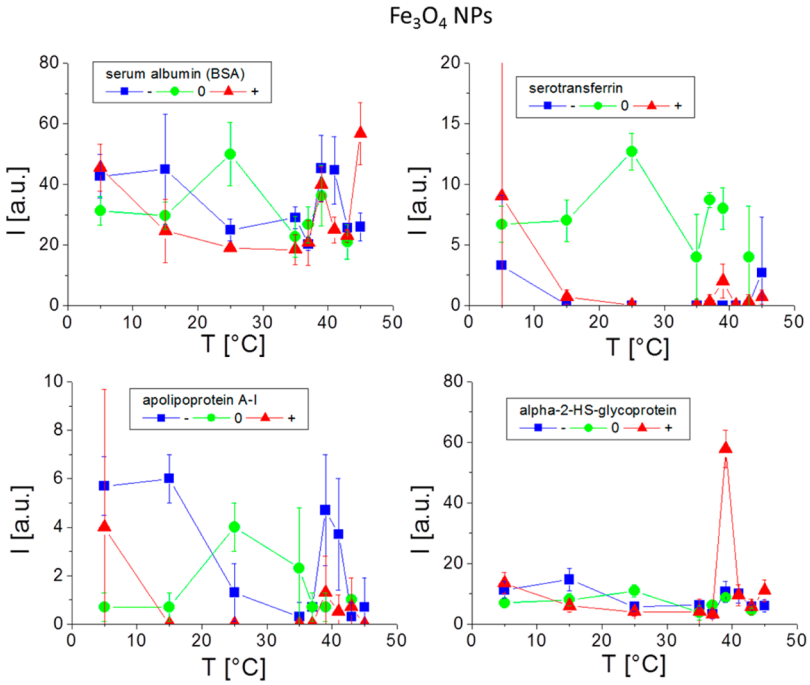

Figure 3. Temperature-dependent amounts of specific proteins in the protein corona of negatively charged (−), positively (+), charged, and neutral (0) FeO_x NPs, as obtained from LC-MS/MS data. Mean values over three independent measurements are shown with their corresponding standard deviations.

and colloidal dispersion, the data presented here rather have to be interpreted in a qualitative than in a quantitative way. Also, in the FCS data on FePt NPs, a noticeable difference in the protein corona was observed between room temperature and 43 °C. Thus, our data indicate that the composition of the corona strongly depends on the temperature at which the corona is formed (*i.e.*, the incubation temperature).

NP Interaction with Cells. Cellular endocytotic processes are intrinsically temperature-dependent.[26−28] For example, below 4 °C, active internalization is suppressed. Also the protein layers formed on the NP surface affect their uptake and trafficking inside cells.[29,30] We have demonstrated above that the formation of the protein corona is temperature-dependent. Thus one may ask how much of this temperature-dependent formation of the protein corona is reflected in temperature-dependent internalization of NPs by cells. In order to investigate this, uptake of fluorescence-labeled FePt NPs under serum-free and serum-containing conditions was analyzed with confocal microscopy at different incubation temperatures. Active cellular uptake of NPs involves the transfer of NPs into endosomes and subsequently lysosomes.[1] Thus we quantified uptake in terms of the amount of NPs found inside cells and of the amount of NPs found inside lysosomes.

In accordance with previous studies,[14,22,30,31] we noticed that NP uptake was reduced by protein corona formation compared to bare NPs, as inferred from measurements with incubation in serum-containing *versus* serum-free medium (*cf.* Figure 4c,f). We also observed a clear enhancement of NP uptake (in terms of mean NP intensity inside cells) with increasing temperatures, as well as with serum-free (Figure 4a) and serum-containing media (*cf.* Figure 4b). This trend was not as clear in the case where only NPs inside lysosomes were considered (*cf.* Figure 4c,d). In order to infer whether the protein corona plays a role in the temperature-dependent uptake of NPs, we analyzed the temperature dependence of the ratio of the uptake of NPs under serum-free and serum-containing conditions. Within our experimental errors we at best can speculate that the amount of NPs internalized by cells may rise faster with temperature under serum-free than under serum-containing conditions (*cf.* Figure 4c). In the case where NP uptake is quantified only by NPs localized inside lysosomes a different tendency was observed (*cf.* Figure 4f). Thus, even without considering that the impact of identical NPs on various cells can be significantly different[4,32,33] our data do not allow for deriving a sharp conclusion about the correlation between the temperature-dependence of protein corona formation and NP uptake. Taking into account the different methods of quantification we applied, neither can we prove that the temperature-dependent formation of the protein corona around NPs may have some influence on the temperature-dependence of NPs uptake by cells, nor can we claim the opposite. Other temperature-dependent effects, such as active NP transport, are likely to play important roles in the temperature dependence in NP uptake, and thus the importance of the temperature dependence of protein

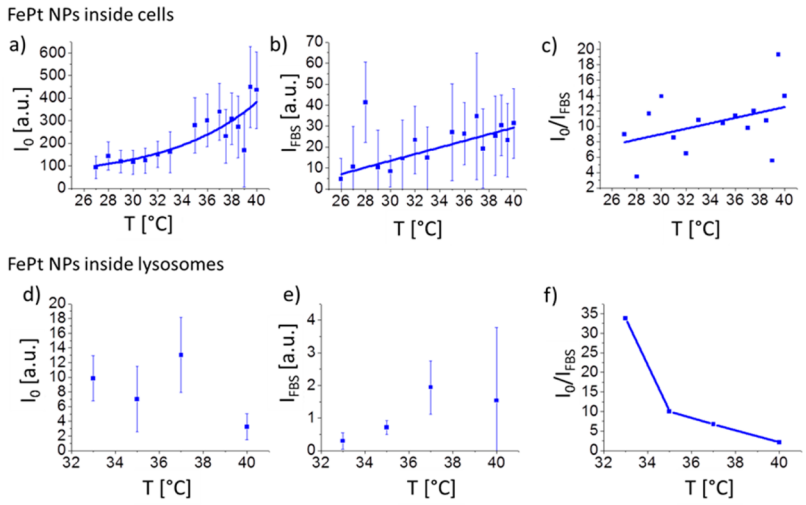

Figure 4. Uptake of fluorescently labeled FePt(−) NPs by HeLa cells after 3 h of incubation. Mean fluorescence intensities *I* of NPs upon using serum-free (I_0) and serum-containing (I_{FBS}) culture media are plotted. (a, b, c) Mean fluorescence intensities *I* of NPs that are localized inside cells. Each data point corresponds to the mean value of at least 2000 analyzed cells and the corresponding standard deviation. Exponential curves are added in order to serve as guide to the eyes. Also the ratio I_0/I_{FBS} is plotted for the different incubation temperatures *T*. (d, e, f) Mean fluorescence intensities *I* of NPs that are localized inside lysosomes. Each data point corresponds to the mean value of at least 30 analyzed cells and the corresponding standard deviation.

corona formation on the temperature dependence in NP uptake can be fully elucidated with more sophisticated assays. Also entanglement of size and protein corona formation needed to be considered, as NP uptake is also size-dependent.[34] In Figure 1 we demonstrated that at the same protein concentration the effective NP radius can be significantly different due to different corona formation, and a detailed analysis also would need to take size effects into account.

CONCLUSIONS

In this study, we have investigated the influence of the exposure temperature, ranging from 5 to 45 °C, on the formation and composition of the protein corona on magnetic NPs. The influence of temperature on NP−cell interactions was also investigated. We have shown that changes in the incubation temperature can cause significant effects in protein corona formation and composition, although this is not necessarily always the case. Temperature effects for the NPs investigated by us were especially pronounced in the physiologically highly relevant temperature window of 37−41 °C. Thus, our findings suggest that studies on the formation of a protein corona on NPs should be carried out at well-controlled temperatures to enable comparison and reproduction of results from different laboratories. The results presented are expected to apply to other classes of NPs, such as fluorescent or plasmonic NPs, with similar surface functionalization, although we did not prove this yet experimentally.

MATERIALS AND METHODS

Synthesis of FePt NPs and Investigation of Adsorbed HSA with FCS. Synthesis of polymer-coated FePt NPs with a fluorophore (DY-636) in the polymer shell has been reported previously.[21] Our two-focus fluorescence correlation spectroscopy setup has recently been described.[24] For incubation with proteins, FePt NPs and proteins were mixed and incubated at a controlled temperature, *T*, for 10 min. HSA and apo-Tf were purchased from Sigma Aldrich as lyophilized powders (A8763 and T4382, respectively). The proteins were suspended in PBS without Ca^{2+} and Mg^{2+} ions (PAA Laboratories) at room temperature at a concentration of 1 mM or less. Subsequently, FCS measurements were carried out for 4 min at the same temperature, *T*. A 40 μL amount of solution was filled into a sample chamber consisting of a small borosilicate glass cylinder glued to a coverslip with epoxy. The sample chamber was kept in a small water bath within an aluminum block heated or cooled to the desired temperature with a Peltier element. Thermal expansion effects due to temperature changes in the objective led to small variations in the focusing properties and, thus, to slight changes of the confocal volume, as was observed by measuring the point spread function (PSF) using laser light reflected off 100 nm gold NPs. We compensated the temperature effect by changing the position of the correction collar normally used to correct for different coverslip thicknesses. The position of the correction collar was adjusted so as to achieve maximum fluorescence intensity, which also correlates with the smallest dimensions of the measured confocal volume. Furthermore, we measured deviations in the interfoci distance resulting from temperature changes with a reference sample, Atto655 in buffer solution. The measured size of the NPs was corrected according to the calibration obtained with the reference sample. Temperature was directly measured in the sample solution. Hydrodynamic radii, r_h, were determined by FCS and plotted *versus* the HSA concentration in solution, *c*(HSA), as shown in Figure 1. At saturation, the hydrodynamic radius of one NP was calculated according to[21]

$$r_h(N_{max}) = r_h(0)\sqrt[3]{1 + cN_{max}} \quad (1)$$

where $c = V_p/V_0$ is the volume ratio of protein molecules to NP. For the NPs, the volume was simply calculated by using $V_0 = (4\pi/3)(r_h(0))^3$. For apo-Tf, the volume was estimated from the physical dimensions, *i.e.*, $V_p = 10 \times 7 \times 4.2 = 294$ nm^3. Likewise,

for HSA, the volume of a triangular prism with 8 nm side length and 3 nm thickness was computed, *i.e.*, $V_p = 3 \times (8/2) \times (8^2 - 4^2)^{1/2} = 83\ nm^3$. Note that, for HSA, which is a compact globular protein, V_p can equally well be calculated by using $V_p = (M_w/N_A)/\rho_p$, with the molecular weight, M_w, of HSA, Avogadro's constant, N_A, and the protein density, $\rho_p = 1.35\ g/cm^3$. N_{max} is the maximum number of adsorbed molecules. Concentration-dependent adsorption was described by the Hill equation,

$$N = N_{max} \frac{1}{1 + (K'_D/[Pr])^n} \quad (2)$$

where N is the number of adsorbed protein molecules per NP, K'_D represents the concentration of protein molecules for half coverage, and n is the Hill coefficient, which determines the steepness of the binding curve.[21]

Synthesis of FeO_x NPs and Investigation of Adsorbed FBS with PAGE and MS. Syntheses of dextran-coated FeO_x NPs (SPIONs, inorganic core diameter) with negative, neutral, and positive surface charges were performed according to our previously published protocols (hydrodynamic radii together with their characterization are presented in the Supporting Information).[35] To study the interactions of the NPs with FBS, 100 μL of NP solution (with a concentration of 100 μg/mL) was mixed with 900 μL of FBS and incubated at T = 5, 15, 25, 35, 37, 39, 41, 43, and 45 °C. The protein/NP mixtures were run through a strong magnetic field using a magnetic-activated cell sorting system. NPs were trapped inside the magnetic column, and the flow-through fraction (two washing steps with 500 μL of PBS buffer) was removed. We ensured that all washing solutions were at the same temperature as the media used during incubation. Finally, the column was removed from the magnetic field, and the released NPs were collected. The protein/NP mixtures were immediately resuspended in protein loading buffer containing 10% dithiothreitol, followed by boiling for 5 min at 100 °C to remove the proteins from the NPs.[3] To quantify the amount of proteins on the surface of the various NPs, equal sample volumes of the solution were loaded into sodium dodecyl sulfate polyacrylamide gel electrophoresis (1D SDS-PAGE). Gel electrophoresis was carried out at 120 V, 400 mA, for about 60 min each, until the proteins approached the end of the gel. While the NPs stick in the wells of the gels, the desorbed proteins migrate in the applied electric field. The gels were stained by silver nitrate in order to visualize the proteins and scanned using a Biorad GS-800 calibrated densitometer scanner, and gel densitometry was performed using Image J (1.410 version). Intensity profiles of the stained proteins along the migration direction of the proteins were recorded to quantify the total amount of protein in each lane and the contribution of the proteins of different molecular weight to the total amount. An example of a gel after SDS-PAGE is shown in Figure 2a. To determine the relative amounts of proteins adsorbed onto different NPs, the collected proteins were digested with trypsin and analyzed by LC-MS/MS. A semiquantitative evaluation of the data was done by using the peptide spectrum matches (*i.e.*, "spectral counts") assigned to a distinct protein by Proteome Discoverer software.

Uptake of FePt NPs by Cells. HeLa cells were incubated with polymer-coated FePt NPs with integrated fluorophore (DY-636) at different temperatures for 3 h with and without serum (FBS) in the culture medium. Nuclei, membranes, and lysosomes of the cells were stained, and fluorescence images of these cellular compartments together with images of the NP distribution were recorded with confocal microscopy (for details refer to the Supporting Information). Cellular compartments were identified with the open source software CellProfiler. NPs located in the specific compartments (here either inside cells or inside lysosomes) were identified by overlay of a mask corresponding to the locations of the compartments with the image of the NP distribution.[36] As well, the total amount of NPs incorporated per cell (as quantified by the mean fluorescence intensity I inside cells), as the amount of NPs that co-localized with the lysosome (as quantified by the mean fluorescence intensity I inside lysosomes),[37] was determined. Please note the limited depth resolution of confocal microscopy, which makes it complicated to distinguish between NPs only adherent to the outer cell surface and internalized NPs. One could clearly distinguish between both cases using pH-sensitive fluorophores attached to the NPs[38,39] In our case we also stained the cell membrane. We did not observe a significant amount of NPs at positions close to the cell membrane, and thus the error in the quantification of internalized NPs by wrongfully counting also NPs attached to the outer membrane is very small.

Conflict of Interest: The authors declare no competing financial interest.

Acknowledgment. This work was supported by the Deutsche Forschungsgemeinschaft DFG (grants CFN, NI291/7, and NI291/8 to G.U.N. and grant PA794/4-2 to W.J.P.). The authors thank Faheem Amin for helping with the synthesis and polymer coating of FePt NPs, Dr. Andreas Schaper for discussions about TEM, Alexander Hepting for his efforts with the temperature-controlled measurement chamber, and Dominik Hühn for proofreading the manuscript.

Supporting Information Available: Full methodology and additional data are available free of charge *via* the Internet at http://pubs.acs.org.

REFERENCES AND NOTES

1. Nel, A. E.; Madler, L.; Velegol, D.; Xia, T.; Hoek, E. M. V.; Somasundaran, P.; Klaessig, F.; Castranova, V.; Thompson, M. Understanding Biophysicochemical Interactions at the Nano-Bio Interface. *Nat. Mater.* **2009**, *8*, 543–557.
2. Mahmoudi, M.; Lynch, I.; Ejtehadi, M. R.; Monopoli, M. P.; Bombelli, F. B.; Laurent, S. Protein-Nanoparticle Interactions: Opportunities and Challenges. *Chem. Rev.* **2011**, *111*, 5610–5637.
3. Monopoli, M. P.; Walczyk, D.; Campbell, A.; Elia, G.; Lynch, I.; Bombelli, F. B.; Dawson, K. A. Physical-Chemical Aspects of Protein Corona: Relevance to *in Vitro* and *in Vivo* Biological Impacts of Nanoparticles. *J. Am. Chem. Soc.* **2011**, *133*, 2525–2534.
4. Laurent, S.; Burtea, C.; Thirifays, C.; Hafeli, U. O.; Mahmoudi, M. Crucial Ignored Parameters on Nanotoxicology: The Importance of Toxicity Assay Modifications and "Cell Vision". *PLoS One* **2012**, *7*, e29997.
5. Walczyk, D.; Bombelli, F. B.; Monopoli, M. P.; Lynch, I.; Dawson, K. A. What the Cell "Sees" in Bionanoscience. *J. Am. Chem. Soc.* **2010**, *132*, 5761–5768.
6. Cedervall, T.; Lynch, I.; Foy, M.; Berggad, T.; Donnelly, S.; Cagney, G.; Linse, S.; Dawson, K. Detailed Identification of Plasma Proteins Adsorbed on Copolymer Nanoparticles. *Angew. Chem., Int. Ed.* **2007**, *46*, 5754–5756.
7. Lundqvist, M.; Stigler, J.; Cedervall, T.; Berggard, T.; Flanagan, M. B.; Lynch, I.; Elia, G.; Dawson, K. The Evolution of the Protein Corona around Nanoparticles: A Test Study. *ACS Nano* **2011**, *5*, 7503–7509.
8. Tenzer, S.; Docter, D.; Rosfa, S.; Wlodarski, A.; Kuharev, J.; Rekik, A.; Knauer, S. K.; Bantz, C.; Nawroth, T.; Bier, C.; *et al.* Nanoparticle Size Is a Critical Physicochemical Determinant of the Human Blood Plasma Corona: A Comprehensive Quantitative Proteomic Analysis. *ACS Nano* **2011**, *5*, 7155–7167.
9. Maiorano, G.; Sabella, S.; Sorce, B.; Brunetti, V.; Malvindi, M. A.; Cingolani, R.; Pompa, P. P. Effects of Cell Culture Media on the Dynamic Formation of Protein-Nanoparticle Complexes and Influence on the Cellular Response. *ACS Nano* **2010**, *4*, 7481–7491.
10. Gebauer, J. S.; Malissek, M.; Simon, S.; Knauer, S. K.; Maskos, M.; Stauber, R. H.; Peukert, W.; Treuel, L. Impact of the Nanoparticle-Protein Corona on Colloidal Stability and Protein Structure. *Langmuir* **2012**, *28*, 9673–9679.
11. Casals, E.; Pfaller, T.; Duschl, A.; Oostingh, G. J.; Puntes, V. F. Time Evolution of the Nanoparticle Protein Corona. *ACS Nano* **2010**, *4*, 3623–3632.
12. Milani, S.; Bombelli, F. B.; Pitek, A. S.; Dawson, K. A.; Radler, J. Reversible *versus* Irreversible Binding of Transferrin to Polystyrene Nanoparticles: Soft and Hard Corona. *ACS Nano* **2012**, *6*, 2532–2541.

13. Walkey, C. D.; Chan, W. C. Understanding and Controlling the Interaction of Nanomaterials with Proteins in a Physiological Environment. *Chem. Soc. Rev.* **2012**, *41*, 2780–2799.
14. Hühn, D.; Kantner, K.; Geidel, C.; Brandholt, S.; De Cock, I.; Soenen, S. J. H.; Rivera Gil, P.; Montenegro, J.-M.; Braeckmans, K.; Müllen, K.; *et al*. Polymer-Coated Nanoparticles Interacting with Proteins and Cells: Focusing on the Sign of the Net Charge. *ACS Nano* **2013**, *7*, 3253–3263.
15. Lesniak, A.; Campbell, A.; Monopoli, M. P.; Lynch, I.; Salvati, A.; Dawson, K. A. Serum Heat Inactivation Affects Protein Corona Composition and Nanoparticle Uptake. *Biomaterials* **2010**, *31*, 9511–9518.
16. Petersdorf, R. G. Chills and Fever. In *Harrison's Principles of Internal Medicine*; McGraw-Hill: New York, 1974.
17. Hasday, J. D.; Singh, I. S. Fever and the Heat Shock Response: Distinct, Partially Overlapping Processes. *Cell Stress Chaperones* **2000**, *5*, 471–480.
18. Rhoades, R. A.; Pflanzer, R. G. *Human Physiology*.; Saunders College Publishing: Philadelphia, PA, 1989; pp 823−840.
19. Yang, J. M.; Yang, H.; Lin, L. W. Quantum Dot Nano Thermometers Reveal Heterogeneous Local Thermogenesis in Living Cells. *ACS Nano* **2011**, *5*, 5067–5071.
20. Donner, J. S.; Thompson, S. A.; Kreuzer, M. P.; Baffou, G.; Quidant, R. Mapping Intracellular Temperature Using Green Fluorescent Protein. *Nano Lett.* **2012**, *12*, 2107–2111.
21. Röcker, C.; Pötzl, M.; Zhang, F.; Parak, W. J.; Nienhaus, G. U. A Quantitative Fluorescence Study of Protein Monolayer Formation on Colloidal Nanoparticles. *Nat. Nanotechnol.* **2009**, *4*, 577–580.
22. Jiang, X.; Weise, S.; Hafner, M.; Röcker, C.; Zhang, F.; Parak, W. J.; Nienhaus, G. U. Quantitative Analysis of the Protein Corona on FePt Nanoparticles Formed by Transferrin Binding. *J. R. Soc., Interface* **2010**, *7*, S5–S13.
23. Lehmann, A. D.; Parak, W. J.; Zhang, F.; Ali, Z.; Röcker, C.; Nienhaus, G. U.; Gehr, P.; Rothen-Rutishauser, B. Fluorescent-Magnetic Hybrid Nanoparticles Induce a Dose-Dependent Increase in Proinflammatory Response in Lung Cells *in Vitro* Correlated with Intracellular Localization. *Small* **2010**, *6*, 753–762.
24. Maffre, P.; Nienhaus, K.; Amin, F.; Parak, W. J.; Nienhaus, G. U. Characterization of Protein Adsorption onto FePt Nanoparticles Using Dual-Focus Fluorescence Correlation Spectroscopy. *Beilstein J. Nanotechnol.* **2011**, *2*, 374–383.
25. Bailey, S.; Evans, R. W.; Garratt, R. C.; Gorinsky, B.; Hasnain, S.; Horsburgh, C.; Jhoti, H.; Lindley, P. F.; Mydin, A.; Sarra, R.; *et al*. Molecular-Structure of Serum Transferrin at 3.3-A Resolution. *Biochemistry* **1988**, *27*, 5804–5812.
26. Mamdouh, Z.; Giocondi, M. C.; Laprade, R.; LeGrimellec, C. Temperature Dependence of Endocytosis in Renal Epithelial Cells in Culture. *Biochim. Biophys. Acta* **1996**, *1282*, 171–173.
27. Weigel, P. H.; Oka, J. A. Temperature-Dependence of Endocytosis Mediated by the Asialoglycoprotein Receptor in Isolated Rat Hepatocytes - Evidence for 2 Potentially Rate-Limiting Steps. *J. Biol. Chem.* **1981**, *256*, 2615–2617.
28. Hong, G. S.; Wu, J. Z.; Robinson, J. T.; Wang, H. L.; Zhang, B.; Dai, H. J. Three-Dimensional Imaging of Single Nanotube Molecule Endocytosis on Plasmonic Substrates. *Nat. Commun.* **2012**, 3.
29. Jedlovszky-Hajdu, A.; Bombelli, F. B.; Monopoli, M. P.; Tombacz, E.; Dawson, K. A. Surface Coatings Shape the Protein Corona of Spions with Relevance to Their Application *in Vivo*. *Langmuir* **2012**, *28*, 14983–14991.
30. Lesniak, A.; Fenaroli, F.; Monopoli, M. R.; Aberg, C.; Dawson, K. A.; Salvati, A. Effects of the Presence or Absence of a Protein Corona on Silica Nanoparticle Uptake and Impact on Cells. *ACS Nano* **2012**, *6*, 5845–5857.
31. Mirshafiee, V.; Mahmoudi, M.; Lou, K.; Cheng, J.; Kraft, M. L. Protein Corona Significantly Reduces Active Targeting Yield. *Chem. Commun.* **2013**, *49*, 2557–2559.
32. Mahmoudi, M.; Laurent, S.; Shokrgozar, M. A.; Hosseinkhani, M. Toxicity Evaluations of Superparamagnetic Iron Oxide Nanoparticles: Cell "Vision" *versus* Physicochemical Properties of Nanoparticles. *ACS Nano* **2011**, *5*, 7263–7276.
33. Mahmoudi, M.; Saeedi-Eslami, S. N.; Shokrgozar, M. A.; Azadmanesh, K.; Hassanlou, M.; Kalhor, H. R.; Burtea, C.; Rothen-Rutishauser, B.; Laurent, S.; Sheibani, S.; *et al*. Cell "Vision": Complementary Factor of Protein Corona in Nanotoxicology. *Nanoscale* **2012**, *4*, 5461–5468.
34. Chithrani, B. D.; Chan, W. C. W. Elucidating the Mechanism of Cellular Uptake and Removal of Protein-Coated Gold Nanoparticles of Different Sizes and Shapes. *Nano Lett.* **2007**, *7*, 1542–1550.
35. Mahmoudi, M.; Simchi, A.; Milani, A.; Stroeve, P. Cell Toxicity of Superparamagnetic Iron Oxide Nanoparticles. *J. Colloid Interface Sci.* **2009**, *336*, 510–518.
36. Rivera Gil, P.; Yang, F.; Thomas, H.; Li, L.; Terfort, A.; Parak, W. J. Development of an Assay Based on Cell Counting with Quantum Dot Labels for Comparing Cell Adhesion within Cocultures. *Nano Today* **2011**, *6*, 20–27.
37. Schweiger, C.; Hartmann, R.; Zhang, F.; Parak, W. J.; Kissel, T.; Rivera Gil, P. Quantification of the Internalization Patterns of Superparamagnetic Iron Oxide Nanoparticles with Opposite Charge. *J. Nanobiotechnol.* **2012**, *10*, 28.
38. Semmling, M.; Kreft, O.; Muñoz Javier, A.; Sukhorukov, G. B.; Käs, J.; Parak, W. J. A Novel Flow-Cytometry-Based Assay for Cellular Uptake Studies of Polyelectrolyte Microcapsules. *Small* **2008**, *4*, 1763–1768.
39. Zhang, F.; Lees, E.; Amin, F.; Rivera Gil, P.; Yang, F.; Mulvaney, P.; Parak, W. J. Polymer-Coated Nanoparticles: A Universal Tool for Biolabelling Experiments. *Small* **2011**, *7*, 3113–3127.

Particle & Particle Systems Characterization
www.particle-journal.com

The Toxicity of Silver Nanoparticles Depends on Their Uptake by Cells and Thus on Their Surface Chemistry

*Encarnación Caballero-Díaz, Christian Pfeiffer, Lena Kastl, Pilar Rivera-Gil, Bartolome Simonet, Miguel Valcárcel, Javier Jiménez-Lamana, Francisco Laborda, and Wolfgang J. Parak**

A set of three types of silver nanoparticles (Ag NPs) are prepared, which have the same Ag cores, but different surface chemistry. Ag cores are stabilized with mercaptoundecanoic acid (MUA) or with a polymer shell [poly(isobutylene-alt-maleic anhydride) (PMA)]. In order to reduce cellular uptake, the polymer-coated Ag NPs are additionally modified with polyethylene glycol (PEG). Corrosion (oxidation) of the NPs is quantified and their colloidal stability is investigated. MUA-coated NPs have a much lower colloidal stability than PMA-coated NPs and are largely agglomerated. All Ag NPs corrode faster in an acidic environment and thus more Ag(I) ions are released inside endosomal/lysosomal compartments. PMA coating does not reduce leaching of Ag(I) ions compared with MUA coating. PEGylation reduces NP cellular uptake and also the toxicity. PMA-coated NPs have reduced toxicity compared with MUA-coated NPs. All studied Ag NPs were less toxic than free Ag(I) ions. All in all, the cytotoxicity of Ag NPs is correlated on their uptake by cells and agglomeration behavior.

1. Introduction

Silver nanoparticles (Ag NPs) are frequently used in industry, mainly because of their antimicrobial properties,[1] with applications in an increasing number of medical and consumer products. However, their antibacterial features and extremely small size, which makes them to have a high surface area and to be more reactive, also suggest a toxicological risk when these NPs come into contact with biological systems.[2] Countless toxicological studies involving Ag NPs have already been carried out in different organisms ranging from bacteria to humans.[3–5] Although it is generally known that corrosion (oxidation) and subsequent release of Ag(I) ions is a major source of toxicity,[6,7] there is still a lack of detailed general knowledge concerning the origin of the Ag NPs' toxicity. Most important shortcomings are that individual studies are often based on different NPs, and also on different types of cells, which complicate the comparison and extrapolation of results. In some studies, the final toxicity resulted to be an unclear combination of effects among the Ag NPs and their released Ag(I) ions, whereas in other works the Ag(I) ions showed a greater (or even the only) contribution to the toxicity than the Ag NPs per se.[3,7–9] Several studies describe the release of Ag(I) ions upon NP oxidation and subsequent partial dissolution of the Ag NPs over time as amplification of the toxicity of the (undissolved) Ag NPs, which can cause intracellular reactions, as, for example, in the mitochondria.[5] Other studies even claim that the only effect originates from Ag ions, which acts on the cell membrane, whereas under the same conditions Ag NPs had no effect.[9] Studies indicate that toxicity depends on size,[10] shape,[11] charge,[12] and colloidal stability[13] of the Ag NPs.

Although correlation of the physicochemical properties of NPs to their interaction with cells is attempted by a large-body research studies, a comprehensive picture is still missing (not only for Ag NPs but in general) albeit many effects are well established. This is partly due to the fact that not all physicochemical properties are easy to be determined experimentally, and most of them are entangled (e.g., loss in colloidal stability/reduced dispersion also increases the effective hydrodynamic diameter of the NPs).[14] The interaction of NPs with cells is not only governed directly but also it is strongly influenced by interplay with the medium. Salt can reduce colloidal stability, and the NP surface will be covered with a corona of proteins, which provides signature to the NP surface.[15] This interaction is not static, but rather dynamic and may change with time.[16] Although this already gives a complex scenario for the NP–medium interaction, modern techniques such as fluorescence correlation spectroscopy (FCS) allow for detailed

E. Caballero-Díaz, C. Pfeiffer, L. Kastl,
Dr. P. Rivera-Gil, Prof. W. J. Parak
Fachbereich Physik
Philipps Universität Marburg
Marburg, Germany
E-mail; wolfgang.parak@physik.uni-marburg.de
E. Caballero-Díaz, Dr. B. Simonet, Prof. M. Valcárcel
Department of Analytical Chemistry
University of Cordoba
Córdoba, Spain
J. Jiménez-Lamana, Prof. F. Laborda
Group of Analytical Spectroscopy and Sensors (GEAS)
Institute of Environmental Sciences (IUCA)
University of Zaragoza
Zaragoza, Spain
Prof. W. J. Parak
CIC Biomagune
San Sebastian, Spain

DOI: 10.1002/ppsc.201300215

These are not the final page numbers

investigation of the physicochemical properties of NPs in many protein-containing media[17] (but not in all, for instance, not in blood). Characterization is, however, complicated as soon as NPs enter cells. Going back to the dynamic picture of the protein corona,[15] its composition certainly will change inside cells. Enzymes in endo/lysosomal compartments can, for example, digest part of the protein corona. [18] Also the pH in these compartments, in which NPs are typically residing, is highly acidic. In particular in the case of Ag NPs, this may enhance oxidation of the inorganic NP core by release of Ag(I) ions, which in turn would affect toxicity. In order to single out such effects, highly defined NPs, in which parameters are varied in a controlled way, and appropriate test media, are warranted.

In the present study, we wanted to investigate two hypotheses. The first one is that toxicity of Ag NPs is correlated with their uptake by cells, i.e., the more internalized Ag NPs, the greater their toxicity. This was motivated by previous studies based on different types of NPs.[19] In order to test this hypothesis, cells need to be exposed to the same amounts of Ag NPs, but different amounts are internalized. One possibility to enhance uptake of Ag NPs is coupling them to magnetic NPs. Enhanced internalization of Ag NPs via magnetofection has been demonstrated to increase cytotoxicity.[20] In our study, we wanted to attempt an alternative strategy. Ag NPs are internalized via endocytotic pathways,[21] whereby uptake can be controlled by the surface chemistry of the NPs. Polyethylene glycol (PEG) of 10 kDa molecular weight is commonly used to reduce NP uptake by cells in vitro [22] and also to increase in vivo retention times.[23] Thus, in this study, we modulate uptake of Ag NPs by PEGylation and compare toxic effects obtained for Ag NPs with PEG to those obtained for the same Ag NPs but without PEG. The second hypothesis is that toxicity of Ag NPs is correlated to how fast they corrode, i.e., how fast they dissolve under physiological conditions. Also this hypothesis has been motivated by previous reports.[7] As pointed out above, one hereby needs to consider that NPs internalized in endo/lysosomal structures are exposed to highly acidic pH, which enhanced NP dissolution, in contrast to the neutral pH in extracellular media. In our study, we attempt to modulate oxidation of Ag NPs by different protective surface coatings. Often Ag NPs are capped by a monolayer of surfactant, and thus have been also termed previously as monolayer-protected clusters.[24] Additionally, we protected and stabilized the NP surface by wrapping a polymer around the original surfactant shell.[25] Altogether the key point of our study is that all experiments are based on the same Ag cores. By modification of the surface chemistry, both uptake by cells and oxidation are controlled. As the actual Ag cores of the different Ag NPs are identical, and also the final Ag NPs are well defined and characterized, comparative studies can be performed.

2. Materials and Methods

2.1. Synthesis of Hydrophobic Ag NPs [26]

Ag NPs capped with dodecylthiol were synthesized following the protocol of Mari et al.[27] These hydrophobic NPs were dispersed in chloroform and had a core diameter (i.e., the diameter of the inorganic Ag NP, excluding the organic capping [14] of d_c = 4.2 ± 0.4 nm and an experimentally determined molecular extinction coefficient of $\varepsilon = 16.9 \times 10^6\ M^{-1}\ cm^{-1}$ at the surface plasmon peak at 430 nm. Based on this, we calculated that each Ag NP in average contains $N_{Ag} \approx 2200$ Ag atoms in total, whereby ≈30% ($N_{Ag,surf} \approx 650$) Ag atoms are located on the surface of each NP. For a detailed description of the synthesis protocol and the calculations, we refer to the Supporting Information. In the following section, different strategies on how these NPs were transferred to aqueous phase will be described.

2.2. Synthesis of Hydrophilic Ag NPs

The hydrophobic Ag NPs were transferred via two strategies to aqueous phase. First, the hydrophobic dodecylthiol ligands were replaced with hydrophilic mercaptoundecanoic acid (MUA) ligands by a ligand-exchange procedure, resulting in water-soluble Ag–MUA NPs. Second, an amphiphilic polymer (dodecylamine-modified poly(isobutylene-alt-maleic anhydride) PMA) was wrapped around the original ligand shell, leading to water-soluble Ag–PMA NPs. Advantages and disadvantages of both procedures have been compared in previous works.[28] The resulting Ag NPs were stringently purified by gel electrophoresis and size exclusion chromatography, which allows for sufficient removal of excess of reactants and polymeric micelles[29] (for the case of polymer-coating). Using EDC (1-ethyl-3-(3-dimethylaminopropyl)carbodiimide) chemistry, 10 kDa amino-modified polyethylene glycol NH_2–PEG–CH_3 (Rapp Polymere) was linked via the amino group to the carboxyl groups on the surface of Ag–PMA NPs. NPs saturated with PEG (Ag–PMA–satPEG NPs) and with exactly one PEG per NP (Ag–PMA–1PEG NPs) were obtained and fractionated via gel electrophoresis. Thus, four different surface modifications based on the same original hydrophobic NPs were obtained: Ag–MUA, Ag–PMA, Ag–PMA–1PEG, Ag–PMA–satPEG (**Figure 1**). Details of the surface modification protocols are reported in detail in the Supporting Information.

2.3. Characterization of Colloidal Properties

The colloidal properties of the Ag NPs were characterized according to our standard protocols,[30] including determination of the hydrodynamic diameter (d_h) by dynamic light scattering (DLS), the zeta-potential (ζ) [31] by laser Doppler anemometry (LDA), and stability in salt-containing solutions (**Table 1**). For the stability assays, changes in the d_h upon the presence of NaCl were recorded (**Figure 2**).

2.4. Characterization of NP Oxidation

Despite stringent purification after synthesis, the Ag cores of the Ag NPs corrode over time, leading to the release of Ag(I) ions.[7] Release of Ag(I) was quantified both, at neutral (pH = 7) and acidic (pH = 3) conditions using ultrafiltration and inductively coupled plasma mass spectrometry (ICP-MS).

These are not the final page numbers

DOI: 10.1002/ppsc.201300215

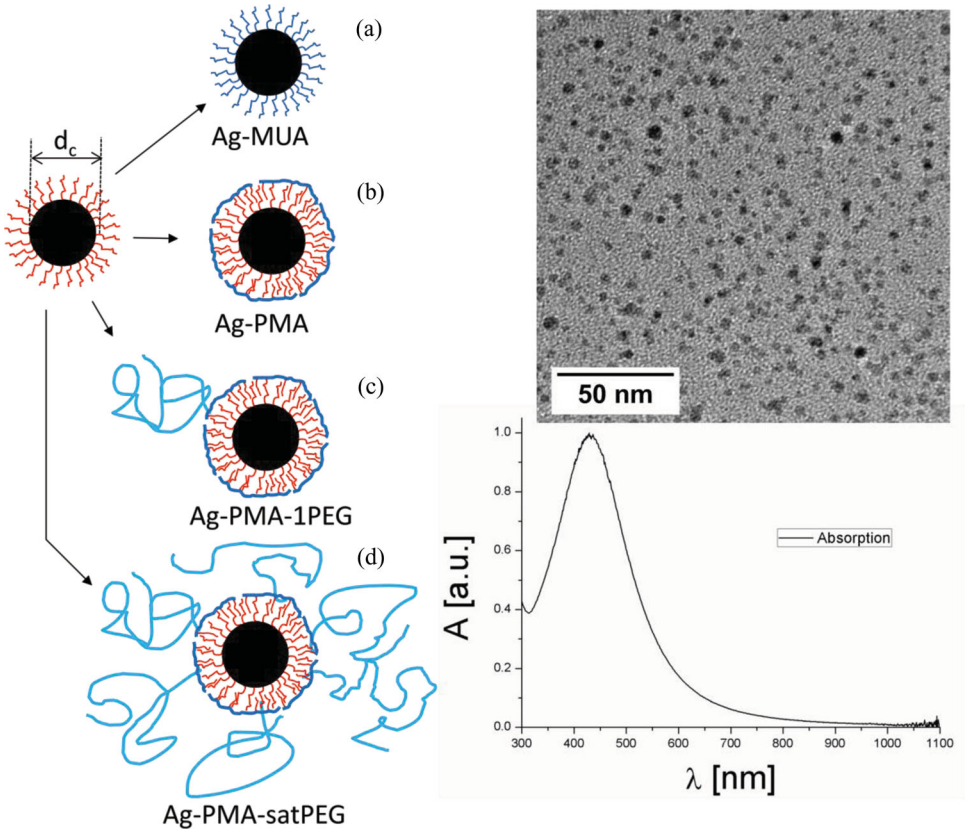

Figure 1. Sketch of the four types of surface modifications, which were applied to the same hydrophobically capped Ag NPs. The Ag cores (with core diameter d_c) are depicted in black, and the original hydrophobic ligand shell is depicted in red. The following surface modifications have been applied to obtain water-soluble NPs. a) Ligand exchange to mercaptoundecanoic acid (Ag–MUA NPs; the hydrophilic ligands are depicted in blue). b) Overcoating with an amphiphilic polymer (Ag–PMA NPs). c) Overcoating with an amphiphilic polymer and conjugation with one PEG molecule per NP (Ag–PMA–1PEG NPs). d) Overcoating with an amphiphilic polymer and subsequent saturation of the surface with polyethyleneglycol (Ag–PMA–satPEG NPs).

2.5. Analysis of NP uptake by Cells

The cellular uptake of Ag NPs was analyzed by confocal laser scanning microscopy (CLSM). NIH/3T3 embryonic fibroblasts were seeded on Ibidi-Plates at cell densities of $2 \times 10^{[4]}$ cells/well in 300 µL growth medium (DMEM-F12 Ham's basal medium supplemented with 10% calf serum, 1% L-glutamine, and 1% penicillin/streptomycin). The next day, the cells were rinsed with phosphate-buffered saline (PBS) and incubated with Dy636-modified fluorescent Ag NPs (Supporting Information) at a concentration of c(Ag NP) = 10×10^{-9} M ($\lambda_{excitation}$ 645 nm and $\lambda_{emission}$ 671 nm) for 15 h at 37 °C and 5% CO_2. The cells were then analyzed with a CLSM (Zeiss LSM Meta; **Figure 3**).

Table 1. Colloidal (hydrodynamic diameter d_h and zeta-potential ζ) and toxic properties (concentration of half viability, LD_{50}) of Ag NPs with different surface coating, with a core diameter of $d_c = 4.2$ nm. The concentrations refer to the number of Ag atoms in solution (c(Ag)). The LD_{50} value for $AgNO_3$ was determined as $0.022 \pm 1.24 \times 10^{-5} \times 10^{-3}$ M.

Sample	d_h [nm]	ζ [mV]	LD_{50} [$\times 10^{-3}$ M]
Ag–MUA	11 ± 4	–24.9 ± 1.7	$0.04 \pm 2.83 \times 10^{-4}$
Ag–PMA	12 ± 3	–31.0 ± 1.3	$0.65 \pm 8.66 \times 10^{-3}$
Ag–PMA–1PEG	13 ± 4	–41.1 ± 1.5	$0.73 \pm 6.48 \times 10^{-3}$
Ag–PMA–satPEG	12 ± 3	–10.9 ± 0.4	$1.34 \pm 2.49 \times 10^{-2}$

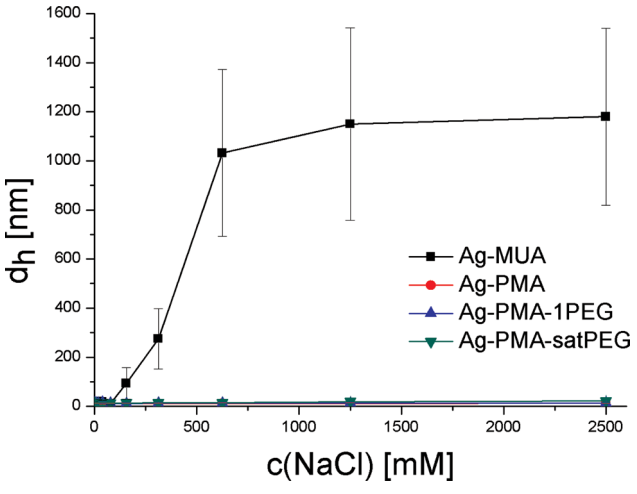

Figure 2. Change of the hydrodynamic diameter (d_h) of the Ag NPs upon the presence of NaCl (d_h was detected directly after exposure of the Ag NPs to AgCl). The error bars belong to the width of the peak.

These are not the final page numbers

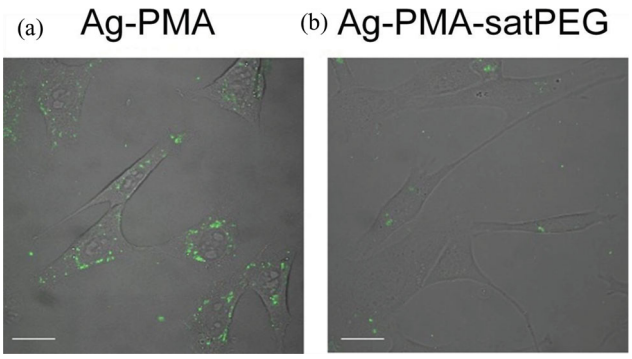

Figure 3. Fluorescence images of 3T3 fibroblasts, which had been exposed for 15 h to fluorescence (DY636) labeled a) polymer-coated Ag NPs or b) polymer-coated Ag NPs whose surface has been saturated with 10 kDa PEG molecules. The images correspond to the overly images of the transmission and fluorescence channel. Scale bars correspond to 20 µm.

2.6. Analysis of Cell Viability

Viability of NIH/3T3 embryonic fibroblasts upon incubation with Ag NPs was probed with a standard resazurin assay.[32] Silver nitrate was used as positive control. Resazurin is a blue, non-fluorescent sodium salt, which is converted to resorufin by metabolically active cells. Resorufin is a pink, fluorescent sodium salt that accumulates outside the cells. This reduction process requires functional mitochondrial activity, which is inactivated immediately after cell death. Thus, cell viability was assessed by the increase in the fluorescence signal and is given as mean of normalized intensities against the concentration of Ag. The response curves were fitted with a sigmoidally shaped curve, of which the point of inflection was taken as LD_{50} value, i.e., the concentration when cell viability was reduced by half (**Figure 4**).

3. Results and Discussion

3.1. Colloidal Properties

Four different surface modifications applied to the same Ag cores were compared. All NP samples have comparable hydrodynamic diameters (Table 1) in PBS. PEGylation increases the diameter, which is indicated in gel electrophoresis and size exclusion chromatography experiments (Supporting Information). Surprisingly, we were reproducibly not able to observe this also with DLS, which is however within the error bars. In the DLS data, MUA and PMA provide negative charge to the NPs and thus colloidal stability via electrostatic repulsions

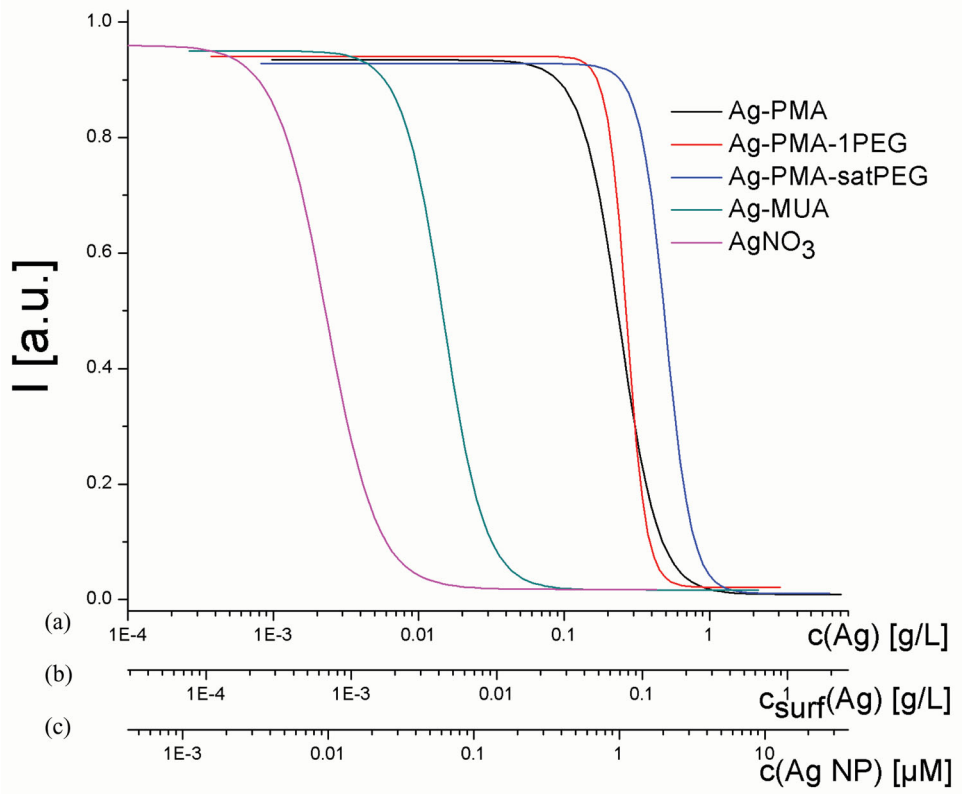

Figure 4. Resazurin-based viability test of 3T3 fibroblasts, which had been incubated for 24 h with Ag NPs. Onset of fluorescence (as quantified by the measured intensity I) is an indicator for viability of cells. The amount of Ag is quantified in a) the total amount of Ag (c(Ag)), b) the amount of Ag atoms, which are present on the NP surface (c_{surf}(Ag)), and c) the amount of Ag NPs (c(Ag NP)). The following scaling factors were used (Supporting Information): $c_{surf}(Ag) = 0.29\ c(Ag)$ and $c(Ag\ NP) = 4.2 \times 10^{-9}$ mol mg^{-1} c(Ag). In case of $AgNO_3$ as silver source, only the c(Ag) concentration scale is valid; in case of all the NPs, all three concentration scales are valid .

(the zeta-potential data in Table 1). Saturation of the NPs surface with PEG (Ag–PMA–satPEG NPs) reduces the negative charge, but the colloidal stability is conducted by steric repulsions. However, as soon as NaCl is added to PBS, dramatic differences in colloidal stability of the NPs are visible. While for Ag–PMA NPs, the hydrodynamic diameter upon the presence of NaCl (up to 2.5 M) remains relatively unaffected, Ag–MUA NPs completely agglomerate, which is visible by their huge hydrodynamic diameters (Figure 2). Please note that colloidal characterization was performed in neutral PBS buffer containing different amounts of NaCl, not in the actual cell media. The presence of NaCl can provoke electrostatic screening and thus induces agglomeration. The presence of proteins (in serum-containing cell media) also could act on colloidal stability. However, as proteins and the NPs in this study have hydrodynamic radii on the same order of magnitude DLS is hard to perform.[33] Data with similar NPs (the same polymeric surface coating but Au instead of Ag cores) demonstrate that the presence of proteins can under our experimental conditions further reduce colloidal stability.[33] Thus, we can conclude that Ag–MUA NPs are highly agglomerated even at neutral pH and without the presence of proteins, whereas Ag–PMA NPs (with/without PEGylation) are much better dispersed. This is due to the more negative zeta-potential of PMA versus MUA coatings, which leads to stronger electrostatic repulsion for Ag–PMA NPs than for Ag–MUA NPs. For PEGylated NPs, the loss of colloidal stability due to electrostatic screening by NaCl is compensated by steric repulsions.

3.2. NP Oxidation

The Ag NPs were stringently cleaned after synthesis, leading to the removal of excess Ag(I) ions in solution. Kittler et al.[7] demonstrated release of Ag(I) from the Ag NPs due to oxidation. In order to study the release of Ag(I), NP samples incubated in water were analyzed by ultrafiltration followed by ICP-MS. At pH 7, even after 7 days of incubation, the amount of Ag(I) released from the Ag NPs was below the detection limit (<0.0015%; Supporting Information for details). On the other hand, after 7 days of incubation at pH 3 solution, around 1% of the Ag from the Ag NPs was detected as Ag(I) in solution. This suggests that Ag NPs inside acidic endo/lysosomal compartments release more Ag(I) than NPs in the extracellular neutral medium. No significant differences among the four different NP samples were observed. This can be explained by the fact that all are capped by thiolated hydrocarbon chains of comparable length (mercaptoundecanoic acid for Ag–MUA NPs and dodecylthiol for Ag–PMA NPs, respectively). Thus, changes in the outer surface cappings as PEGylation did not have significant effects on NPs oxidation. We also found in agreement with Kittler et al.[7] that Ag NPs are not completely dissolved and only a certain amount of Ag(I) is released. Analyses were performed in water at different pH, and not in the cell medium. To the best of our knowledge, proteins as particular enzymes in the cell medium can partly disintegrate the organic shell around,[18] but not extensively dissolve inorganic (e.g., Ag) cores.

3.3. NP Internalization

As can be clearly seen in Figure 3, the uptake of Ag–PMA NPs was strongly reduced when the surface of the NPs was saturated with PEG molecules of 10 kDa size (Ag–PMA–satPEG NPs vs Ag–PMA NPs). We did not quantify uptake as this has been already previously done with similar NPs,[22,33] and the qualitative results are sufficiently indicative. Data also clearly demonstrate that Ag–PMA NPs are internalized to a much higher extent than Ag–PMA–satPEG NPs. Unfortunately, we were not able to quantitatively compare the uptake of Ag–MUA NPs and Ag–PMA NPs. This is due to the fact that on the basis of different surface chemistry, the Dy636 fluorescence labels were attached differently to the NPs. Besides different amount of fluorophore per NP, they also will have different distance to the Ag cores and thus different quenching effects. The main statement of the uptake experiments thus is that PEGylation drastically reduces the uptake of NPs by cells, in accordance with previous works.

3.4. Cell Viability

As expected, free Ag(I) ions ($AgNO_3$ solution as positive control) significantly reduce the viability of NIH/3T3 cells, as quantitatively demonstrated in dose-response curves (one time point, one type of assay, and one cell type; Figure 4). Also in case Ag(I) is introduced in the cells via Ag NPs, the cell viability is reduced. In comparison to the MUA coating, the PMA coating was effective in reducing the toxicity of the Ag NPs. The surface modification of PMA-coated Ag NPs with one single PEG molecule (10 kDa) per NP (Ag–PMA–1PEG NPs) exhibited a similar dose-response curve (with similar LD_{50} values) to Ag–PMA NPs. In contrast, dose-response curve for Ag–PMA–satPEG NPs was strongly shifted to higher concentrations values. This indicates that much lower concentrations of nonPEGylated Ag NPs than of PEGylated NPs are necessary to induce cell death.

4. Conclusions

Correlation of the interaction of the NPs with cells and their physicochemical properties allows for a set of conclusions. i) Toxicity of Ag NPs was lower in comparison to Ag(I) ions, in case of normalization of the absolute amount of Ag. In Figure 4 NP concentration is given in terms of c(Ag) gram per liter, which allows for direct comparison. Even if one assumed that in the case of Ag–MUA NPs all Ag atoms on the NP surface went into solution, there is still a lower toxic effect in comparison to the same amount of free Ag(I) ions (from $AgNO_3$). Even in the worst case (Ag–MUA NPs), the toxicity from all Ag atoms on the surface still is lower than the one for free Ag(I), in case the c_{surf}(Ag) scale for Ag NPs is compared with the c(Ag) scale for $AgNO_3$. In addition, while ≈30% of the Ag within Ag NPs is bound on surface, our ICP-MS data indicated that even at pH 3, only ≈1% of Ag is released from the Ag NPs into solution. Thus, under our experimental conditions, Ag NPs are less toxic compared to Ag(I) ions in terms of absolute amounts of Ag, as most of the Ag in NPs is bound to the NPs and not available as Ag(I).

These are not the final page numbers

Please note that this is the opposite as reported by Cronholm et al.,[9] who, however, worked under different experimental conditions (other NPs and cells). In our case, even if one assumed the outer capping of Ag NPs to be oxidized there is still lower toxicity compared to $AgNO_3$. Additionally, PMA coating did not reduced the release of Ag(I) versus MUA coating, but reduced cytotoxicity. ii) Toxicity of Ag NPs depends on their uptake by cells. One may argue that the 1% of released Ag(I) ions from internalized Ag NPs has a more cytotoxic effect than assuming a scenario in which all Ag atoms situated at the Ag NP surface (≈30%) would be released extracellularly. Ag(I) as free ion is not membrane permeable (although it can be complexed by serum proteins) and thus Ag NPs are an efficient carrier to transport Ag(I) ions inside cells. The difference between intracellular and extracellular Ag is demonstrated upon comparison of Ag–PMA and Ag–PMA–satPEG NPs. PEGylation reduces cellular uptake, which goes hand in hand with a lower cytotoxicity. iii) Agglomeration is a key parameter in Ag NPs toxicity. Comparing the cytotoxic effects between Ag–MUA NPs and Ag–PMA NPs, different agglomeration behavior is the most likely reason. Ag–MUA NPs showed a greater tendency to agglomerate what finally resulted in an increased cytotoxicity. Toxic effects may be explained by clouding the cell membrane, as has been speculated previously.[34] Although our data clearly demonstrate that toxicity due to intracellular Ag is higher than that due to extracellular Ag (note that in contrast in the report by Cronholm et al.,[9] toxicity was generated by the extracellular interaction of Ag(I) to the cell membrane, unfortunately we could not quantify this in terms of the contribution of Ag from Ag(I) or Ag NPs. Characterization of physicochemical properties of internalized NPs still remains a future challenge, which, however, is strongly needed for further unraveling pathways of cytotoxic effects and their attribution to distinct physicochemical properties.

Acknowledgements

E.C-D. and C.P. contributed equally to this work. This work was supported by the BMBF Germany (project UMSICHT to WJP). E.C.-D. also would like to thank the Spanish Ministry of Education for the award of a FPU fellowship (Grant AP2008-02955).

Received: June 10, 2013
Published online:

[1] a) C. Marambio-Jones, E. M. V. Hoek, *J. Nanopart. Res.* **2010**, *12*, 1531; b) M. J. Hajipour, K. M. Fromm, A. A. Ashkarran, D. J. d. Aberasturi, I. R. d. Larramendi, T. Rojo, V. Serpooshan, W. J. Parak, M. Mahmoudi, *Trends Biotechnol.* **2012**, *30*, 499; c) S. Chernousova, M. Epple, *Angew. Chem Int. Ed.* **2013,** *52,* 1636.

[2] S. W. P. Wijnhoven, W. J. G. M. Peijnenburg, C. A. Herberts, W. I. Hagens, A. G. Oomen, E. H. W. Heugens, B. Roszek, J. Bisschops, I. Gosens, D. Van de Meent, S. Dekkers, W. H. De Jong, M. Van Zijverden, A. J. A. M. Sips, R. E. Geertsma, *Nanotoxicology* **2009**, *3*, 109.

[3] C. Beer, R. Foldbjerg, Y. Hayashi, D. S. Sutherland, H. Autrup, *Toxicol. Lett.* **2012**, *208*, 286.

[4] a) J. S. Teodoro, A. M. Simoes, F. V. Duarte, A. P. Rolo, R. C. Murdoch, S. M. Hussain, C. M. Palmeira, *Toxicol. In Vitro* **2011**, *25*, 664; b) R. Liu, S. J. Lin, R. Rallo, Y. Zhao, R. Damoiseaux, T. Xia, S. Lin, A. Nel, Y. Cohen, *Plos One* **2012**, *7, e35014*; c) E. Demir, G. Vales, B. Kaya, A. Creus, R. Marcos, *Nanotoxicology* **2011**, *5*, 417; d) C. Greulich, J. Diendorf, J. Gessmann, T. Simon, T. Habijan, G. Eggeler, T. A. Schildhauer, M. Epple, M. Koller, *Acta Biomater.* **2011**, *7*, 3505; e) S. Shrivastava, T. Bera, S. K. Singh, G. Singh, P. Ramachandrarao, D. Dash, *ACS Nano* **2009**, *3*, 1357.

[5] P. V. AshaRani, G. Low Kah Mun, M. P. Hande, S. Valiyaveettil, *ACS Nano* **2009**, *3*, 279.

[6] a) J. Liu, D. A. Sonshine, S. Shervani, R. H. Hurt, *ACS Nano* **2010**, *4*, 6903; b) J. Liu, R. H. Hurt, *Environ. Sci. Technol.* **2010**, *44*, 2169.

[7] S. Kittler, C. Greulich, J. Diendorf, M. Koller, M. Epple, *Chem. Mater.* **2010**, *22*, 4548.

[8] R. Foldbjerg, P. Olesen, M. Hougaard, D. A. Dang, H. J. Hoffmann, H. Autrup, *Toxicol. Lett.* **2009**, *190*, 156.

[9] P. Cronholm, H. L. Karlsson, J. Hedberg, T. A. Lowe, L. Winnberg, K. Elihn, I. O. Wallinder, L. Moller, *Small* **2013**, *9*, 970.

[10] a) M. V. Park, A. M. Neigh, J. P. Vermeulen, L. J. de la Fonteyne, H. W. Verharen, J. J. Briede, H. van Loveren, W. H. de Jong, *Biomaterials* **2011**, *32*, 9810; b) H.-J. Yen, S.-h. Hsu, C.-L. Tsai, *Small* **2009**, *5*, 1553; c) C. Carlson, S. M. Hussain, A. M. Schrand, L. K. Braydich-Stolle, K. L. Hess, R. L. Jones, J. J. Schlager, *J. Phys. Chem. B* **2008**, *112*, 13608.

[11] L. C. Stoehr, E. Gonzalez, A. Stampfl, E. Casals, A. Duschl, V. Puntes, G. J. Oostingh, *Part. Fibre Toxicol.* **2011**, *8*, 36.

[12] A. M. El Badawy, R. G. Silva, B. Morris, K. G. Scheckel, M. T. Suidan, T. M. Tolaymat, *Environ. Sci. Technol.* **2010**, *45*, 283.

[13] I. Romer, T. A. White, M. Baalousha, K. Chipman, M. R. Viant, J. R. Lead, *J. Chromatogr. A* **2011**, *1218*, 4226.

[14] P. Rivera-Gil, D. Jimenez de Aberasturi, V. Wulf, B. Pelaz, P. del Pino, Y. Zhao, J. de la Fuente, I. Ruiz de Larramendi, T. Rojo, X.-J. Liang, W. J. Parak, *Acc. Chem. Res.* **2013**, *46*, 743.

[15] M. P. Monopoli, C. Aberg, A. Salvati, K. A. Dawson, *Nat. Nanotechnol.* **2012**, *7*, 779.

[16] S. Milani, F. B. Bombelli, A. S. Pitek, K. A. Dawson, J. Radler, *ACS Nano* **2012**, *6*, 2532.

[17] a) C. Röcker, M. Pötzl, F. Zhang, W. J. Parak, G. U. Nienhaus, *Nat. Nanotechnol.* **2009**, *4*, 577; b) X. Jiang, S. Weise, M. Hafner, C. Röcker, F. Zhang, W. J. Parak, G. U. Nienhaus, *J. R. Soc. Interface* **2010**, *7*, S5.

[18] M. Chanana, P. Rivera-Gil, M. A. Correa-Duarte, W. J. Parak, L. M. Liz-Marzán, *Angew. Chem Int. Ed.* **2013**, *52*, 4179.

[19] N. Lewinski, V. Colvin, R. Drezek, *Small* **2008**, *4*, 26.

[20] R. Di Corato, D. Palumberi, R. Marotta, M. Scotto, S. Carregal-Romero, P. Rivera-Gil, W. J. Parak, T. Pellegrino, *Small* **2012**, *8*, 2731.

[21] C. Greulich, J. Diendorf, T. Simon, G. Eggeler, M. Epple, M. Koller, *Acta Biomater.* **2011**, *7*, 347.

[22] C. Brandenberger, C. Mühlfeld, Z. Ali, A.-G. Lenz, O. Schmid, W. J. Parak, P. Gehr, B. Rothen-Rutishauser, *Small* **2010**, *6*, 1669.

[23] M. Lipka, M. Semmler-Behnke, R. A. Sperling, A. Wenk, S. Takenaka, C. Schleh, T. Kissel, W. J. Parak, W. G. Kreyling, *Biomaterials* **2010**, *31*, 6574.

[24] D. E. Cliffel, F. P. Zamborini, S. M. Gross, R. W. Murray, *Langmuir* **2000**, *16*, 9699.

[25] C.-A. J. Lin, R. A. Sperling, J. K. Li, T.-Y. Yang, P.-Y. Li, M. Zanella, W. H. Chang, W. J. Parak, *Small* **2008**, *4*, 334.

[26] Y. Sun, *Chem. Soc. Rev.* **2013**, *42*, 2497.

[27] A. Mari, P. Imperatori, G. Marchegiani, L. Pilloni, A. Mezzi, S. Kaciulis, C. Cannas, C. Meneghini, S. Mobilio, L. Suber, *Langmuir* **2010**, *26*, 15561.

[28] T. Pellegrino, S. Kudera, T. Liedl, A. M. Javier, L. Manna, W. J. Parak, *Small* **2005**, *1*, 48.

These are not the final page numbers

[29] M. T. Fernández-Argüelles, A. Yakovlev, R. A. Sperling, C. Luccardini, S. Gaillard, A. S. Medel, J.-M. Mallet, J.-C. Brochon, A. Feltz, M. Oheim, W. J. Parak, *Nano Lett.* **2007**, *7*, 2613.
[30] C. Geidel, S. Schmachtel, A. Riedinger, C. Pfeiffer, K. Müllen, M. Klapper, W. J. Parak, *Small* **2011**, *7*, 2929.
[31] T. L. Doane, C. H. Chuang, R. J. Hill, C. Burda, *Acc. Chem. Res.* **2012**, *45*, 317.
[32] J. O'Brien, I. Wilson, T. Ortaon, F. Pognan, *Toxicology* **2001**, *164*, 132.
[33] D. Hühn, K. Kantner, C. Geidel, K. Chiad, S. Brandholt, S. Soenen, U. Linne, P. Rivera-Gil, J. M. Montenegro, K. Braeckmans, K. Müllen, U. G. Nienhaus, M. Klapper, W. J. Parak, *ACS Nano* **2013**, *7*, 3253.
[34] C. Kirchner, T. Liedl, S. Kudera, T. Pellegrino, A. Muñoz Javier, H. E. Gaub, S. Stölzle, N. Fertig, W. J. Parak, *Nano Lett.* **2005**, *5*, 331.

C. Pfeiffer[#], B. D. Johnston[#], ..., W. Kreyling, W. J. Parak

Colloidal stability in addition to surface chemistry as key factor of the composition of the protein corona of nanoparticles.

[#]both authors contributed equally to this work

Introduction

The formation of a so called protein corona is the fate of every kind of nanoparticle which is introduced into a biological matter. The properties of the corona and how it is build depends on various physicochemical properties of the covered particle{Lundqvist, 2008 #15544}. The most important once are (I) size, (II) charge, (III) surface chemistry and (IV) the colloidal stability. By changing the size of a particle and with this its curvature radius the contact angel between the particle and the protein is changed which influences the interaction. A decreased curvature radius leads to a decreased contact angle which leads to a weaker interaction between NP and protein{Walkey, 2012 #20875; Tenzer, 2011 #20889; Pelaz, 2013 #24459}. Charged, hydrophobic particles tend to form more stable complexes with proteins than neutral hydrophilic once due to electrostatic interactions. The absorption of proteins can also be modified by the use of so called anti fouling polymers. The surface of the NP is covered with hydrophilic, charge-neutral polymers like PEG, polysaccharides, or zwitterionic poly(carboxybetaine methacrylate) which leads to a minimized protein absorption{Mei, 2008 #13292; Moros, 2010 #17110; Breus, 2009 #15558}. This effect is called passivation of a NP. Another very important parameter is the colloidal stability of the NP. Weak stable NP often aggregate and precipitate out of the solvent when they are introduced into biological media whereas stable NP can build a stable protein corona{Safri, 2011 #21271}. The corona also influences active the uptake of a NP by a cell. A passivated NP for example shows a decreased uptake than a not passivated one{Chang, 2005 #17676; Moros, 2012 #20064}. It is also important to mention that the protein corona, once it is formed, is not stable but shows a highly dynamic structure. The outer part of the corona the so called soft corona shows a dynamic exchange of absorbed proteins whereas the closer, hard corona shows less exchange but is still not stable{Lynch, 2008 #23810; Lundqvist, 2011 #23850; Milani, 2012 #20888}. Also the size of the corona can shrink after a certain time{Jedlovszky-Hajdu, 2012 #23863}. Not only the absorbed proteins change the properties of the covered NP the same is true the other way around. The covered particle can influence the shape of the protein which can change the fate of the protein. The overall structure of the protein can be intact so that the protein keeps intact but it can also lead to full denaturation of the protein{Aubin-Tam, 2005 #11591}.

In this article five different stabilized Au NPs were used to analyze the formation of the protein corona in a quantitative way. All modifications were done starting with the same commercial Au NPs so that all particles have the same inorganic core diameter (d_c) about 5 nm. By using this method the differences in the properties and the protein corona belong to the surface coatings and not to different cores. Before the protein coronas were analyzed the physicochemical properties were investigated using various methods. Amongst others transmission electron microscopy (TEM) for measuring the inorganic core diameter, UV/Vis spectroscopy for measuring the absorbance, dynamic light scattering (DLS) for measuring the hydrodynamic diameter (d_h) and laser Doppler anemometry (LDA) for measuring the zeta potential (ζ) were used to characterize the particles. Additionally to measure the stability of the particles, the agglomeration behavior was investigated by measuring the hydrodynamic diameter at different times and

under different salt concentrations. As protein source the pooled serum of four mice and the pooled BAL from 50 mice were used and incubated with the different particles at 37°C. The particles and protein corona were analyzed by atomic force microscopy (AFM), differential centrifugal sedimentation, SDS gel electrophoresis and hybrid mass spectroscopy.

Materials and Methods

All materials were used without further purification before use. A complete list of all used chemicals can be found in the supporting information. A more detailed description of the different modifications methods is in the supporting information, too. All modifications were done using citrate stabilized, 5 nm sized Au NPs from British BioCell International.

Ligand exchange with Bis(p-sulfonatophenyl)phenylphosphine dihydrate dipotassium salt (Phosphine):

The citrate stabilized Au NPs were mixed with Bis(p-sulfonatophenyl)phenylphosphine dihydrate dipotassium salt and stirred for 4 hours at RT. The particles were separated from the exchanged citrate molecules and the excess Phosphine molecules by using a centrifuge filter (100kDa MWCO).

Ligand exchange with thiol capped PEG (PEG-SH):

A stock solution of the thiol capped PEG (5 kDa) was mixed with the citrate stabilized Au NPs and stirred for 24 hours at RT. The particles were separated from excess PEG molecules and exchanged citrate molecules by using a centrifuge filter (100kDa MWCO).

Transfer to the organic phase and polymer coating:

The phase transfer was inspired by the synthesis of Au NPs from Brust et al.{Brust, 1994 #7593}. The phase transfer to the organic phase was done by using Tetraoctylammonium bromide (TOAB) as phase transfer agent. The TOAB was dissolved in toluene and placed into a separation funnel. The citrate stabilized Au NPs were added and shaken for 10 minutes. Afterwards the aqueous phase was trashed and the organic phase was reduced to 1/3 of its original volume. Dodecanethiol was added, the mixture was heated up to 65°C and stirred for 4 hours to replace the TOAB. The particles were separated by precipitation by adding acetone (four times the volume of the toluene). The precipitated particles were centrifuged for 5 minutes at 2000 rpm. The supernatant was discarded and the particles were resuspended in Chloroform. The polymer coating could be done described in the literature{Lin, 2008 #11245}. Therefore the Au NPs were mixed with the amphiphilic polymer (Dodecylamine modified Poly(isobutylene-alt-maleic anhydride)). The Chloroform was removed under reduced pressure and the particles were resuspended in a basic aqueous buffer (50 mM sodium borate, pH 12). By dissolving the particles in the basic buffer, the anhydride rings opened leading to carboxylic acid groups at the surface of the particles.

Additional modification with amine capped PEG:

The addition of amine capped PEG (2 kDa) to the surface was done by *N*-(3-Dimethylaminopropyl)-*N*′-ethylcarbodiimide hydrochloride (EDC) chemistry. The carboxylic acid groups from the polymer react with the amine from the PEG leading to an amide bond. The particles were mixed with the polymer using an excess of 500 amine groups per particle. The ratio of EDC per particle were set to 64000:1 and added

to the mixture of polymer and particles and stirred. After 2.5 hours of reaction at RT the particles were given into a 2% agarose gel and purified via gel electrophoresis (1 h, 10 V/cm).

Formation of the protein corona:

The experimental design of the formation of the protein corona is shown in figure 1. Serum or BAL with concentration of 400-800µg/ml were mixed with the Au NPs with a concentration of 3-5· 10^{-6} M and incubated at 37°C for 15 minutes or 24 hours. The mixture was centrifuged at 75000 x g to concentrate the particles. The supernatant was discarded and the particles were washed three times with PBS. Afterwards the particles and the particle corona were characterized.

Gel electrophoresis:

All particles were purified after modification using gel electrophoresis. Therefore a 2% agarose gel was prepared and placed into an electrophoresis chamber filled with Tris-borate-EDTA (TBE) buffer (0.5x). The particles were placed in a pocket inside the gel and run for 1 hour at 10 V/cm. Afterwards the band including the nanoparticles was cut of the gel and placed into a dialysis membrane (50 kDa MWCO). The membrane was filled with TBE buffer, locked and placed back into the electrophoresis chamber. By running the particles again at 10 V/cm they run out of the gel but keep trapped inside the dialysis membrane. By using a centrifuge filter (100 kDa MWCO) at 2500 rpm the particles were concentrated for further purification/characterization.

Size exclusion chromatography:

After purification by gel electrophoresis all particles were purified by using high pressure liquid chromatography (HPLC). An Agilent Technologies 1100 Series system with a self packed Sephacryl S-300 HR from GE Health Care was used. The system was run using phosphate buffered saline (PBS) as eluent with a flow rate of 1 ml/min. A centrifuge filter was used to concentrate the particles again for further characterization. The Au NPs stabilized by Phosphine could not be purified by HPLC because they didn´t pass the column and stuck to the material (see supporting information).

Ultraviolet-visible spectroscopy

The concentration of the Au nanoparticle suspension was calculated by measuring the absorbance of the suspension and using Beer-Lambert law. The molar extinction coefficient (9696000 $M^{-1}\cdot cm^{-1}$) was given from the company. An Agilent Technologies 8453 UV-Vis spectrometer was used for measuring the absorbance. A blank spectrum of the solvent was used for background correction.

Dynamic light scattering (DLS) and laser Doppler anemometry (LDA)

For measuring the hydrodynamic diameter and the zeta potential a Malvern Zetasizer Nano ZS was used. The measurements were performed using a red laser light source at 173° backscatter detection mode. The samples were equilibrated for 15 minutes at 25°C before measurement. For measuring the zeta potential the Malvern Dip Cell Kit was used.

Transmission electron microscopy (TEM):

For measuring the nanoparticles with transmission electron microscopy a Jeol JEM-3010 TEM was used. A drop of the particle suspension was placed on a copper grid and dried in the dark for four days.

Atomic force microscopy (AFM):

##done by Blair##

Results and Discussion

Colloidal stability

Beginning with a commercial Au NP with a core diameter of around 5 nm four different surface modifications were done. Two were done by replacing the original citrate molecules by hydrophilic molecule (Bis(p-sulfonatophenyl)phenylphosphine dihydrate dipotassium salt (Phosphine)) and a thiol capped polymer (α-thiol-polyethylene glycol (PEG-SH) (5 kDa)). The citrate can be removed easily because of its weak binding to the Au core. The Phosphorus from the Phosphine, as well as the Sulfur from the polymer show a much higher affinity to the gold. The two other samples were stabilized by coating the Au NP with an amphiphilic polymer. Therefore the original particle had to be transferred to the organic phase first. This was done by replacing the citrate first with a phase transfer ligand which was replaced by a hydrophobic ligand in a second step. Afterwards the Au NPs were stable in organic phase and could be coated with an well established amphiphilic polymer which is already know in literature{Lin, 2008 #11245}. After coating the particles the surface of one sample was saturated with 2 kDa PEG molecules by using EDC chemistry. All particles showed similar UV/Vis spectra containing the typical plasmon peak at 520 nm (see supporting information). No change in the core could be seen in TEM (see supporting information) showing similar sizes for all samples (Table 1). The hydrodynamic diameter of the two samples with polymer saturated surfaces (Au-PEG-SH + Au-PMA-satPEG) was about doubled the diameter of the polymer coated sample (Au-PMA) and three times the size of the original and the Phosphine stabilized particles (Table 1). The different hydrodynamic diameters could also be seen in gel electrophoresis (figure 2). The stability of different samples was measured by measuring the hydrodynamic diameter under different salt concentrations up to 2.5 M of sodium chloride. The diameters were measured directly after addition and after 24 hours. The not modified citrate stabilized particles, as well as the Phosphin stabilized particles showed the weakest stability and aggregate with certain amounts of salt after 24 hours. Here the particles were completely aggregated and settled down to the bottom of the cuvette (figure 4). These particles already showed an increased hydrodynamic diameter directly after addition of the salt. The other three samples in contrast kept stable even after 24 hours with a concentration of 2.5 M NaCl (Table 2). Similar results could already been shown for silver nanoparticles{XXX not yet added to endnote}.

Protein corona formation

The results of the two size measuring methods (AFM + differential centrifugal sedimentation) it could be clearly seen that the two particle types showing the lowest colloidal stability (citrate and Phosphine stabilized) again show the tendency to behave similar. Both types show agglomeration with serum protein whereas the other three samples did not (see supporting information). The colloidal stability seemed to be the key factor for the formation of the protein corona more than the surface chemistry. The well stabilized particles (PEG-SH, PMA and PMA-satPEG stabilized) showed similar results in AFM and also in LC MS/MS. For all the samples a huge number of proteins could be identified by MS spectroscopy for the incubation with serum as well as for incubation with BAL (Table 3 + figure 5). The PEG-SH stabilized

particles were expected to behave more similar to the other samples which were modified by simple ligand exchange and less like the polymer coated samples. But here the way how a ligand is bound to the polymer seemed to be less important than the effect which it had to the colloidal stability of the Au NPs. The PEG-SH modified particles and the PMA-satPEG stabilized particles showed also almost the same abundance of proteins. Here the PMA coated particles differed from all the other samples. The citrate and the Phosphine stabilized particles again showed similar results. The similarity of the good stabilized and the bad stabilized particles could also be seen in the protein profile heat maps after 15 minutes and 24 hours after incubation with mouse serum (figure 6). Here the profiles of the bad stabilized particles looked pretty much the same and the profiles of the good stabilized particles too.

=> from the protein corona the NPs with the lowest colloidal stabiliy are closest

=> major parameter for formation of protein corona seem colloidal stability

also PEGylated NPs, regardless how PEG was introduced similar

and PEG + polymer coated NPs more similar than citrate / phosphine stabilized NPs (good versus bad colloidal stability)

include

Tables

	d_c [nm]	d_h [nm]	ζ [mV]
Au-citrate		6.82 ± 1.8	-19 ± 2.5
Au-Phosphine	5.31 ± 0.73	6.30 ± 1.8	-51 ± 4.8
Au-PEG-SH	5.44 ± 0.78	21.47 ± 5.8	-44 ± 7.7
Au PMA	5.24 ± 0.69	9.48 ± 2.9	-33 ± 6.4
Au-PMA-satPEG	5.63 ± 0.77	18.64 ± 5.1	-45 ± 4.4

Table 1: Summary of core diameter *via* TEM (d_c), hydrodynamic diameter *via* DLS (d_h) and zeta potential *via* LDA (ζ).

t = 0 h

c(NaCl)	0 mM	160 mM	625 mM	2.5 M
Au-citrate	7.10±1.9nm	149.8±49.4nm	833±324nm	898±315nm
Au-Phosphine	6.30±1.8nm	6.49±1.8nm	539±248nm	693±297nm
Au-PEG-SH	21.47±5.8nm	23.08±5.7nm	22.16±5.9nm	26.51±7.4nm
Au-PMA	9.48±2.9nm	10.00±2.6nm	10.78±3.0nm	12.34±3.1nm
Au-PMA-satPEG	18.64±5.1nm	17.75±5.0nm	21.06±5.7nm	22.50±5.9nm

t = 24 h

c(NaCl)	0 mM	160 mM	625 mM	2.5 M
Au-citrate	7.26±2.0nm	$\rightarrow\infty$	$\rightarrow\infty$	$\rightarrow\infty$
Au-Phosphine	6.68±1.8nm	7.40±1.9nm	$\rightarrow\infty$	$\rightarrow\infty$
Au-PEG-SH	21.31±5.8nm	22.47±4.9nm	21.80±5.9nm	25.08±7.2nm
Au-PMA	9.10±2.7nm	10.43±2.9nm	13.39±4.7nm	15.39±4.4nm
Au-PMA-satPEG	18.57±5.1nm	18.65±5.2nm	18.65±5.2nm	22.63±6.1nm

Table 2: Summary of mean hydrodynamic diameters d_h and their corresponding standard deviation.

Serum		BAL	
Acc.	**Gene**	**Acc.**	**Gene**
C3	Complement factor 3	GELS	Gelsolin
Alb	Albumin	DPYL2	Dihydropyrimidinase
Mug1	Murinoglobulin 1	ACTG	Actin, cytoplasmic
Fn	Fibronectin 1	ANXA1	Annexin 1
Hbb-b1	Hemoglobin, beta adult major chain	CO3	Complement 3
Cfh	Complement component factor h	MOES	Moesin
TrF	Transferrin	VINC	Vinculin
Hba-a2	Apolipoprotein B	HSP7C	Heat Shock cognate 71kDa
Thbs-1	Thrombospondin 1	PRDX6	Peroxiredoxin 1
Serpinc1	Serine (or cystein) peptidase inhibitor	AL1A1	Retinal dehydrogenase
Ahsg	Alpha 2-HS-glycoprotein	SBP1	Selenium binding protein 1
Hpx	Hemopexin	SPA3K	Serine protease inhibitor
Apoa4	Apolipoprotein A-IV	TBB2C	Tubulin beta 2C chain
Plg	Plasminogen	GSTM1	Glutathione-S-transferase
Apoa1	Apolipoprotein A-I	KPYM	Pyrovate kinase lysoymes M1/M2
Pon1	Paraoxonase I	INMT	Indolethylamine N-methyltransferase
Ttr	Transthyretin	G3P	Glyceraldehyde-3-phosphate
H2-Q10	Histocompatability-2, Q region, locus 10	ENOA	Alpha-enolase

Table 3: List of the proteins bound to Au NP-TPPMS ligand/Orbitrap MS detection.

Figures

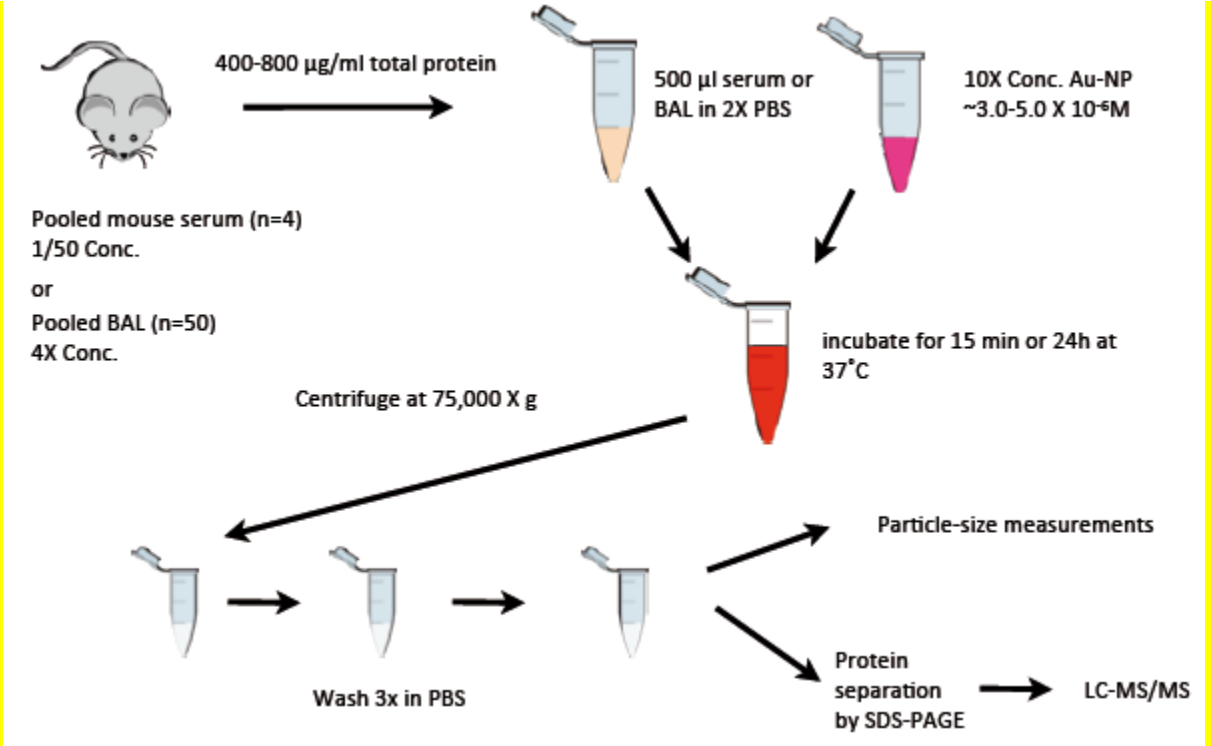

Figure 1: Experimental design for the protein corona formation.

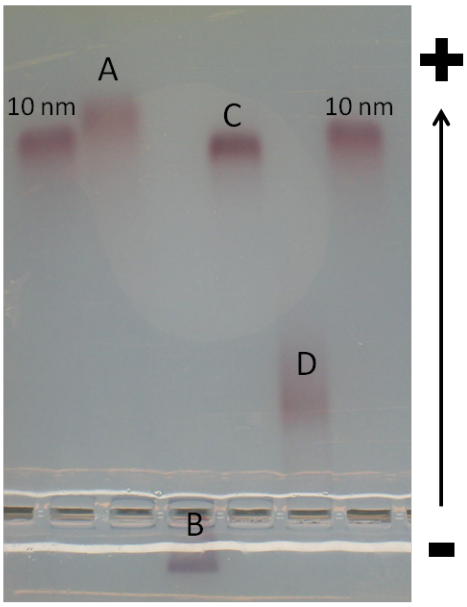

Figure 2: 2% Agarose gel after 1 hour of gel electrophoresis (10 V/cm). A-D show the four different stabilized Au NPs (A: Phosphine, B: PEG-SH, C: PMA coated, D: PMA coated + saturated with 2 kDa PEG). The original citrate stabilized NPs did not enter the gel. Additionally 10 nm Au NPs were used as reference.

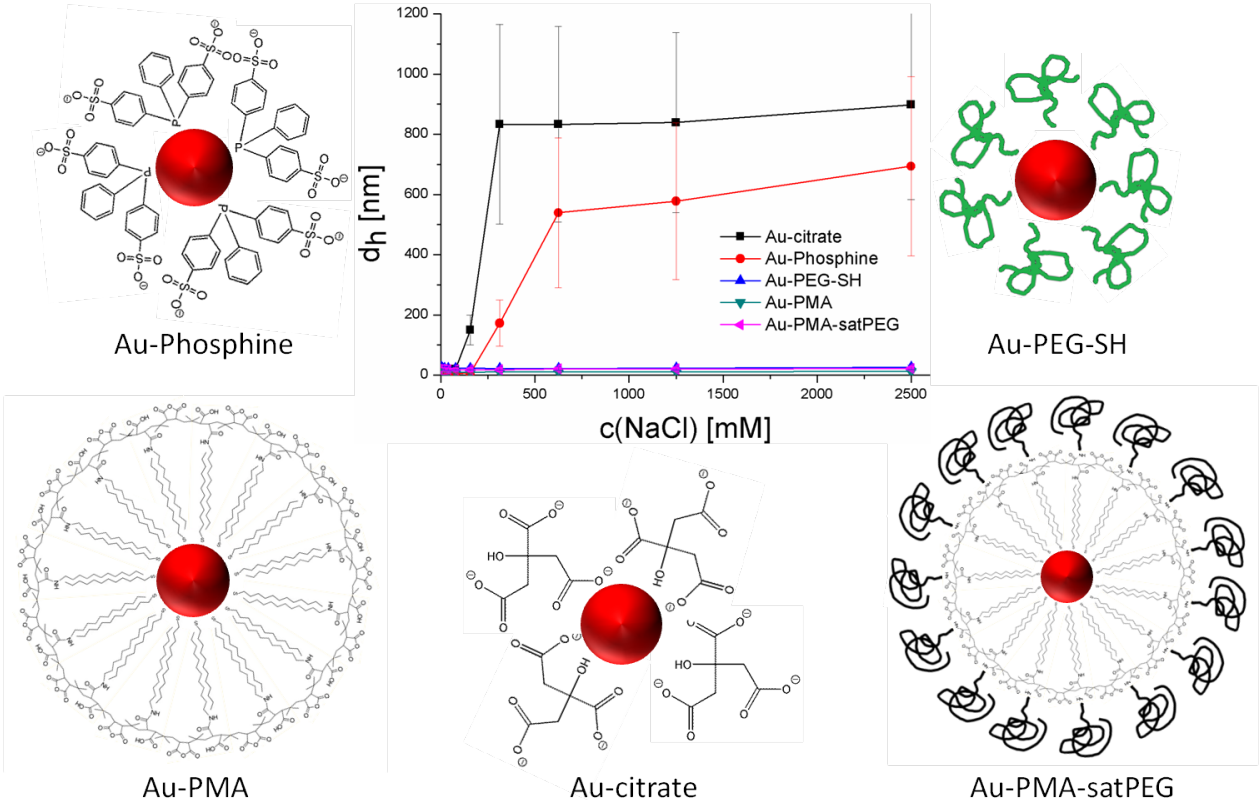

Figure 3: Sketches of the four different modified Au NPs and the original citrate stabilized particle. The diagram shows the hydrodynamic diameter of the different particles in dependency of the added sodium chloride concentration directly after addition.

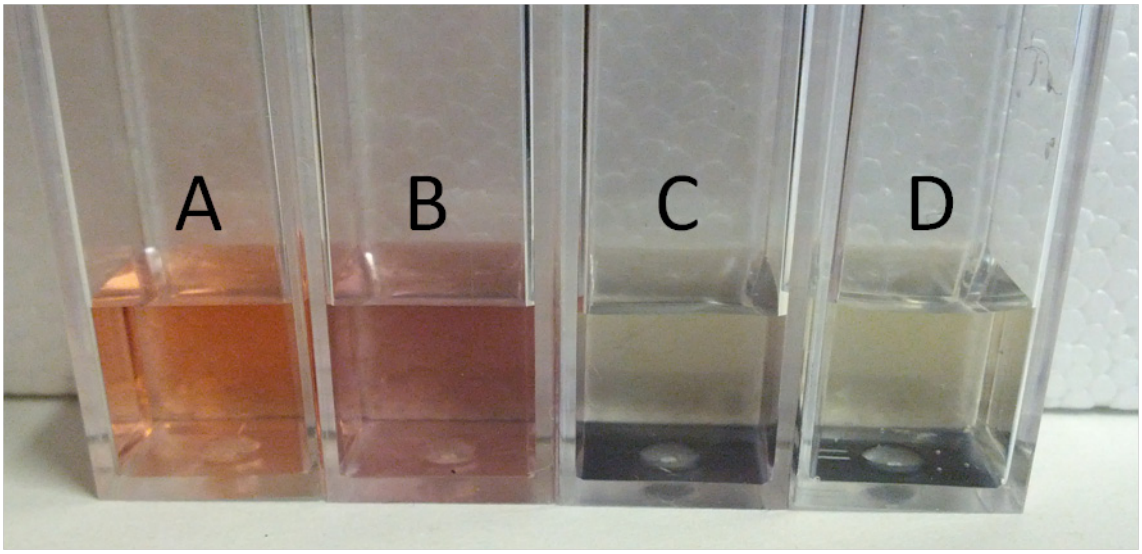

Figure 4: Picture of Au-Phosphine NPs with different sodium chloride concentrations after 24h [(A) 0mM, (B) 160mM, (C) 625mM, (D) 2.5M]. The change in color indicates the increased size. In C+D the particles are completely aggregated and precipitated at the bottom of the cuvette.

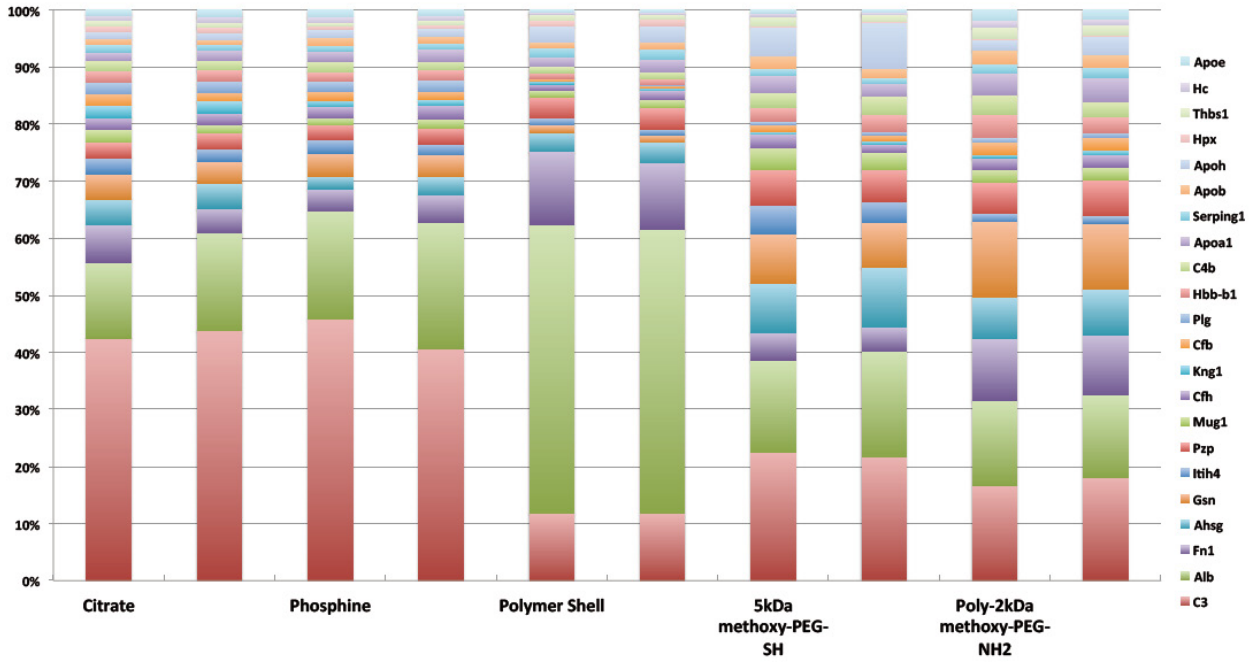

Figure 5: Protein profiles of Au NPs incubated with mouse serum for 15 minutes.

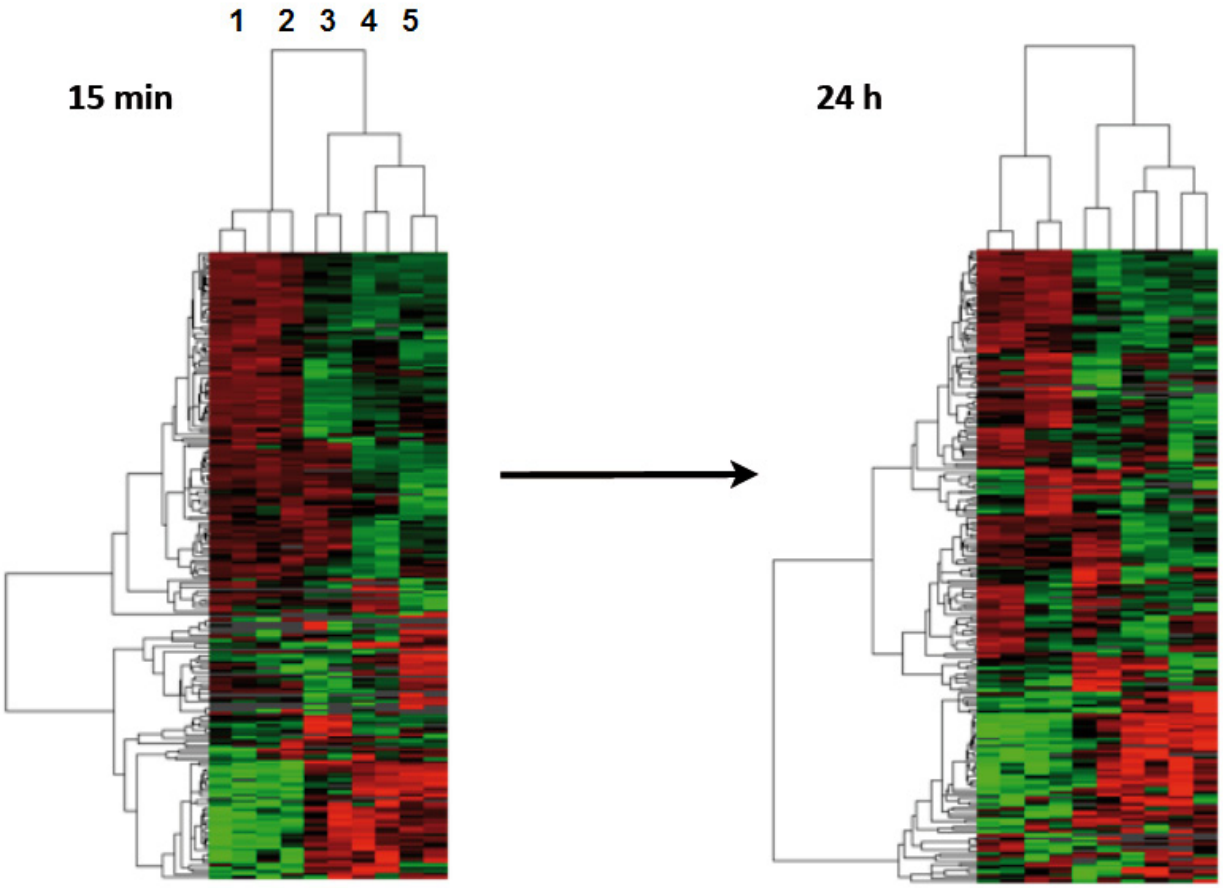

Figure 6: Protein profiles of Au NPs incubated with mouse serum for 15 minutes and 24 hour. Heat map of all proteins across 5 ligands. (1: Citrate, 2: Phosphine, 3: PMA, 4: PEG-SH, 5: PMA-satPEG)

References